THE TURBULENT INCOMPRESSIBLE HYDRODYNAMIC BOUNDARY LAYER

by

Marcel Paul Escudier
B.Sc.(Eng.), A.C.G.I., D.I.C.
Beit Scientific Research Fellow

Thesis submitted for the degree of
Doctor of Philosophy
in the Faculty of Engineering
University of London

October 1967

ABSTRACT

The entrainment and kinetic-energy methods for the calculation of turbulent hydrodynamic boundary layers are discussed in detail. The main concern is with the auxiliary relations used by the two methods. Most of the previous proposals for these relations are shown to be deficient in accuracy of prediction, range of applicability and, often, ease of use. New empirical formulae, free from the drawbacks of earlier proposals, are recommended; and predictions of boundary-layer development are presented to demonstrate the adequacy of the new relations. A critical discussion of the predictions leads to the conclusion that, where poor results are obtained, the most likely cause is a lack of two-dimensionality of the mean flow. However, some discrepancies are attributed to failure to comply with other restrictions by which the calculation methods are bound.

An important outcome of the above work is a table which gives details of many of the experimental data reported in the literature.

The influence of augmenting artificially the level of turbulence intensity within a boundary layer is investigated experimentally. The most significant effect is found to be upon the peak shear stress, which is considerably increased by quite modest increases in the intensity.

ACKNOWLEDGEMENTS

I wish to acknowledge with gratitude the advice, guidance and assistance of my supervisor, Professor D.B. Spalding of Imperial College, who suggested the work and provided many of the original ideas described in this thesis.

I am also indebted to Drs. J.H. Whitelaw, E. Baker and B.E. Launder who have always been willing to give of their time to discuss problems and make many useful suggestions for their solution.

Thanks are also due to my other colleagues, too numerous to mention individually, who have contributed to the successful completion of this work.

The provision of personal financial support by the Trustees of the Beit Scientific Research Fellowships, for the major part of the time spent on this research, is also gratefully acknowledged.

Finally, I must express my gratitude to the following writers who have been willing to provide unpublished details of their experimental work: Mr. P. Bradshaw, Prof. F.H. Clauser, Mr. F. Erian, Dr. V. Kruka, Dr. W. B. Nicoll, Dr. G.B. Schubauer, Mr. W. Spangenberg and Dr. B.S. Stratford; and also to Mr. J.A.P. Stoddart, who supplied details of the Ludwieg-Tillman experiments.

CONTENTS

CHAPTER		PAGE
1.	INTRODUCTION	5
2.	MATHEMATICAL THEORY	14
3.	THE ENTRAINMENT METHOD	31
4.	THE KINETIC - ENERGY METHOD	62
5.	CALCULATIONS OF BOUNDARY - LAYER DEVELOPMENT	111
6.	THE EXPERIMENTAL INVESTIGATION	136
7.	CONCLUSIONS	164
	REFERENCES	169
	NOMENCLATURE	180
	TABLES	185
	FIGURES	227
	APPENDICES	274

CHAPTER 1

INTRODUCTION

1.1 Historical background

The subject of the turbulent boundary layer is one about which there exists an already extensive and still rapidly-growing literature. This alone is testimony both to its importance and to its complexity. But, if additional evidence is required as to the importance of the problem, it is necessary only to mention a few of the multitude of situations where an accurate method is required for the calculation of the development of turbulent boundary layers. It is necessary in the estimation of aircraft drag, for the design of rocket motors, combustion chambers and heat exchangers, and of diffusers, pumps and compressors. Indeed, the limiting performance of almost all turbomachinery is governed by stall - the separation of boundary layers.

The fundamental difficulty of turbulent shear flows is attributable to the fact that when the Navier-Stokes equations of fluid motion are time-averaged in order to make them tractable, six Reynolds stresses appear as additional unknowns. No universally-valid expressions are yet known for relating these to the mean velocity distribution, the turbulent kinetic energy, etc.

Therefore, in contrast with laminar flows, no physically exact solutions of the boundary-layer equations are possible. In order to proceed at all, empirical information is necessary; but the complexity of the flow, and the difficulty of measuring turbulence quantities, such as the Reynolds stresses, has long been an insurmountable barrier to establishing empirical laws valid for more than a limited range of situations.

For laminar flows, the numerical solution of any general problem has always been possible in principle, but it is only the advent of large high-speed computers which has made this a practicable possibility. Even so, approximate integral methods for the solution of laminar boundary-layer problems are still being developed (e.g. Curle, 1967). Similarly for turbulent boundary layers, the formidable problem of mathematically exact computation is shunned, and integral, or profile, techniques have been developed as a means for simplifying the problem. The main advantage of such methods is that they maximise the information obtainable from a given number of differential equations; the reason being that when selecting the profile family, guidance usually is taken from, and so implicitly knowledge is incorporated of, the general experimental behaviour.

The integral methods used in turbulent-boundary-layer calculations can take two typical forms, distinguished by the choice of dependent variables. They are: (1) The explicit method, which employs explicit formulae for the drag coefficient, and other quantities, in terms of the dependent variables of the naturally-occurring differential equations. The majority of available integral procedures are of this type; examples are those of Truckenbrodt (1952), Head (1958) and Walz (1965). They have the advantage that their very nature can ensure agreement of the auxiliary relations with experiment. On the other hand, the previously-existing explicit procedures are of limited applicability and generally incapable of extension. Also, as Thompson (1964) convincingly showed in his critical review of explicit methods developed prior to 1963, in all cases bar one (Head's method) they are decidedly unreliable. (2) The parametic-profile method, in which the auxiliary quantities are expressed in terms of certain parameters. The latter are usually quantities which appear in the formulae used to describe the velocity profile; they are used as the dependent variables of the differential equations. The methods of Spalding (1964a), Patankar and Spalding (1965) and Lewkowicz and Horlock (1966) are parametric ones. This type of method has the advantage of poten-

tially greater flexibility, but at the expense of mathematical simplicity and computational convenience. Also, a parametric-profile method generally brings some loss of freedom, to adjust constants etc. to fit experimental findings, so far as the auxiliary relations are concerned.

In the original version of his 'Unified Theory', Spalding (1964a) drew attention to the desirability of a single calculation procedure, applicable both to 'conventional' boundary layers, where the velocity increases monotonically from zero at the wall to its mainstream value, and also to the so-called wall jet - the flow downstream of an injection slot, for which the profiles of velocity can exhibit a maximum. No previously-existing explicit method is so applicable; and examination, for example, of the considerable German literature on the subject of turbulent-boundary-layer calculation reveals that almost all of the recent work carried out in Germany has been founded on a structure emanating from the work of Ludwieg and Tillmann (1949) and entirely unsuitable for extension to jet-like boundary-layer flows (the reasons are elaborated in section 3 of CHAPTER 4).

The major part of this thesis records the writer's contributions to both a parametric-profile method and to an explicit method of turbulent boundary-layer calculation. The profile method is that of Spalding's

original 'Unified Theory'; it employs as an auxiliary relation an entrainment law, and is similar to the method of Head (1958), though of wider range of applicability. The other method examined is that based upon the equation for the conservation of mean-flow kinetic energy. This has been developed along two distinct lines, one resulting in the parametric-profile procedure of Patankar and Spalding (1965), and the other in the explicit procedure of Escudier and Nicoll (1966b). A special feature of the present writer's kinetic-energy method is that the basic structures of the empirical relations on which it relies were suggested by consideration of a parametric profile. This new explicit method appears to be the first which is continuously applicable to the wide range of flows with separating boundary layers at one extreme, and wall jets in still surroundings at the other.

1.2 The purposes of the present study

The broad outlines of the theoretical part of the present study have been indicated in section 1.1; they may be stated more precisely as follows: (1) To survey the available experimental data on turbulent boundary layers for information about the wall shear stress and the profiles of velocity (thicknesses, shape factors, etc.) and shear stress. (2) To use the information

collected so as to establish empirically the auxiliary relations necessary to two integral procedures for the calculation of turbulent boundary layers: the entrainment method and the kinetic-energy method. (3) To apply the calculation methods so established to the prediction of the development of particular boundary layers, the information of (1) being used as data for comparison.

In addition to the above, experiments were to be carried out to provide further experimental information, particular attention being paid to the effect, on the downstream development of a boundary layer, of altering (increasing) the upstream level of turbulence intensity (turbulent kinetic energy) within the layer.

Restrictions

The present research has been confined to flows subject to the following restrictions: (1) The density and viscosity of the fluid are uniform throughout the stream, and when any fluid is injected into the boundary layer it has the same composition and fluid properties as that of the primary flow. (2) The wall on which the boundary layer is developing is smooth, plane and impermeable. (3) Gravitational, centrifugal and other body forces are negligible. (4) The mean flow is steady and two-dimensional in character (this means that the mean-velocity and shear-stress profiles depend upon only two space vari-

ables; consideration may thus be given to converging and diverging flows). (5) Outside the shear layer is a mainstream of effectively unlimited extent and negligible turbulence intensity.

1.3 Outline of the thesis

The main body of this thesis is divided into seven chapters, of which this INTRODUCTION is the first.

The second chapter introduces the partial differential equations which govern turbulent-boundary-layer development. Integral forms of these equations are also presented, initially in dimensional form, and then in non-dimensional 'working' form. Finally, outlines are given of the entrainment and kinetic-energy methods of calculation to be discussed in subsequent chapters.

CHAPTER 3 is devoted to the entrainment method. First, the proposals of Spalding's 'Unified Theory' are outlined. This is followed by a critical examination of the velocity-profile assumption. Then, theoretical and experimental information about the entrainment law is discussed and a recommendation for this law is made. Finally, a review is given of the advantages and disadvantages of the entrainment method.

CHAPTER 4 describes the writer's work on the kinetic-energy method. It opens with a comparison of the method with the entrainment procedure of the previous chapter. Then, the three auxiliary relations necessary to the explicit kinetic-energy method are discussed individually in detail. As in CHAPTER 3, new recommendations for the auxiliary relations are made, and these are compared where possible with previous recommendations.

In CHAPTER 5 the results are presented of calculations of the development of particular boundary layers carried out using the new calculation procedures. These results are compared with the calculations reported in Thompson's review paper. Finally, reasons are discussed for the discrepancies between calculation and experiment which occur in some circumstances.

In CHAPTER 6, the experimental investigation of the writer into boundary layers with augmented upstream turbulence intensity is presented. The experimental apparatus and the methods of measurement and data analysis are described. The results of the experiments are then discussed. This is followed by a re-examination of the empirical relations of the kinetic-energy calculation procedure, and by the application of this method in an attempt to predict the development of the somewhat unusual boundary layers described.

Finally, in CHAPTER 7, the achievements of CHAPTERS 3, 4, 5 and 6 are summarised and re-appraised. Suggestions are made for future theoretical and experimental work.

Several TABLES are included, after the list of REFERENCES and the nomenclature section. The first of these gives details of all the experimental data collected from the literature by the writer; and the others summarise recommendations which have been made for the various auxiliary relations. Also included are three APPENDICES, one of which is concerned with the analysis of the electrical signals obtained from a hot-wire anemometer, and in particular with a new procedure developed by the writer which retains its validity even for highly turbulent flows.

CHAPTER 2

MATHEMATICAL THEORY

2.1 Introductory remarks

In the present chapter, the equations are presented on which are based the calculation procedures to be discussed in CHAPTERS 3 and 4.

First, the time-averaged Navier-Stokes equations, which describe two-dimensional turbulent shear flow, are stated together with the restrictions and conditions particular to the present study.

This section is followed by an outline of the derivation of the integral equations. These are ordinary differential equations derived by formal integration of the partial differential equations of continuity and x-momentum after multiplication of the latter by weighting functions. There is no limit to the number of integral equations which may be so derived, although it is impracticable in an explicit calculation method to consider more than two or three such equations because of the difficulty of including in the auxiliary functions more than that number of arguments. Parametric-profile methods are better suited to the employment of a larger number of equations, although in many circumstances no more than two are necessary, since only one or two integral quan-

tities are needed to define quite closely the velocity profile (Thompson, 1964).

The choice of integral equations to be used is largely arbitrary, although it has become traditional (though not necessary) always to include the integral momentum-deficit equation. The reason is the obvious physical significance of this equation, and the fact that it contains one of the quantities of greatest interest - the wall shear stress. Indeed, this and the other two integral equations discussed in the present thesis alone share the distinction that they may be derived, in an alternative manner to formal mathematical manipulation of the partial differential equations, by consideration of the fluxes through a control volume of physically meaningful quantities: those of mass, momentum and mean kinetic energy.

The integral momentum-deficit equation, when combined with the integral mass-conservation equation, forms the basis of 'the entrainment method' discussed in CHAPTER 3. In 'the kinetic-energy method' of CHAPTER 4, the second equation is the integral mean kinetic-energy-deficit equation.

A fourth integral conservation equation presented is that for the turbulent kinetic energy; it is given primarily to illustrate a point of nomenclature.

The specific forms of the equations which are used here were suggested by Spalding.

2.2 Partial differential equations of motion and turbulence

The equations of motion to be considered are those governing the mean-steady, two-dimensional, laterally converging or diverging, turbulent flow of an incompressible fluid over an impermeable surface of negligible curvature. They may be written as:

mass-conservation, or continuity:

$$\frac{\partial(\omega\overline{u})}{\partial x} + \frac{\partial(\omega\overline{v})}{\partial y} = 0 \qquad (2.2\text{-}1),$$

x-momentum:

$$\overline{u}\frac{\partial\overline{u}}{\partial x} + \overline{v}\frac{\partial\overline{u}}{\partial y} = -\frac{1}{\rho}\frac{\partial\overline{p}}{\partial x} + \frac{1}{\rho}\frac{\partial\tau}{\partial y} - \frac{\partial\overline{u'^2}}{\partial x} \qquad (2.2\text{-}2),$$

y-momentum:

$$\overline{u}\frac{\partial\overline{v}}{\partial x} + \overline{v}\frac{\partial\overline{v}}{\partial y} = -\frac{1}{\rho}\frac{\partial\overline{p}}{\partial y} - \frac{\partial\overline{u'v'}}{\partial x} - \frac{\partial\overline{v'^2}}{\partial y} \qquad (2.2\text{-}3),$$

(the viscous terms have been omitted except in so far as they contribute to the total shear stress). u and v are the components of velocity in the co-ordinate directions x and y, x being measured along the wall, and y normal to, and outward from, it; p is the static pressure; and ρ and ν are the fluid density and molecular

kinematic viscosity, respectively. Overbars indicate temporal mean quantities, and primes fluctuating componets (i.e. $u = \overline{u} + u'$, etc.). τ here denotes the total (laminar-plus-turbulent) shear stress,

i.e. $$\frac{\tau}{\rho} = \nu \frac{\partial \overline{u}}{\partial y} - \overline{u'v'} \qquad (2.2\text{-}4),$$

although the viscous (Newtonian) shear stress is negligible compared with the turbulent (Reynolds) shear stress ($-\overline{u'v'}$), except in the immediate vicinity of the wall (viscous sub-layer) and, possibly, in the outermost regions of the boundary layer.

The quantity ω, appearing in the continuity equation (2.2-1), may be regarded as the width separating imaginary "streamplanes" which are normal to the surface. Thus $d\omega/dx$ measures the extent to which the mean flow converges or diverges (ω depends only upon x for two-dimensional flows). Other writers (e.g. Kehl, 1943 and Bradshaw and Ferriss, 1965) account for this effect by referring x to the virtual origin of the convergence, x_o,

i.e. $$\frac{1}{\omega}\frac{d\omega}{dx} = \frac{1}{x-x_o} \qquad (2.2\text{-}5).$$

Terms involving ω in the integral equations are included in the present section for two reasons. Firstly, as a reminder that converging/diverging flows come under

the heading of two-dimensional flows (although this appellation, so far as boundary layers are concerned, usually implies that ω is assumed constant). The second reason is the important one that the ω terms do not appear in the shape-factor equations given in section 2.3, so that it becomes apparent that the subsequent use of these equations neither involves the assumption that ω is constant nor requires the specification of $d\omega/dx$.

The boundary conditions to which (2.2-1), (2.2-2) and (2.2-3) are subject are as follows:

$y = 0$: $\overline{u} = \overline{v} = u' = v' = 0$; $\overline{p} = p_S$; $\tau = \tau_S = \mu(\partial\overline{u}/\partial y)_S$,

$y = y_G$: $\overline{u} = u_G$; $\overline{v} = v_G$; $\overline{p} = p_G$; $\tau = 0$.

It is usual to assume further that the mainstream turbulence intensities are negligibly small.

The subscript S denotes conditions at the surface, and G those in the mainstream. The symbol y_G denotes the (arbitrarily-specified) outer limit of the boundary layer - the 'boundary-layer thickness'.

Use of the mainstream boundary conditions permits the relationship between the mainstream velocity, u_G, and pressure, p_G, to be deduced from (2.2-2):

$$u_G \frac{du_G}{dx} = -\frac{1}{\rho}\frac{dp_G}{dx} \qquad (2.2\text{-}6),$$

i.e. the Bernoulli equation. Thus the x-momentum equa-

tion (2.2-2) may be written as

$$\bar{u}\frac{\partial\bar{u}}{\partial x} + \bar{v}\frac{\partial\bar{u}}{\partial y} = u_G\frac{du_G}{dx} + \frac{1}{\rho}\frac{\partial\tau}{\partial y} - \frac{1}{\rho}\frac{\partial}{\partial x}(\bar{p}-p_G) - \frac{\partial\overline{u'^2}}{\partial x} \quad (2.2\text{-}7).$$

If the 'boundary-layer approximation' is invoked, the last two terms on the right-hand side of (2.2-7) may be discarded as negligible. In certain situations, however, such as the important one of a turbulent boundary layer near separation, the validity of the approximation has been questioned by a number of writers (e.g. Newman, 1951; Ross, 1953; Trezek and Robertson, 1965; and Moses, 1964). The writer has followed the approach adopted by a number of these authors in attempts to include the effects of these additional terms in calculation procedures. It is assumed that the cross-flow static-pressure gradient is due to high turbulence intensity alone, so that the y-momentum equation (2.2-3) reduces to

$$0 = -\frac{1}{\rho}\frac{\partial\bar{p}}{\partial y} - \frac{\partial\overline{v'^2}}{\partial y} \quad (2.2\text{-}8),$$

which may be integrated to give

$$p_S - \bar{p} = \rho\overline{v'^2} \quad (2.2\text{-}9).$$

Then (2.2-7) may be written as

$$\bar{u}\frac{\partial\bar{u}}{\partial x} + \bar{v}\frac{\partial\bar{u}}{\partial y} = u_G\frac{du_G}{dx} + \frac{1}{\rho}\frac{\partial\tau}{\partial y} + \frac{\partial}{\partial x}(\overline{v'^2}-\overline{u'^2}) \quad (2.2\text{-}10).$$

The merit of this procedure is that it allows at least a

qualitative estimate to be made of the importance and direction of influence of the normal-pressure gradient.

However, it is observed experimentally (e.g. see Newman, 1951 and Schubauer and Klebanoff, 1951) that near separation the thickness of a boundary layer increases very rapidly, so that the magnitude of $\bar{v}$ is unlikely to be negligible compared with that of $\bar{u}$, and the boundary-layer approximation ceases to be valid. Neither is (2.2.10) then valid, and further progress requires either consideration of both the x- and y-momentum equations or, possibly, information to relate $(\bar{p} - p_G)$ and $\overline{u'^2}$ to the other quantities appearing in (2.2-7).

Finally, in this section, a fourth differential equation is introduced; it is that for the conservation of mean turbulent kinetic energy. This equation, which may be derived from the Navier-Stokes equations (see e.g. Hinze, 1959 and Rotta, 1962), may be written as

$$\bar{u}\frac{\partial \bar{k}}{\partial x} + \bar{v}\frac{\partial \bar{k}}{\partial y} = -\overline{u'v'}\frac{\partial \bar{u}}{\partial y} + (\overline{v'^2}-\overline{u'^2})\frac{\partial \bar{u}}{\partial x} - \frac{\partial}{\partial y}\left(\overline{kv'} + \overline{\frac{p'v'}{\rho}}\right) + \nu\frac{\partial^2}{\partial y^2}(\bar{k} + \overline{v'^2}) - \varepsilon \qquad (2.2\text{-}11),$$

wherein k is the turbulent kinetic energy,

i.e. $$k \equiv \tfrac{1}{2}(\overline{u'^2} + \overline{v'^2} + \overline{w'^2}) \qquad (2.2\text{-}12),$$

w' being the fluctuating velocity in a plane parallel with the surface and normal to the x-y plane. The terms on the left-hand side of (2.2-11) represent the advection (or convection) of $\overline{k}$ with the flow, and those on the other side of the equation, respectively, the production (by shear and normal stresses), turbulent diffusion, viscous diffusion and viscous dissipation (ε) of $\overline{k}$.

The present writer will not be concerned with the employment in a calculation method of the turbulent kinetic-energy equation, but merely with the implications of an integral equation which can be derived from it (see section 2.3). However, three new procedures for the numerical solution of the turbulent-boundary-layer equations, proposed by Glushko (1965), Bradshaw, Ferris and Atwell (1967) and Patankar and Spalding (1967), do consider this as a third equation to be solved simultaneously with the continuity and x-momentum equations.

2.3 Integral equations

The first integral equation to be derived is that known as the integral mass-conservation equation. It is obtained from (2.2-1) by direct integration in the y-direction, from the wall to the outer edge of the boundary layer; there results

$$\frac{1}{\omega}\frac{d}{dx}\left(\omega\int_0^{y_G}\overline{u}\,dy\right) = -v_G + u_G\frac{dy_G}{dx} \qquad (2.3\text{-}1).$$

The right-hand side of this equation represents the total rate of entrainment into the boundary layer of mass from the irrotational fluid of the mainstream. (2.3-1) may be written as

$$\frac{1}{\omega}\frac{d}{dx}\left(\omega\int_o^{y_G}\overline{u}\,dy\right) = \frac{-\dot{m}''_G}{\rho} \qquad (2.3\text{-}2),$$

where $-\dot{m}''_G$ is the entrainment rate per unit area, defined by

$$-\dot{m}''_G \equiv \rho\left(-v_G + u_G\frac{dy_G}{dx}\right) \qquad (2.3\text{-}3).$$

The integral mass-conservation equation, and the idea of entrainment, seem first to have been introduced into turbulent-boundary-layer theory by Head (1958).

The next equation to be considered is von Kármán's integral <u>momentum-deficit</u> equation. It is obtained by integrating the x-momentum equation (2.2-7) across the boundary layer, after eliminating the normal-velocity component $\overline{v}$ by use of the continuity equation (2.2-1). The final result is the equation

$$\frac{1}{\omega}\frac{d}{dx}\left[\omega\int_o^{y_G}\overline{u}(u_G-\overline{u})\,dy\right] + \frac{d}{dx}\int_o^{y_G}(\overline{v'^2} - \overline{u'^2})\,dy + \frac{du_G}{dx}\int_o^{y_G}(u_G-\overline{u})\,dy = \frac{\tau_S}{\rho} \qquad (2.3\text{-}4),$$

which will be referred to for brevity as the momentum equation.

The third integral equation is that for the mean-kinetic-energy deficit. It is obtained in a similar manner to the momentum equation (2.3-4) after multiplication of the x-momentum equation (2.2-7) by the weighting function $\bar{u}$. The resulting equation is

$$\frac{1}{\omega}\frac{d}{dx}\left[\omega\int_o^{y_G}\bar{u}\,\tfrac{1}{2}(u_G^2-\bar{u}^2)dy\right]+\int_o^{y_G}\bar{u}\,\frac{\partial}{\partial x}\,(\overline{v'^2}-\overline{u'^2})dy$$

$$=\int_o^{y_G}\frac{\tau}{\rho}\,\frac{\partial\bar{u}}{\partial y}\,dy \qquad (2.3\text{-}5),$$

which will be referred to for brevity as the kinetic-energy equation. This equation appears first to have been employed by Wieghardt (1945).

The final integral equation to be given here is one which can be deduced from the turbulent-kinetic-energy equation. The result in this case is

$$\frac{1}{\omega}\frac{d}{dx}\,(\omega\int_o^{y_G}\bar{u}\,\bar{k}\,dy)-\int_o^{y_G}(\overline{v'^2}-\overline{u'^2})\,\frac{\partial\bar{u}}{\partial x}\,dy$$

$$-\int_o^{y_G}-\overline{u'v'}\,\frac{\partial\bar{u}}{\partial y}\,dy+\int_o^{y_G}\varepsilon\,dy=0 \qquad (2.3\text{-}6).$$

The integral equations (2.3-2), (2.3-4), (2.3-5) and (2.3-6) will now be expressed in dimensionless form, in accordance with the practice of Spalding and others; the following definitions are used:

Variables: $z \equiv \bar{u}/u_G$ (2.3-7),

$\xi \equiv y/y_G$ (2.3-8),

$s \equiv \tau/(\rho u_G^2)$ (2.3-9).

Integrals: $I_n \equiv \int_o^1 z^n \, d\xi \quad (n=1,2,3)$ (2.3-10),

$\bar{s} \equiv \int_o^1 s \, (\partial z/\partial \xi) d\xi$ (2.3-11).

Reynolds numbers: $R_G \equiv u_G y_G/\nu$ (2.3-12),

$R_m \equiv I_1 R_G$ (2.3-13),

$R_1 \equiv (1-I_1)R_G$ (2.3-14),

$R_2 \equiv (I_1-I_2)R_G$ (2.3-15),

$R_3 \equiv (I_1-I_3)R_G$ (2.3-16),

$R_x \equiv \int_o^x (u_G/\nu)dx$ (2.3-17).

Shape factors: $H_1 \equiv R_m/R_2$ (2.3-18),

$H_{12} \equiv R_1/R_2$ (2.3-19),

$H_{32} \equiv R_3/R_2$ (2.3-20).

Drag coefficient: $s_S \equiv \tau_S/(\rho u_G^2)$ (2.3-21)

(a more commonly-used symbol for the local drag coefficient is $c_f/2$; s_S is used here to preserve consistency in the notation and to simplify the writing of many of

the equations).

Pressure-gradient parameter:

$$F_2 \equiv R_2 d(\ln u_G)/dR_x \qquad (2.3\text{-}22).$$

Dimensionless entrainment rate:

$$m_G \equiv \dot{m}''_G/(\rho u_G) \qquad (2.3\text{-}23).$$

It may be helpful to note that the Reynolds numbers R_1, R_2 and R_3 are those based upon δ_1, the displacement thickness, δ_2, the momentum-deficit thickness, and δ_3, the mean-kinetic-energy-deficit thickness, respectively. Also, H_1 is the shape factor introduced by Head (1958) $[= (y_G-\delta_1)/\delta_2]$, and H_{12} and H_{32} are the conventional shape factors usually defined by the ratios δ_1/δ_2 and δ_3/δ_2, respectively.

The above definitions, when inserted into the four integral equations, give:

Mass-conservation:

$$\frac{dR_m}{dR_x} + R_m \frac{d(\ln \omega)}{dR_x} = -m_G \qquad (2.3\text{-}24),$$

Momentum:

$$\frac{dR_2}{dR_x} + R_2 \frac{d(\ln \omega)}{dR_x} + (1+H_{12})F_2 + \frac{1}{u_G^2} \frac{d}{dx} \int_o^{y_G} \overline{(v'^2-u'^2)}\, dy = s_S \qquad (2.3\text{-}25),$$

Kinetic-energy:

$$\frac{dR_3}{dR_x} + R_3 \frac{d(\ln \omega)}{dR_x} + 2H_{32}F_2 + \frac{2}{u_G^2}\int_o^{y_G} \frac{\bar{u}}{u_G}\frac{\partial}{\partial x}\left(\overline{v'^2}-\overline{u'^2}\right)$$

$$= 2\bar{s} \qquad (2.3\text{-}26),$$

Turbulent-kinetic-energy:

$$\bar{s} = \frac{1}{u_G^3}\int_o^{y_G}\left[\nu\left(\frac{\partial \bar{u}}{\partial y}\right)^2 + \varepsilon\right]dy - \frac{1}{u_G^3}\int_o^{y_G}\left(\overline{v'^2}-\overline{u'^2}\right)\frac{\partial \bar{u}}{\partial x}\,dy$$

$$+ \frac{1}{\omega u_G^3}\frac{d}{dx}\left(\omega\int_o^{y_G}\bar{u}\,\bar{k}\,dy\right) \qquad (2.3\text{-}27).$$

The quantity $\bar{s}$ is called here 'the shear-work integral', because its integrand represents the amount of shear work done per unit volume. Some writers, however, (e.g. Truckenbrodt, 1951 and Spalding, 1965a) have chosen to call it 'the dissipation integral' because, as (2.3-27) shows, $\bar{s}$ is approximately equal to the integral of total viscous dissipation (the first term on the right-hand side of (2.3-27)) in many situations. The condition to be satisfied is that the last term in the equation, which represents the net advection of turbulent kinetic energy with the flow, is negligible (in laminar flow it is zero). Thus $\bar{s}$ is likely to be little different from the dissipation integral in flows

for which the history is unimportant (no transport of turbulent kinetic energy from upstream).

It may be noted, in passing, that the overbar in $\bar{s}$ may be regarded as denoting that this quantity represents the total (dimensionless) shear stress, s, averaged over the boundary layer with respect to mean velocity.

Two important equations which can be obtained from the first three integral equations, (2.3-24) to (2.3-26), are the shape-factor equations. The mass-conservation and momentum equations may be combined to yield

$$R_2 \frac{dH_1}{dR_x} = -m_G - H_1 s_S + (H_{12}+1)H_1 F_2 - \frac{H_1}{u_G^2} \frac{d}{dx} \int_o^{y_G} \overline{(u'^2-v'^2)}\,dy \qquad (2.3\text{-}28),$$

and the momentum and kinetic-energy equations to give

$$R_2 \frac{dH_{32}}{dR_x} = 2\bar{s} - H_{32} s_S + (H_{12}-1)H_{32} F_2 - \frac{H_{32}}{u_G^2} \frac{d}{dx} \int_o^{y_G} \overline{(u'^2-v'^2)}\,dy + \frac{2}{u_G^2} \int_o^{y_G} \frac{\bar{u}}{u_G} \frac{\partial}{\partial x} \overline{(u'^2-v'^2)}\,dy \qquad (2.3\text{-}29).$$

A significant feature of these shape-factor equations is that they show that convergence (or divergence) has no direct influence on shape-factor growth. Such influence as there is comes about indirectly through the Reynolds number R_2, which must either be specified or

calculated simultaneously from the momentum equation.

2.4 Methods for the solution of the integral equations

The calculation methods which are considered in the present study rest upon two important assumptions. The first was mentioned in section 2.1; it is that two integral properties provide an adequate description of the mean velocity profile. The other is perhaps more important, and has certainly been the subject of controversy in recent years. It is that the distribution of shear stress through a turbulent boundary layer is determined uniquely by the local velocity profile. This implies the existence of local equilibrium between the dissipation and production of turbulent kinetic energy, and the negligibility of the advection and diffusion of this energy. Thus the quantity $\bar{s}$ is assumed to be a function of R_2 and H_{32} alone. The papers of Bradshaw and Ferriss (1965), Felsch (1965) and Goldberg (1966) have been concerned specifically with the validity of such an assumption; and all three conclude that the shear stress must depend not only upon the local velocity profile, but also upon the upstream history of the flow.

The assumption is an over-simplification, therefore. Its adoption is <u>not</u> necessary because of an

inability to handle mathematically the complications of equations incorporating 'history effects', but rather that there is little information about these additional influences; and this may be taken as an indication that in most circumstances they are relatively unimportant.

The calculation methods considered in CHAPTERS 3 and 4 are as follows:

(1) CHAPTER 3: The entrainment method, which requires the simultaneous integration of the mass-conservation and momentum equations. An explicit approach would require that H_{12}, s_S and $-m_G$ be related, by explicit formulae, to R_m, R_2 and, perhaps also, F_2. This is the procedure adopted by Head (1958). An alternative, adopted by Spalding (1964a) and followed here, is to relate H_{12} and s_S to R_m and R_2 through formulae derived from a parametric velocity profile (formulae which are therefore unlikely to be explicit). Still required, however, is an equation to connect $-m_G$ with known quantities. The establishment of a suitable entrainment law, and examination of an appropriate velocity profile, are the primary purposes of CHAPTER 3.

(2) CHAPTER 4: The kinetic-energy method. Here again both explicit and parametric-profile methods are possible. In the latter case H_{32} and s_S would be re-

lated to R_2 and R_3 through profile-derived formulae; and the shear-work integral would also have to be related to these quantities. The procedure of Patankar and Spalding (1965), for example, is to evaluate $\bar{s}$ using a velocity profile and assuming a (known) universal distribution to exist for the Prandtl mixing length. In the present thesis, the alternative procedure is followed, explicit formulae being given for the relationships between H_{12}, s_S and $\bar{s}$ and R_2 and R_3. It is with these relationships that CHAPTER 4 is concerned.

CHAPTER 3

THE ENTRAINMENT METHOD

3.1 Introduction

Spalding's Unified Theory

The original form of the 'Unified Theory' (Spalding, 1964a) contained a general theoretical framework for the prediction of friction, heat transfer and mass transfer in turbulent boundary layers. The procedure for calculating the development of the hydrodynamic boundary layer required integration of the mass-conservation and momentum equations; the auxiliary functions employed were:

(1) A two-parameter velocity profile having two components; one accounting for the effects of momentum transfer to the wall, and the other for interactions with the mainstream and departures from the wall profile.

(2) A formula which relates to the profile and flow parameters the rate of mass-entrainment into the boundary layer from the mainstream.

Neither of the two elements of the Unified Theory was new; two-part velocity profiles were first suggested by Rotta (1950) and popularised by Coles (1956); and the idea of entrainment was introduced into boundary-layer theory by Head (1958). The novelty of the

Unified Theory was two-fold; first it combined the appealing physical simplicity of the entrainment hypothesis with the flexibility of two-parameter velocity profiles, and secondly it considered, apparently for the first time within a single theoretical framework, boundary layers both with and without velocity maxima.

Aims of CHAPTER 3

The purposes of the present chapter are:

(1) To examine the velocity-profile assumption made by Spalding, in respect of its ability to represent measured profiles, and also of its implications so far as the drag law and shape-factor relation ($H_{12} \sim H_1$) are concerned.

(2) To collect together and examine the available experimental data for information about entrainment rates and relevant velocity-profile parameters; to compare with this information the entrainment laws of both Head (1958) and Spalding (1964a, b, 1965a); and to recommend, if necessary and possible, an improved entrainment law.

In CHAPTER 5, the results will be presented and discussed of calculations of boundary-layer development performed using the best available entrainment law together with Spalding's velocity profile.

3.2 The mean-velocity-profile assumption

Introductory remarks

Two main possibilities are open when choosing the form of mean-velocity profile to be adopted, the choice depending largely upon the number of parameters to be employed. If great flexibility is required, many parameters must be used. It is then difficult, and usually unnecessary, to specify the velocity profile in such a way that the parameters and components of the profile have physical significance. Thus the polynomial profile might be chosen:

$$z = \sum a_i \xi^{b_i} \qquad (3.2\text{-}1),$$

wherein it is likely that the a_i will be the parameters and dependent variables of the integration, and b_i chosen integers or fractions.

When only a few parameters are employed, it is provident to select profiles guided by, and so implicitly incorporating some knowledge of, the general experimental behaviour. The profile model chosen here, that recommended by Spalding (1964a), is an analytical representation of the form found by Coles (1956) adequately to systematise a large amount of experimental data.

Coles wrote

$$u^+ = f\{y^+\} + \frac{2\Pi}{\kappa} g\{\xi\} \qquad (3.2\text{-}2),$$

where $$u^+ \equiv u/(\tau_S/\rho)^{\frac{1}{2}} \qquad (3.2\text{-}3),$$

and $$y^+ \equiv y(\tau_S/\rho)^{\frac{1}{2}}/\nu \qquad (3.2\text{-}4).$$

Π is a profile parameter and κ a universal constant (von Kármán's). The functions $f\{y^+\}$ and $g\{\xi\}$ are supposed universal, the former being known as the 'law of the wall' and the latter, after Coles, as the 'law of the wake'.

The 'log-plus-cos' velocity profile

In the fully-turbulent region near an impermeable wall, the velocity profile for an incompressible boundary layer may be shown by dimensional analysis to take the universal form (the law of the wall)

$$u^+ = f\{y^+\} = \frac{1}{\kappa} \ln (Ey^+) \qquad (3.2\text{-}5),$$

or $$u^+ = \frac{1}{\kappa} \ln (y^+) + C \qquad (3.2\text{-}6),$$

where κ, E and C are universal constants for smooth walls (E and C otherwise vary with wall roughness). A fairly wide range of values has been proposed for these, there being uncertainty because κ is a measure of the slope of the velocity profile in a region where

the profile itself is difficult to measure with high accuracy because of large velocity gradients and high turbulence intensity. In addition, it is necessary to know the value of τ_S before a measured profile can be cast in terms of u^+ and y^+.

The values adopted here are those recommended by Spalding (1964b),

$$\kappa = 0.41, \quad E = 7.7, \quad (C = 4.98).$$

Coles (1956) determined the form of the wake law by examination of many experimental velocity profiles. His recommendation was expressed by means of a table of numbers; these define a curve nearly symmetrically sigmoidal, and well-represented by the formula adopted by Spalding (1964a), and also by Hinze (1959), McDonald and Stoddart (1965) and Cornish (1960),

i.e. $$g(\xi) = [1 - \cos(\pi\xi)]/2 \qquad (3.2\text{-}7).$$

If the above expressions for the laws of the wall and wake are substituted into (3.2-2), the formula for the complete mean profile may be written

$$u^+ = \frac{1}{\kappa} \ln(Ey^+) + \frac{\Pi}{\kappa} [1-\cos(\pi\xi)] \qquad (3.2\text{-}8),$$

or, in the alternative form of Spalding,

$$z = z_E[1+\ln(\xi)/\ell'] + (1-z_E)[1-\cos(\pi\xi)]/2 \qquad (3.2\text{-}9),$$

where the profile parameters z_E and ℓ' are defined by

$$\ell' \equiv \ln(ER_G s_S^{\frac{1}{2}}) \qquad (3.2\text{-}10),$$

and

$$z_E \equiv s_S^{\frac{1}{2}} \ell'/\varkappa \qquad (3.2\text{-}11).$$

The unrealistic behaviour of the profile recommendation for very small distances from the wall is of little importance so far as the evaluation of integral quantities is concerned.

The profile parameter z_E is a very important quantity in the present work; it may be interpreted as the ratio of the law-of-the-wall velocity at the outer edge of the boundary layer to the mainstream velocity, u_G. Thus $(1-z_E)$ is a measure of the relative magnitude of the wake component. z_E also serves the useful purpose of distinguishing between conventional boundary layers and those for which the velocity profiles exhibit a maximum. In the former case, the value of z_E may vary from zero (for a separating flow) to about unity (for an accelerated boundary layer); the zero-pressure-gradient flat-plate boundary layer has a value of z_E close to 0.9. Boundary layers for which the dimensionless mean velocity, z, may somewhere exceed unity are characterised by $z_E > 1$.

The formulation of Spalding is preferable here to that of Coles because the profile is adequately characterised by only one of the two parameters: ℓ' varies slowly with x for any particular boundary, rarely falling outside the range 8 to 12. Values of both z_E and ℓ', determined from the experimental data of many authors, are listed in TABLE 1.

The velocity profile given by (3.2-9) is referred to as the 'log-plus-cos profile'.

Some further experimental justification for separating a turbulent boundary layer into two regions, one dominated by the wall and the other behaving as a free-shear zone, has come recently from Uzkan and Reynolds (1967). These authors considered separately the two influences of the presence of a wall on turbulent shear flow; its direct effect of inhibiting the turbulent fluctuations in its vicinity, and its indirect action of assisting in the maintenance of mean velocity gradients which generate new turbulence. In the usual Reynolds-number range, their experiments suggested that the inhibiting effects would be confined to the inner 5 or 10% of the boundary layer.

Direct comparison of the log-plus-cos profile with experiment

It is not possible to state what velocity-profile

expression gives the closest agreement with experiment, for there is no limit to the shapes of profiles which may actually be generated. However, in order to show how well reality can be described by (3.2-9), a few diagrams are presented here. In figure 3.1 are shown six sets of experimental profiles, compared with the best-fitting curves according to (3.2-9). The criterion for the best fit was that the values of z_E and ℓ' selected should be those which minimize* the square deviation, R, defined by

$$R \equiv \sum_i \left[z\{y_i\} - z_i \right]^2 ,$$

where z_i is the measured velocity ratio at y_i, and $z\{y_i\}$ the value given by (3.2-9) at the same point.

In figure 3.1(a) are shown four profiles measured by Smith and Walker (1959) in boundary layers developing along a smooth flat plate under zero pressure gradient. There is some evidence of a small, but apparently systematic, deviation from the measured profile in the region of $\xi = 0.3$. However, values of the shape factor H_{12} calculated from the fitted profiles differ by only about 4% from the reported experimental ones.

Similar remarks to the above can be made about the comparison with the profiles of Bradshaw and Ferriss (1965), run 2, shown in figure 3.1(b). These

*The computer program to perform the fitting procedure was written and developed by W.B. Nicoll.

data were obtained for a boundary layer in zero pressure gradient recovering from the effects of an adverse pressure gradient upstream; this explains the relatively large wake component at station 1 where $z_E \approx 0.67$. Although the plotted curves give the impression that the profile expression fits these data less well than those of Smith and Walker, in this case the greatest difference between the reported experimental and computed values of H_{12} is less than 3%.

The profiles of Schubauer and Klebanoff (1951), shown in figure 3.1(c), were obtained for a boundary layer subjected to an adverse pressure gradient which eventually caused the layer to separate from the wall, a little beyond station 16. Here again the profiles appear to be well-fitted by the theoretical expression, although for the two downstream profiles shown the fitted profile is clearly inadequate near the wall. The profile at station 16 has a large wake component, the value of z_E in this case being about 0.29, and in this instance the shape factor calculated from the fitted profile is about 2.38, compared with the value 2.30 computed from the experimental profile.

The final set of profiles, for $z_E < 1$, was reported by Stratford (1959) for a boundary layer having continuously-zero wall shear. In this case the least-squares-

fitting procedure was not used, since z_E should be identically equal to zero, so that the profile expression reduces to the pure wake form

$$z = [1 - \cos(\pi\xi)]/2.$$

This expression, it may be observed from figure 3.1(d), is not a good representation of Stratford's data. For $z_E = 0$, the assumed profile expression gives the unique result $H_{12} = 4$, whereas Stratford's experiments give values ranging from about 1.8 to 2.6. Indeed, the log-plus-cos profile completely fails to accord with the theoretical zero-wall-shear profile, for which the velocity near the wall is proportional to the square root of the distance from the wall.

The measurements shown in figures 3.1(e) and 3.1(f) were obtained by Nicoll (1965) for boundary-layer flows exhibiting velocity maxima; these are characterised by $z_E > 1$. For all these data, the assumed profile deviates from the measurements in the same way, being too low near the edge of the layer and too high in the middle. Also, the magnitude of the theoretical maximum is roughly correct, but the point at which it is predicted to occur is always further from the wall than measured. The deviations are seen to increase in magnitude as z_E increases, that is as the wake (or, more

appropriately here, jet) component becomes increasingly dominant. In fact, Jayatillaka (1966) showed that for the limiting case of a wall jet in stagnant surroundings ($z_E = \infty$), the linear wake function proposed by Rotta (1950) gives a better fit to the data than does the log-plus-cos formula. But this is not the case in general, as the data on the accuracy of the drag laws implicit in velocity-profile expressions, given in TABLE 5, shows.

Coles (1956) also found that it was not possible to find satisfactory values of the profile parameters to make his recommendation fit a profile, measured by Klebanoff and Diehl (1952), downstream of a point of boundary-layer re-attachment. There were also shown to be definite indications, in experiments performed by Wieghardt (1944), of changes in both the shape and the amplitude of the wake component in flow at constant pressure when the level of free-stream turbulence was varied. In later work, Coles (1962) showed that an external turbulence level of about 2% would halve the normal magnitude of the wake component, and one of 4.5% would reduce it to zero. However, no further work, either qualitative or quantitative, appears to have been done on this subject.

Finally, it should be noted that difficulties are encountered in attempts to apply a two-parameter calcu-

lation procedure to the flow just downstream of an injection slot (parallel with the wall). The reason is that the velocity profiles there always exhibit a dent, as a result of the existence of boundary layers on either side of the lip of the slot, and cannot be fitted by a profile such as that given here. The consequence of this is that predictions of such flows are generally forced to begin ten or more slot-heights downstream of the slot.

Drag law implicit in the log-plus-cos profile

Implicit in any velocity profile of the wall-plus-wake type, (3.2-2), is a drag law. That this is so may be seen from Spalding's form of such profiles, of which the log-plus-cos is an example. Thus, if values are given for the profile parameters z_E and ℓ', (3.2-11) gives s_S from

$$s_S = (\kappa z_E/\ell')^2 \qquad (3.2\text{-}12).$$

This may be related to a thickness Reynolds number and a shape factor, for example R_2 and H_{12}, via the expressions given in CHAPTER 2,

$$R_2 = (I_1-I_2)R_G \qquad (2.3\text{-}15),$$

and

$$H_{12} = (1-I_1)/(I_1-I_2) \qquad (2.3\text{-}19),$$

and also $$R_G = \exp(\ell')/(Es_S^{\frac{1}{2}})$$

(from the definition of ℓ', 3.2-10). The integral quantities I_1 and I_2 may be evaluated using the profile expression (the formulae deducible for these from the log-plus-cos profile are given in APPENDIX 1).

Probably the best known drag law for $z_E < 1$ is the empirical one proposed by Ludwieg and Tillmann (1949),

$$s_S = 0.123 \cdot 10^{-0.678\ H_{12}}\ R_2^{-0.268} \qquad (3.2\text{-}13).$$

(It should be noted, however, that the Ludwieg-Tillmann formula is inapplicable to flows where $z_E > 1$, because then $R_2 < 0$. This point is discussed more extensively in section 3 of CHAPTER 4.) It is with this formula that the drag law implicit in the log-plus-cos profile is compared in figure 3.2. The trends of both drag laws are similar, in respect of the variation with both Reynolds number and shape factor. The values of s_S obtained for the log-plus-cos drag law are generally lower than those given by the Ludwieg-Tillmann formula, except for the behaviour for the lower values of H_{12} at very high Reynolds numbers, the deviations increasing with H_{12}. This is in accordance with reality, since the Ludwieg-Tillmann law predicts that s_S will not fall to zero until H_{12} becomes infinite, whereas the implicit law gives $H_{12} = 4$ for the separation condition, a value

much closer to that of about 2.7 indicated by experiment.

The log-plus-cos drag law is compared directly with experimental data for both $z_E < 1$ and $z_E > 1$ in figure 3.3. The agreement is evidently fairly satisfactory over the whole of the very wide range of values of s_S examined: the rms deviation from all the data (including those for $z_E = \infty$) is only 14%, which compares well with the lowest value of 11% so far achieved by any drag law, and also with the value of 19% obtained for the Ludwieg-Tillmann drag law (in its range of application). Comparisons with other drag laws, both implicit and explicit, are made in TABLE 5; and a discussion of drag laws in general is given in section 3 of CHAPTER 4.

Shape-factor relationship, $H_{12} \simeq H_1$

The entrainment method, it will be remembered, requires the integration of the momentum equation (2.3-25) and the shape-factor equation (2.3-28). It is therefore necessary to be able to relate the shape factor H_{12} to the dependent variables of these equations, R_2 and H_1. In the explicit procedure of Head (1958) this relationship was empirical, being a fit to the data of Newman (1951) and Schubauer and Klebanoff (1951). In the present method it is, like the drag law, implicit in the profile assumption. Curves representing the

relationship (for $z_E < 1$) are shown in figure 3.4 where they are compared with Head's recommendation and with experimental data collected by the writer.

Head's neglect of the Reynolds-number influence on the $H_1 \sim H_{12}$ relation is seen to be fairly well supported by the implications of the log-plus-cos profile, and the agreement with Head's recommendation is evidently satisfactory. The experimental data, however, are very widely scattered, with H_1 generally greater for any given value of H_{12} than is indicated by the theoretical curves. Undoubtedly much of the scatter may be attributed to uncertainties in the experimental values of y_G (selected by 'eye' from the measured velocity profiles). The direction of the discrepancy is a little surprising, since it seems more likely that y_G would be underestimated than overestimated, although the values of H_1 $[= (y_G-\delta_1)/\delta_2]$ are indicating the opposite tendency.

In view of the uncertainties in the data, and the agreement with Head's proposal, which can be regarded as an independent interpretation of the data, it seems reasonable to accept the implications of the log-plus-cos profile as an acceptable representation of the relationship between H_{12} and H_1.

Concluding remarks about the log-plus-cos velocity profile

(1) Spalding's log-plus-cos velocity-profile expression has been shown to be an adequate representation of measured mean-velocity profiles for a wide range of conditions, although deviations become increasingly significant when z_E is either very large or small.

(2) The drag law implicit in the profile expression is an appreciable improvement over the widely-used (for $z_E < 1$) Ludwieg-Tillmann formula, both in respect of accuracy of prediction, particularly at high values of the shape factor H_{12}, and range of applicability.

(3) The relationship implied by the profile between the shape factors H_1 and H_{12}, and the Reynolds number R_2, is in good agreement with Head's proposal and the experimental data for $z_E < 1$, although the latter show a very marked degree of scatter.

3.3 The entrainment law

The hypotheses of Head and Spalding

The entrainment hypotheses of both Head (1958) and Spalding (1964a) are similar in concept. Head suggested that the rate at which the irrotational fluid outside a boundary layer is entrained into it ($-\dot{m}''_G$) is dependent only upon the boundary-layer thickness, the velo-

city outside the boundary layer, u_G, and the distribution of velocity in the outer regions of the layer. The length-scale $(y_G-\delta_1)$ was chosen as the measure of boundary-layer thickness*, and the shape-factor H_1 to characterise the shape of the velocity profile. Dimensional analysis then led to the functional form

$$-m_G \equiv -\dot{m}''_G/(\rho u_G) = f\{H_1\} \qquad (3.3\text{-}1).$$

The dependence of $-m_G$ upon H_1 was obtained by Head from an analysis of a limited amount of experimental data - those of Newman (1951) and Schubauer and Klebanoff (1951). Difficulty was experience by Head in selecting the best-fitting curve due to the wide spread exhibited by the data.

Each of Spalding's several proposals (1964a, b, 1965a) for an entrainment law assumes the same functional dependence:

$$-m_G \equiv -\dot{m}''_G/(\rho u_G) = f\{z_E\} \qquad (3.3\text{-}2).$$

That is, the entrainment rate, $-\dot{m}''_G$, is proportional to the mainstream mass flux, ρu_G, and otherwise dependent only upon the velocity difference across the wake component of the velocity profile. Indeed, Spalding (1965a) suggested that the entrainment rate might be proportional to this velocity difference,

---

*Strictly speaking, Head chose $y_{.995}$ rather than y_G, $y_{.995}$ being the value of y for which z = 0.995. The differences between the two quantities are unimportant.

i.e. $$-m_G = \text{constant}. \left|1-z_E\right| \qquad (3.3\text{-}3),$$

which is clearly plausible in the light of knowledge about free turbulent flows. The implication of (3.3-3) that $-m_G$ falls to zero when z_E approaches unity is certainly in accord with reality, for this is the case of a boundary layer in which the mean velocity profile is logarithmic over the whole boundary layer. This condition is closely satisfied by the accelerated similar boundary layer which has constant thickness Reynolds numbers (R_G, R_2, etc.) and is thus non-entraining.
It will be shown below that the general run of experimental data also lends support to an entrainment law with the simple linear form of (3.3-3).

Determination of entrainment rates from experimental data

The immediately obvious way to determine entrainment rates is from measured velocity profiles. The information required is the variation of R_m with R_x, since, from (2.3-24):

$$-m_G = dR_m/dR_x^*.$$

To deduce R_m from experimental profiles it is necessary first to know the boundary-layer thickness, y_G; and it is evidently desirable to use a consistent procedure for determining this somewhat arbitrarily-defined quantity.

*The ω-term has not been included in this equation. It was in any case nominally zero in all the experiments for which data were examined.

One such procedure is to fit to the measured points an assumed profile, such as the log-plus-cos formula, (3.2-9), which will yield not only y_G, but also R_m, z_E and any other profile quantities of interest. Alternatively, integral properties of experimental profiles, such as R_2 and H_{12}, can be matched with those given by the adopted profile, and the profile parameters determined in this way.

These two methods of data analysis are complementary and, if the profile assumption is a good representation of measured profiles (as the log-plus-cos profile has been shown to be), any differences which arise in the final results should be small. However, it is important to note at this stage that two essentially inaccurate processes are involved in the determination of $-m_G$: the specification of y_G, and the differentiation (performed graphically) of quantities derived from experimental data.

Analysis of the data for $z_E < 1$

All the information for values of z_E less than unity has been extracted by the writer from published experimental data. The measured velocity profiles were often available only in the form of small-scale graphs, and their retrieval difficult, inaccurate and time-

consuming. For these reasons, the profile parameters here were calculated from the published values of R_2 and H_{12}, these being the most commonly-reported properties of measured profiles.

Analysis of the data for $z_E \geq 1$*

In this case two different procedures were adopted. Full details of the data of Nicoll (1965) were available; it was therefore possible to apply the least-squares method (see p.38) to fit the log-plus-cos formula to his measured profiles. The available information about the other data for $z_E > 1$ was less detailed, so the profile parameters were determined from the most frequently-reported experimental quantities in these cases: z_m and $y_{\frac{1}{2}}$, where z_m is the ratio to u_G of the maximum velocity in the boundary layer and $y_{\frac{1}{2}}$ is the value of y (further from the wall) at which $z = (z_m+1)/2$. $y_{\frac{1}{2}}$ is a quantity well-defined experimentally, in contrast with y_m (where $z = z_m$) which is not.

Comparison of Head's recommendation with experimental data for $z_E \leq 1$

Head (1958) gave his recommendation for the entrainment law in graphical form; it is shown in figure 3.5

*The data for $z_E > 1$ were analysed by W.B. Nicoll.

plotted in the way in which it was presented, i.e. $-m_G$ vs H_1. Also plotted are points and curves deduced from experimental data. Head's curve clearly has the correct trend, except for the behaviour where H_1 becomes large ($z_E \to 1$), when the data and theoretical knowledge show $-m_G \to 0$, whereas Head's curve levels off at $-m_G \approx 0.01$.

Comparison of Spalding's recommendations with experimental data

Spalding's first proposal (1964a) was

$$z_E < 1 \qquad -m_G = 0.1023\ (1-z_E)(1+\tfrac{1}{3}z_E)$$

$$z_E > 1 \qquad -m_G = 0.09\ (z_E-1)(1+\tfrac{1}{3}z_E)/(1+z_E) \qquad (3.3.4).$$

The basic structure of these formulae (which are seen to include $1 - z_E$ as a factor) was arrived at by consideration of information relating to free mixing layers. The constants were determined, somewhat indirectly, from analyses of the equilibrium zero pressure-gradient boundary layer, and of the spread and velocity-decay information available for boundary layers with velocity maxima.

In an annotated version of the paper last cited, Spalding (1964b) noted that equations (3.3-4) considerably over-estimate entrainment rates, and that these relations are unjustifiably elaborate. A direct study of experimental data revealed that greater support is given to the

simpler expressions

$$z_E < 1 \qquad -m_G = 0.06\ (1-z_E)$$
$$z_E > 1 \qquad -m_G = 0.03\ (z_E-1) \qquad (3.3\text{-}5).$$

These relations, of course, are in the linear form of (3.3-3).

Spalding's final recommendation (1965a) was based upon further examination of experimental data, which were found to be better fitted by

$$z_E < 1 \qquad -m_G = 0.06 - 0.05z_E$$
$$z_E > 1 \qquad -m_G = 0.03z_E - 0.02 \qquad (3.3\text{-}6).$$

Curves representing (3.3-4) to (3.3-6), for $z_E < 1$, have been plotted in figure 3.6, in the form of $-m_G$ vs z_E; points and curves deduced from experimental data are also shown. The data confirm that Spalding's first proposal does indeed considerably overestimate $-m_G$ over most of the range of z_E values. The second and third recommendations are in far better accord with the data, although the former relation is in fact better than the latter so far as the bulk of these are concerned.

For $z_E > 1$, the data* again show that Spalding's first proposal overestimates $-m_G$, although the deviations

---

*Details of these are not available to the writer. They were shown, however, by W.B. Nicoll in the paper by Escudier and Nicoll (1966a).

are not great. The differences between the second and third recommendations are small, and both are in good agreement with the data, although these show wide scatter, particularly for $z_E > 10$.

The present writer's recommendation for the $-m_G(z_E)$ function

The data shown in figure 3.6, although showing considerable scatter, certainly lend support to the suggestion made earlier that $-m_G$ should be proportional to $1-z_E$, the constant of proportionality being about 0.075 (25% higher than that for Spalding's second proposal). Thus the writer's recommendation, which is used in CHAPTER 5 in the prediction of a number of particular boundary layers, is

$$z_E < 1 \qquad \boxed{-m_G = 0.075(1-z_E)} \qquad (3.3\text{-}7).$$

For $z_E > 1$, Spalding's final proposal is as good a fit to the data as any, and may thus be recommended,

i.e. $$\boxed{-m_G = 0.03z_E - 0.02} \qquad (3.3\text{-}8).$$

Supporting evidence for the recommended entrainment law

(1) The procedure outlined above for the determination of entrainment rates is not the only one which may be used.

Another has been demonstrated by Spalding (1965b) in the form of an interesting theorem. The result of this is the identity

$$-\dot{m}''_G \equiv -\left(\frac{\partial\tau/\partial y}{\partial u/\partial y}\right)_G \qquad (3.3\text{-}9),$$

or

$$-m_G = -(\partial s/\partial z)_G \qquad (3.3\text{-}10).$$

That is, $-m_G$ is equal to minus the slope of the s~z curve at the outer edge of a shear layer. This result is the more interesting when it is realised that the area <u>enclosed by this curve</u> and the co-ordinate axes is simply the quantity $\bar{s}$, the counterpart of $-m_G$ so far as the kinetic-energy method of calculation is concerned. Another noteworthy feature of (3.3-10) is that it removes the arbitrariness until now attached to the quantity $-m_G$, although the difficulties involved in measuring accurately the shear stress present other problems.

The data of several authors have been analysed using (3.3-10); the results for $z_E < 1$ are shown in figure 3.7, and for $z_E > 1$ in figure 3.8, where they are plotted in the form $-m_G$ vs z_E for comparison with the recommendation made above, (3.3-8). Again there is a great deal of scatter in both graphs, although the more recent, and probably more reliable, data are in good agreement with (3.3-8). The earlier data give $-m_G$ values which are

generally too low; and, although these may well be in error, in the case of Schubauer and Klebanoff (1951) the error suggested by Coles (1956) is such as to raise rather than to lower the values found for $-m_G$.

Typical plots of s vs z are shown in figure 4.8, where they are given to illustrate the method of determining $\bar{s}$.

(2) The arbitrariness in $-m_G$ is also removed to some extent when consideration is paid to those flows where the shape of the velocity profile changes slowly with x; that is, to similar or equilibrium boundary layers. And, it may be noted that, if the assumption that $-m_G$ depends only upon the local velocity profile were correct, then an entrainment law derived for equilibrium flows would be generally valid.

The shape-factor (H_1) equation (2.3-38), with the cross-flow pressure-gradient terms omitted, may be written

$$R_2 dH_1/dR_x = -m_G - H_1 s_S + (1+H_{12})H_1 F_2$$

≈ 0, since the profile shape is changing but slowly. This equation may be rearranged to give $-m_G$ as

$$\boxed{-m_G = -m_{G,eq} = H_1 s_S [1+\beta(1+1/H_{12})]} \qquad (3.3\text{-}21),$$

where β is the pressure-gradient parameter defined by Clauser (1954) as a constant for a given equilibrium flow:

$$\beta \equiv (\delta_1/\tau_S)dp_G/dx = -H_{12}F_2/s_S \qquad (3.3\text{-}22).$$

Also, for equilibrium boundary layers, it may be shown that β is a unique function of the shape factor, G, of the velocity-defect profile, $(u_G-\overline{u})/u_\tau$. G is related to H_{12} and s_S by

$$G \equiv (1-1/H_{12})s_S^{-\frac{1}{2}} \qquad (3.3\text{-}23).$$

An empirical formula for the G~β relationship (for $z_E<1$), given by Nash (1965), is

$$G = 6.1\,(\beta+1.81)^{\frac{1}{2}} - 1.7 \qquad (3.3\text{-}24).$$

(3.3-21), (3.3-23) and (3.3-24), together with the log-plus-cos profile formula, have been used to determine the curves in figure 3.9 of $-m_G$ plotted vs z_E, with ℓ' as parameter. These clearly show the same trends as the data for equilibrium flows, which are also plotted, and confirm that ℓ' has a relatively small influence on the $-m_G$ relation. In the vicinity of $z_E = 0.8$, however, the equilibrium curves predict more than twice as much entrainment as (3.3-7), and are in better agreement with the data in that region. This perhaps indicates why Spalding (1965a) was led to propose the relation (for $z_E < 1$)

$$-m_G = 0.06 - 0.05z_E$$

which gives values for $-m_G$ more in keeping with the flat-plate boundary-layer data.

Arguments of the entrainment function in addition to z_E

The hypothesis of Spalding (1964a) that $-m_G$ depends upon z_E alone has been adopted in the present work also. It is certain, however, that other quantities will also influence $-m_G$, although their effects are likely to be of secondary importance. Examples of quantities which might be expected to enter the $-m_G$-function are ℓ', which would contribute essentially a Reynolds-number influence, and dz_E/dR_x, which would account for the upstream history of the flow.

However, $-m_G$ is a particularly difficult quantity to determine with accuracy from experimental data, so that a plot of $-m_G$ vs z_E, for example, shows a considerable degree of scatter. Consequently, it is impossible to determine from the data the dependence of $-m_G$ on any quantity which might exert an influence secondary to that of z_E. It is possible, however, that calculations of boundary-layer development carried out using the recommended entrainment law, may indicate the need to include other arguments in the entrainment function.

Concluding remarks about the entrainment law

(1) z_E is a preferable quantity to H_1 as the argument of the entrainment function, because a linear relationship between $-m_G$ and z_E is both theoretically plausible and also fairly well supported by the data analysed.

(2) Entrainment rates determined in three different ways are in reasonably good agreement with each other, although there is a very high degree of scatter in the data, mainly due to the arbitrariness associated with $-m_G$.

(3) The best recommendation that can at present be made for the entrainment law is

$$z_E < 1 \qquad -m_G = 0.075(1-z_E)$$

$$z_E > 1 \qquad -m_G = 0.03z_E - 0.02.$$

(4) Because the rate of entrainment is experimentally ill-defined, the dependence of $-m_G$ on quantities other than z_E, say, is impossible to determine.

(5) The adequacy of the recommended entrainment relation remains to be judged by its ability to allow accurate prediction of boundary-layer development; this will be examined in CHAPTER 5.

3.4 Advantages and disadvantages of the entrainment method

It is appropriate in this concluding section of CHAPTER 3 to list the advantages and disadvantages of the entrainment method as a prediction procedure.

The entrainment method possesses four innate advantages over other methods of calculation: (1) Any integral equation derived from the continuity equation (2.2-1), an example being the mass-conservation equation (2.3-34) used in the entrainment method, is formally exact for two-dimensional flow. Those based upon the momentum equation introduce the boundary-layer approximations and the associated assumption that u' and v' are negligible when compared with $\overline{u}$. (2) The phenomenon of entrainment is associated primarily with events occurring at the outer edge of a shear layer, and so mass transfer and surface roughness may be expected to have little direct influence on entrainment. (3) Only knowledge about the mean-velocity profile is essential to the determination of entrainment rates. Thus there is a very large pool from which to draw information about entrainment. (4) There is the simplicity of the idea of entrainment itself; a great aid to guessing about a suitable form for the entrainment function.

In addition to the above, there is the very real advantage that it has been shown by Thompson (1964) that, of previously-existing explicit calculation procedures, Head's entrainment method is the only one to give uniformly-acceptable predictions of boundary-layer development. It remains to be seen, however, whether the present implicit entrainment procedure gives results as good as Head's.

In spite of the very definite advantages listed above, the entrainment method suffers from several serious drawbacks: (1) The arbitrariness of the bounday-layer thickness, y_G, which influences not only the entrainment rate itself, but also the shape factor H_1. Even if sufficient information were available to allow $-m_G$ to be determined from shear-stress measurements, say, using (3.3-10), the uncertainties in the shape-factor relation would remain. The data for this at present available have been found to be subject to an almost intolerable degree of scatter, attributable essentially to the arbitrariness of y_G. (2) There is the inevitable desire to extend the entrainment function to situations in which density variations are important. There is little experimental information about the effects of such variations, and apparently no theoretical clue even as to the direction of such influences. (3) There are flow

situations where the concept of entrainment is totally inapplicable. These are duct flows, such as occur in pipes and channels, where the boundary layers on opposite walls have joined up; yet the wake component of the velocity profile may well be large, and will certainly be varying until fully-developed conditions are reached.

CHAPTER 4

THE KINETIC - ENERGY METHOD

4.1 Introduction

Comparison with the entrainment method

The previous chapter closed with a list of the advantages and disadvantages of the entrainment method. The disadvantages indicated are serious impediments to progress, and one at least (inapplicability to certain confined flows) is an irremediable defect. It is as well, therefore, to be sure from the outset that the kinetic-energy method is free from these and other innate drawbacks.

So far as this method is concerned, it may be said that: (1) the arbitrariness of the position of the outer boundary of the flow does not arise at all. The counterparts here of $-m_G$ and H_1 are the shear-work integral, $\bar{s}$, and H_{32}, respectively; and the integrands of the various integrals associated with these quantities vanish outside the boundary layer. (2) There is no reason to suppose that the $\bar{s}$-function for confined flows is fundamentally different from that for external flows, for $\bar{s}$ is as much dependent on events near the wall as those far removed from it. (3) Spalding (1965a) has proposed a reasonable hypothesis concerning the way in

which density variations influence the $\bar{s}$-function. Thus the kinetic-energy method is apparently free from the inherent disadvantages of the entrainment method.

There are, however, some disadvantages of this method which contrast directly with the advantages of the entrainment method: (1) Because $\bar{s}$ is dependent upon events throughout the boundary layer, the $\bar{s}$-function is likely to have a more complex form than the $-m_G$ function. Associated with this is the expectation that mass transfer and wall roughness will exert appreciable influence on the $\bar{s}$-function.* (2) Shear-stress data from which to obtain information about $\bar{s}$ are scarce and of doubtful accuracy. In principle, of course, $\bar{s}$ could be determined from the kinetic-energy equation (2.3-26); but this involves differentiation of experimentally-determined quantities, and is of unreliable accuracy. (3) The reliability of predictions of boundary-layer development using previously-existing kinetic-energy methods was shown by Thompson (1964) to be far from acceptable, even though probably the most widely known and used calculation procedure is a kinetic-energy method - that of Truckenbrodt (1952).

---

*Information about roughness effects may be found in the thesis of Jayatillaka (1966) and those of mass transfer in that of Baker (1967).

This unreliability is somewhat surprising, particularly when compared with the success of Head's (1958) entrainment method which contains far more inherent arbitrariness and uncertainty. The most likely explanation is that the disadvantages of the kinetic-energy method itself led to basically unsound early proposals being made for the $\bar{s}$-function (the unacceptable features of these was demonstrated by Spalding (1965a); they are discussed below). Nevertheless, none of the drawbacks associated with the kinetic-energy method are irremediable; and the likelihood is that ultimately it will be preferable to use it rather than the entrainment method. The main requirement is the provision of an acceptable $\bar{s}$-function, applicable in as wide a range of situations as the $-m_G$ function of CHAPTER 3.

Spalding's review of the kinetic-energy method

The paper by Spalding (1965a) throws light onto the reasons for the poor predictions of previously-existing kinetic-energy methods. This pointed out that probably the greatest single deficiency of the $\bar{s}$-functions proposed by Rotta (1950) and Rubert and Persh (1951), for example, is their implication that $\bar{s}$ falls to zero for a separating boundary layer. That this is in conflict with reality is shown both by experiment and by simple

theoretical considerations (see section 4.4, below). Truckenbrodt's (1952) proposal, too, is found to be an unreliable description of the behaviour of $\bar{s}$, since it indicates a dependence only upon R_2, and even this is such that $\bar{s}$ falls in an adverse pressure gradient.

The other main drawback of these early $\bar{s}$-functions is their limited range of applicability: none is valid when mass transfer is present, when there are density variations or when the velocity profile exhibits a maximum. Much the same criticism may be made of the more recent proposals of Meuller, Korst and Chow (1964), Felsh (1965), Walz (1965) and Goldberg (1966). Support for the point regarding inapplicability when $R_2 < 0$ is given by the list of relations given in TABLE 6, which in the majority of cases contain a term like $R_2^{-1/6}$ - the inheritance from Ludwieg and Tillmann (1949) mentioned in CHAPTER 1 (p.8).

Thus Spalding's paper demonstrated the lack of an acceptable $\bar{s}$-function. The information given by Spalding about $\bar{s}$, and guidance as to a suitable functional form, provides the basis for the recommendation given in section 4.4, below.

Other auxiliary relations required

The equations upon which the kinetic-energy method

is based are those describing the variation of the momentum-thickness Reynolds number, R_2,(2.3-25), and the shape-factor H_{32}, (2.3-29). Thus, in addition to a relationship connecting $\bar{s}$ with these quantities, formulae are required to relate to them the local drag coefficient, s_s, and the shape-factor H_{12}.

Every procedure so far proposed for the calculation of turbulent boundary-layer development makes use of an equation for the conservation of momentum. A knowledge of the way in which skin friction (drag) is influenced by the thickness, velocity profile and other properties of the layer is thus essential. The consequence is that many previous writers have made recommendations for a drag law, although all explicit drag laws have been limited in application either to flows without velocity maxima or to those with velocity maxima but with zero mainstream velocity. Also, as the relations lised in TABLE 3 show, their formulation generally precludes extension to the whole range of boundary-layer flows - again due to the way in which the Reynolds-number influence was introduced.

Generally-valid drag laws are implicit in all formulae for the velocity profile which have the wall-plus-wake form discussed in CHAPTER 3, though their proposers usually were concerned only with conventional boundary layers ($R_2 > 0$). But such drag laws lack computational

convenience if R_2 and H_{32} are the dependent variables in use. Indeed Spalding (1965c) indicated that in some regions the determination of unequivocal values of the profile parameters is not possible. Furthermore, the wide validity of the profile-based drag laws is not always matched by their accuracy in fitting the experimental data. Thus there is a need for a generally-valid, accurate, explicit drag law with R_2 and H_{32} as variables.

Similar remarks to the above may be made about the relationship between H_{12}, H_{32} and R_2. The limitations of previous recommendations are the same, as are the drawbacks of profile-based relations. Again, therefore, a new explicit relationship is called for.

Aims of CHAPTER 4

In the light of the preceding paragraphs, the purposes of the present chapter may be stated as being:

(1) To examine the available theoretical and experimental information about $\bar{s}$ and relevant velocity-profile parameters; and to recommend an explicit $\bar{s}$-function applicable to separating boundary layers at one extreme, and wall jets in still surroundings at the other.

(2) To recommend an explicit drag law covering the same range of flow situations as the $\bar{s}$-function.

(3) To recommend an explicit shape-factor relationship, again as widely-valid as the $\bar{s}$-function.

In CHAPTER 5, the results will be presented and discussed of calculations of boundary-layer development performed using the recommended $\bar{s}$-function, drag law and shape-factor relation.

4.2 The shape-factor relation

Insensitivity to Reynolds-number variation

Curves representing the variation of H_{12} with H_{32} implied by the log-plus-cos velocity profile are shown in figure 4.1. The parameter on the curves is ℓ' rather than R_2, because the latter must change sign near H_{12} equal to unity, whereas the values of ℓ' fall within very narrow limits (values are listed in TABLE 1). Also plotted are points representing data* taken from the experiments, for positive values of R_2, of Bradshaw and Ferriss (1965), Clauser (1954), Fage and Falkner (1930), Herring and Norbury (1967), Klebanoff (1955), Moses (1964), Newman (1951), Schubauer and Klebanoff (1951) and Schubauer and Spangenberg (1960). The data for negative values of R_2 are those of Erian and Eskinazi (1964), Kruka and Eskinazi (1964) and Nicoll (1965). All the data are listed in

---

*In every case values of H_{12}, H_{32} and R_2 were computed by the writer from the reported velocity profiles using the same integration procedure - Simpson's rule generalised for integration with unevenly-spaced pivotal points.

TABLE 1.

Three observations may be made about figure 4.1: (1) The theoretical curves shown fit most of the experimental data extremely well. The sole exception is the set of data reported by Erian and Eskinazi, which lies considerably below the general run of data. The discrepancy here is almost certainly attributable to there being but scanty information in this case about the velocity distributions between the wall and the velocity maximum. (2) The curves for ℓ' equal to 8 and 12 are virtually indistinguisable, except in the region of $H_{12}=1$. These two observations indicate that the inclusion of a Reynolds-number influence is superfluous to the shape-factor relation. (3) There are gaps in the theoretical curves in the vicinity of $H_{12} = 1$. Although there are no experimental data available in this region, these gaps must be a true reflection of reality, since it is here that all the boundary-layer <u>deficit</u> thicknesses (δ_1, δ_2, δ_3 etc.) change sign and so are generally close to zero. Since they do not all pass through zero at the same point*,

---

*The proof of this (suggested by S.V. Patankar) is as follows. The definitions of δ_1, δ_2 and δ_3 show that

$$\delta_1-\delta_2 \equiv \int_o^{y_G} (1-\bar{u}/u_G)^2 dy \quad \text{and} \quad 2\delta_2-\delta_3 \equiv \int_o^{y_G} (\bar{u}/u_G)(1-\bar{u}/u_G)^2 dy.$$

The integrands of both integrals are always positive (in the absence of negative velocities); so δ_1 is positive and δ_3 negative when δ_2 equals zero.

infinite and zero values of the shape factors occur, resulting in gaps in the $H_{12} \sim H_{32}$ curves.

The other (dashed) curve in figure 4.1 also represents the implications of a velocity profile; it is discussed below (p.77).

The new recommendation for the shape-factor relation

As was stated above, both the theoretical curves and the experimental data shown in figure 4.1 clearly support the proposal that there exists a unique relationship between the shape factors H_{12} and H_{32} (a contrast may be drawn with the scant support for a unique relationship between H_{12} and H_1, the shape factor of the entrainment method - see section 3.2).

It is found that the following empirical relations fit the data as well as any

$$\boxed{H_{32} = 1.431 - 0.0971/H_{12} + 0.775/H_{12}^2} \quad (4.2\text{-}1),$$

$(10^3 < R_2 < 8\times10^4, \quad 1.25 < H_{12} < 2.8)$

and

$$\boxed{H_{32} = 0.82 + 1.10/H_{12}} \quad (4.2\text{-}2).$$

$(4\times10^3 < -R_2 < 6\times10^5, \quad 0.06 < H_{12} < 0.85)$

The former equation fits the available data with an rms deviation of only 1.03%.

Also of interest is the limiting case of the wall jet in still surroundings, for which H_{12} falls to zero and H_{32} becomes infinite; but the product $H_{12} \cdot H_{32}$ remains finite and non-zero, as may be seen from the definitions of these quantities. For this situation, (4.1-2) implies

$$H_{12} \cdot H_{32} = 1.10,$$

a value which has been substantiated by the experiments reported by Jayatillaka (1966) and Baker (1967) for the radial wall jet, the former with wall roughness and the latter with mass transfer.

The discussion earlier indicated why gaps in the H_{12}~H_{32} data are unavoidable near $H_{12} = 1$. However, a continuous relationship is convenient in a calculation procedure, so the following interpolation formula is recommended

$$\boxed{H_{32} = 2.67 - 0.66\, H_{12}} \qquad (4.2\text{-}3),$$

$$(0.85 < H_{12} < 1.25)$$

Little error will be engendered by its use because the shape factors which appear in the integral equations are always multiplied by R_2, which is small in the region in question.

The complete recommendation for the shape-factor relation, represented by (4.2-1) to (4.2-3), is shown in figure 4.2 together with the data on which it is based. Inset to a larger scale are the data and recommendation for $R_2 > 0$. Although the data in this region show more scatter than do those for $R_2 < 0$, no evidence of a systematic trend with Reynolds number was discernible.

Previous recommendations for the shape-factor relation

The recommendations of a number of authors for an explicit shape-factor relation for $R_2 > 0$ are listed in TABLE 2. So far as is known to the writer, no previous explicit recommendations have been made for $R_2 < 0$.

Complementary to the explicit formulae are the relationships implicit in velocity-profile recommendations. The only writers, other than Spalding (1965a), to have made specific use of a two-parameter profile to generate shape-factor relations are Rotta (1951) and Truckenbrodt (1952), who made use of the wall-plus-wake profile with a linear wake function. Although these authors did not recognise the wider implications of their recommendations, so far as flows with velocity maxima are concerned, the log-plus-linear profile was found by Jayatillaka (1966) and Baker (1967) to be a better representation than the log-plus-cos formula of their radial wall-jet data.

The more recent explicit relations fit the data as well as the new recommendation, except where H_{12} falls below about 1.5, when H_{12} is generally underestimated by them. The profile-based relations fit the data quite well for both $R_2 > 0$ and $R_2 < 0$, except in the regions near the gap and where H_{12} exceeds about 2.

Conclusions

The recommended shape-factor relation appears to possess overall superiority to previous recommendations in respect of: range of applicability, accuracy of prediction and computational convenience.

Much of this work on the shape-factor relation may be found in the paper of Nicoll and Escudier (1966).

4.3 The drag law

Introduction

The influence on the local drag coefficient, s_S, for zero-pressure-gradient boundary layers, of the momentum-thickness Reynolds number, R_2, was recognised long ago by Prandtl (1921), Squire and Young (1938), Falkner (1943) and others. The experimental investigation of Ludwieg and Tillmann (1949), on boundary layers developing in streams with adverse and favourable pressure gradients, showed that, at a given value of R_2, the value

of s_S could vary widely. Ludwieg and Tillmann found that the variation could be correlated with the shape factor H_{12}; and, as has already been noted, they recommended the formula

$$s_S = 0.123 \times 10^{-0.678H_{12}} R_2^{-0.268} \qquad (4.3\text{-}1).$$

Although many later authors have proposed other relations, (4.3-1) is still widely used for the calculation of s_S for turbulent boundary layers. The reason, perhaps, is that the majority of authors have retained the Ludwieg-Tillmann form, but their modifications have by no means always improved the accuracy. These points are illustrated by TABLES 3 and 4.

The Ludwieg-Tillmann recommendation is a fairly satisfactory correlation formula in the limited range of conditions studied by its originators, but is seriously deficient as a drag law for general use. One obvious shortcoming, to which allusion has already been made, is its inapplicability to flows where R_2 is negative. Another is the implication that s_S does not fall to zero until H_{12} is infinite, whereas it is well know that the shape factor for boundary-layer separation is around 2.7.

This section of the present chapter is based upon the papers by Escudier and Nicoll (1965) and Escudier, Nicoll and Spalding (1966); in the latter paper a new

formula, free from the shortcomings of (4.3-1), was proposed for the calculation of drag. Its form was chosen so that it could be applied to the whole range of turbulent boundary layers. Empirical constants were chosen systematically, so as to reduce to a minimum the discrepancies between the formula and data taken from the experiments of many authors. Like all previous proposals, however, it was assumed that s_S depends at most upon two locally-measurable properties.

Choice of arguments of the new drag law

The arguments of the s_S-function are taken to be R_2 and H_{32}, rather than the more usual combination of R_2 and H_{12}. The reasons are: (1) The drag law can then be used immediately in the kinetic-energy calculation procedure. (2) H_{32} is less sensitive to density variations across the boundary layer than is H_{12}*. In any case, the results reported in section 4.2 show that a

---

*That this is so may be seen from the way in which the density enters the fuller definitions of H_{12} and H_{32} appropriate to the non-uniform-density case:

$$H_{12} \equiv \int_o^{y_G} \left(1 - \frac{\rho\bar{u}}{\rho_G u_G}\right) dy \Bigg/ \int_o^{y_G} \frac{\rho\bar{u}}{\rho_G u_G}\left(1 - \frac{\bar{u}}{u_G}\right) dy$$

and $$H_{32} \equiv \int_o^{y_G} \frac{\rho\bar{u}}{\rho_G u_G}\left(1 - \frac{\bar{u}^2}{u_G^2}\right) dy \Bigg/ \int_o^{y_G} \frac{\rho\bar{u}}{\rho_G u_G}\left(1 - \frac{\bar{u}}{u_G}\right) dy.$$

close relation exists between H_{32} and H_{12} for uniform-density boundary layers; so it is easy to replace H_{32} by H_{12} if this is desired.

Establishment of a suitable form for the drag law

(consideration of wall-plus-wake velocity profiles)

An appropriate way of introducing H_{32} into the drag law, and of accommodating both positive and negative values of R_2, is indicated by considering the drag law implied by the general wall-plus-wake velocity-profile relation. In the previous chapter, it was shown that this drag law could be written

$$s_S = (\varkappa z_E/\ell')^2 \qquad (4.3\text{-}2).$$

Consideration is given to the much simplified form of the velocity profile, which results when the first term of the profile expression (3.2-9) is given at all y its value at the edge of the boundary layer, and the wake function $g(\xi)$ is taken as linear. Then the profile relation becomes

$$z = \zeta + (1-\zeta)\xi \qquad (4.3\text{-}3),$$

wherein z_E has been replaced by ζ to emphasize the fact that (4.3-3) is but a crude representation of real profiles. It is, nevertheless, the simplest formula for the velocity profile which imitates the qualitative fea-

tures of real profiles, including both jet-like and reversed flows, if ζ is suitably chosen.

The dashed curve shown in figure 4.1 represents the variation of H_{12} with H_{32} implied by (4.3-3),

i.e. $$H_{32} = 1.125/H_{12} + 0.75 + 0.125H_{12} \qquad (4.3\text{-}4).$$

Though this equation does not fit the data quite as well as either the shape-factor relation recommended in the previous section or that implicit in the log-plus-cos profile, it does predict the main trends remarkably well. Also its form is very close to that of (4.2-2) (particularly when $H_{12} \to 0$).

From (4.3-3) it may be deduced that

$$H_{32} = \frac{3(1+\zeta)^2}{2(1+2\zeta)} \qquad (4.3\text{-}5),$$

and $$R_2/R_G = (1-\zeta)(1+2\zeta)/6 \qquad (4.3\text{-}6).$$

Since H_{32} experimentally is a well-defined quantity, it is convenient to regard (4.3-5) as <u>defining</u> the new parameter ζ; (4.3-5) may be solved to give ζ explicitly in terms of H_{32}, thus

$$\boxed{\zeta = \tfrac{2}{3}H_{32} - 1 + \left[\tfrac{2}{3}H_{32}\left(\tfrac{2}{3}H_{32} - 1\right)\right]^{\frac{1}{2}}} \qquad (4.3\text{-}7)$$

(only the positive square root being physically of in-

terest for forward flows, where H_{32} exceeds 1.5). In a similar way, (4.3-6) may be taken as the definition of the boundary-layer-thickness Reynolds number, R_G, an otherwise somewhat arbitrary quantity.

From the above it is evident that s_S will be given approximately by

$$s_S = (\varkappa\zeta/\ell')^2 \qquad (4.3\text{-}8)$$

with

$$\ell' = \ln\left[\frac{6ER_2\, s_S^{\frac{1}{2}}}{(1-\zeta)(1+2\zeta)}\right] \qquad (4.3\text{-}9).$$

This, of course, is very nearly in the required form: $s_S = f\{R_2, H_{32}\}$.

Generalisation of the drag formula

Since (4.3-3) does not describe real velocity profiles very precisely, (4.3-8) cannot be expected to give accurate predictions of drag unless modifications are made, such as by the addition of extra terms and the adjustment of constants.

Before examining what modifications are necessary, it is observed that the presence of s_S within the argument of the logarithm ℓ' does not accord with the requirement of explicitness. Since s_S varies in practice from zero to infinity, its influence on ℓ' can hardly be ignored. Instead it is removed to a less influential place by substitution for s_S from the right-hand side

of (4.3-8); there results

$$s_S = \left[\frac{\varkappa\zeta}{\ln\left\{\frac{6ER_2\varkappa\zeta}{(1-\zeta)(1+2\zeta)\ell'}\right\}} \right]^2 \qquad (4.3\text{-}10).$$

It is now recalled that for all the turbulent boundary layers for which data have been collected, the values of ℓ' lie between 8 and 12. It therefore seems permissible to replace the whole of the argument of the logarithm by the expression $CR_2\zeta/[(1-\zeta)(1+2\zeta]$, C being a constant to be determined empirically.

To allow further flexibility in fitting the available data, the numerator of (4.3-10) will be replaced by a function of ζ. Thus the form of the drag law adopted is

$$\boxed{s_S = \frac{f\{\zeta\}}{\left[\ln\left\{\frac{CR_2\zeta}{(1-\zeta)(1+2\zeta)}\right\}\right]^2}} \qquad (4.3\text{-}11),$$

where the constant C and the function $f\{\zeta\}$ are to be determined by fitting to experimental data. The symbol ℓ will be used to denote the modified form of the logarithmic function appearing in the denominator of (4.3-11).

Limiting form of the drag law for wall jets

For the wall jet in still surroundings, u_G is zero and so s_S, ζ etc. are infinite. However, integral pro-

perties which remain finite for u_G equal to zero may be introduced as follows

$$\eta_i \equiv \int_o^{y_G/y_m} \left(\frac{u}{u_m}\right)^i d\left(\frac{y}{y_m}\right) \qquad (i = 1,2,3) \qquad (4.3\text{-}12),$$

where y_m is the position of the maximum velocity, u_m. Then for this limiting case (4.3-11) transforms to

$$\sigma_S = \frac{\frac{16}{9}\left(\frac{\eta_3}{\eta_2}\right)^2 \lim_{\zeta\to\infty}\left[\frac{f(\zeta)}{\zeta^2}\right]}{\left[\ln\left(\frac{3C}{8}\frac{\eta_2^2}{\eta_3}R_{max}\right)\right]^2} \qquad (4.3\text{-}13),$$

where $$\sigma_S \equiv \tau_S/(\rho u_m^2) \qquad (4.3\text{-}14)$$

and $$R_{max} \equiv u_m y_m/\nu \qquad (4.3\text{-}15).$$

Most experimental data for wall jets are expressed in the literature as $\sigma_S(R_{max})$; the data of Myers, Eustis and Schauer (1961) and Bradshaw and Gee (1962) are listed in TABLE 1.

Examination of the velocity profiles of Sigalla (1958) and Myers et al. indicates that the values of the η's are approximately constant; they have the values*

$$\eta_2 = 4.91 \qquad \text{and} \qquad \eta_3 = 4.02.$$

---

*These values were obtained by W.B. Nicoll.

Concluding remarks about the form of the drag law

The following remarks are made to establish necessary conditions if the adoption of (4.3-11) as the form of the drag law is not to conflict with established knowledge: (1) When ζ becomes very large, as in wall jets, (4.3-13) shows that the argument of the logarithm ℓ remains finite. (2) Another feature at large ζ, which again may be seen from (4.3-13), is that $f(\zeta)$ must increase in proportion to ζ^2. (3) At the other extreme, when ζ becomes small, s_S also becomes small. If the value of ζ for zero shear stress is taken as zero (as would be the case if (4.3-10) were exact), then (4.3-5) shows that the zero-drag value of H_{32} is 1.5. This is close to that found in practice - the shape-factor relation (4.2-1) shows the corresponding value of H_{12} to be 2.71. (4) In the intermediate region, where R_2 and R_3 pass through zero, it is noted that for the argument of ℓ to remain finite and positive, it is necessary again to violate the rule given in section 4.1 by making R_2 and $1-\zeta$ change sign together. (4.3-5) shows that H_{32} must then equal 2, and so $R_2 = R_3 = 0$. It will be shown in the following section that this also imposes restrictions on the form of the $\bar{s}$-function, if this is to be compatible with the drag law.

The experimental data examined

The data, and their sources, which are used in establishing constants in the drag law are listed in TABLE 1.* Some important features of the data should be noted: (1) In few cases were direct measurements of drag available: the bulk of the data were obtained by the writer using the method of Clauser (1954), with the values $\kappa = 0.41$ and $E = 7.7$ as the log-law constants. The resultant values of s_s are generally consistent both with each other and also with values obtained, for similar flow conditions, by more direct measurement. (2) Many of the more direct measurements themselves rely upon the existence of a universal distribution of velocity near the wall. (3) The data display considerable scatter; the measurements of individual workers often show irregular variations in the streamwise direction of from 5 to 10%. This can only be attributed to experimental uncertainty.

Determination of the constant C

The logarithmic term ℓ of the drag-law equation (4.3-11) was obtained as an approximation to the term ℓ' which appears in the profile-based drag formula (4.3-2) (see also 3.2-10). The value of C which gives

*Most of the data for $R_2 < 0$ were collected by W.B.Nicoll.

maximum accuracy to this approximation is found to be 3.389. Two observations may be made: (1) The inaccuracy in ℓ' due to uncertainties in R_G are small, because $\partial\ell'/\ell' = (1/\ell')\partial R_G/R_G$, and of course the value of ℓ' is usually close to 10. (2) Although the agreement between the two logarithmic quantities is very good, there are indications of a systematic tendency for ℓ to exceed ℓ' by about 2% when $\ell' \approx 11$, and to fall short by about the same amount when $\ell' \approx 9$. The deviations are small, however, compared with the scatter in the drag data themselves, so no further adjustments to ℓ have been made.

Determination of the function $f\{\zeta\}$

The drag law which has finally been adopted can be arranged as

$$s_S \left[\frac{\ln\{CR_2\zeta/[(1-\zeta)(1+2\zeta)]\}}{\zeta}\right]^2 = g\{\zeta^{-1}\} \quad (4.3\text{-}16)$$

where $g\{\zeta^{-1}\}$ now replaces $f\{\zeta\}$ as the function to be determined. ζ^{-1} has been chosen as the argument of $g\{\ \}$ because this allows all the data, including those for wall jets, to be presented compactly (there are no data for ζ precisely equal to zero).

The limiting form of (4.3-16), when ζ becomes infinite, can be written

$$\frac{9}{16}\,\sigma_S\left[\frac{\eta_2}{\eta_3}\ln\left(\frac{3C}{8}\,\frac{\eta_2}{\eta_3}^{2}\,R_{max}\right]^{2}\right. = g(0) \qquad (4.3\text{-}17).$$

Since C, η_2 and η_3 are now known, the left-hand sides of both (4.3-16) and (4.3-17) can be evaluated for each experimental condition. The values are plotted against ζ^{-1} in figure 4.3.

Over most of the range of ζ^{-1}, the data are adequately represented by a quadratic in ζ^{-1}. However, the ordinates for ζ^{-1} equal to zero have a mean which is appreciably higher than that for small, but non-zero, ζ^{-1}. This requires that the g-function must possess much greater curvature in this region than is possible with a simple quadratic. A suitable form for $f(\zeta^{-1})$, consistent with both these observations, is

$$g = C_o + C_1\zeta^{-1} + C_2\zeta^{-2} + C_3/(1+C_4\zeta^{-1}) \qquad (4.3\text{-}18).$$

The values of the constants C_i, which reduce to a minimum the mean-square deviation between s_S calculated from (4.3-11) and experimental values, are found to be

$C_o = 0.243$, $C_1 = 0.0376$, $C_2 = 0.00106$, $C_3 = 0.0914$ and $C_4 = 65$.

The final result

The recommended drag law is

$$s_S = \frac{0.243\zeta^2 + 0.0376\zeta - 0.00106 + \frac{0.0914\zeta^2}{1+65/\zeta}}{\left[\ln\left\{\frac{3.389R_2\zeta}{(1-\zeta)(1+2\zeta)}\right\}\right]^2} \qquad (4.3\text{-}19)$$

where $\zeta \equiv \frac{2}{3}H_{32} - 1 + \left[\frac{2}{3}H_{32}\left(\frac{2}{3}H_{32} - 1\right)\right]^{\frac{1}{2}}$ (4.3-7).

For the limiting case of the wall jet, (4.3-19) reduces to

$$\sigma_S = 0.398/[\ln(7.62R_{max})]^2 \qquad (4.3\text{-}20).$$

The implications of (4.3-19), for s_S as a function of the shape factors H_{12} and H_{32}, are shown graphically in figure 4.4. The dependence on H_{12} was determined with the aid of the H_{12}~H_{32} relation given by (4.2-1) to (4.2-3). The parameters on the curves are R_2 and $R_2/(1-\zeta)$. The former is both conventional and satisfactory for flows without velocity maxima; it is, however, less convenient for the range of flows considered here, where the values encountered in practice range from about 10^6 down to minus infinity. The parameter $R_2/(1-\zeta)$ is more satisfactory; it takes on values in the relatively restricted range 10^3 to 10^5 (approximately).

Comparison with experiment

One measure of the capacity of an empirical relation to correlate experimental data is the rms deviation, R, between the predicted and experimental values. The deviations for the recommended drag law are

$8 \times 10^4 > R_2 > 7 \times 10^3$ $1.9 > H_{32} > 1.5$ $2.9 > H_{12} > 1.2$	153 data points	R = 11.0%
$2 \times 10^6 > -R_2 > 4 \times 10^3$ $12.5 > H_{32} > 2.3$ $0.8 > H_{12} > 0.09$	44 data points	R = 12.9%
$-R_2 = \infty$	44 data points	R = 8.0%
Overall	241 data points	R = 10.9%.

Probably the irreducible experimental scatter has an rms deviation little less than 10%.

The range of finite s_s values encompassed by the data is shown in figure 4.5, in which the drag predicted from R_2 and H_{32} is plotted against experimental drag.

Boundary-layer separation

For the extreme case of a separating boundary layer, for which s_s is by definition zero, the present recommendation implies

$$\zeta = 0.024, \quad H_{32} = 1.501 \quad \text{and} \quad H_{12} = 2.707.$$

These values of H_{32} and H_{12} are consistent with those observed in practice.

The wall jet in still surroundings

The comparison of prediction with experiment for the limiting case of the wall jet is shown in figure 4.6; the ordinate is σ_S [$\equiv \tau_S/(\rho u_m^2)$] and the abscissa R_{max} ($\equiv u_m y_m/\nu$). Both the limiting form of the present drag-law recommendation (4.3-20) and previous proposals are shown. The former agrees well with the experimental data.

Comparison with previous recommendations

Previously-recommended drag laws may be classified as either explicit or implicit. For those in the first category, which include the present recommendation, s_S is expressed explicitly in terms of experimentally well-defined properties of the velocity profile, such as R_2 and H_{12} or H_{32}. The explicit drag laws examined are summarised in TABLE 3. The implicit drag laws considered here were all derived from a velocity-profile assumption, some being modified to obtain more satisfactory agreement with experiment.

With the exception of that of Nash (1965), all the implicit laws can be expressed as

$$G = G\{\Pi\} \qquad (4.3\text{-}21)$$

where G is the shape factor of the velocity-defect profile introduced in CHAPTER 3,

$$G = (1-1/H_{12})s_S^{-\frac{1}{2}} ,$$

and Π is Coles' wake parameter, also introduced in CHAPTER 3. Nash's drag law can be expressed as a relation between G and K, where the latter is defined as

$$K \equiv (s_S^{-\frac{1}{2}}/\varkappa)\ln(ER_2H_{12}) \qquad (4.3\text{-}22).$$

The implicit drag laws are summarised in TABLE 4.

The rms deviations between the new drag law and experimental data are compared in TABLE 5 with those of previous recommendations. Values of s_S were computed from the recommended formulae as nearly as possible in the way proposed by their originators - usually from R_2 and H_{12}. Values of H_{32} are unavailable for the data of Ludwieg and Tillmann (1949) and Moses (1964); because they are needed as inputs to the present law and that of Walz (1965), the necessary values were computed using (4.2-1) from the reported values of H_{12}.

Two observations may be made: (1) For each of the three types of flow ($R_2 > 0$, $R_2 < 0$ and $R_2 = -\infty$), the present recommendation correlates the experimental data with the lowest rms deviation. (2) For $R_2 > 0$ and $R_2 = -\infty$, the new law represents a substantial improve-

ment over previous explicit recommendations.

Conclusions

The drag law represented by (4.3-18) appears to be superior to previously-recommended formulae in respect of: accuracy of prediction and range of applicability, and also, in many cases, convenience of computation.

However, its limitations must be remembered. These include: (1) Many of the data which the formula has been adjusted to fit were deduced using Clauser's method from measured velocity profiles, a procedure which may introduce systematic errors. (2) The data in any case are limited in number, accuracy and range of conditions. (3) The formula is limited to uniform-property boundary layers.

4.4 The shear-work-integral relation

Introduction

It was mentioned in section 4.1 that Spalding's (1965a) review of the kinetic-energy method revealed that previous proposals for the shear-work-integral, $\bar{s}$, relation are inadequate for two main reasons: (1) Their implication that $\bar{s}$ falls to zero for a separating boundary layer. (2) Their inapplicability to boundary layers with velocity maxima. Spalding showed further

that an $\bar{s}$-relation free from these drawbacks could be deduced from the simple linear velocity profile (used in the previous section in establishing a form for the drag law) and a generalized form of Clauser's (1954) constant eddy-viscosity hypothesis. In more recent work a ramp-function distribution of the Prandtl mixing length has superseded the Clauser hypothesis; it is, for example, the main empirical input to the current version of the general, finite-difference calculation procedure of Patankar and Spalding (1967). A brief discussion of this mixing-length distribution is given below, after which it is shown that Spalding's $\bar{s}$-relation is consistent with a ramp-function mixing-length profile. The basic form of this $\bar{s}$-relation is modified to comply with the drag-law requirement that R_2 and R_3 both pass through zero at the same point; and constants in the relation are adjusted to fit the available experimental data.

The Prandtl mixing-length distribution

Most theories so far developed for turbulent flows have made use of either an eddy-viscosity or mixing-length hypothesis. For boundary layers, the assumption of a constant eddy viscosity in the region away from the wall was popularised by Clauser (1954), who proposed the relation

$$\nu_{eff} \equiv \tau/(\partial\bar{u}/\partial y) = 0.018\, u_G \delta_1 \qquad (4.4\text{-}1).$$

Although Clauser, and also later authors such as Libby, Baronti and Napolitano (1964), Mellor and Gibson (1966) and Mellor (1966), have shown this to be an acceptable hypothesis for the calculation of boundary layers without velocity maxima, it is unsuitable for general use; for flows with velocity maxima it implies a negative effective viscosity. An alternative formulation for ν_{eff} in terms of the Prandtl mixing length is free from this defect.

The dimensionless Prandtl mixing length is defined by

$$s \equiv \tau/(\rho u_G^2) = \lambda^2 |\partial z/\partial\xi| \partial z/\partial\xi \qquad (4.4\text{-}2),$$

where $\lambda \equiv \ell/y_G$, and ℓ is the mixing length. In the outer region of the boundary layer, a reasonable assumption consistent with the available data, is that λ has a uniform value of about 0.075,

i.e. $\lambda = \lambda_G \approx 0.075.$

The constant mixing length is a well-known empirical feature of free-turbulent flows. The main influence of the presence of a wall is to reduce the mixing length; it is found that the experimental data support a linear variation of λ with ξ,

i.e. $\lambda = \varkappa\xi$

where κ is the von Kármán constant, the value of which was taken earlier as 0.41. This linear distribution, of course, is consistent with the existence of a logarithmic velocity profile in the fully-turbulent, uniform shear stress, wall region.

Experimental information in support of the ramp-function mixing-length distribution was collected by Escudier (1965); figure 4.7 shows representative data extracted from his survey. When assessing the degree of similarity between the curves shown, it is helpful to remember: (1) Shear stress is proportional to the square of mixing length; so the $\lambda\{\xi\}$ representation tends to minimise the differences in the shear-stress-velocity relation. (2) Where ξ lies between 0.8 and 1.0, although λ rises rapidly (to an infinite value as $\xi \rightarrow 1.0$) and the differences between profiles may be great, the velocity gradients are small; consequently the shear stresses are small and errors in λ of slight importance. (3) Values of λ rest on the determination of y_G and the slope of the velocity profile; the inevitable experimental error then introduces a large scatter into the $\lambda\{\xi\}$ curves. In this respect, therefore, this method of presentation magnifies the differences between boundary layers.

Mixing-length distributions were also deduced from the wall-jet data of Schwarz and Cosart (1961), Bradshaw

and Gee (1962), Mathieu (1961) and Mathieu and Tailland (1963). It was again found that λ was fairly uniform over the outer region of the boundary layer, although the value was greater than before, at about 0.1.

It can hardly be doubted that λ depends upon other variables additional to ξ. So far, however, no equation has been found which links the mixing-length function to other arguments; nor is it known to what extent the function is influenced by the presence of non-uniform density. Therefore, for the time being, it seems appropriate to adopt generally the ramp-function proposal of Escudier (1965),

$$\begin{array}{|ll|}\hline \xi \leqslant \lambda_G/\varkappa : & \lambda = \varkappa\xi, \quad \varkappa = 0.41 \\ \xi \geqslant \lambda_G/\varkappa : & \lambda = \lambda_G, \quad \lambda_G = 0.075 \\ \hline \end{array} \qquad (4.4\text{-}3).$$

Other authors who have examined the mixing-length hypothesis in relation to boundary-layer theory include Szablewski (1951), Philip (1959) and Shigemitsu (1962).

Establishment of a suitable form for the $\bar{s}$-relation

The quantity $\bar{s}$ was defined in CHAPTER 2 as

$$\bar{s} \equiv \int_0^1 s(\partial z/\partial \xi)d\xi \qquad (4.4\text{-}4).$$

In the immediate vicinity of the wall, the dimensionless

shear stress, s, is not sensibly different from its wall value, s_S, so that (4.4-4) may be expanded as

$$\overline{s} = s_S z_S + \int_{\xi_S}^{1} s(\partial z/\partial \xi)\partial \xi \qquad (4.4\text{-}5),$$

where z_S is the velocity ratio at the edge of the constant shear-stress region, and ξ_S its thickness. The adoption of the linear velocity profile of section 4.3,

$$z = \zeta + (1-\zeta)\xi,$$

in which the physical thickness of the constant-stress region has been reduced to nothing, leads to the identification of z_S with ζ and of ξ_S with zero. The evaluation of the integral in (4.4-5) using this profile together with the mixing-length formula (4.4-3) leads to the result

$$\overline{s} = \zeta s_S + \lambda_G{}^2[1-2\lambda_G/(3\kappa)]\ |1-\zeta|^3 \qquad (4.4\text{-}6),$$

or

$$\overline{s} = \zeta s_S + 0.00494\ |1-\zeta|^3 \qquad (4.4\text{-}7),$$

when the recommended values of κ and λ_G are inserted.

The corresponding result deduced by Spalding (1965a) from the constant eddy-viscosity hypothesis, together again with the straight-line velocity profile, is

$$\overline{s} = \zeta s_S + (0.018/2)\ |1-\zeta|^3 \qquad (4.4\text{-}8).$$

Clearly, the only difference between (4.4-7) and (4.4-8) is in the value of the constant multiplying $|1-\zeta|^3$.

However, it is unlikely, in view of the crudeness of the assumptions involved in their derivations, that either (4.4-7) or (4.4-8) will fit experimental data well. But, the form of the $\bar{s}$-relation so derived may serve well enough if constants are adjusted to fit the data; thus the relation is taken as

$$\bar{s} = \zeta s_S + C|1-\zeta|^n \qquad (4.4\text{-}9),$$

where C and n are now regarded as empirical constants. However, as will be shown below, theoretical requirements put an upper limit of 3 on the values of n for $\zeta \to \infty$. Also, the requirement that R_2 and R_3 pass through zero at the same point necessitates modification of the ζs_S term.

Two important, and correct, implications of (4.4-9) are: (1) That for the flat-plate, zero-pressure-gradient boundary layer, where ζ is of the order of unity, $\bar{s}$ and s_S are approximately equal. That this must be so is shown by the plot of s vs z for the data of Klebanoff (1955) shown in figure 4.8. (2) When ζ becomes very small, as separation is approached, $\bar{s}$ increases with decrease in ζ.

Theoretical requirements of the $\bar{s}$-relation for $\zeta \to 1$.

Examination of the logarithm, ℓ, which appears in the denominator of the drag-law expression of Escudier,

Nicoll and Spalding (1966), (4.3-19), reveals that $R_2/(1-\zeta)$ must remain finite and non-zero as $R_2 \rightarrow 0$ if absurd predictions are to be avoided. For this to be so, it is clear that

$$\lim_{R_2 \rightarrow 0} \zeta = 1 \qquad (4.4\text{-}10)$$

(and hence, incidentally, $H_{32} \rightarrow 2$)

and also $$\lim_{R_2 \rightarrow 0} (dR_2/d\zeta) = \text{finite} \qquad (4.4\text{-}11).$$

That these results impose restrictions on the $\bar{s}$-relation, and in fact necessitate modification of (4.4-9), may be shown as follows.

In the immediate vicinity of the region under discussion, R_1, R_2 and R_3 are negligibly small, so the momentum and shape-factor equations reduce to

$$dR_2/dR_x = s_S$$

and $$R_2 dH_{32}/dR_x = 2\bar{s} - H_{32} s_S.$$

If H_{32} is substituted for by ζ, through the use of (4.3-4), and R_x eliminated, there results

$$\frac{dR_2}{d\zeta} = \frac{R_2}{2\bar{s}/s_S - H_{32}} \frac{dH_{32}}{d\zeta} \qquad (4.4\text{-}12).$$

Thus, for (4.4-11) to be satisfied

$$\lim_{\zeta \rightarrow 1} (\bar{s}/s_S) = 1 \qquad (4.4\text{-}13).$$

Application of l'Hopital's rule to (4.4-12) reveals further

$$\lim_{\zeta \to 1} (dR_2/d\zeta) = \frac{\lim_{\zeta \to 1} \left[\frac{dH_{32}}{d\zeta} \frac{dR_2}{d\zeta} + R_2 \frac{d^2 H_{32}}{d\zeta^2} \right]}{\lim_{\zeta \to 1} \left[2 \frac{d}{d\zeta} \left(\frac{\bar{s}}{s_S} \right) - \frac{dH_{32}}{d\zeta} \right]} .$$

So that $\lim_{\zeta \to 1} [d(\bar{s}/s_S)/d\zeta] = \lim_{\zeta \to 1} (dH_{32}/d\zeta) = \frac{2}{3}$ (4.4-14).

A modified form of the $\bar{s}$-relation (4.4-9) which satisfies both (4.4-13) and (4.4-14) is

$$\boxed{\bar{s} = \tfrac{1}{3}(2\zeta+1)s_S + C|1-\zeta|^n} \qquad (4.4\text{-}15).$$

This is the final form of the $\bar{s}$-relation, although C and n are constants which remain to be determined by fitting the experimental data for $\bar{s}$.

Limiting form of the $\bar{s}$-relation for wall jets ($\zeta=\infty$)

The integral quantities η_2 and η_3 which were introduced in the previous section (p.80) allow the definition of $\bar{s}$, (2.3-11) to be transformed, for $\zeta \to \infty$, to

$$\boxed{\frac{\bar{s}}{\zeta^3} \to \left(\frac{3}{4}\frac{\eta_2}{\eta_3}\right)^2 \int_0^1 \frac{\tau}{\rho u_m^2} \frac{\partial(\bar{u}/u_m)}{\partial \xi} d\xi} \qquad (4.4\text{-}16).$$

Since the right-hand side of this equation remains finite

for $\zeta \to \infty$, $\bar{s}$ must vary in proportion to ζ^3 when ζ becomes very large. Thus $n \to 3$ if the second term of (4.4-15) is to contribute to $\bar{s}$ when $\zeta \to \infty$.

Experimental information about $\bar{s}$

Experimental information about $\bar{s}$ comes from two main sources: (1) Measurements of shear stress made using hot-wire equipment. (2) Measurements of successive velocity profiles, values of $\bar{s}$ being determined by way of either the kinetic-energy equation (2.3-26) or the shape-factor equation (2.3-29). However, both methods are of doubtful reliability.

Few extensive experimental studies have been reported of the shear-stress distributions in turbulent boundary layers, because accurate hot-wire measurements are difficult to make in general, and particularly difficult in highly-turbulent flows such as occur in severe adverse pressure gradients (some of the reasons for the uncertainties are given in APPENDIX 3). In TABLE 1, details are given of all the data available to the writer. In addition to the data listed there, measurements have been reported by Townsend (1950), Mueller, Korst and Chow (1964) and Kruka and Eskinazi (1964); but it has not been possible to obtain sufficiently detailed information about these to allow their inclusion here.*

*Also, the data of Goldberg (1966) and Spangenberg, Rowland and Mease (1967) became available too recently to be included here.

Figure 4.8 contains, on the left-hand side, graphs of the velocity and shear-stress profiles for three typical situations: (a) shows the data of Klebanoff (1955) for a zero-pressure-gradient boundary layer; (b) shows the data of Bradshaw and Ferriss (1965), run 1, for a boundary layer in adverse pressure gradient; and (c) represents the situation some 38 slot-heights downstream of a slot from which fluid was injected into a boundary layer at a velocity, u_c, considerably in excess of that of the mainstream. The data shown are those of Erian and Eskinazi (1964). On the right-hand side of figure 4.8 are shown corresponding plots of shear stress versus velocity: the shaded areas on the s~z plane represent the values of $\bar{s}$.

The data listed in the column in TABLE 1 headed $\bar{s}_{eq}$ pertain to equilibrium boundary layers. The values of $\bar{s}$ given there were obtained from the shape-factor (H_{32}) equation (2.3-29) which, for equilibrium flows, becomes

$$2\bar{s} - H_{32}s_S + H_{32}(H_{12}-1)F_2 \approx 0 \qquad (4.4\text{-}17),$$

since H_{32} is slowly-varying in such cases. This may be re-arranged to give $\bar{s}_{eq}$ as

$$\boxed{\bar{s} = \bar{s}_{eq} = \tfrac{1}{2}H_{32}s_S[1+\beta(1-1/H_{12})]} \qquad (4.4\text{-}18),$$

where β is the pressure-gradient parameter defined by

(3.3-22),

i.e. $$\beta \equiv -H_{12}F_2/s_S.$$

Of course, errors are engendered by the assumption that dH_{32}/dR_x is negligible and that (4.4-18) can be used to calculate $\bar{s}$ from velocity profiles measured for equilibrium boundary layers. That the errors are probably small in most cases, however, is evident from the adjacent figures in the $\bar{s}$-column of TABLE 1 (where available). These are values of $\bar{s}$ determined from either hot-wire measurements or from shear stresses computed from the measured velocity profiles by an exact equilibrium-boundary-layer analysis.

Data of especial interest, perhaps, are those deduced from the velocity-profile measurements of Stratford (1955) for the limiting case of an equilibrium boundary layer with continuously zero wall shear stress, so that (4.4-17) reduces further to

$$\bar{s}_{eq} = -\tfrac{1}{2}H_{32}(H_{12}-1)F_2 \qquad (4.4\text{-}19).$$

It will be seen shortly that the information about $\bar{s}$ obtained in this way from Stratford's data are quite consistent with the rest of the available data.

(4.4-19) is important too in a more fundamental way: it provides decisive proof that $\bar{s}$ is non-zero for a separating boundary layer.

The available shear-stress measurements for boundary layers with velocity maxima (but non-zero u_G) are limited to those reported by Erian and Eskinazi (1964). These cover the limited range of values $1.5 < \zeta < 2.5$, and are of doubtful value in view of the remarks made earlier about the velocity profiles for these experiments (p.69): the absence of information about the flow near the wall is clearly indicated by the curves in figure 4.8(c). $\overline{s}$-data covering a wider range have been obtained, by the writer, using the kinetic-energy equation (2.3-26), with the ω-term omitted, from the velocity-profile data reported by Nicoll (1965). The $\overline{s}$-values so obtained are again listed in TABLE 1.

Determination of the constants C and n in the $\overline{s}$-relation

It was found when fitting (4.4-15) to experimental data that best overall agreement was realised when C and n were given a different pair of values for $\zeta < 1$ and $\zeta > 1$. The continuous nature of the $\overline{s}$-relation is still retained, although the slope is discontinuous at $\zeta = 1$.

(a) $\zeta < 1$

A least-squares-fitting procedure applied to (4.4-15) and the data for $\zeta < 1$ led to the values 0.00565

and 2.715 for C and n, respectively, so that the $\bar{s}$-relation is

$$\zeta < 1: \quad \boxed{\bar{s} = \tfrac{1}{3}(2\zeta+1)s_S + 0.00565(1-\zeta)^{2.715}} \quad (4.4\text{-}20).$$

The data for $\zeta < 1$ are plotted in figure 4.9, on logarithmic scales in the form $\bar{s} - \frac{1}{3}(2\zeta+1)s_S$ versus $(1-\zeta)$. Also plotted is a straight line representing (4.4-20). The open circles represent data obtained from hot-wire measurements; the data for equilibrium boundary layers, obtained using (4.4-18), are denoted by solid symbols, those tagged representing information deduced from Stratford's experiments.

Although the data shown in figure 4.9 are generally consistent, clearly there is considerable scatter. For values of ζ near unity, in particular, this was to be expected because both ordinate and abscissa quantities become small in this region, and uncertainties about the values of ζ affect both but in opposite directions. Also, in most cases, neither $\bar{s}$ nor s_S is known very precisely, so there may well be significant errors in the difference between $\bar{s}$ and $\frac{1}{3}(2\zeta+1)s_S$.

However, before dismissing the spread in the data as due to experimental scatter alone, it was considered worthwhile examining the data for consistent trends in

the spread. Except in the procedure of Goldberg (1966), a brief discussion of which is given below, so far as the writer is aware the only parameter other than velocity-profile shape factors and Reynolds numbers (or, what is essentially the same thing, s_S) to have received attention is a pressure-gradient parameter, such as F_2. This was included in the correlation of Rubert and Persh (1951) and, implicitly, in that of Felsch (1965). In figure 4.10, therefore, the data of figure 4.9 have been replotted with symbols chosen to represent various F_2 ranges. No consistent trend <u>across</u> the band of points is discernible, although, of course, the higher F_2-values are associated with the lower ζ (higher H_{12}) data.

For the time being at least, therefore, the spread in the data must be regarded as the result of experimental uncertainty, and (4.4-20) is thus taken as the $\bar{s}$-relation for $\zeta < 1$.

The data are compared directly with this equation in figure 4.11. The parameter on the curves is ℓ, the logarithmic function appearing in the drag law. Clearly, most of the data are contained within the space between the curves for $\ell = 8$ and 12.

(b) <u>$\zeta > 1$</u>

Comparison of (4.4-16) with the limiting form of (4.4-15) for $\zeta = \infty$ (with $n = 3$) allows values of C to be

obtained for this case. Three sets of data are available: those of Mathieu (1961) and Bradshaw and Gee (1962) obtained using hot-wire equipment, and those of Schwarz and Cosart (1961), for which shear stresses were calculated from measured velocity profiles. Values for the integral $\int_0^1 [\tau/(\rho u_m^2)\partial(\bar{u}/u_m)/\partial\xi]d\xi$ for these cases were given by Spalding (1965c); they are 0.0128, 0.0155 and 0.0134, respectively. Thus from (4.4-16), with the values of η_2 and η_3 given on p. 80, there is obtained

$$\bar{s}/\zeta^3 = 0.0099 \quad \text{(Mathieu)}$$
$$0.0119 \quad \text{(Bradshaw and Gee)}$$
$$0.0103 \quad \text{(Schwarz and Cosart).}$$

The differences between these values is probably of the same order as the experimental uncertainty involved, so it is reasonable to take the mean as representative,

i.e. $$\bar{s}/\zeta^3 = 0.011.$$

The limiting form of (4.4-15) for this case is

$$\bar{s}/\zeta^3 = \frac{2}{3}s_S/\zeta^2 + C,$$

and that of the drag law (4.3-18)

$$s_S/\zeta^2 = 0.334/\ell^2 \approx 0.0033 \text{ (since } \ell \approx 10).$$

Thus, finally, there is obtained

$$C \approx 0.011 - 0.002 \approx 0.01,$$

so that for flows with $\zeta \gg 1$ it is expected that the $\overline{s}$-relation will be little different from

$$\boxed{\overline{s} = \tfrac{1}{3}(2\zeta+1)s_S + 0.01(\zeta-1)^3} \qquad (4.4\text{-}21).$$

If the coefficient of $(\zeta-1)^3$ in (4.4-6) is equated with the value 0.01 given above, and the value 0.41 retained for $\varkappa$, it is found that $\lambda_G = 0.11$. This is evidently much greater than the value 0.075 adopted earlier (p.91), but is remarkably close to the value deduced by Escudier (1965) from the data for $\zeta = \infty$.

The data for $1 < \zeta < \infty$ are shown plotted in figure 4.12, those of Erian and Eskinazi (1964) being denoted by open circles to distinguish them from the data of Nicoll (1965), which are represented by solid circles. Also shown is a straight line representing (4.4-21). Perhaps surprisingly, this fits as well as any the data for $\zeta > 2$, which show remarkably little scatter in view of their method of derivation. For ζ near unity, however, there is again the not unexpected scatter: the remarks made earlier (p.102) apply equally here. In addition, and also noted earlier (p.69), there are uncertainties about the data of Erian and Eskinazi which lie mainly in this region.

Again, therefore, the scatter will be disregarded, and (4.4-21) retained as the $\overline{s}$-relation for all $\zeta > 1$.

Thus the complete final recommendation is

$$\bar{s} = \frac{1}{3}(2\zeta+1)s_S + \begin{cases} 0.00565(1-\zeta)^{2.715}, & \zeta < 1 \quad (4.4\text{-}20) \\ 0.01(\zeta-1)^3, & \infty \geq \zeta \geq 1 \quad (4.4\text{-}21). \end{cases}$$

Supporting evidence for the recommended $\bar{s}$-relation

(1) In the previous chapter it was shown that for equilibrium boundary layers an entrainment law could be constructed, for $\zeta < 1$, with the aid of Nash's (1965) $G \sim \beta$ relationship, using the degenerate form of the shape-factor equation (3.3-21) for H_1 = constant. In a similar way the curves plotted in figure 4.13 were obtained from the shape-factor equation (4.4-18) with H_{32} = constant, together with the shape-factor relation and drag law given earlier, (4.2-1) and (4.3-19), and also again Nash's relation.

These curves clearly fit the experimental data quite well, and resemble closely those shown in figure 4.11, with the exception of the levelling-out near $\zeta = 0$.

(2) Spalding (1965c) showed that $\bar{s}$ can be related explicitly to the dimensionless entrainment rate, $-m_G$, through the expression

$$\bar{s} = H_{32}[-m_G(H_{12}-1)/(2H_1) + s_S]/(H_{12}+1) \qquad (4.4\text{-}22),$$

where H_1 is Head's shape factor, defined by (2.3-18).

This result may be obtained by combining the degenerate forms of the two shape-factor equations (3.3-21) and (4.4-18), which are applicable to equilibrium boundary layers, with the elimination of the pressure-gradient parameter β. Spalding's derivation, perhaps, was somewhat more general in that the result was deduced from the complete shape-factor equations, (2.3-28) and (2.3-29), with the assumption that $\bar{s}$, $-m_G$ and s_S are not directly influenced by the pressure gradient.

If the variation of $\bar{s}$ is to be determined from (4.4-22), it is necessary to relate $-m_G$ and H_1 to the other profile parameters. The relations adopted here are those proposed in CHAPTER 3 - the entrainment law given by (3.3-7) and (3.3-8) and the log-plus-cos profile for the shape-factor relation. Curves deduced for $\zeta < 1$ are shown in figure 4.14 and for $\zeta > 1$ in figure 4.15. For $\zeta < 1$, the curves again closely resemble those of figure 4.11; and the fit to the data is also good. For $\zeta > 1$, the agreement with the data is also most satisfactory.

The reason for good agreement, both here and previously, when equilibrium-boundary-layer relations were being considered, may be regarded as an indication of an overall consistency in the data and data analysis, and also in the implications and trends of the various rela-

tions recommended. Thus there is good reason to suppose that the new $\bar{s}$-relation, unlike those considered in Thompson's (1964) review, will lead to predictions of boundary-layer development of an accuracy on a par with that of Head's (1958) entrainment method.

Previous recommendations for the $\bar{s}$-relation

All previous recommendations for an $\bar{s}$-relation are limited to $\zeta < 1$; and most are explicit in character. The exceptions are those of Rotta (1950), which was based upon the log-plus-linear velocity profile and what appears to be essentially an equilibrium-boundary-layer analysis, and Goldberg (1966). Goldberg's is a kinetic-energy method, but differs from all others, including that of the present thesis, in that it attempts to allow for the effects of the upstream history of the boundary layer by the use of a differential equation for $\bar{s}$ (to be solved simultaneously with those for momentum and kinetic energy):

$$R_2 d\bar{s}/dR_x = K(\bar{s}_{eq}-\bar{s}),$$

where $\bar{s}_{eq}$ is the value of $\bar{s}$ for an equilibrium boundary layer and K is a constant. Goldberg did not appear to be aware that an expression for $\bar{s}_{eq}$ could be arrived at through the shape-factor (H_{32}) equation (4.4-18) itself, as demonstrated on p.99, but gave instead an empirical

correlation, relating $\bar{s}_{eq}$ to R_2 and F_2, which reduces to Truckenbrodt's (1952) $\bar{s}$-relation for zero-pressure-gradient boundary layers.

As has already been mentioned, the main reasons for re-examining the kinetic-energy method, and for recommending a new $\bar{s}$-relation, are the theoretical inadequacy and limited applicability of previous proposals. For the sake of completeness, and for reference purposes, these are listed in TABLE 6, although they are put to no further use in the present work. In view of the paucity of, and uncertainty in, the available experimental data, it has not been considered worthwhile making comparisons between the abilities of the various proposals to fit the data, as was done in the case of the drag law in section 4.3. The most notable feature of many of these empirical $\bar{s}$-relations is their extreme complexity, which stems basically from a lack of theoretical guidance in their derivation.

Concluding remarks

(1) The recommended $\bar{s}$-relation is

$$\bar{s} = \tfrac{1}{3}(2\zeta+1)s_S + \begin{cases} 0.00565(1-\zeta)^{2.715}, & \zeta < 1 \quad (4.4\text{-}20) \\ 0.01(\zeta-1)^3, & \infty \geqslant \zeta > 1 \quad (4.4\text{-}21). \end{cases}$$

(2) The degree to which these formulae correlate experimental data is probably as good as can be expected in view

of the paucity and poor quality of the available data.

(3) The new relation is superior to previously-recommended formulae in respect of: range of applicability and, in most cases, theoretical propriety.

(4) There is good agreement between values of $\overline{s}$ given by the recommended formulae and those deduced from the entrainment law recommended in CHAPTER 3 and from an equilibrium-boundary-layer analysis incorporating Nash's relation.

(5) The adequacy of the recommended relation remains to be judged by its ability to allow accurate prediction of boundary-layer development when used in conjunction with the shape-factor relation and drag law given in sections 4.2 and 4.3. This will be examined in the chapter which follows.

CHAPTER 5

CALCULATIONS OF BOUNDARY - LAYER DEVELOPMENT

5.1 Introductory remarks

In this chapter the calculation methods developed in CHAPTERS 3 and 4 are applied to the prediction of the development of particular boundary layers which have been reported in the literature. The main intention is to test the auxiliary relations which have been recommended, and to compare the relative abilities of the entrainment and kinetic-energy methods to give accurate predictions.

Inevitably there will be some failures, so that an additional task is to examine critically the calculations presented, and also the data with which they are compared, to see why the failures occur, and if possible to suggest means for remedying the defects.

Consideration here is restricted for the most part to conventional boundary layers, for which the velocity profiles do not exhibit a maximum. Calculations for negative values of R_2 have been carried out using the same computer programs as those used here. The results have been reported in the papers by Escudier and Nicoll (1966a, b).

All the integrations of differential equations were performed numerically on the University of London Atlas computer using the Runge-Kutta method. The steplength

generally used was one twentieth of the distance between measuring stations for the first three stations, and one tenth of that distance for the remainder. The use of smaller steps was found to make no difference to the results except for those calculations where R_2 changed sign, when (in the region of $R_2 = 0$) much finer spacing was necessary. The time taken for a typical calculation was 3 seconds on the Atlas computer.

5.2 Experimental inputs required

(1) Initial conditions: In all cases, the initial conditions required were taken as, or computed from, the experimentally-determined values of R_2 and H_{12}* at the furthest upstream x-station for which data were available.

(2) External pressure gradient and x-Reynolds number: Values of R_x, the independent variable, were calculated in each case from the measured variation of u_G with x using the trapezoidal rule. The pressure gradient, $d(\ln u_G)/dR_x$, at each x-station was calculated from the slope of a parabola fitted to the value of u_G at that station and those adjacent to it (values at the end points were obtained by extrapolation).

---

*Wherever possible, the values of R_2 and H_{12} used were those re-calculated by the writer from the measured velocity profiles; otherwise, the reported values were used.

(3) Convergence/divergence: In no case was explicit allowance made for the ω-terms appearing in the mass-conservation, momentum and kinetic-energy equations. However, in those calculations where only one of the shape-factor equations, (2.3-28) and (2.3-29), was integrated, implicit allowance was made by adopting the experimentally-determined variation of R_2.

5.3 Application of the entrainment method: change of dependent variables

Before presenting and discussing the results of calculations of R_2 and H_{12}, some explanation of the method of application of the entrainment procedure is appropriate.

In a parametric-profile calculation procedure, such as the entrainment method, it is convenient to use as the dependent variables of the differential equations the profile parameters (z_E and ℓ', in the present case) rather than the naturally-occurring variables (H_1 and R_2). The reason is that the values of the profile parameters must in any case be known at each stage of the calculation to permit the evaluation of other quantities, such as H_{12}, s_S, $-m_G$ etc. But the determination of z_E and ℓ' from H_1 and R_2 is not straightforward and (in terms of computer time) is very time consuming, because iterative techniques are usually required. Indeed with other variables, or more than two variables, the task may become

prohibitive. Where only two or three parameters are involved, it is a simple matter to write the differential equations with the profile parameters themselves as the dependent variables, but with more parameters matrix-inversion techniques are necessary (see Spalding, 1966).

The differential equations to be solved in the case of the entrainment method are the momentum equation (2.3-25) and the shape-factor (H_1) equation (2.3-28). The equations which result when these are transformed to differential equations with z_E and ℓ' as the dependent variables are set out in APPENDIX 1.

The kinetic-energy method, of course, is explicit in terms of R_2 and H_{32}, although there would be no difficulty in working with ζ and ℓ, say, as the dependent variables if desired.

5.4 Check on mean-flow two-dimensionality

Consideration has been limited in this thesis to nominally two-dimensional flows with no convergence or divergence. Lack of two-dimensionality in such flows, however, is one of the main causes to which the failure of prediction procedures is sometimes attributed. A check on the momentum balance has been made, therefore, for all the boundary layers to which the calculation procedures have been applied. The method adopted was to integrate the two-dimensional momentum equation

(2.3-25) with the ω- and normal-stress terms omitted. The values of H_{12} and F_2 required were taken as those determined experimentally. But, in order that a single, consistent procedure could be adopted, experimental values of s_S were not used, even where available; instead, values were calculated from the drag law proposed in CHAPTER 4, (4.3-19). It is unlikely that this procedure led to any appreciable error in the results, as (4.3-19) is the best-available representation of experimentally-determined drag.

The full curves in figure 5.1 represent the variations with R_x of R_2 calculated as described above, and the points the experimental values of R_2. In most cases the computed (two-dimensional) values of R_2 agree well with the experimental ones - the short vertical line drawn through the last experimental point in each case indicates $\pm$10% of that value of R_2. A notable point is that, where reported, the majority of runs in a series of experiments performed in the same wind tunnel tend to be either accurately two-dimensional or very badly non two-dimensional. The experiments of Klebanoff and Diehl, excepting run 2, Moses, with the exception of runs 4 and 6, and Schubauer and Spangenberg fall into the first category; and those of Ludwieg and Tillman, excepting runs 1 and 2, into the second. This latter result is

perhaps surprising in view of the prominence in the literature of the experimental work of these authors. Other particularly notable failures, in respect of poor agreement between calculated two-dimensional values of R_2 and experiment, are those for the flows reported by Brebner and Bagley, run 1, von Doenhoff and Tetervin, runs 1 and 4, Newman, run 2, and Schubauer and Klebanoff. The majority of these experiments, it should be noted, refer to flows in strong adverse pressure gradients. It should be taken into account, however, that in some cases the lack of two-dimensionality may be merely local: comparisons should be made between the slopes of the curves and of the experimental data. In the case of Klebanoff and Diehl, run 2, for example, the near-constant difference downstream is due to a very great discrepancy upstream.

Unfortunately, there is no way of telling, without further information, whether the departures of the curves from the experimental points indicate a true lack of two-dimensionality, brought about by stress-terms like $\partial(\overline{w'v'})/\partial z$, or merely planwise convergence or divergence of the mean flow, the effects of which could be included if information about the ω-term were available. Bradshaw and Ferriss (1965) maintain that the latter is generally the case, and that true secondary flows are indeed absent (however, in a private communication, Bradshaw

concedes that in the case of the experiments reported recently by Spangenberg, Rowland and Mease (1967) real secondary flows may be occurring). In addition there is uncertainty about the importance of the cross-flow pressure gradient, brought out by streamline curvature and the normal stresses, although it is unlikely that this becomes important until the value of H_{12} exceeds about two.

Little more can be said than to observe that the most common form of discrepancy is the failure of dR_2/dR_x to grow sufficiently rapidly towards the end of a run where, in adverse pressure gradient, s_s is usually falling quite rapidly. This can be interpreted as indicating flow convergence, due to the growth of sidewall boundary layers, and/or to the increasing importance of the cross-flow pressure gradient.

The dashed and chain-dotted curves shown in figure 5.1 represent the results of calculations of R_2 carried out using the entrainment and kinetic-energy methods. They will be discussed below.

5.5 Calculations of momentum-thickness Reynolds number, R_2

The dashed curves shown in figure 5.1 represent values of R_2 calculated using the entrainment method, with simultaneous solution of the mass-conservation and momentum

equations. In general the results are satisfactory, and follow closely the trends of the full curves which were discussed in section 5.4. The dashed curves generally lie a few per cent lower than the full ones, resulting in appreciably better agreement with experiment in, for example, the cases of Herring and Norbury, run 2, Ludwieg and Tillmann, run C, and Moses, runs 1 and 2. In the case of Klebanoff and Diehl, run 2, the agreement is also improved, although here the dashed curve lies above the full one.

The chain-dotted curves in figure 5.1 represent the results of calculations performed using the kinetic-energy method, with simultaneous solution of the momentum and kinetic-energy equations. The results again are little different from those represented by the full curves, although again too there are small differences which in some instances lead to better agreement with the data, as in the case of Gault, run 2, and all seven of the Klebanoff and Diehl boundary layers.

In general, the kinetic-energy method leads to slightly better agreement with experiment than does the entrainment method, although the differences between the two sets of calculations are quite small. Little more can be added to the discussion until after the shape-factor calculations have been presented.

5.6 Calculations of shape factor H_{12}

In most calculation procedures, including those considered in the present thesis, the main aim is accurate calculation of the shape factor H_{12} (although H_{32}, for example, would do equally well). For once this is achieved, together with values of R_2, the other quantities of interest, principally s_s, are known too.

The dashed curves in figure 5.2 represent the results of calculations of H_{12} performed using the entrainment method, and the full curves those obtained for the kinetic-energy method. The points plotted again represent the experimental data.

The following observations may be made: (1) There is a definite correlation between the achievement of satisfactory agreement here and the existence of accurate two-dimensionality, as indicated by the full curves of figure 5.1. (2) In all cases both calculation methods give similar results, although values of H_{12} for the entrainment method are generally a few per cent higher than those for the kinetic-energy method, and usually (for that reason) in better agreement with the data. There are several exceptions to this last point, however, the most notable, perhaps, being Moses' run 3, where the kinetic-energy method gives excellent agreement with the data (and where, incidentally, the best agreement

between two-dimensional and experimental R_2 was found). However, in no case does one method succeed where the other has failed badly. (3) It is interesting to note that the wide differences (in some cases) between the calculated and experimental values of H_{12} are not reflected in the R_2-calculations of figure 5.1. The reason for this is that if H_{12} is too small then s_S will be too large, and vice versa, and, as the momentum equation shows, the effects tend to be self-cancelling:

$$dR_2/dR_x = s_S + (1+H_{12})(-F_2) ,$$

since $-F_2$ is positive for adverse pressure gradient.

A question which must arise, but to which there is no immediate answer, is why are the results for the entrainment method generally in better agreement with the data than those for the kinetic-energy method? This is certainly a surprising feature of the results, although the differences are not great, in view of the uncertainties associated with the former method. Both the drag law and shape-factor relation used in the kinetic-energy method correlate the available data appreciably better than the corresponding relations for the entrainment method. Also, although the data on which both the $-m_G$- and $\bar{s}$-relations are based show considerable scatter, the doubts associated with values of $-m_G$ and with the $-m_G(z_E)$ correlation are certainly greater.

For flows with velocity maxima, both methods give rise to satisfactory agreement with the data of Kruka and Eskinazi (1964) and Nicoll (1965). The results of additional calculations performed using only the kinetic-energy method compare well with the data of Whitelaw (1966), but less well with those of Erian and Eskinazi (1964). The discrepancies in the latter case may again be associated with the uncertainties in the data themselves (see p. 69). The differences between the results of the two calculation methods are slight, and the deviations from the data appreciably less than for $R_2 > 0$.

Calculations have also been carried out for the experiments of Wieghardt (1943) and Whitelaw (1966) in which R_2 changed from negative to positive. It will be remembered that it was necessary to modify the basic form of the $\bar{s}$-relation, deduced in CHAPTER 4 from simple theoretical considerations, to ensure that calculation could proceed without difficulty through the point where R_2 becomes zero. The results of these calculations, carried out by the writer, are shown in the paper by Escudier, Nicoll, Spalding and Whitelaw (1967), where values of R_1 and R_2 are given rather than the more usual combination of R_2 and H_{12} ($\equiv R_1/R_2$) because the latter quantity loses its usual significance in the region where R_1 and R_2 change sign. Although the predicted values of both R_1 and R_2 are generally too high (probably indi-

cating lack of mean-flow two-dimensionality), the calculations convincingly demonstrate the adequacy of the measures taken to ensure that the zero-R_2 point could be traversed.

Another question to be answered is how does the accuracy of the calculations presented in figures 5.1 and 5.2 compare with those of other available calculation procedures? A review of these calculation methods, and the application of them to the data considered here, is neither appropriate nor possible in the present thesis. However, previous writers, principal among them Thompson (1964), have made such reviews and have demonstrated which are the most accurate procedures available.

Thompson showed the results of shape-factor calculations carried out using the methods of Head (1958), Maskell (1951), Rubert and Persh (1951), Spence (1952, 1956) and Truckenbrodt (1952). Comparisons were made with the data of Clauser, runs 1 and 2, von Doenhoff and Tetervin, runs 1, 2 and 3, Newman, run 2, Schubauer and Klebanoff, Schubauer and Spangenberg, runs C, D and E, Schmidbauer (1936) (for a boundary layer on a convex wall) and also with a considerable amount of zero-pressure-gradient data. Thompson showed quite convincingly that Head's method is superior to the other procedures considered.

In all the cases shown by Thompson, Head's method gives rise to values of H_{12} larger than does either of the procedures considered here. The consequence is that in the cases of the experiments of von Doenhoff and Tetervin, Newman and Schubauer and Klebanoff, the results of Head's method are in better agreement with the data than those of the present entrainment method. However, for the experiments of Clauser, Schubauer and Spangenberg and for the zero-pressure gradient data, both new methods represent a significant improvement over Head's. It is unfortunate that Thompson was unable to make comparisons with the experiments of Moses, for it is almost certain that for these data Head's method would give values of H_{12} larger than those measured, and so in poorer agreement than the results of the new methods.

Some justification for this claim is to be found in the work of Goldberg (1966) who carried out calculations with the methods of von Doenhoff and Tetervin (1943), Escudier and Spalding (1966), Head, Moses (1964), Rubert and Persh, Schuh (1955) and Spence (1960). The results of these calculations were compared with Goldberg's own data, obtained in an experimental set-up similar to that of Moses for boundary layers in adverse pressure gradients, including cases where recovery in zero pressure gradient was allowed (similar to Moses' runs 5 and 6).

5.6 Calculations of shape factor H_{12}

In most calculation procedures, including those considered in the present thesis, the main aim is accurate calculation of the shape factor H_{12} (although H_{32}, for example, would do equally well). For once this is achieved, together with values of R_2, the other quantities of interest, principally s_s, are known too.

The dashed curves in figure 5.2 represent the results of calculations of H_{12} performed using the entrainment method, and the full curves those obtained for the kinetic-energy method. The points plotted again represent the experimental data.

The following observations may be made: (1) There is a definite correlation between the achievement of satisfactory agreement here and the existence of accurate two-dimensionality, as indicated by the full curves of figure 5.1. (2) In all cases both calculation methods give similar results, although values of H_{12} for the entrainment method are generally a few per cent higher than those for the kinetic-energy method, and usually (for that reason) in better agreement with the data. There are several exceptions to this last point, however, the most notable, perhaps, being Moses' run 3, where the kinetic-energy method gives excellent agreement with the data (and where, incidentally, the best agreement

Goldberg's conclusion was that, of the prediction methods he considered, that of Escudier and Spalding gave best agreement with his data, although in most cases Goldberg's own method (discussed briefly on p.108), tailored to fit his own data, gave better agreement still. However, application of this method, by the present writer, reveals that this characteristic is not retained in general circumstances. The method of Escudier and Spalding referred to was an early version of the kinetic-energy method of CHAPTER 4; it gives results little different from the new procedure.

Carmichael and Pustintsev (1966) have also demonstrated the adequacy of the empirical relations recommended by Escudier and Spalding in leading to satisfactory predictions of the performance of conical diffusers.

In view of the above paragraphs, it seems safe to conclude that the results of calculations performed using the entrainment method of CHAPTER 3 and the kinetic-energy method of CHAPTER 4 are at least as accurate as other available procedures. The major advantage of both methods is their far wider range of applicability than earlier methods.

Although the new procedures give satisfactory results in many cases, the causes of failure in other, apparently similar, situations remains to be explained. The dis-

cussion in the section which follows is intended to throw some light on this.

5.7 Discussion of the reasons for discrepancies between calculation and experiment

The causes of the inconsistencies and discrepancies which exist between some of the calculations and experiment should be sought systematically. It is suggested that an examination of the causes of error might conveniently be carried out under the following headings:

(1) Inaccuracy of measurements

- (a) static pressure
- (b) mean velocity
- (c) local shear stress
- (d) wall shear stress

(2) Inaccurate processing of data

- (a) integral velocity-profile quantities
- (b) shear-work integral
- (c) pressure gradient

(3) Inadequacy of presumed empirical inputs

- (a) shape-factor relations
- (b) drag law
- (c) entrainment relation
- (d) shear-work-integral relation

(4) Failure of experimental situations to conform with conditions presumed in theory

(a) turbulent flow

(b) steady mean flow

(c) uniform fluid properties

(d) two-dimensional mean flow

(e) boundary-layer flow

(f) plane walls

Some of these points will be discussed below and, although no attempt can be made to present an exhaustive examination of the causes of error, detailed discussion will be given where appropriate. For obvious reasons, however, much of the discussion must be largely speculative.

(1) Inaccuracy of measurements

Although doubt from this source should diminish with increase in the number of experiments considered, it is not at all unlikely that some generally-used measurement techniques are subject to systematic errors. For example, most reported velocity profiles are measured using flattened pitot tubes, for which the effects of turbulence intensity, pitch, velocity gradient, viscosity etc. are uncertain and, for the most part, ignored. Also, the questionable assumption is often made that

the static pressure at a given x-station is everywhere equal to the value indicated by a wall tapping.

The use of a hot-wire anemometer for mean-velocity measurement removes some of these uncertainties, but introduces others. Some discussion of the use of this instrument is given in CHAPTER 6 and APPENDIX 3, with particular reference to the writer's own experimental work on highly-turbulent flows (discussed in CHAPTER 6).

As was mentioned in CHAPTER 4, few extensive experimental investigations of the shear stress in turbulent boundary layers have been reported, and the serious doubts associated with some of those which have been reported have also been mentioned already. Some of the reasons for these doubts are given later, in the discussion of hot-wire anemometry referred to in the previous paragraph.

Direct methods for the determination of wall shear stress, such as the use of a floating element, are not well established because of the practical difficulties involved. However, the values yielded by various indirect devices, such as Stanton or Preston tubes, a heated element, or the use of a Clauser plot, are generally in good agreement with each other, as was demonstrated by Goldberg (1966). Therefore it is usually assumed that the values so obtained are of acceptable accuracy.

The underlying difficulty, of course, is that for most of the measurements made in turbulent flows there are no true standards of comparison or accuracy, so that the only possible checks on precision are provided by self-consistency of the data: for example, agreement between the wall shear stress and the extrapolation of the shear-stress profile to the wall; the balance of the conservation equations; the lack of scatter; etc. Generally, however, it is impossible for any person other than the experimenter himself to guess even the direction of measurement inaccuracies (particularly when most writers give so few details of their measurements).

(2) Inaccurate processing of data

Many of the remarks made above are of equal relevance here. However, little doubt usually attaches to the evaluation of R_1, R_2 and R_3, and less still to their ratios, H_{12} and H_{32}, although as Thompson (1964) has shown, and as the writer himself has found, appreciably different values of H_{12}, say, are sometimes calculated from the same velocity profile by different workers.

Such errors as arise in the evaluation of $\overline{s}$ are likely to be due to the scatter resulting from inaccuracies in the determination of the shear stress itself, and also to the absence of data for small values of z (see the plots of s versus z in figure 4.8).

As with any quantity which requires the differentiation of experimental data, errors in the evaluation of $d(\ln u_G)/dR_x$ may be appreciable, particularly where pressure differences across the layer are ignored. Part of the uncertainty could be removed if mainstream velocities or pressures between profile-measuring stations were reported.

(3) Inadequacy of presumed empirical inputs

CHAPTERS 3 and 4 were concerned largely with discussion of the empirical inputs for the entrainment and kinetic-energy calculation procedures, so only a few general points will be made here. First of all, of course, the adequacy of any empirical relation depends upon the accuracy of the data upon which it is based, upon the flexibility and theoretical propriety of the correlation form, and upon the degree of correlation achieved. Associated with this, in the case of the $-m_G$- and $\bar{s}$-relations, is the assumption of local equilibrium referred to earlier, in CHAPTER 2 p.28, which underlies the present work and also most other calculation schemes. As has already been mentioned (p.108) the only explicit calculation method to attempt to include the effects of upstream history is that of Goldberg (1966), and this gives results generally inferior to those of the present methods.

Nevertheless, it is reasonable to suppose that a theory employing an equation requiring an initial condition for dH_{12}/dR_x, say, can be made to give better agreement with experiment than any local-equilibrium theory.

(4) Failure of experimental situations to conform with conditions presumed in theory

Although it is here that the causes of the discrepancies between calculation and experiment probably lie, a number of the points raised under this heading as likely sources of error can be ruled out immediately. These include the conditions that the flow should be turbulent, steady in the mean and have uniform fluid properties. Even so, it should be noted that Whitelaw (1966) attributed the lack of balance between dR_2/dR_x and s_s (for $F_2=0$) to secular changes in his slot velocity.

Another condition certainly satisfied in the majority of cases is that the wall should be plane. In the case of some aerofoil experiments, however, this may not be so, as there may be significant curvature in the x-y plane. Thompson (1965) has shown that calculations for the experiments of von Doenhoff and Tetervin, Schmidbauer and Schubauer and Klebanoff, all for boundary layers on convex walls,can be improved significantly if empirical allowance is made for the effect of curvature in these

cases (the direction of influence is the same in all cases). Mellor (1966) and Bradshaw (1967) also suggest ways in which to allow for the influence of curvature; and, as Bradshaw remarks, the effect is on the behaviour of the turbulence, and hence the empirical relations, not the equations (to the boundary-layer approximation, at least).

The experiments of Moses (and also, incidentally, of Goldberg) were performed on boundary layers developing along a circular cylinder (axisymmetric flow), so that here again curvature effects were involved, though now it is probably only the equations which require modification. The present writer did not include such modifications, although it is fairly easy to do so. The a posteriori justification for this is the acceptable accuracy (in most instances) of the calculations in these cases.

In section 5.3, in the discussion of the calculations carried out to check mean-flow two-dimensionality, it was pointed out that lack of agreement between calculation and experiment could be due to planwise convergence or divergence of the mean flow, and/or to the non-negligibility of the cross-flow pressure gradient, that is to the invalidity of the boundary-layer approximation. The same remarks apply to the calculations of shape-

factor development. However, as was indicated in CHAPTER 2 (p.27) no terms involving ω appear in the shape-factor equations, (2.3-28) and (2.3-29), so that calculations of H_{12} based upon either of these equations, with R_2 taken from experiment, would include implicit allowance for the effects of convergence or divergence. Such calculations have been carried out by the writer for both the entrainment and the kinetic-energy methods. The values of H_{12} obtained in both cases are slightly higher than those in figure 5.2, although in general the results were scarcely different from the earlier calculations.

The influence of the cross-flow pressure gradient is less easy to ascertain although, again as suggested in CHAPTER 2 (p.19), attempts in the past have been made to estimate its importance by assuming it to arise through high turbulence intensity alone. Calculations based upon this assumption, together with a simple hypothesis to relate the normal stresses to known quantities (details of the analysis are given in APPENDIX 2), have been carried out by the writer, again for both calculation procedures. In the case of the kinetic-energy method, the values of H_{12} so obtained were again slightly increased in most instances, although again too the differences were too slight to result in any significant improvement in the comparisons with experimental data.

The effect on the entrainment-method calculations was much greater, presumably because only the momentum equation is affected (see p.59). Again H_{12} was generally increased, resulting in most cases in poorer agreement with the data.

From the results of these two sets of calculations* it may be concluded that lack of agreement with experimental data is not due to the influence of planwise convergence or divergence. Neither is it likely that the cause is the neglect of the cross-flow pressure gradient, although this is less certain because of the assumptions necessary before this can be estimated.

Finally there is the possibility that the discrepancies are caused by a true lack of two-dimensionality. Some evidence for the plausibility of this is the apparently random manner in which boundary layers are affected by the factor(s) causing the discrepancies. For example, the results of calculations on two apparently similar boundary layers (i.e. having similar shape-factor distributions) may be quite different: boundary layers where this is seen to be so are those of von Doenhoff and Tetervin, runs 2 and 3, and Newman, run 2; Schuabuer and Klebanoff and Schubauer and Spangenberg, run E; and

---

*The results are not shown in the present thesis, but those for the kinetic-energy method are given in the paper by Escudier and Nicoll (1966b).

Moses, run 4, and Schubauer and Spangenberg,runs B and D. In the first two cases it is possible that the reason may be the neglect of curvature effects mentioned earlier. Another possible explanation is the invalidity of the local-equilibrium assumption, although this seems most unlikely.

A further point in favour of this being the cause is that it seems reasonable to assume that the dominant influence on the degree to which the flow is, or is not, two-dimensional is the geometry of the set-up, i.e. the tunnel aspect ratio, plate length, width and inclination, etc. Consistent with this is the observation in section 5.4, p.115, that good agreement between calculation and experiment is obtained for most of the flows in the series of experiments reported by Schubauer and Spangenber and by Moses (to these can probably be added the series of Goldberg), whereas, in contrast, poor results have been obtained for most of the layers reported by von Doenhoff and Tetervin and Ludwieg and Tillmann.

5.8 Concluding remarks

(1) Calculations performed using both the parametric-profile entrainment method of CHAPTER 3 and the explicit kinetic-energy method of CHAPTER 4 lead to values of R_2 in good agreement with those given by the two-dimensional

momentum equation evaluated using experimental data.

(2) In the majority of cases, values of H_{12} calculated using the methods mentioned above agree well with experimental values; and the results for the entrainment method are slightly better than those of the kinetic-energy method.

(3) The predictions of H_{12} are usually in poor agreement with the data in cases where there is an indicated lack of two-dimensionality of the mean flow.

(4) The results of calculations for $R_2 < 0$, although not shown here, are generally in better agreement with the data than those for $R_2 > 0$.

(5) The causes for the discrepancies between calculation and experiment are uncertain, but they are probably due to true lack of two-dimensionality (rather than convergence or divergence) although in some cases the neglected effects of wall curvature may be of significance.

(6) The inclusion in calculation procedures of the effects of the upstream history of the flow should lead to improved results, although in general application the one attempt, by Goldberg (1966), to do so (in an explicit method) does not.

CHAPTER 6

THE EXPERIMENTAL INVESTIGATION

6.1 Introduction

The calculation procedures discussed in CHAPTERS 3 to 5 rest upon the assumption that the shear stress within a turbulent boundary layer is determined uniquely by the local mean-velocity profile. Therefore, in the calculations the only trace of the upstream history of a boundary layer is in the initial velocity profile. A number of authors, among them Bradshaw and Ferriss (1965) and Goldberg (1966), have suggested that further account of upstream conditions should be taken. The reason is that it is only for specially contrived 'equilibrium' flows that the assumption of a unique relationship between the shear-stress and velocity profiles is satisfied exactly. In more general situations, the shear-stress profile develops less rapidly than that of the mean velocity.

In the experiments of the present writer, which are reported below, violent changes in the shear-stress and velocity profiles of a boundary layer were brought about by the injection of air (in the y-direction) into the boundary layer. Such a highly perturbed boundary layer is far from equilibrium, and provides, therefore, a severe test of the recommended auxiliary relations and

calculation procedures.

Previous investigators, who have reported boundary layers which develop from an initially perturbed state, include Klebanoff and Diehl (1952), Moses (1964) and Bradshaw and Ferriss (1965). However, the accuracy of the predictions, shown in figure 5.2, of the development of these flows (downstream of the perturbation) is not noticeably poorer than for those of near-equilibrium boundary layers. Also, the quantities R_2, H_{12}, H_{32}, s_S and $\bar{s}$, where available for these 'recovering' flows, were found in CHAPTER 4 to be governed by the same relations as the data for other situations.

One of the reasons why such good predictions were obtained, for the boundary layers mentioned above, may be that the initial perturbations were not particularly severe. Also, all these flows developed subsequently in zero pressure gradient, whereas those of the present writer were subjected to a severe adverse pressure gradient.

The data, on which were based the correlation formulae recommended in CHAPTER 4, were obtained from experiments in conditions far less extreme (closer to equilibrium) than those of the present writer's experments. Consequently, as mentioned above, the new data will provide an exacting test of the recommended formulae,

and also of the calculation procedure of CHAPTER 4. The extent of the agreement, between the writer's data and the predictions of the recommendations, may be taken as an indication of the general efficacy of the latter.

6.2 Experimental apparatus

Wind tunnel

The experiments reported below were carried out in the 12in x 18in x 36in working section of a closed-circuit wind tunnel. The tunnel is powered by two English Electric induction motors: one of 5h.p, for airspeeds up to about 50ft/s in the unoccupied working section, and the other of 120h.p, for speeds up to 240ft/s. Fine speed control was achieved by running the 5h.p motor close to its maximum speed.

A heat exchanger built into the tunnel circuit permitted the air temperature to be stabilised within $\pm 0.5^{\circ}C$.

The working section of the wind tunnel, and its main dimensions, are shown in figure 6.1. For practical reasons, the cross section of the working section was reduced to 8in x 12in; the overall contraction ratio then was just over 9:1, and the free-stream turbulence intensity between 0.5 and 1.0%. The reduced flow area raised the maximum velocity available with the 5h.p motor to about 80ft/s.

The test plate itself is a $\frac{1}{2}$in thick sheet of perspex (plexiglass), 12in wide, with 1in dia. holes along its centre-line at $2^1/4$in intervals. Into these holes were inserted plugs which carried static-pressure tappings and which could be removed to allow a probe to be inserted into the boundary layer. The x-stations along the test plate, at which measurements were made, are indicated in figure 6.1 by the numbers 1 to 9. The first station is 2.6in downstream of the trailing edge of the blowing region; and subsequent stations are separated by $2^1/4$in intervals.

The 'step' near the end of the test plate is simply a metal sheet set normally to and across the plate. This step provides an adverse pressure gradient which cannot fail to cause the boundary layer to separate from the wall. The perforated sheet above the test plate was installed to allow the pressure distribution to be adjusted, by altering the inclination of the sheet and/or covering some of the perforations with adhesive tape.

Two blowing sections, each 1in wide, were used in the experiments. One blowing strip was $^1/8$in thick Porosint grade E (porous sintered bronze with a porosity of 37% (quoted by Harrison, 1960)), and the other perforated steel sheet with 0.026in dia. holes set 0.052in apart (23% open area). A 3/32in thick strip of Porosint

grade E was set behind the perforated strip to increase the pressure drop and create a uniform distribution of flow through the perforated material.

The fan used to blow air through the injection region, via a plenum chamber set behind the plate, has an available pressure head of about 8in of water. This head corresponds with a maximum injection velocity, v_S, through the porous strip of about 7ft/s.

Instrumentation

For the reader's convenience, the items of instrumentation are given in the form of a list.

1. 0 - 50°C mercury-in-glass thermometer; used to measure tunnel-air temperature.
2. TEM NPL-tye 36 tube (25in range) manometer, with paraffin (specific gravity 0.787) as working fluid; used to measure static and total (pitot-tube) pressures.
3. 0.01in dia. tappings in removable plugs inserted in test-plate holes; used to measure wall static pressure.
4. Disc probe, 3/8in. dia. and 0.1in thick; used to measure mainstream static pressure.
5. Pitot tubes, manufactured from stainless steel hypodermic tubing: (a) 0.043in dia.; used to measure mainstream total head,

(b) 0.064in dia.; used as a Preston tube.

(c) 0.064in dia., with tip flattened to give opening 0.0043in high and walls thinned to give tip height of 0.0096in; used to measure total-head profiles.

6. DISA 55A01 constant-temperature hot-wire anemometer, with 55A25 miniature single-wire probe (wire normal to probe axis); used to measured longitudinal mean velocity and turbulence intensity.

7. Two DISA 55A01 anemometers, 55A06 random-signal indicator and correlator, and 55A32 cross-wire probe; used to measure Reynolds stresses.

8. 1.097in dia. orifice in plate set in 2in dia. delivery pipe; used to measured injection-air flow rates, according to procedure laid down in BS 1042 (1951).

9. Single sloping-tube manometer, with paraffin as working fluid; used to measure pressure drop across orifice plate.

10. Vertical U-tube manometer, with water as working fluid; used to measure pressure upstream of orifice plate.

11. Probe-traversing mechanism with sliding block, upon which probes were mounted, driven by 0 - 1in micrometer.

Hot-wire calibration

The calibration law adopted was that of Collis and Williams (1959) (see APPENDIX 3); it may be written as

$$E^2 = A + B\, u_N^{0.45} ,$$

where E is the voltage drop across the wire and u_N the velocity normal to the wire. For constant-temperature operation, A and B are constants (to be determined by calibration).

Wires were calibrated at the beginning and end of each test run, because appreciable changes in the values of A and B occurred during some tests. The values of the constants at any stage of a run were obtained by linear interpolation in time. Clearly, a quick method of determining A and B was essential, so calibrations were carried out at the x-station where measurements were to be made, and the minimum information necessary was used: two values of u_N and the corresponding values of E. These values of u_N were those in the mainstream for the tunnel run at its lowest possible speed and at the working speed.

Test conditions

The velocity u_1 at station 1 (see figure 6.1) for the experiments reported below was about 80ft/s. At the start of every test the speed was adjusted to give

a Reynolds number per unit length, u_1/ν, of 5×10^5/ft.

A series of three experiments was carried out; the first for zero blowing, and the other two for air injection through the porous and perforated strips. The average injection velocity, v_S, in the tests with blowing was 5.6ft/s; this rate corresponds to an injection ratio, v_S/u_1, of about 0.07.

For each experiment, measurements were made of the wall shear stress and of the profiles of the mean velocity and Reynolds stresses at stations 1, 3, 5, 7, 8 and 9 (see figure 6.1). In a few cases, measurements of some quantities were made at stations 2, 4 and 6.

6.3 Methods of measurement and data analysis

Mainstream velocity, u_G

Values of u_G were measured with a single-hot-wire probe, and subsequently confirmed by the results obtained from a pitot tube and a disc static-pressure probe. Initial measurements of the mainstream static pressure, p_G, determined with the disc probe, were found to be in error, apparently due to flow along the probe stem. Therefore, the probe was modified to eliminate this flow in the confirmatory experiments.

Distance from wall, y

Traverses were always started at the wall position.

Wall contact for both the pitot and single-hot-wire probes was determined by bringing the probes up against the test plate, and then adjusting the micrometer screw by 0.0005in intervals until a gap between the tube tip, or wire-support prongs, was just visible. A change in the manometer or anemometer reading confirmed the contact position so determined.

Local mean velocity, $\bar{u}$

Mean velocities were calculated from the differences between the local total head, indicated by the flattened pitot tube, and the static pressure, $\bar{p}$. The latter was assumed to vary through the boundary layer according to the relation

$$p_S - \bar{p} = (p_S - p_G)\xi^2 \qquad (6.3\text{-}1),$$

which is an approximation to the static-pressure profiles of Bradshaw and Galea (1967). p_S was taken as the pressure indicated by a wall tapping. p_G was obtained from the local value of u_G and the mainstream total head indicated by a pitot tube.

The pitot-tube-displacement correction of MacMillan (1956) was applied to the mean-velocity profiles, although the effects of this correction are negligible except in the region very close to the wall. There is a lack of general agreement as to the effects on the pitot tube of

viscosity, high-turbulence intensity, etc. (see Dean, 1963 and Hinze, 1959). Consequently no adjustments for these effects have been made.

Longitudinal turbulence intensity, $(\overline{u'^2})^{\frac{1}{2}}$

Over extensive regions of turbulent boundary layers in strong adverse pressure gradients, the values of the rms turbulence intensity $\tilde{u}'$ $[\equiv(\overline{u'^2})^{\frac{1}{2}}]$ are very large; but the conventional method for the analysis of the electrical signals obtained from a hot-wire anemometer loses its validity for high intensities. Consequently, a re-examination was made of the method, and a new procedure recommended; this study and its results are reported in APPENDIX 3. Turbulence-intensity and mean-velocity data presented below have been calculated from hot-wire signals by the new method.

Other turbulence quantities: $\overline{v'^2}$, $\overline{w'^2}$ and $-\overline{u'v'}$

Also considered in APPENDIX 3 are the methods of analysis for signals obtained from the hot-wire anemometers and from the random-signal correlator used with a cross-wire probe. The conclusion reached is that the conventional procedure leads, for highly-turbulent flow, to results which are considerably in error, particularly for the Reynolds shear stress, $-\overline{u'v'}$. However,

the new method cannot be used, in general, to separate $\overline{v'^2}$ from $\bar{v}^2$, $\overline{u'v'}$ from $\bar{u}.\bar{v}$, etc. Consequently, the little information given below about $\overline{v'^2}$ and $-\overline{u'v'}$ was obtained by the conventional method of analysis.

6.4 Presentation and discussion of results

Tabulated details of the experimental data presented below are given in TABLE 7.

Mainstream velocity

The mainstream-velocity variation, $u_G(x)$, is shown in figure 6.2; the normalising velocity, u_1, is the value of u_G at station 1. It may be seen that blowing has no direct effect on the variation of u_G, although the differences near the step may be attributable to the influence of blowing on the displacement thickness.

Longitudinal turbulence intensity

Profiles of $\tilde{u}'/u_1$ $[\equiv(\overline{u'^2})^{\frac{1}{2}}/u_1]$ are shown in figure 6.3* for each of the three experiments.

For no blowing, the data in figure 6.3(a) show that:

1. The profiles for stations 1 and 5 are little different.
2. The peak intensity moves away from the wall with

---

*Some points near the wall, and also some complete profiles, have been omitted from this figure in the interests of visual clarity.

increase in x.

3. The increase in peak intensity is only about 20%, and the final value of $\tilde{u}'$ only about $0.12u_1$, even though the flow at station 9 was actually within the separated-flow region near the step.

Results similar to the above, shown in figure 6.3(b), were obtained for the porous strip. The only significant difference is in the profile at station 1, which is slightly fuller than that for zero blowing (shown dashed) and has a peak away from the wall. The profiles in figure 6.3(c) show that the effect of fluid injection through the perforated strip was more severe than for the porous strip, and closer to that intended. The initial profile is markedly different from that for no blowing (again shown dashed): the peak is about 40% higher than before, and again away from the wall. Another difference is the decay in peak intensity, between the blowing region and station 5, before the rise as separation was approached.

Profiles of $\tilde{u}'/\overline{u}$ are shown in figure 6.4. These profiles give little more information than those of $\tilde{u}'/u_1$ plotted in figure 6.3, except to show the true levels of turbulence intensity involved, and to re-emphasize the relative effects of blowing through the porous and perforated strips. The spatial-average values of $\tilde{u}'/\overline{u}$

at station 1 are 0.0582, 0.0666 and 0.151, for no blowing, for the porous strip and for the perforated strip, respectively.

Mean-velocity profiles

In figure 6.5 are shown mean-velocity profiles determined with the flattened pitot tube. The profiles are plotted in the form $\overline{u}/u_G$ versus $\log(u_G y/\nu)$ to permit the determination of the local drag coefficient, s_S, by comparison of the logarithmic portion of each profile with a 'standard' log-law profile (Clauser's (1954) method). The log-law constants adopted are those consistent with Patel's (1965) Preston-tube calibration: $\varkappa = 0.419$ and $E = 9.79$. These values are slightly different from those used earlier in this thesis (0.41 and 7.7), but the differences have little effect on the values of s_S obtained.

The logarithmic region is exceptionally well defined in most instances, including that for the profile just downstream of the perforated strip, where the indicated values of $\tilde{u}'/\overline{u}$, for $u_G y/\nu < 2\text{x}10^3$, varied from 0.88 to 0.56. Also, the hump in the profile near $u_G y/\nu = 10^3$ appears to diminish as s_S falls. Nevertheless, uncertainties must attach themselves to mean-velocity measurements when the indicated turbulence intensities are as

high as those found in the present experiments.

The profiles for station 9 in figures 6.5(a) and 6.5 (c) show a region of mean-flow reversal near the wall ($y < 0.25$in). However, it should be noted that a forward-facing pitot tube does not measure accurately the total head in a reversed flow, but rather something close to the static pressure. The profile at station 9 in figure 6.5(b) also shows anomalous behaviour near the wall. But, here again, the velocities determined are unlikely to be of high precision because of the very small values involved (less than 6ft/s for $y < 0.5$in).

Total-pressure profiles

In a flow where there is a rapid pressure rise, the shear forces in the outer part of the boundary layer are small compared with the inertia forces or the pressure gradient. It is easily shown, as follows, that in such a flow the total pressure, P, will remain constant along a streamline, and that this conservation of total pressure can be used as a convenient check on two-dimensionality.

A stream function, ψ, is defined by

$$\frac{\partial \psi}{\partial y} \equiv \omega\overline{u} \quad \text{and} \quad \frac{\partial \psi}{\partial x} \equiv -\omega\overline{v} \qquad (6.4\text{-}1).$$

Then the momentum equation, (2.2-2), may be written in the von Mises form as follows

$$\rho\overline{u}\left.\frac{\partial\overline{u}}{\partial x}\right|_{\psi} + \left.\frac{\partial\overline{p}}{\partial x}\right|_{\psi} = \omega\overline{u}\left.\frac{\partial\tau}{\partial\psi}\right|_{x}$$

(the normal-stress term has been omitted),

or $$\boxed{\frac{\partial}{\partial x}(\overline{p} + \tfrac{1}{2}\rho\overline{u}^2) \equiv \frac{\partial P}{\partial x} = \omega\overline{u}\frac{\partial\tau}{\partial\psi}} \qquad (6.4\text{-}2).$$

Thus, when the stress gradient is negligible, (6.4-2) integrates to give

$$\overline{p} + \tfrac{1}{2}\rho\overline{u}^2 \approx P\{\psi\} ,$$

i.e. the total pressure is constant along a constant-ψ line.

In figure 6.6, total pressures, made non-dimensional with respect to P_G, are plotted against the quantity Ψ. Ψ is defined by

$$\Psi \equiv \int_0^y \overline{u}\, dy \qquad (6.4\text{-}3)$$

and given the dimension of length by division by u_1. Clearly, any lack of two-dimensionality (ω not constant) results in Ψ not being proportional to ψ, and hence in variations from a single curve of the data in figure 6.6 for regions where the stress gradient is negligible.

The data shown in figure 6.6(a), for no blowing, suggest that the condition of two-dimensionality is well satisfied from station 5 onwards. The drop in total pressure upstream, where the static-pressure gradient was

not severe, is consistent with the negative stress gradients which exist in the outer region of a boundary layer.

For the two blowing cases, shown in figure 6.6(b) and (c), the data collapse on to a single curve only for stations 7, 8 and 9. Upstream of station 7, the drop in total pressure may again be attributed to the non-negligibility of the stress gradients, which were almost certainly increased by the action of blowing. An interesting feature of these two figures is that the unique curves to which the downstream profiles eventually collapse are almost identical with each other, but appreciably lower than the corresponding curve for no blowing. This difference also can be attributed to the increased importance of the upstream (negative) stress gradients in the two blowing experiments.

Shape-factor (H_{12}) distribution

Values of H_{12}, determined from velocity profiles measured with both the pitot tube and the hot-wire anemometer, are plotted against distance along the test plate in figure 6.7.

The following observations may be made:

1. For values of H_{12} up to about 2, there is generally good agreement between the two sets of data. For larger values of H_{12}, for which the turbulence intensities are

much greater, the differences become appreciable. The hot wire generally leads to the higher values.

2. The shape factors at station 1 for blowing are evidently higher than for no blowing; and the highest values are for the perforated strip.

3. There is an initial drop in H_{12} downstream of the perforated strip, over the same region as the decay in turbulence intensity noted earlier. But differences between the three sets of data remain all the way along the test plate.

4. The values of H_{12} at station 9 are undoubtedly lower than they should be, because of the measurement errors in the negative velocities observed to occur near the wall.

Wall shear stress

Values of s_S were determined both by Clauser's (1954) method (from the mean-velocity profiles) and from Preston-tube readings with the calibration recommended by Patel (1965). The results are plotted against distance along the test plate in figure 6.8.

The following observations may be made:

1. The agreement between the results of the two methods of determination of s_S is very good; this agreement was to be expected because both procedures are based upon similar assumptions about the universality of the velocity

distribution near the wall.

2. The effect of blowing through the porous strip is nearly to halve the value of s_S at station 1; and for the perforated strip s_S is reduced almost to zero.

3. Downstream of the perforated strip there is a much greater 'recovery' in s_S than downstream of the porous strip.

4. The values of s_S are consistent with those of the shape factor H_{12} (demonstrated quantitatively below).

5. The separation point in each of the three experiments occurs about two step-heights upstream of the step.

Some comment is appropriate at this point on the possible artificiality of values of s_S obtained by the Clauser method*. This artificiality is the result of the possibility that κ and E are not universal constants, but may be altered, for example, by increasing the turbulence intensity of a flow. From the expression for the law-of-the-wall velocity distribution, (3.2-5), which may be written as

$$z = (s_S^{\frac{1}{2}}/\kappa)[\ln(u_G y/\nu)+\ln(E\kappa\{s_S^{\frac{1}{2}}/\kappa\})],$$

---

*Similar remarks apply to other methods which rely upon the universality of the velocity distribution near a wall (e.g. Preston tube).

it is easily seen that the only quantities which can be determined, from the logarithmic region of a mean-velocity profile, are $s_S^{\frac{1}{2}}/\varkappa$ and $E\varkappa$.

In principle, the value of $E\varkappa$ provides the only true test of the 'normality' of the measured velocity distribution near a wall. However, the small inaccuracies present even in the most precise mean-velocity measurements in a turbulent flow, and the strong dependence (through an exponential function) of $E\varkappa$ on the slope of the velocity profile, precludes the test from being a reliable one. For example, the values of $E\varkappa$ indicated by the measurements shown in figure 6.5(a), for no blowing, vary from 1 to 16, compared with the normal value of 4.1.

Nevertheless, if values of s_S are to be determined by the Clauser method, the values of $\varkappa$ and E must be known. Consequently, even for the present writer's blowing experiments, the normal values have been assumed, although it is realised that their use may give rise to artificial values of s_S.

Reynolds-stress profiles

Profiles of the dimensionless total shear stress, s ($\approx -\overline{u'v'}/u_G^2$), at station 1 are shown in figure 6.9. For no blowing the maximum value of s is about 0.0020, for the porous strip 0.0046, and for the perforated strip

0.0040. The profiles of $\tilde{v}'/u_G$, also plotted in figure 6.9, show trends similar to those of the corresponding shear-stress profiles.

The profiles plotted in figure 6.4 show that the values of $\tilde{u}'/\overline{u}$ at the points of maximum shear stress are 0.12, 0.14 and 0.34 for, respectively, no blowing, the porous strip and the perforated strip. Therefore, it seems implausible that the shear stress in the second blowing case was really lower than in the first. It is more likely that the indicated drop is attributable to the invalidity of the method of analysis for highly-turbulent flows (see APPENDIX 3).

The magnitude of the increase in peak shear stress for the porous strip is an important result. The profiles of $\tilde{u}'/u_G$ and $\tilde{v}'/u_G$, in figure 6.9(b), suggest that the rise in $-\overline{u'v'}/u_G^2$ is largely due to the increase in $\tilde{v}'/u_G$. This suggestion is supported by the fact that the correlation coefficient, $-\overline{u'v'}/\tilde{u}'\tilde{v}'$, for no blowing is only a little smaller than that for the porous-strip data. However, since $\tilde{u}'$ is the largest contributor to the turbulent kinetic energy, $\overline{k}$, it is clear that the increase in $-\overline{u'v'}$ is not related to a similarly great increase in $\overline{k}$: $-\overline{u'v'}/\overline{k}$ is not constant.

6.5 Comparisons of data with recommended empirical relations

Shape-factor relation: $H_{12} \sim H_{32}$

Values of H_{12} and H_{32}, deduced both from the data of the pitot tube and from those of the hot-wire anemometer, are plotted in figure 6.10. The numbers adjacent to some of the points indicate the x-stations to which the data refer. The curve shown represents the empirical relation (4.2-1).

The following observations may be made:

1. Both the pitot-tube and the hot-wire data, for $H_{12} < 2.5$, are in satisfactory agreement with the curve.

2. The data at stations 1, 2 and 3 downstream of the perforated strip show appreciable deviations from the curve. The deviations are perhaps due to measurement errors caused by the very high turbulence intensities in these cases. However, it is not improbable that the discrepancy results from the unusual way in which the profile was formed.

3. The discrepancies for the data at station 9 may be attributed to measurement inaccuracies, associated both with the negative velocities near the wall and with the high turbulence intensities at station 9. It is interesting to note that at station 9 the hot-wire data lie

closer to the empirical curve than do the pitot-tube data, although it is unlikely that either instrument indicates the correct velocity in reversed flow.

Drag law

In figure 6.11, experimental values of s_S are plotted against values calculated from the formula recommended in CHAPTER 4, (4.3-19). The experimental values correspond to the smooth curve drawn through the Clauser-plot and Preston-tube data of figure 6.7. The solid symbols designate values of s_S computed from R_2 and H_{32}, and the open ones values obtained from R_2 and H_{12} with the aid of the shape-factor relation, (4.2-1). The numbers against some of the points again designate x-stations.

The following observations may be made:

1. For the most part, the difference between calculation and experiment is less than 10%. It is possible, of course, that the agreement is artificially introduced, because the bulk of the data on which (4.3-19) was based were obtained by the Clauser method. The discussion on p. 153 relates to this point.

2. The discrepancies between calculation and experiment, greatest when s_S is small, are reduced when s_S is calculated from R_2 and H_{12}, rather than by the more direct method from R_2 and H_{32}.

Shear-work-integral ($\bar{s}$) relation

The table below shows comparisons between values of $\bar{s}$, computed from the shear-stress profiles at station 1 shown in figure 6.9, and values obtained from the correlation formula recommended in CHAPTER 4, (4.4-20).

	Experiment	(4.4-20)
No blowing	0.0015	0.0014
Porous strip	0.0027	0.0015
Perforated strip	0.0022	0.0025

The following conclusions are drawn from the comparisons:

1. The agreement for no blowing is within the experimental uncertainty.

2. The discrepancy for the porous strip indicates that the increase in shear stress in this situation was far larger than expected and the correlation formula is clearly inadequate in this case.

3. The direction of the discrepancy for the perforated strip adds confirmation to the conclusion, drawn on p.155, that the measurements here are seriously in error.

The lack of reliable information about the shear stress, and so $\bar{s}$, for the downstream stations leaves an

unfortunate gap in this section. However, some further conclusions about the adequacy of the $\bar{s}$-relation are drawn from the shape-factor calculations, discussed below.

6.6 Predicted values of R_2 and H_{12}

R_2-calculations

The results are shown in figure 6.12(a) of calculations carried out to check the two-dimensionality of the mean flow for the three experiments reported. The closed symbols represent data obtained with the pitot tube, and the open ones the hot-wire data. The calculations were performed in a manner similar to that for the calculations discussed in CHAPTER 5. Experimental values of H_{12}, F_2 and s_S were used to evaluate the right-hand side of the momentum equation (2.3-25); and the ω- and cross-flow pressure-gradient terms were omitted. The full curves represent calculations in which the pressure gradient was evaluated from the pressure distribution along the wall, $p_S\{x\}$; and the dashed curves were determined with $p_G\{x\}$.

The following observations may be made:

1. The use of p_S rather than p_G in some of the calculations more than compensates for the omission of the cross-flow pressure-gradient term.

2. The calculations based upon p_S are in better agreement with the data than those which use p_G. Even so, the full curves (p_S) still fall somewhat below the data for the farthest-downstream stations; and it should be remembered that the 'true' curve must lie somewhere in between the S and G curves.

3. For no blowing, the agreement between the calculations and experiment is at least as good as for many previously-reported comparable situations (see figure 5.1). And even in the two blowing cases, the discrepancies are only of the same order as the experimental uncertainty (indicated by the differences between the hot-wire and pitot-tube data).

4. The agreement between the calculated and experimental distributions of R_2 adds confirmation to the conclusion drawn from the total-pressure profiles, plotted in figure 6.6, that the flows reported here were quite accurately two-dimensional.

Shape-factor (H_{12}) calculations

Predictions of H_{12} are compared with experiment in figure 6.12(b)*. As in figure 6.12(a), the closed symbols

*It should be noted that the calculations were terminated once the value of s_S had fallen to zero, i.e. H_{12} to about 2.71. Also, it has not been considered realistic to present data downstream of station 8 (it will be recalled that some of the data at station 9 were found to indicate reversed flow).

represent the pitot-tube data and the open ones the hot-wire data; again, too, the full curves are based upon p_S and the dashed ones upon p_G. The calculations were carried out with the kinetic-energy method of CHAPTER 4.

The following conclusions are drawn from the calculations:

1. The values of H_{12} based upon p_S are significantly higher than those based upon p_G, and generally in better agreement with the experimental data.

2. For the two blowing cases, the fall in H_{12} just downstream of the blowing section is predicted to occur either not at all or much too slowly. That this failure can be attributed directly to the fact that the theoretical values of $\overline{s}$ (obtained from 4.4-20) are too small can be seen from the shape-factor equation, (2.3-29):

$$R_2 dH_{32}/dR_x = 2\overline{s} - H_{32}s_S + (H_{12}-1)H_{32}F_2$$

(normal-stress term omitted). This equation shows that if the value of $\overline{s}$ is too small, so too will be that of H_{32}, and hence (from the shape-factor relation, 4.2-1) the value of H_{12} will be too big.

3. The data downstream of the perforated strip are of particularly uncertain precision, because of the high turbulence intensities encountered. However, additional calculations started at station 3 downstream of the per-

forated strip are evidently in better agreement with the remaining data.

4. In the region where H_{12} is decreasing, the calculations have suggested that the theoretical values of $\overline{s}$ are too small. The discrepancies far downstream, where H_{12} is increasing, suggest that there smaller values would be appropriate. The conclusion might be drawn from these two observations that $\overline{s}$ should depend upon dH_{12}/dR_x. However, it is quickly seen from the shape-factor equation that a dependence upon F_2 amounts to the same thing as a dependence upon dH_{12}/dR_x. It was shown in CHAPTER 4 (p.103) that the available data for $\overline{s}$ lend no support to the proposition that F_2 should be one of the arguments of the $\overline{s}$-function.

6.7 Concluding remarks

1. Injection of air through a perforated strip increases the average level of turbulence intensity in the boundary layer by almost ten times the amount achieved by blowing at the same rate through porous material.

2. The changes in R_2, H_{12}, H_{32} and s_S brought about by blowing are appreciable, but these quantities are still quite well correlated by the formulae recommended in CHAPTER 4. The greatest discrepancies arise when the turbulence intensity is so great as to give rise to serious

doubt about the measurements themselves.

3. In all three experiments, the turbulence intensity, $\tilde{u}'/\bar{u}$, was for the most part too high (> 30%) to permit the evaluation of $-\overline{u'v'}$ and $\overline{v'^2}$ from hot-wire measurements.

4. Just downstream of the porous strip, an increase in the value of $\tilde{u}'/\bar{u}$ of only about 20% over the value for no blowing was associated with more than a 100% increase in $-\overline{u'v'}$.

5. Indirect evidence, deduced from calculations of H_{12} performed with the kinetic-energy method of CHAPTER 4, suggests that the value of $\bar{s}$ (and hence those of $-\overline{u'v'}/u_G^2$) was greatly increased by blowing through the perforated strip.

6. The results of the shape-factor calculations were more satisfactory when the pressure gradient was evaluated from p_S rather than p_G. This observation suggests that in the present experiments the cross-flow pressure gradient is not negligible so far as the shape-factor calculations are concerned.

CHAPTER 7

CONCLUSIONS

7.1 Principal results of the present study

The aims of this study, which were set out in section 1.2, have in the main been achieved, specifically:

1. The survey of experimental data on turbulent boundary layers has yielded the collection of data listed in TABLE 1.

2. Previous recommendations for the auxiliary relations used in the entrainment and kinetic-energy calculation procedures were discussed in detail in CHAPTERS 3 and 4, respectively. It was concluded that for the most part these recommendations are limited in range of applicability, incapable of extension to situations other than those for which they were devised, and of poor accuracy of prediction. Where necessary, new empirical recommendations were given which are free from the drawbacks of the earlier proposals. The new and old recommendations for the auxiliary relations used in the kinetic-energy method are summarised in TABLES 2, 3, 4 and 6.

3. Both the entrainment and kinetic-energy calculation procedures, with the recommended auxiliary relations, have been used to calculate the development of a large

number of boundary layers. The results of these two sets of calculations, which were reported in CHAPTER 5, were little different. This finding contrasts with the behaviour of previously-existing calculation methods, reported by Thompson (1964), for which the results varied widely.

4. In general, the accuracy of the predictions of H_{12} obtained with the new methods is as high as for the best of the earlier procedures, though the latter are of much more limited applicability. It was concluded in CHAPTER 5 that where poor predictions are obtained, usually in severe adverse pressure gradients, the cause is probably a lack of two-dimensionality of the mean flow. In some cases, however, some of the restrictions laid down in CHAPTER 1 are not well satisfied; this too may have contributed to the discrepancies observed.

5. The experimental investigation, reported in CHAPTER 6, revealed that the total shear stress in a boundary layer is considerably increased by quite modest increases in the turbulence intensity. This conclusion was supported by the results of shape-factor calculations performed with the kinetic-energy method. Unfortunately, however, the turbulence intensities encountered in the experiments were too great in most regions to permit the direct measurement of the shear stress.

Except in the immediate vicinity of the perforated strip, the experimental data were well correlated by the shape-factor relation and drag law recommended in CHAPTER 4.

7.2 Re-appraisal of the present study, and suggestions for further work

The two calculation methods which have been discussed in detail in this thesis are of wider validity than any previously-recommended procedure. Also, the auxiliary relations used in the two methods, and particularly the kinetic-energy method, are more accurate in both their qualitative and quantitative predictions than earlier proposals. The kinetic-energy method can be recommended for use where the requirement is for a quick and accurate calculation procedure. This method also has the advantage of being easy to understand and use.

Nevertheless, the disadvantage of any integral procedure is that it is limited to types of flow for which experimental data are available. Interpolation is possible, but extrapolation generally uncertain. Extension to situations where mass-transfer surface-roughness or variable-property effects are important is also impossible, and progress requires more and more experimental data. The writer considers, therefore, that future

theoretical work must be aimed at providing a more fundamental link between the profiles of shear stress, velocity, turbulent kinetic energy, etc., than, say, an $\overline{s}$-relation.

The mathematical difficulties involved in the solution of the partial differential conservation equations for mass, momentum and turbulent kinetic energy have been overcome to a large extent by Patankar and Spalding (1967). Also, an acceptable shear-stress hypothesis may not be too difficult to provide, for Patankar and Spalding have shown that the simple ramp-function mixing-length proposal of Escudier (1965) leads to quite accurate predictions of many of the features of turbulent flows. And there is little doubt that the Kolmogorov (1942) - Prandtl (1945) turbulent-kinetic-energy hypothesis will lead to even better predictions.

The predictions of the methods discussed in the present thesis may be regarded as setting the standards of accuracy which more fundamental procedures must equal and eventually surpass. New procedures must also, of course, predict correctly the relationships between R_2, H_{12}, H_{32}, s_S, $\overline{s}$, etc.; the recommendations of CHAPTER 4 provide the means for checking these predictions.

The paucity of extensive experimental investigations of the shear stress in turbulent boundary layers was mentioned in CHAPTER 4; and even some of the measurements

which have been reported are of uncertain reliability. Far more information about the shear stress is undoubtedly required, particularly for boundary layers in extreme adverse pressure gradients and also for those with abnormally high turbulence intensities.

REFERENCES

1. Baker, E. "Influence of mass transfer on surface friction at a porous surface." Mech. Eng. Dept., Imperial Col., Ph.D. Thesis, 1967.

2. Bradshaw, P. "The turbulence structure of equilibrium boundary layers." NPL Aero. Rep. 1184, 1966.

3. Bradshaw, P. Progress report on work reported in Bradshaw, Ferriss and Atwell (1967), 1967.

4. Bradshaw, P. and Ferriss, D.H. "The response of a retarded equilibrium turbulent boundary layer to the sudden removal of pressure gradient." NPL Aero. Rep. 1145, 1965.

5. Bradshaw, P., Ferriss, D.H. and Atwell, N.P. "Calculation of boundary-layer development using the turbulent energy equation." J. Fluid Mech. 28, p.593, 1967.

6. Bradshaw, P. and Galea, P.V. "Step-induced separation of a turbulent boundary layer in incompressible flow." J. Fluid Mech. 27, p.111, 1967.

7. Bradshaw, P. and Gee, M.T. "Turbulent wall jets with and without an external stream." ARC R&M 3252, 1962.

8. Bradshaw, P. and Johnson, R.F. "Turbulence measurements with hot wire anemometers." NPL Notes on Appl. Sci. No.33, 1963.

9. Bradshaw, P. and Pankhurst, R.C. "The design of low-speed wind tunnels." From "Progress in Aeronautical Science." 5, p.1, Pergamon Press: London, 1964.

10. Brebner, G.G. and Bagley, J.A. "Pressure and boundary-layer measurements on a two-dimensional wing at low speed." ARC R&M 2886, 1956.

11. "British Standard Code: Flow measurement." B.S. 1042, British Standards Institution, London, 1951.

12. Carmichael, A.D. and Pustintsev, G.N. "Prediction of turbulent boundary layer development in conical diffusers." J. Mech. Eng. Sci. 8, p.426, 1966.

13. Clauser, F.H. "Turbulent boundary layers in adverse pressure gradients." J. Aero. Sci. 21, p.91, 1954.

14. Clauser, F.H. "The turbulent boundary layer." Adv. in App. Mech., IV, pt.1, New York: Academic Press, 1956.

15. Coles, D. "The law of the wake in the turbulent boundary layer." J. Fluid Mech. 1, p.191, 1956.

16. Coles, D.E. "The turbulent boundary layer in a compressible fluid." Rand Corp. Rep. R-403-PR, 1962.

17. Collis, D.C. and Williams, M.J. "Two-dimensional convection from heated wires at low Reynolds numbers." J. Fluid Mech. 6, p.357, 1959.

18. Cornish, J.J. "A universal description of turbulent boundary layer profiles with or without transpiration." Mississippi State Univ., Aerophys. Dept., Res. Rep. 29, 1960.

19. Curle, N. "A two-parameter method for calculating the two-dimensional incompressible laminar boundary layer." J. Roy. Aero. Soc. 71, p.117, 1967.

20. Dean, R.C. "Aerodynamic measurements." MIT Press, Cambridge, Mass., 1963.

21. Doenhoff, A.E. von and Tetervin, N. "Determination of general relations for the behaviour of turbulent boundary layers." NACA TR 772, 1943.

22. Dwight, H.B. "Mathematical tables of elementary and some higher mathematical functions." 2nd Edn., Dover Publications: New York, 1958.

23. Emmons, H.W. "Shear-flow turbulence." Proc. 2nd U.S. Nat. Congr. App. Mech. ASME, p.1, 1954.

24. Erian, F. and Eskinazi, S. "The wall-jet in a longitudinal pressure gradient." Mech. and Aerospace Eng. Dept., Syracuse Univ., Rep. ME 937-6410F, 1964.

25. Escudier, M.P. "The distribution of the mixing length in turbulent flows nears walls." Mech. Eng. Dept., Imperial Col., Rep. TWF/TN/1, 1965.

26. Escudier, M.P. and Nicoll, W.B. "A single explicit drag law for uniform-density turbulent boundary layers and wall jets on smooth impermeable walls." Mech. Eng. Dept., Imperial Col., Rep. TWF/TN/5, 1965.

27. Escudier, M.P. and Nicoll, W.B. "The entrainment function in turbulent boundary-layer and wall-jet calculations." J. Fluid Mech. 25, p.337, 1966a.

28. Escudier, M.P. and Nicoll, W.B. "The shear-work-integral relation in calculations of turbulent boundary layers." Mech. Eng. Dept., Imperial Col., Rep. TWF/TN/18, 1966b.

29. Escudier, M.P., Nicoll, W.B. and Spalding, D.B. "An explicit drag law for uniform-density turbulent bounday layers on smooth, impermeable walls." Mech. Eng. Dept., Imperial Col., Rep. TWF/TN/12, 1966.

30. Escudier, M.P., Nicoll, W.B., Spalding, D.B. and Whitelaw, J.H. "Decay of a velocity maximum in a turbulent boundary layer." Aero. Qtly. 18, p.121, 1967.

31. Escudier, M.P., and Spalding, D.B. "A note on the turbulent uniform-property hydrodynamic boundary layer on a smooth impermeable wall; comparisons of theory with experiment." ARC CP 875, 1966.

32. Fage, A. "Profile and skin-friction aerofoil drags." ARC R&M 1852, 1938.

33. Fage,A. and Falkner, V.M. "An experimental determination of the intensity of friction on the surface of an aerofoil." ARC R&M 1315, 1930.

34. Falkner, V.M. "The resistance of a smooth flat plate with turbulent boundary layer." Aircraft Eng. 15, 1943.

35. Felsch, K.-O. "Beitrag zur Berechnung turbulenter Grenzschichten in zweidiminsionaler inkompressibler Strömung." Technischen Hochschule, Karlsruhe, Dr.-Ing. Dissert, 1965.

36. Fernholz, H. "A new empirical relationship between the form-parameters H_{32} and H_{12} in boundary layer theory." J. Roy. Aero. Soc. 66, p.588, 1962.

37. Fernholz, H. von "Halbempirische Gesetze zur Berechnung turbulenter Grenzschichten nach der Methode der Integralbedingungen." Ing. Arch. 33, p.384, 1964.

38. Gault, D.E. "Boundary-layer and stalling characteristics of the NACA 63-009 airfoil section." NACA TN 1894, 1949.

39. Glauert, M.B. "The wall jet." J. Fluid Mech. 1, p. 625, 1956.

40. Glushko, G.S. "Turbulent boundary layer on a flat plate in an incompressible fluid." Izv. Akad. Nauk. SSSR Mekh. 4, p.13, 1965.

41. Goldberg, P. "Upstream history and apparent stress in turbulent boundary layers." MIT GTL Rep. 85, 1966.

42. Goldstein, R.J., Shavit, G. and Chen, T.S. "Film-cooling effectiveness with injection through a porous section." J. Heat Trans. 87, p.353, 1965.

43. Harrison, L. "Powder metallurgy." Eng. Materials and Design Conf., London, 1960.

44. Head, M.R. "Entrainment in the turbulent boundary layer." ARC R&M 3152, 1960.

45. Herring, H.J. and Norbury, J.F. "Some experiments on equilibrium boundary layers in favourable pressure gradients." J. Fluid Mech. 27, p.541, 1967.

46. Hinze, J.O. "Turbulence. An introduction to its mechanism and theory." McGraw-Hill: New York, 1959.

47. Hudimoto, B. "Momentum equations for the boundary layer and their application to the turbulent boundary layer." Mem. Fac. Eng., Kyoto Univ., 13, p.162, 1951.

48. Jayatillaka, C.L.V. "The influence of Prandtl number and surface roughness on the resistance of the laminar sub-layer to momentum and heat transfer." Imperial Col., Mech. Eng. Dept., Ph.D. Thesis, 1966.

49. Kawasaki, T. "On an approximate solution of the two-dimensional turbulent boundary layer." Trans. Jap. Soc. Aero. and Space Sci. 4, p.1, 1961.

50. Kehl, A. "Untersuchungen über konvergente und divergente turbulente Reibungsschichten." Ing. Arch. 13, p.293, 1943.

51. King, L.V. "On the convection of heat from small cylinders in a stream of fluid." Phil. Trans. Roy. Soc. 214, p.373, 1914.

52. Klebanoff, P.S. "Characteristics of turbulence in a boundary layer with zero pressure gradient." NACA Rep. 1247, 1955.

53. Klebanoff, P.S. and Diehl, Z.W. "Some features of artificially thickened fully developed turbulent boundary layers with zero pressure gradient." NACA Rep. 1110, 1952.

54. Kolmogorov, A.N. Izv. Akad. Nauk SSSR ser. phys. 1-2, 1942.

55. Kruka, V. and Eskinazi, S. "The wall jet in a moving stream." J. Fluid Mech. 20, p.555, 1964.

56. Lewkowicz, A.K. and Horlock, J.H. "An implicit approach to calculation of two-dimensional turbulent boundary layers." Mech. Eng. Dept., Liverpool Univ. ULME B.19, 1966.

57. Libby, P.A., Baronti, P.O. and Napolitano, L. "Study of the incompressible turbulent boundary layer with pressure gradient." AIAA J. 2, p.445, 1964.

58. Ludwieg, H. and Tillmann, W. "Untersuchungen über die Wandschubspannung in turbulenten Reibungsschichten." Ing. Arch. 17, p.288, 1949. Translated as: "Investigations of the wall shearing stress in turbulent boundary layers." NACA TM 1285, 1950.

59. Macmillan, F.A. "Experiments on pitot tubes in shear flow." ARC R&M No.3028, 1956.

60. Maskell, E.C. "Approximate calculation of the turbulent boundary layer in two-dimensional incompressible flow." RAE Rep. Aero. 2443, 1951.

61. Mathieu, J. "Contribution a l'etude aerothermique d'un jet plan evoulant en presence d'une paroi." Publ. Sci. et Tech. 374, 1961.

62. Mathieu, J. and Tailland, A. "Etude d'un jet plan dirige tangentiellement a une paroi." C.R. Acad. Sci. Aerodynamique 256, 1963.

63. McDonald, H. and Stoddart, J.A.P. "On the development of the incompressible turbulent boundary layer." BAC Aero. Rep. 223, 1965.

64. Mellor, G.L. "Turbulent boundary layers with arbitrary pressure gradients and divergent or convergent cross flows." Dept. Aerospace and Mech. Sci., Princeton Univ., Rep. 775, 1966.

65. Mellor, G.L. and Gibson, D.M. "Equilibrium turbulent boundary layers." J. Fluid Mech. 24, p.225, 1966.

66. Moses, H.L. "The behaviour of turbulent boundary layers in adverse pressure gradients." MIT GTL Rep. 73, 1964.

67. Mueller, T.J., Korst, H.H. and Chow W.L. "On the separation, reattachment, and redevelopment of incompressible turbulent shear flow." J. Basic Eng., Trans. ASME 84D, p.221, 1964.

68. Myers, G.E., Schauer, J.J. and Eustis, R.H. "The plane turbulent wall jet. Pt.1, Jet development and friction factor." Mech. Eng. Dept., Stanford Univ., Tech. Rep. 1, 1961.

69. Nash, J.F. "A note on skin-friction laws for the incompressible turbulent boundary layer." NPL Aero. Rep. 1135, 1965.

70. Newman, B.G. "Some contributions to the study of the turbulent boundary layer near separation." ARCC Rep. ACA-53, 1951.

71. Nicoll, W.B. "Wall jet velocity profiles and entrainment." Mech. Eng. Dept., Imperial Col., Rep. IC/HRJ/23, 1965.

72. Nicoll, W.B. and Escudier, M.P. "Empirical relationships between the shape factors H_{32} and H_{12} for uniform-density turbulent boundary layers and wall jets." AIAA J. 4, p.940, 1966.

73. Patankar, S.V. and Spalding, D.B. "A calculation procedure for heat transfer by forced convection through two-dimensional uniform-property turbulent boundary layers on smooth impermeable walls." Proc. 3rd Int. Ht. Trans. Conf., Chicago, 2, p.50, 1966.

74. Patankar, S.V. and Spalding, D.B. "A finite-difference procedure for solving the boundary-layer equations for two-dimensional flows." Mech. Eng. Dept., Imperial Col., Rep. TWF/TN/20, 1967.

75. Patankar, S.V. and Wolfshtein, M. "A computer programme for hydrodynamic and heat-transfer calculations of turbulent boundary layers and wall jets." Mech. Eng. Dept., Imperial Col., Rep. TWF/TN/16, 1966.

76. Patel, R.P. "Measurement of the Reynolds stresses in a circular pipe as a means of testing a DISA constant-temperature hot wire-anemometer." Mech. Eng. Res. Lab., McGill Univ. TN 63-6, 1963.

77. Patel, V.C. "Calibration of the Preston tube and limitations on its use in pressure gradients." J. Fluid Mech. 23, p.185, 1965.

78. Philip, J.R. "Analysis of turbulent boundary layers with zero pressure gradient." ZAMP 10, 1959.

79. Prandtl, L. Reports of the Aerod. Versuchsanst. Göttingen, 1st series 136, 1921.

80. Prandtl, L. "Uber die ausgebildete Turbulenz." ZAMM 5, 1925.

81. Prandtl, L. "Uber ein neues Formelsystem für die ausgebildete Turbulenz." Nach. Akad. Wiss. Göttingen, Math-phys., p.6, 1945.

82. Ross, D. "Integration of the Reynolds equations for incompressible turbulent boundary layers." Ord. Res. Lab., Penn. State Univ., Rep. NOrd 7958-286, 1953a.

83. Ross, D. "Evaluation of the momentum integral equations for turbulent boundary layers." J. Aero. Sci. 20, p.502, 1953b.

84. Ross, D. and Robertson, J.M. "A superposition analysis of the turbulent boundary layer in an adverse pressure gradient." J. App. Mech. 18, p.95, 1951.

85. Rotta, J. "Uber die theorie der turbulenten Grenzschichten." Mitt. MPI Strömm. Forsch. 1, 1950. Translated as: "On the theory of the turbulent boundary layer." NACA TM 1344, 1953.

86. Rotta J. "Schubspannungs verteilung und Energiedissipation bei turbulenten Grenzschichten." Ing. Arch. 20, p.195, 1952.

87. Rotta,J. "Näherungsverfahren zur Berechnung turbulenter Grenzschichten unter Benutzung des Energiesatzes." Mitt. MPI Strömm. Forsch. 8, 1953.

88. Rotta, J.C. "Turbulent boundary layers in incompressible flow." From: "Progress in Aeronautical Sciences." 2, p.1, Pergamon Press: London, 1962.

89. Rubert, K.F. and Persh, J. "A procedure for calculating the development of turbulent boundary layers under the influence of adverse pressure gradients." NACA TN 2478, 1951.

90. Sandborn, V.A. and Slogar, R.J. "Study of the momentum distribution of turbulent boundary layers in adverse pressure gradients." NACA TN 3264, 1955.

91. Schlichting, H. "Boundary layer theory." 4th Edn., McGraw-Hill: New York, 1960.

92. Schmidbauer, H. "Turbulente Reibungsschicht an erhaben gekrümmten Flächen." Luftfahrtforschung 13, p.160, 1936. Translated as: "Turbulent friction layers along convex surfaces." NACA TM 791, 1936.

93. Schubauer, G.B. and Klebanoff, P.S. "Investigation of separation of the turbulent boundary layer." NACA Rep. 1030, 1951.

94. Schubauer, G.B. and Spangenberg, W. "Forced mixing in boundary layers." J. Fluid Mech. 8, p.10, 1960.

95. Schuh, H. "On determining turbulent boundary layer separation in incompressible flow." J. Aero. Sci. 22, 1955.

96. Schultz-Grunow, F. "Neues Reibungswiderstandsgesetz für glatte Platten." Luftfahrtforschung 17, p.239, 1940. Translated as: "New frictional resistance law for smooth plates." NACA TM 986, 1941.

97. Schwarz, W.H. and Cosart, W.P. "The two-dimensional turbulent wall jet." J. Fluid Mech. 10, p.481, 1961.

98. Shigemitsu, Y. "Velocity defect law of turbulent boundary layer." Rep. of Transportation Tech. Res. Inst., Rep. 51, 1962.

99. Sigalla, A. "Experimental data in turbulent wall jets." Aircraft Eng. 30, p.131, 1958.

100. Smith, D.W. and Walker, J.H. "Skin friction measurements in incompressible flow." NACA TN 4231, 1958.

101. Spalding, D.B. "A unified theory of friction, heat transfer and mass transfer in the turbulent boundary layer and wall jet." ARC 25 925, 1964a.

102. Spalding, D.B. "A unified theory of friction, heat transfer and mass transfer in the turbulent boundary layer and wall jet." Mech. Eng. Dept., Imperial Col., 1964b. (annotated version of Spalding, 1964a).

103. Spalding, D.B. "The kinetic-energy-deficit equation of the turbulent boundary layer." AGARDograph 97, pt.1, 1965a.

104. Spalding, D.B. "A relation between entrainment rate, shear-stress gradient and velocity gradient. Mech. Eng. Dept., Imperial Col., Rep. TWF/TN/8, 1965b.

105. Spalding, D.B. "Notes on the present form and status of the 'unified theory'." Mech. Eng. Dept., Imperial Col., 1965c.

106. Spalding, D.B. "Progress in the development of a unified theory of friction, heat transfer and mass transfer, in boundary layers and jets." Mech. Eng. Dept., Imperial Col., Rep. TWF/TN/10, 1966.

107. Spalding, D.B. "Heat transfer from turbulent separated flows." J. Fluid Mech. 27, p.97, 1967.

108. Spangenberg, W., Rowland, W.R. and Mease, N.E. "Measurements in a turbulent boundary layer maintained in a nearly separating condition." From: "Fluid Mechanics of internal flow." p.110, Elsevier Publ. Co.: Amsterdam, 1967.

109. Spence, D.A. "The development of turbulent boundary layers." J. Aero. Sci. 23, p.3, 1956.

110. Spence, D.A. Ph.D. Dissertation, Cambridge University, 1952.

111. Spence, D.A. "Prediction of the characteristics of two-dimensional aerofoils." J. Aero. Sci. 21, p.577, 1954.

112. Spence, D.A. "The calculation of the boundary layer." From: "Incompressible Aerodynamics II." Oxford University Press, 1960.

113. Squire, H.B. and Young, A.D. "The calculation of the profile drag of aerofoils." ARC R&M 1838, 1938.

114. Stratford, B.S. "An experimental flow with zero skin friction throughout its region of pressure rise." J. Fluid Mech. 5, p.17, 1959.

115. Szablewski, W. "Berechnung der turbulenten Strömung längs der ebenen Platte." ZAMM 31, 1951.

116. Tani, I. "Energy dissipation in turbulent boundary layers." J. Aero. Sci. 23, p.606, 1956.

117. Thompson, B.G.J. "A critical review of existing methods of calculating the turbulent boundary layer." ARC 26 109, 1964.

118. Thompson, B.G.J. "The calculation of shape-factor development in incompressible turbulent boundary layers with or without transpiration." AGARDOgraph 97, p.159, 1965.

119. Townsend, A.A. "The structure of the turbulent boundary layer." Proc. Camb. Phil. Soc. 47, p.375, 1951.

120. Trezek, G.J. and Robertson, J.M. "On the energy equation of turbulent boundary-layer flow." Univ. of Illinois Rep., 1965.

121. Truckenbrodt, E. "Ein Quadraturverfahren zur Berechnung der laminaren und turbulenten Reibungsschicht bei ebener und rotationssymmetrischer Strömung." Ing. Arch. 20, p.211, 1951. Translated as: "A method of quadrature for calculation of the laminar and turbulent boundary layer in case of plane and rotationally symmetrical flow." NACA TM 1379, 1955.

122. Uram, E.M. "Skin-friction calculation for turbulent boundary layers in adverse pressure distributions." J. Aero/Space Sci. 27, p.75, 1960.

123. Walz, A. "Beitrag zur Näherungstheorie kompressibler turbulenter Grenzschichten." DVL-B No.84, 1959.

124. Walz, A. "Beitrag zur Näherungstheorie kompressibler turbulenter Grenzschichten." DVL-B No.136, 1960.

125. Walz, A. "Uber Fortschritte in Näherungstheorie und Praxis der Berechnung kompressibler laminarer und turbulenter Grenzschichten mit Wärmeübergang." Zeit. Flug. 13, p.89, 1965.

126. Whitelaw, J.H. "An experimental investigation of the two-dimensional wall jet." ARC Rep. 28 179, HMT 106, 1966.

127. Wieghardt, K. "Zum Reibungswiderstand rauher Platten." ZWB, KWI, Göttingen,U&M 6612, 1944.

128. Wieghardt, K. "Turbulente Reibungsschichten." Göttinger Monograph B5, 1945.

129. Wieghardt, K. "Hot air discharge for de-icing." AAF Translation No.F-Ts-919-RE, 1946.

130. Dryden, H.L. "Some recent contributions to the study of transition and turbulent boundary layers." NACA TN 1168, 1947.

NOMENCLATURE

Symbol	Meaning	Equation of first appearance
a_i, b_i	constants and/or parameters in polynomial mean-velocity profile	3.2-1
A, B	constants in hot-wire-response equation	A.3-1
C	universal constant (roughness dependent) in law-of-wall velocity distribution (intercept for $\ln(y^+) = 0$)	3.2-6
C	empirical constant in logarithmic function in denominator of new drag law	4.3-11
C	empirical constant in new $\overline{s}$-relation	4.4-9
C_i	empirical constants in $g\{\zeta^{-1}\}$ function of new drag law	4.3-18
E	universal constant (roughness dependent) in law-of-wall velocity distribution [$= \exp(\varkappa C)$]	3.2-5
E	instantaneous voltage drop across hot wire	A.3-1
$f\{...\}$	function of ...	
F_2	pressure-gradient parameter	2.3-22
G	shape factor of mean-velocity-defect profile	3.3-23
H_1	shape factor of mean-velocity profile defined by Head (1958)	2.3-18
H_{12}	shape factor of mean-velocity profile	2.3-19
H_{32}	shape factor of mean-velocity profile	2.3-20
I_n	integral function of mean-velocity profile	2.3-10
k	instantaneous turbulent kinetic energy	2.2-11

K	function appearing in Nash's (1965) drag law	4.3-22
K	constant of proportionality in Goldberg's (1966) differential equation for $\overline{s}$	-
ℓ	logarithmic function in denominator of new drag law	-
ℓ	Prandtl mixing length	-
ℓ'	logarithmic function (parameter) appearing in Spalding's (1964a) form of wall-plus-wake mean-velocity-profile expression	3.2-9
$-\dot{m}''_G$	rate of entrainment into boundary layer from mainstream	2.3-2
m_G	dimensionless value of $\dot{m}''_G$	2.3-23
n	exponent of $\lvert 1-\zeta \rvert$ in new $\overline{s}$-relation	4.4-9
n	exponent of u_N in hot-wire-response equation	A.3-1
p	instantaneous local static pressure	2.2-2
P	instantaneous local total (dynamic-plus-static) pressure	-
R	rms deviation	-
R_G	Reynolds number based upon u_G and y_G	2.3-12
R_m	Reynolds number based upon flow rate within boundary layer	2.3-13
R_{max}	Reynolds number based upon u_m and y_m	4.3-13
R_x	Reynolds number based upon u_G and x	2.3-17
R_1	Reynolds number based upon u_G and δ_1	2.3-14
R_2	Reynolds number based upon u_G and δ_2	2.3-15
R_3	Reynolds number based upon u_G and δ_3	2.3-16

s	dimensionless value of τ	2.3-9
s_S	local skin-friction (wall-drag) coefficient (conventional symbol $c_f/2$)	2.3-21
$\bar{s}$	shear-work integral	2.3-11
u, v, w	instantaneous velocity components in three coordinate directions, x, y, z	2.2-1
$-\overline{u'v'}$, $-\overline{v'w'}$, $-\overline{w'u'}$	Reynolds shear stresses	2.2-3
$\overline{u'^2}$, $\overline{v'^2}$, $\overline{w'^2}$	Reynolds normal stresses (turbulence intensities)	2.2-2
u_G	mainstream velocity	2.2-6
u_m	maximum value of $\bar{u}$ in boundary layer	4.3-12
u_N	instantaneous (total) velocity normal to hot wire	A.3-1
u_τ	friction velocity	-
u^+	dimensionless value of $\bar{u}$	3.2-2
v_S	local normal velocity at wall (of fluid injected into boundary layer)	-
w_1	difference between $\bar{u}$ and $\bar{v}$	A.3-19
w_2	sum of $\bar{u}$ and $\bar{v}$	A.3-21
x	distance measured along wall in mainstream direction	2.2-1
x_o	virtual origin of converging or diverging boundary layer	2.2-5
y	distance measured normal to and outward from wall	2.2-1
y_C	height of slot for tangential injection of fluid	-
y_G	thickness of boundary layer: value of y for which $\bar{u} = u_G$	2.3-1
y^+	dimensionless value of y	3.2-2

z	dimensionless value of $\bar{u}$	2.3-7
z	distance measured normal to x-y plane	-
z_E	Spalding's (1964a) mean-velocity-profile wake parameter	3.2-9
α	angle which principal axis of turbulent stress tensor makes with direction of mean flow	-
β	Clauser's (1954) pressure-gradient parameter	3.3-21
δ_1	displacement thickness of boundary layer	3.3-22
δ_2	momentum-deficit thickness of boundary layer	-
δ_3	mean-kinetic-energy-deficit thickness of boundary layer	-
ε	dissipation rate of mean turbulent kinetic energy	2.2-11
ζ	shape factor defined in terms of H_1 or H_{32}	A.2-6, 4.3-3
η_i	integral function of mean-velocity profile in wall jet	4.3-12
$\varkappa$	von Kármán's mixing-length constant (slope of log-law velocity distribution)	3.2-2
λ	dimensionless value of Prandtl mixing length	4.4-2
λ_G	value of λ in central and outer regions of boundary layer	4.4-3
μ	molecular dynamic viscosity of boundary-layer fluid	-
ν	molecular kinematic viscosity of boundary-layer fluid	2.2-4
ν_{eff}	effective (total) kinematic viscosity of fluid in turbulent flow	4.4-1

ξ	dimensionless value of y	2.3-8
Π	Coles' (1954) mean-velocity profile wake parameter	3.2-2
ρ	density of boundary-layer fluid	2.2-1
σ_S	local skin-friction (wall-drag) coefficient for wall jet	4.3-13
τ	total (viscous-plus-turbulent) shear stress	2.2-2
ψ	stream function	6.4-1
Ψ	function defined by ψ/ω	6.4-3
ω	distance between adjacent stream-planes normal to wall	2.2-1

Subscripts	Condition pertained to
eq	equilibrium boundary layer
G	edge of boundary layer
m, max	maximum value of $\overline{u}$ in boundary layer
S	wall
S	edge of constant-stress layer near wall
sepn	separating boundary layer
$\frac{1}{2}$	position in boundary layer, farthest from wall, where $\overline{u} = (u_m+u_G)/2$
1,2	wires 1 and 2 in a crossed-wire hot-wire probe

Overbars, etc.

straight overbar	(e.g. $\overline{E}$) temporal mean value	)
curly overbar	(e.g. $\tilde{E}'$) rms value	)of a time-varying quantity
prime	(e.g. E') fluctuating component	)

Author(s)	Date	x(ft)	u_G(ft/s)	R_2	H_{12}	H_{32}	ζ	$10^3 s_S$	ℓ'	z_E	$10^3\overline{s}$	$10^3\overline{s}_{eq}$	Comments
1. Bradshaw	1966	1.92 3.92 5.42 6.92	143 129 123 119	9.17,3 1.48,4 1.83,4 2.17,4	1.451 1.386 1.389 1.397	1.735 1.759 1.753 1.747	0.582 0.625 0.610 0.605	1.12 1.055 1.015 0.94	10.04 10.42 10.70 10.75	0.820 0.824 0.830 0.803	 1.04	1.27 1.16 1.13 1.04	1) Equilibrium flow, β=0.9. 2) s_S from Preston tube. 3) $\overline{s}$ from hot wires. 4) ν=1.6x10^{-4} ft^2/s.
2. Bradshaw and Ferriss 1	1965	1.92 3.92 5.42 6.92	145 121 112 105	1.50,4 2.62,4 3.22,4 3.79,4	1.653 1.591 1.556 1.564	1.643 1.664 1.675 1.671	0.418 0.458 0.478 0.470	0.725 0.66 0.625 0.615	9.97 10.33 10.43 10.45	0.655 0.648 0.636 0.632	 1.516	1.798 1.669 1.530 1.517	1) Equilibrium flow, β=5.4. 2) s_S from Preston tube. 3) $\overline{s}$ from hot wires. 4) ν=1.6x10^{-4} ft^2/s.
3. Bradshaw and Ferriss 2	1965	3.92 4.42 4.92 5.42 5.92 6.92 7.92	114 112 110 110 110 110 110	2.46,4 2.67,4 2.77,4 2.80,4 2.78,4 2.86,4 2.92,4	1.572 1.557 1.522 1.471 1.426 1.377 1.343	1.669 1.674 1.686 1.705 1.724 1.747 1.764	0.467 0.476 0.497 0.531 0.564 0.603 0.631	0.675 0.695 0.745 0.835 0.89 0.94 0.96	10.55 10.60 10.70 10.70 10.84 10.96 11.04	0.668 0.682 0.713 0.754 0.789 0.820 0.835	1.497 1.392 1.349 1.221 1.189 1.128 1.110		1) Boundary layer recovering from $\beta\approx$5.4 to β=0. 2) s_S from Preston tube. 3) $\overline{s}$ from hot wires. 4) ν=1.6x10^{-4} ft^2/s.

TABLE 1. Summary of experimental data for uniform-property turbulent boundary layers.

Author(s)	Date	x(ft)	u_G(ft/s)	R_2	H_{12}	H_{32}	ζ	$10^3 s_S$	ℓ'	z_E	$10^3\overline{s}$	$10^3\overline{s}_{eq}$	Comments
4. Brebner and Bagley 1	1956	1.57 1.99 2.245 2.38 2.50	105 101 97.2 95.1 96.8	9.23,2 1.69,3 2.15,3 2.48,3 3.38,3	1.873 1.429 1.371 1.338 1.220								1) Boundary layer on symmetrical wing RAE 101, 0° incidence. 2) $\nu=1.56\times10^{-4}$ ft²/s.
5. Brebner and Bagley 2	1956	0.75 1.00 1.57 1.99 2.25 2.38 2.50	125 120 110 103 98.3 95.8 93.4	1.18,3 1.76,3 2.94,3 3.91,3 4.68,3 5.14,3 6.85,3	1.321 1.351 1.584 1.498 1.536 1.566 1.594								1) 4.09° incidence. 2) $\nu=1.56\times10^{-4}$ ft²/s.
6. Brebner and Bagley 3	1956	0.75 1.00 1.57 1.99 2.25 2.38 2.50	134 127 113 105 99.4 96.9 95.2	2.78,3 3.57,3 4.75,3 6.76,3 7.85,3 8.65,3 1.10,4	1.424 1.459 1.615 1.661 1.725 1.979 1.923								1) 8.18° incidence. 2) $\nu=1.56\times10^{-4}$ ft²/s.
7. Clauser 1	1954	6.92 11.0 12.8 18.6 23.8 26.9 29.7 32.3	32.5 29.1 28.0 25.2 23.6 22.5 21.8 21.2	6.13,3 9.08,3 9.82,3 1.20,4 1.52,4 1.64,4 1.69,4 1.86,4	1.565 1.526 1.512 1.479 1.434 1.462 1.445 1.440	1.712 1.692 1.703 1.713 1.729 1.715 1.721 1.723	0.543 0.508 0.527 0.545 0.572 0.548 0.558 0.562	1.06 0.935 0.94 0.96 0.985 0.93 0.95 0.92	9.53 9.79 9.82 10.03 10.35 10.36 10.48 10.46	0.757 0.730 0.735 0.758 0.793 0.782 0.786 0.775		1.378 1.310 1.307 1.312 1.370 1.360 1.361 1.352	1) Equilibrium flow, $\beta\approx1.8$. 2) s_S from Clauser plot. 3) $\nu=1.58\times10^{-4}$ ft²/s.
8. Clauser 2	1954	7.50 9.00 11.0 12.7 16.2 19.2 23.9 26.7	26.1 24.8 23.5 22.8 21.3 20.2 18.9 18.1	8.26,3 1.00,4 1.15,4 1.37,4 1.82,4 2.03,4 2.67,4 3.11,4	1.768 1.800 1.818 1.820 1.768 1.969 1.846 1.858	1.635 1.608 1.607 1.611 1.626 1.635 1.640 1.636	0.403 0.350 0.348 0.356 0.386 0.403 0.413 0.405	0.63 0.57 0.54 0.53 0.51 0.50 0.47 0.42	9.25 9.36 9.59 9.69 9.93 10.08 10.31 10.41	0.577 0.546 0.538 0.543 0.548 0.549 0.545 0.520		1.557 1.649 1.662 1.672 1.867 2.315 2.699 3.425	1) Equilibrium flow, $\beta\approx8$. 2) s_S from Clauser plot. 3) $\nu=1.58\times10^{-4}$ ft²/s.

Author(s)	Date	x/L	u_G/U	R_2	H_{12}	H_{32}	ζ	$10^3 s_S$	ℓ'	z_E	$10^3\overline{s}$	$10^3\overline{s}_{eq}$	Comments
9. von Doenhoff and Tetervin 1	1943	0.075 0.15 0.25 0.35 0.45 0.55 0.60	1.510 1.508 1.442 1.392 1.308 1.180 1.131	7.65,2 1.04,3 1.33,3 1.86,3 2.34,3 3.42,3 4.27,3	1.808 1.599 1.551 1.572 1.641 1.985 2.593								1) Boundary layer on aerofoil NACA 65(216)-222 (approx.), 8.1° incidence. 2) $UL/\nu = 9.2\times10^5$
10. von Doenhoff and Tetervin 2	1943	0.075 0.15 0.25 0.35 0.45 0.55 0.60	1.550 1.523 1.468 1.419 1.360 1.212 1.141	2.40,3 2.97,3 3.68,3 4.55,3 5.45,3 7.97,3 1.27,4	1.654 1.562 1.510 1.489 1.514 1.872 2.583								1) 8.1° incidence. 2) $UL/\nu = 2.67\times10^6$.
11. von Doenhoff and Tetervin 3	1943	0.075 0.15 0.25 0.35 0.45 0.55	1.616 1.548 1.482 1.428 1.340 1.171	2.44,3 3.31,3 4.00,3 5.58,3 6.83,3 1.24,4	1.563 1.474 1.476 1.522 1.571 2.177								1) 10.1° incidence. 2) $UL/\nu = 2.64\times10^6$.
12. von Doenhoff and Tetervin 4	1943	0.2 0.3 0.4 0.5 0.6 0.7 0.8	1.518 1.478 1.408 1.364 1.323 1.212 1.118	2.54,3 2.98,3 3.36,3 3.88,3 4.60,3 5.83,3 7.95,3	1.370 1.366 1.325 1.326 1.399 1.541 1.902								1) Boundary layer on aerofoil NACA nose-opening shape 13, 9.1° incidence 2) $UL/\nu = 4.18\times10^5$.
		x(ft)	u_G(ft/s)										
13. Fage and Falkner, and Fage 1	1930 1938	1.33 1.67 2.00 2.34	95.2 91.6 88.6 85.3	1.06,3 1.59,3 2.08,3 2.39,3	1.401 1.395 1.404 1.385	1.782 1.772 1.760 1.766	0.661 0.644 0.624 0.634	2.21 2.24 1.92 2.025 1.73 1.89 1.67 1.94	8.54 8.69 8.83 8.95	0.980 0.929 0.885 0.892			1) Boundary layer on Joukowski aerofoil. 2) s_S from Clauser plot; alternate values from

Author(s)	Date	x(ft)	u_G(ft/s)	R_2	H_{12}	H_{32}	ζ	$10^3 s_s$	ℓ'	z_E	$10^3\bar{s}$	$10^3\bar{s}_{eq}$	Comments
13. Fage and Falkner, and Fage 1 (cont.)	1930	2.67	81.6	2.97,3	1.397	1.754	0.618	1.52 1.475	9.00	0.856			Stanton surface tubes.
	1938	3.16	76.4	3.96,3	1.445	1.732	0.577	1.30 1.40	9.11	0.801			3) $\nu=1.59\times10^{-4}$ ft^2/s.
14. Fage and Falkner, and Fage 2	1930	1.67	68.7	1.02,3	1.442	1.765	0.633	2.14 2.16	8.37	0.946			1) s_s from Clauser plot; alternate values from Stanton surface tubes.
	1938	2.00	66.5	1.49,3	1.409	1.766	0.634	1.90 2.11	8.56	0.909			
		2.34	63.9	1.77,3	1.410	1.760	0.624	1.80 2.07	8.65	0.896			
		2.67	61.2	2.23,3	1.429	1.749	0.606	1.64 1.54	8.71	0.860			2) $\nu=1.74\times10^{-4}$ ft^2/s.
		3.16	57.1	2.91,3	1.477	1.733	0.579	1.38 1.345	8.79	0.797			
15. Gault 1	1949	3.0	196	2.64,3	1.386								1) Boundary layer on aerofoil NACA 63-009, 0° incidence.
		3.5	190	3.86,3	1.373								
		4.0	184	5.16,3	1.357								
		4.25	181	5.95,3	1.382								
		4.5	175	6.39,3	1.361								
		4.75	172	6.89,3	1.373								2) $\nu\approx1.6\times10^{-4}$ ft^2/s.
16. Gault 2	1949	1.5	230	5.18,3	1.439								1) 4° incidence.
		2.0	227	6.51,3	1.439								
		2.5	216	7.59,3	1.463								
		3.0	209	9.93,3	1.439								
		3.5	199	1.21,4	1.446								
		4.0	193	1.36,4	1.473								
		4.25	188	1.48,4	1.472								
		4.5	182	1.63,4	1.482								
		4.75	178	1.70,4	1.476								2) $\nu\approx1.6\times10^{-4}$ ft^2/s.
17. Gault 3	1949	1.5	242	7.04,3	1.426								1) 6° incidence.
		2.0	233	8.53,3	1.400								
		2.5	224	1.06,4	1.436								
		3.0	214	1.27,4	1.444								
		3.5	203	1.49,4	1.478								
		4.0	195	1.74,4	1.505								
		4.25	190	1.90,4	1.523								
		4.5	183	1.97,4	1.516								
		4.75	178	2.16,4	1.524								2) $\nu\approx1.6\times10^{-4}$ ft^2/s.

Author	Date	x(ft)	u_G(ft/s)	R_2	H_{12}	H_{32}	ζ	$10^3 s_S$	ℓ'	z_E	$10^3\overline{s}$	$10^3\overline{s}_{eq}$	Comments
18. Gault 4	1949	1.5 2.0 2.5 3.0 3.5 4.0 4.25 4.5 4.75	254 244 231 220 214 195 190 183 178	9.92,3 1.26,4 1.56,4 1.78,4 2.16,4 2.40,4 2.64,4 2.86,4 2.96,4	1.426 1.406 1.446 1.472 1.481 1.583 1.607 1.600 1.595								1) 8.5° incidence. 2) $\nu \approx 1.6\times10^{-4}$ ft²/s.
19. Herring and Norbury 1	1963	2 3 4 5	84.6 90.5 97.1 104	3.58,3 3.75,3 3.97,3 4.29,3	1.294 1.290 1.288 1.287	1.824	0.728	1.795 1.79 1.76 1.775	9.63	0.991	1.485	1.468	1) Equilibrium flow, $\beta \approx -0.35$. 2) s_S from Clauser plot 3) $\nu \approx 1.7\times10^{-4}$ ft²/s.
20. Herring and Norbury 2	1963	3 4	101 115	3.79,3 3.59,3	1.254 1.250	1.848	0.762	1.875 1.91	9.82	1.029	1.54	1.462	1) Equilibrium flow, $\beta \approx -0.53$. 2) s_S from Clauser plot. 3) $\nu \approx 1.7\times10^{-4}$ ft²/s.
21. Klebanoff	1955	10.5	50	7.25,3	1.314	1.788	0.670	1.41	9.97	0.906	1.235	1.251	1) Fully-developed zero pressure-gradient boundary layer. 2) s_S from extrapolated s-ζ profile. 3) $\overline{s}$ from hot-wires. 4) $\nu = 1.69\times10^{-4}$ ft²/s.
22. Klebanoff and Diehl 1	1952	7.5 8.5 9.5 10.5	108	4.37,3 5.45,3 6.36,3 7.17,3	1.46 1.45 1.45 1.52								1) Zero pressure-gradient, natural transition. 2) $\nu = 1.65\times10^{-4}$ ft²/s.

Author(s)	Date	x(ft)	u_G(ft/s)	R_2	H_{12}	H_{32}	ζ	$10^3 s_S$	ℓ'	z_E	$10^3\overline{s}$	$10^3\overline{s}_{eq}$	Comments
23. Klebanoff and Diehl 2	1952	4.17 4.67 5.17 6.0 7.5 10.5	108	1.43,3 2.64,3 2.97,3 4.18,3 4.67,3 7.73,3	1.87 1.66 1.55 1.48 1.42 1.52								1) Zero pressure-gradient, recovering from 0.04 in. rod disturbance. 2) $\nu=1.65\times10^{-4}$ ft^2/s.
24. Klebanoff and Diehl 3	1952	4.17 4.25 4.67 5.17 6.0 7.5 8.5 9.5 10.5	108	5.39,3 5.99,3 4.35,3 5.10,3 6.12,3 7.77,3 8.98,3 1.03,4 1.13,4	2.95 1.98 1.57 1.455 1.405 1.395 1.40 1.35 1.38								1) Zero pressure-gradient, recovering from 0.25 in. rod disturbance. 2) $\nu=1.65\times10^{-4}$ ft^2/s.
25. Klebanoff and Diehl 4	1952	2.0 3.5 4.5 6.5 10.5	43	2.86,3 3.41,3 3.60,3 4.53,3 6.06,3	1.51 1.45 1.48 1.445 1.42								1) Zero-pressure gradient, recovering from mesh-screen disturbance. 2) $\nu=1.65\times10^{-4}$ ft^2/s.
26. Klebanoff and Diehl 5	1952	2.08 2.5 3.0 4.0 5.0 5.5 6.5 7.5 8.5 9.5 10.5	35	2.64,3 2.82,3 2.95,3 3.21,3 3.53,3 3.64,3 4.09,3 4.41,3 4.66,3 4.92,3 5.20,3	1.72 1.59 1.525 1.445 1.445 1.46 1.45 1.415 1.415 1.395 1.42								1) Zero pressure-gradient, recovering from sandpaper-strip disturbance. 2) $\nu=1.65\times10^{-4}$ ft^2/s.
27. Klebanoff and Diehl 6	1952	2.08 2.5 3.0	55	4.05,3 4.32,3 4.54,3	1.77 1.58 1.46								1) Zero pressure-gradient, recovering from

Author(s)	Date	x(ft)	u_G(ft/s)	R_2	H_{12}	H_{32}	ζ	$10^3 s_S$	ℓ'	z_E	$10^3\overline{s}$	$10^3\overline{s}_{eq}$	Comments
27. Klebanoff and Diehl 6 (cont.)	1952	4.0 5.0 5.5 6.5 7.5 8.5 9.5 10.5	55	5.16,3 5.52,3 5.43,3 6.19,3 6.51,3 7.06,3 7.42,3 7.82,3	1.46 1.42 1.45 1.445 1.38 1.385 1.37 1.405								sandpaper-strip disturbance. 2) $\nu=1.65\times10^{-4}$ ft^2/s.
28. Klebanoff and Diehl 7	1952	2.08 2.5 3.0 4.0 5.0 5.5 6.5 7.5 8.5 9.5 10.5	108	7.99,3 8.38,3 8.72,3 9.39,3 1.06,4 1.03,4 1.18,4 1.22,4 1.31,4 1.40,4 1.49,4	1.78 1.53 1.48 1.485 1.415 1.405 1.415 1.39 1.375 1.375 1.35								1) Zero pressure-gradient, recovering from sandpaper-strip disturbance. 2) $\nu=1.65\times10^{-4}$ ft^2/s.
29. Ludwieg and Tillmann A	1949	2.59 4.21 5.85 7.50 9.14 10.3 10.9 11.6 12.3 12.9 13.6 14.2	111 107 101 93.9 89.0 85.5 84.6 81.6 80.4 79.0 77.5 75.9	6.25,3 8.94,3 1.23,4 1.54,4 1.92,4 2.20,4 2.44,4 2.65,4 2.86,4 3.18,4 3.50,4 3.84,4	1.334 1.364 1.383 1.412 1.447 1.475 1.483 1.511 1.536 1.561 1.589 1.615			1.444 1.303 1.122 1.024 0.936 0.864 0.812 0.784 0.773 0.692 0.650 0.605					1) Moderate adverse pressure gradient. 2) s_S from heated element. 3) $\nu\approx1.64\times10^{-4}$ ft^2/s.
30. Ludwieg and Tillmann B	1949	2.59 4.21 5.85 7.50 9.14 10.3 10.9	108 102 94.6 89.0 81.0 77.0 75.2	5.50,3 8.10,3 1.15,4 1.48,4 2.03,4 2.37,4 2.78,4	1.330 1.367 1.443 1.442 1.527 1.598 1.640			1.529 1.274 1.122 1.018 0.829 0.718 0.610					1) High adverse pressure gradient. 2) s_S from heated element.

Author(s)	Date	x(ft)	u_G(ft/s)	R_2	H_{12}	H_{32}	ζ	$10^3 s_S$	ℓ'	z_E	$10^3\overline{s}$	$10^3\overline{s}_{eq}$	Comments
30. Ludwieg and Tillmann B (cont.)	1949	11.6 12.3 12.9	73.7 72.6 72.6	3.25,4 3.70,4 4.76,4	1.721 1.792 2.038			0.538 0.488 0.376					3) $\nu \approx 1.61\times10^{-4}$ ft^2/s.
31. Ludwieg and Tillmann C	1949	2.59 4.21 5.85 7.50 9.14 10.3 10.9 11.6 12.3 12.9 13.6 14.2	37.8 44.0 51.3 58.3 66.4 72.5 75.2 77.9 82.5 84.7 86.7 90.3	1.04,3 1.36,3 1.64,3 2.07,3 2.53,3 2.86,3 2.99,3 3.18,3 3.24,3 3.76,3 3.97,3 4.08,3	1.330 1.276 1.281 1.279 1.295 1.289 1.283 1.278 1.266 1.292 1.287 1.283			2.352 2.237 2.134 2.016 1.849 1.815 1.772 1.747 1.789 1.722 1.697 1.656					1) Favourable pressure gradient. 2) s_S from heated element. 3) $\nu \approx 1.66\times10^{-4}$ ft^2/s.
32. Ludwieg and Tillmann 1	1949	0.62 1.61 2.59 3.58 4.73 5.71 6.54 7.52 8.50 9.50 10.5 11.5 12.4 13.4 14.4	204 194 187 181 174 166 160 154 146 138 131 126 122 120 119	4.06,3 6.51,3 9.31,3 1.15,4 1.41,4 1.73,4 1.97,4 2.23,4 2.66,4 3.18,4 3.80,4 4.46,4 5.11,4 5.72,4 6.05,4	1.396 1.361 1.345 1.352 1.370 1.404 1.398 1.406 1.441 1.502 1.538 1.590 1.627 1.647 1.630								1) Moderate adverse pressure gradient. 2) $\nu \approx 1.66\times10^{-4}$ ft^2/s.
33. Ludwieg and Tillmann 2	1949	2.59 3.58 4.73 5.71 6.54 7.52 8.50	158 156 151 144 138 136 131	7.35,3 1.09,4 1.16,4 1.45,4 1.68,4 1.91,4 2.12,4	1.328 1.328 1.350 1.423 1.406 1.407 1.401								1) Slight adverse pressure gradient. 2) $\nu \approx 1.58\times10^{-4}$ ft^2/s.

	Author(s)	Date	x(ft)	u_G(ft/s)	R_2	H_{12}	H_{32}	ζ	$10^3 s_S$	ℓ'	z_E	$10^3\overline{s}$	$10^3\overline{s}_{eq}$	Comments
33.	Ludwieg and Tillmann 2 (cont.)	1949	9.50 10.5 11.5 12.4 13.4 14.4	127 123 120 117 115 112	2.43,4 2.33,4 3.36,4 3.43,4 3.72,4 3.76,4	1.433 1.470 1.469 1.448 1.442 1.430								
34.	Ludwieg and Tillmann 3	1949	2.59 3.58 4.73 5.71 6.54 7.52 8.50 9.50 10.5 11.5 12.4 13.4 14.4 15.4	182 178 172 167 161 155 148 141 133 127 123 121 118 117	8.15,3 1.01,4 1.20,4 1.46,4 1.70,4 2.00,4 2.34,4 2.92,4 3.52,4 4.22,4 5.18,4 6.66,4 7.12,4 7.66,4	1.308 1.343 1.349 1.330 1.347 1.349 1.377 1.386 1.485 1.560 1.632 1.753 1.819 1.820								1) High adverse pressure gradient. 2) $\nu \approx 1.63 \times 10^{-4}$ ft^2/s.
35.	Ludwieg and Tillmann 4	1949	1.61 2.59 3.58 4.73 5.71 6.54 7.52 8.50 9.50 10.5 11.5 12.4 13.4 14.4 15.4	95.9 94.5 92.5 89.9 88.0 85.0 82.4 79.4 75.8 71.9 68.9 67.6 67.2 65.6 65.0	3.72,3 4.92,3 6.00,3 7.41,3 9.42,3 1.08,4 1.26,4 1.40,4 1.70,4 2.05,4 2.50,4 3.34,4 4.10,4 4.61,4 5.17,4	1.351 1.339 1.350 1.371 1.408 1.417 1.444 1.456 1.501 1.552 1.593 1.693 1.959 2.010 2.012								1) High adverse pressure gradient. 2) $\nu \approx 1.59 \times 10^{-4}$ ft^2/s.
36.	Moses 1	1964	0 0.17 0.33 0.67 1.00 1.33	100 99.8 99.6 99.2 98.8 98.0	7.80,2 9.33,2 1.29,3 1.54,3 1.94,3	1.38 1.41 1.365 1.40 1.36								1) Axisymmetric flow along cylinder, high adverse pressure gradient.

Author(s)	Date	x(ft)	u_G(ft/s)	R_2	H_{12}	H_{32}	ζ	$10^3 s_S$	ℓ'	z_E	$10^3\overline{s}$	$10^3\overline{s}_{eq}$	Comments
36. Moses 1 (cont.)	1964	1.67	97.3	2.15,3	1.40								2) $\nu \approx 1.6\times10^{-4}$ ft^2/s.
		2.00	94.3	2.52,3	1.41								
		2.33	87.2	3.31,3	1.475								
		2.67	73.2	6.75,3	1.85								
37. Moses 2	1964	0	100	7.80,2	1.38			2.42					1) Severe adverse pressure gradient
		0.17	98.2	9.20,2				2.29					2) s_S from Clauser plot.
		0.33	96.1										3) $\overline{s}$ from hot wires.
		0.42	94.8	1.33,3	1.41			2.075					4) $\nu \approx 1.6\times10^{-4}$ ft^2/s
		0.50	93.6										
		0.67	91.0	1.75,3	1.405			1.915					
		0.83	88.8										
		0.92	87.2	2.09,3	1.435	1.749	0.606	1.75	8.59	0.876	1.78		
		1.00	86.5										
		1.17	83.2	2.53,3	1.425			1.585					
		1.33	80.8										
		1.42	79.0	3.16,3	1.46			1.38					
		1.50	78.2										
		1.67	74.3	3.67,3	1.58	1.691	0.503	1.195					
		1.83	71.4										
		1.92	69.9	4.82,3	1.675			0.85					
		2.00	68.4										
		2.17	64.8	5.58,3	1.885			0.53					
		2.33	61.2										
		2.50	60.0	6.43,3	2.425			0.185					
		2.67	59.8										
		2.83	58.1										
		3.00	58.0										
38. Moses 3	1964	0	100	7.80,2	1.380								1) Severe adverse pressure gradient.
		0.17	93.0										2) $\nu \approx 1.6\times10^{-4}$ ft^2/s.
		0.25	89.5	1.26,3	1.43								
		0.33	84.8										
		0.50	78.8	2.05,3	1.51								
		0.67	72.5										
		0.83	66.9	3.30,3	1.70								
		1.00	62.0										
		1.17	58.7	5.19,3	2.15								
		1.33	56.8										
		1.50	55.1										
		1.67	53.5										

Author(s)	Date	x(ft)	u_G(ft/s)	R_2	H_{12}	H_{32}	ζ	$10^3 s_S$	ℓ'	z_E	$10^3\overline{s}$	$10^3\overline{s}_{eq}$	Comments
38. Moses 3 (cont.)	1964	1.83	52.0										
		2.00	51.0										
		2.17	49.2										
		2.33	49.2										
		2.50	47.3										
		2.67	45.6										
		2.83	44.7										
		3.00	44.7										
39. Moses 4	1964	0	100	7.80,2	1.385								1) Severe adverse pressure gradient. 2) $\nu \approx 1.6 \times 10^{-4}$ ft^2/s.
		2	92.8	1.21,3	1.430								
		4	84.9	1.55,3	1.505								
		6	76.2	2.08,3	1.64								
		8	67.2	5.04,3	2.135								
		10	63.9										
		12	64.0										
40. Moses 5	1964	0	100	8.84,2	1.36								1) Initially severe adverse pressure gradient, followed by near-zero gradient. 2) $\nu \approx 1.6 \times 10^{-4}$ ft^2/s.
		0.17	93.0	1.35,3	1.435								
		0.33	83.6	1.96,3	1.475								
		0.50	74.1	2.80,3	1.65								
		0.67	67.2	3.53,3	2.10								
		0.83	62.5	5.46,3	2.145								
		1.00	61.0										
		1.04	60.0	5.93,3	2.16								
		1.17	60.0										
		1.29	58.7	6.18,3	1.805								
		1.33	59.8										
		1.50	59.6	6.29,3	1.587								
		1.67	59.2										
		1.71	59.2	6.50,3	1.465								
		1.83	59.5										
		1.96	59.6	6.66,3	1.40								
		2.00	59.6										
		2.17	59.5	6.88,3	1.39								
		2.33	60.0										
		2.42	59.8	6.90,3	1.35								
		2.50	59.6										
		2.67	60.0	6.87,3	1.35								
		2.83	58.7										
		2.92	58.5	7.00,3									

Author(s)	Date	x(ft)	u_G(ft/s)	R_2	H_{12}	H_{32}	ζ	$10^3 s_S$	ℓ'	z_E	$10^3\overline{s}$	$10^3\overline{s}_{eq}$	Comments
40. Moses 5 (cont.)	1964	3.00 3.17	58.3 54.0										
41. Moses 6	1964	0 0.17 0.33 0.50 0.67 0.83 1.00 1.04 1.17 1.29 1.33 1.50 1.67 1.71 1.83 2.00 2.17 2.33 2.42 2.52 2.67 2.83	100 95.3 88.8 83.0 76.8 74.0 72.9 72.9 72.9 72.9 72.9 72.9 72.9 72.6 72.5 72.6 72.6 73.0 72.9 72.9 71.5 69.3	8.84,2 1.39,3 2.90,3 3.58,3 3.87,3 4.01,3 4.21,3 4.35,3 4.44,3 	1.36 1.37 1.55 1.525 1.51 1.43 1.413 1.368 1.33 								1) Initially moderate adverse pressure gradient followed by near-zero gradient. 2) $\nu \approx 1.6 \times 10^{-4}$ ft^2/s.
42. Newman 1	1951	4.76	33.0	8.96,3	2.204	1.544	0.203	0.225	8.83	0.322	3.85		1) Symmetrical rear-stalling aerofoil, severe adverse pressure gradient. 2) s_S from Clauser plot. 3) $\overline{s}$ from hot wires. 4) $\nu = 1.56 \times 10^{-4}$ ft^2/s.

Author(s)	Date	x(ft)	u_G(ft/s)	R_2	H_{12}	H_{32}	ζ	$10^3 s_S$	ℓ'	z_E	$10^3\overline{s}$	$10^3\overline{s}_{eq}$	Comments
43. Newman 2	1951	2.01	152	5.59,3	1.689	1.653	0.437	0.75	9.15	0.634	1.28		1) Severe adverse pressure gradient. 2) s_S from Clauser plot. 3) $\overline{s}$ from hot wires. 4) $\nu=1.56\times10^{-4}$ ft^2/s.
		2.76	134	9.15,3	1.666	1.645	0.422	0.70	9.58	0.612	1.45		
		3.51	120	1.36,4	1.687	1.628	0.390	0.485	9.63	0.517	1.67		
		4.02	112	1.71,4	1.861	1.595	0.323	0.375	9.73	0.459	1.92		
		4.51	104	2.15,4	1.902	1.581	0.293	0.31	9.80	0.421	2.22		
		4.76	101	2.42,4	2.133	1.551	0.221	0.175	9.71	0.313	3.06		
		4.93	100	2.72,4	2.397	1.522	0.137	0.05	9.17	0.160	3.09		
44. Sandborn and Slogar	1955	0	54	2.68,3	1.413	1.775	0.649	1.60	9.25	0.902	1.50		1) Moderate adverse pressure gradient. 2) s_S from Clauser plot; alternate values (at x=0.25 ft. etc.) from heated element. 3) $\overline{s}$ from hot wires. 4) $\nu=1.74\times10^{-4}$ ft^2/s.
		0.25						1.53					
		1.35	52	3.69,3	1.264	1.843	0.759	1.40	9.55	0.870	1.45		
		1.62						1.78					
		2.84	48	6.14,3	1.393	1.765	0.633	1.15	9.80	0.809	1.37		
		3.09						1.24					
		4.32	43	8.01,3	1.620	1.670	0.469	0.70	9.52	0.614	1.17		
		4.55						0.72					
45. Schubauer and Klebanoff	1951	17.5	160	1.80,4	1.297	1.799	0.688	1.18	11.22	0.939	1.12		1) Boundary layer on aero-foil-shaped shaped wall, severe adverse pressure gradient.
		18.0	159	1.86,4	1.307	1.796	0.683						
		18.5	157	2.00,4	1.318	1.790	0.674	1.05	10.92	0.864	1.06		
		19.0	154	2.21,4	1.338	1.778	0.654						
		19.5	151	2.27,4	1.339	1.778	0.654	0.98	10.93	0.843	1.07		
		20.0	148	2.43,4	1.403	1.772	0.644	0.95	10.99	0.825	1.26		
		20.5	144	2.70,4	1.393	1.750	0.608	0.815	10.80	0.754	1.03		
		21.0	141	2.87,4	1.427	1.736	0.584	0.75	10.81	0.723	1.29		
		21.5	138	3.11,4	1.464	1.718	0.553	0.70	10.88	0.704	1.50		
		22.0	134	3.56,4	1.509	1.704	0.529	0.61	10.88	0.654	1.37		

Author(s)	Date	x(ft)	u_G(ft/s)	R_2	H_{12}	H_{32}	ζ	$10^3 s_S$	ℓ'	z_E	$10^3\overline{s}$	$10^3\overline{s}_{eq}$	Comments
45. Schubauer and Klebanoff (cont.)	1951	22.5	130	4.18,4	1.570	1.672	0.472	0.59	10.84	0.641	1.22		2) s_S from Clauser plot. 3) $\overline{s}$ from hot wires. 4) $\nu \approx 1.6\times10^{-4}$ ft²/s.
		23.0	127	4.41,4	1.608	1.667	0.463	0.48	10.93	0.584	1.35		
		23.5	123	4.62,4	1.666	1.647	0.426	0.43	10.95	0.555	1.50		
		24.0	120	5.39,4	1.835	1.606	0.346	0.29	10.74	0.446	1.75		
		24.5	116	5.78,4	1.976	1.585	0.301	0.225	10.66	0.390			
		25.0	114	6.78,4	2.301	1.530	0.163	0.10	10.34	0.252	2.47		
		25.4	113	7.09,4	2.365	1.523	0.140	0.092	10.32	0.242	2.30		
		25.8	112	7.64,4	2.839	1.500	0.	0.047	10.20	0.170			
46. Schubauer and Spangenberg A	1960	-0.83	83.9	2.81,3	1.255	1.840	0.754	1.70	9.20	0.926			1) Moderate adverse pressure gradient. 2) s_S from Clauser plot. 3) $\nu = 1.65\times10^{-4}$ ft²/s.
		0	82.0	3.53,3	1.285	1.816	0.716	1.58	9.39	0.910			
		0.83	81.1	4.22,3	1.288	1.810	0.706	1.54	9.47	0.906			
		1.67	78.9	5.72,3	1.302	1.800	0.690	1.38	10.00	0.906			
		2.5	75.1	7.31,3	1.439	1.739	0.589	1.15	9.91	0.820			
		3.33	70.7	8.71,3	1.511	1.702	0.526	0.96	9.88	0.747			
		4.17	64.6	1.16,4	1.665	1.652	0.435	0.645	9.85	0.608			
47. Schubauer and Spangenberg B	1960	0	82.0	4,08,3	1.358	1.784	0.664	1.56	9.38	0.904			1) High adverse pressure gradient. 2) s_S from Clauser plot. 3) $\nu = 1.59\times10^{-4}$ ft²/s.
		1.67	79.5	5.47,3	1.328	1.797	0.685	1.37	9.61	0.867			
		3.33	74.5	7.84,3	1.395	1.754	0.614	1.23	10.02	0.859			
		5.00	67.6	1.15,4	1.489	1.710	0.539	0.94	9.99	0.748			
		6.67	61.1	1.57,4	1.640	1.653	0.437	0.67	9.95	0.629			
		8.33	54.9	2.02,4	1.813	1.606	0.346	0.44	9.89	0.506			
		10.0	50.6	2.92,4	2.070	1.536	0.179	0.205	9.85	0.344			
48. Schubauer and Spangenberg C	1960	0	82.0	3.16,3	1.297	1.833	0.743	1.64	9.28	0.917			1) Severe adverse pressure gradient. 2) s_S from Clauser plot. 3) $\nu = 1.68\times10^{-4}$ ft²/s.
		1.67	80.5	5.15,3	1.259	1.824	0.728	1.45	9.96	0.926			
		3.33	78.0	6.80,3	1.290	1.802	0.693	1.34	10.00	0.893			
		5.0	69.8	1.05,4	1.385	1.790	0.674	1.08	10.19	0.816			
		6.67	66.0	1.24,4	1.483	1.731	0.576						
		8.33	61.5	1.60,4	1.566	1.679	0.485	0.76	10.08	0.678			
		10.0	56.9	1.95,4	1.700	1.634	0.401	0.55	9.98	0.571			
		11.7	52.8	2.23,4	1.746	1.620	0.374	0.525	10.10	0.565			
		13.3	48.8	2.70,4	1.845	1.599	0.331	0.42	10.16	0.508			
		15.0	48.3	3.24,4	2.001	1.618	0.370	0.42	10.48	0.524			
		16.7	45.3	4.32,4	2.616	1.519	0.129						
49. Schubauer and Spangenberg D	1960	0	82.0	3.04,3	1.241	1.858	0.782	1.66	9.30	0.925			1) High adverse pressure gradient. 2) s_S from Clauser plot.
		2.5	70.1	6.83,3	1.491	1.713	0.545	1.09	9.53	0.767			
		5.0	58.6	1.47,4	1.776	1.619	0.372	0.52	9.84	0.547			
		7.5	50.3	2.00,4	1.873	1.581	0.293	0.35	9.69	0.442			
		9.58	45.7	2.79,4	2.191	1.526	0.148	0.18	9.71	0.318			

Author(s)	Date	x(ft)	u_G(ft/s)	R_2	H_{12}	H_{32}	ζ	$10^3 s_S$	ℓ'	z_E	$10^3\overline{s}$	$10^3\overline{s}_{eq}$	Comments
50. Schubauer and Spangenberg E	1960	0	82.0	2.94,3	1.227	1.867	0.797	1.69	9.51	0.953			1) Severe adverse pressure gradient. 2) s_S from Clauser plot. 3) $\nu=1.69\times10^{-4}$ ft²/s.
		2.5	79.1	5.31,3	1.365	1.774	0.647	1.45	9.79	0.910			
		5.0	75.1	8.28,3	1.367	1.764	0.631	1.27	10.04	0.874			
		8.33	74.1	1.34,4	1.441	1.725	0.565	1.00	10.10	0.779			
		11.7	59.2	1.66,4	1.548	1.683	0.492	0.80	10.16	0.701			
		13.3	55.0	2.01,4	1.578	1.675	0.478	0.69	10.32	0.662			
		15.0	57.5	2.80,4	1.739	1.627	0.388	0.44	10.40	0.532			
		15.8	50.3	3.59,4	1.928	1.593	0.319	0.23	10.44	0.386			
		16.7	46.0	3.82,4	2.364	1.533	0.172	0.125	10.55	0.288			
51. Schubauer and Spangenberg F	1960	0	82.0	2.99,3	1.243	1.860	0.786	1.68	9.43	0.943			1) High adverse pressure gradient. 2) s_S from Clauser plot. 3) $\nu=1.62\times10^{-4}$ ft²/s.
		4.17	77.1	7.35,3	1.362	1.772	0.644	1.32	10.07	0.892			
		10.0	67.1	1.31,4	1.422	1.733	0.579	1.05	10.12	0.800			
		13.3	63.4	1.76,4	1.431	1.731	0.576	0.94	10.60	0.794			
		15.8	55.3	1.47,4	1.529	1.694	0.512	0.64	10.62	0.656			
		17.5	52.3	3.68 4	1.814	1.605	0.375	0.31	10.51	0.452			
		18.3	49.1	4.53,4	2.085	1.557	0.237	0.15	10.32	0.309			
52. Schultz-Grunow	1940	1.64	63.6	1.77,3	1.429								1) Zero-pressure gradient. 2) s_S from floating element. 3) $\nu=1.54\times10^{-4}$ ft²/s.
		3.28		3.01,3	1.378								
		4.02						1.650					
		4.21						1.636					
		4.83						1.581					
		4.92		4.08,3	1.361								
		5.42						1.563					
		5.81						1.538					
		7.85						1.448					
		8.20		6.06,3	1.308								
		8.79						1.448					
		9.00						1.442					
		9.32						1.435					
		9.42						1.402					
		10.5		7.31,3	1.300								
		10.8						1.371					
		12.0						1.361					
		12.8		8.46,3	1.299								
		13.0						1.352					
		14.4						1.312					
		16.6						1.273					
		17.4		1.08,4	1.285								
		18.4						1.259					

Author(s)	Date	x(ft)	u_G(ft/s)	R_2	H_{12}	H_{32}	ζ	$10^3 s_S$	ℓ'	z_E	$10^3\overline{s}$	$10^3\overline{s}_{eq}$	Comments
53. Stratford 5	1959	2.935	55.0	2.13,3	1.428	1.802	0.693						1) High adverse pressure gradient.
		2.96	52.1	2.54,3	1.522	1.748	0.605						
		3.00	49.9	2.99,3	1.668	1.699	0.521						
		3.48	44.1	4.41,3	1.873	1.608	0.350					1.12	2) s_S for x>3ft nominally zero.
		4.05	42.0	5.05,3	1.798	1.617	0.368					1.23	
		5.26	37.1	6.58,3	1.759	1.624	0.382					1.74	
		6.16	34.1	8.53,3	1.820	1.604	0.342					2.62	3) $\nu=1.61\times10^{-4}$ ft^2/s.
54. Stratford 6	1959	2.935	55.0	2.09,3	1.427	1.804	0.696						1) Severe adverse pressure gradient.
		2.96	51.5	2.47,3	1.541	1.750	0.608						
		3.00	49.1	3.03,3	1.787	1.677	0.482						
		3.47	42.6	4.70,3	2.303	1.541	0.195					3.08	2) s_S for x>3ft nominally zero.
		4.06	39.4	6.24,3	2.327	1.528	0.157					3.76	
		5.28	33.7	9.66,3	2.558	1.500	0.					5.52	
		6.19	31.0	1.20,4	2.529	1.512	0.098					6.24	3) $\nu=1.61\times10^{-4}$ ft^2/s.
55. Erian and Eskinazi	1964	0.42	58.8	-1.74,4	0.458	2.992	2.407	12.9	9.76	2.70	50.1		1) $\nu\approx1.6\times10^{-4}$ ft^2/s.
		0.58	65.0	-1.75,4	0.529	2.748	2.066	8.43	9.86	2.21	26.2		2) y_C=0.131 in.
		0.67	69.2	-1.45,4	0.571	2.592	1.851	7.00	9.83	2.01	18.4		
		0.75	72.4	-1.28,4	0.568	2.527	1.757	6.00	9.80	1.85	15.1		
		0.83	77.2	-1.14,4	0.589	2.436	1.634	5.00	9.89	1.71	10.9		
		0.92	77.3	-1.15,4	0.601	2.410	1.598	4.76	9.97	1.68	9.80		
		1.04	80.0	-1.04,4	0.618	2.343	1.498	4.15	9.93	1.56	7.47		
		1.17	79.8	-1.04,4	0.635	2.313	1.460	3.89	9.90	1.51	6.70		
		1.25	77.9	-1.09,4	0.645	2.311	1.455	3.91	10.02	1.53	6.61		
		1.42	72.5	-1.27,4	0.666	2.318	1.465	4.13	10.30	1.62	7.07		
		1.58	68.4	-1.37,4	0.674	2.325	1.475	4.17	10.31	1.62	7.02		
		1.75	64.9	-1.44,4	0.680	2.329	1.474	4.18	10.26	1.62	7.02		
56. Kruka and Eskinazi 1	1964	0.50	60.0	-2.66,4	0.492	3.058	2.494	14.8					1) s_S from flattened Preston tube.
		1.08	57.7	-2.54,4	0.595	2.690	1.986	7.80					2) y_C=0.131 in.
		1.50	58.3	-2.55,4	0.626	2.566	1.813	6.18					
		2.08	57.9	-2.41,4	0.688	2.445	1.643	4.85					
		3.00	58.0	-2.14,4	0.741	2.339	1.493	3.78					
57. Kruka and Eskinazi 2	1964	0.50	19.7	-1.30,5	0.199	6.267	6.822	102					
		1.50	20.8	-1.11,5	0.322	4.236	4.094	34.1					
		2.08	21.8	-1.04,5	0.375	3.768	3.461	23.2					
		3.00	23.6	-8.37,5	0.453	3.265	2.777	14.2					

Author(s)	Date	x(ft)	u_G(ft/s)	R_2	H_{12}	H_{32}	ζ	$10^3 s_S$	ℓ'	z_E	$10^3\overline{s}$	$10^3\overline{s}_{eq}$	Comments
58. Kruka and Eskinazi 3	1964	0.50	17.8	-5.73,5	0.098	12.18	14.73	507					
		1.08	15.7	-5.55,5	0.131	9.312	10.89	275					
		1.50	16.5	-5.44,5	0.156	8.177	9.377	205					
		2.08	11.4	-8.52,5	0.121	10.10	11.95	290					
		3.00	7.25	-1.33,6	0.096	12.51	15.16	500					
59. Nicoll 1	1965	0.18	49.8	-7.32,4	0.283	4.659	4.67	45	9.82	5.08	566		1) s_S from Clauser plot. 2) $\overline{s}$ from kinetic-energy equation. 3) $\nu=1.6\times10^{-4}$. 4) y_C=0.213 in.
		0.36	49.4	-7.00,4	0.326	4.205	4.07	36	10.15	4.70	374		
		0.53	48.9	-6.93,4	0.362	3.873	3.60	32	10.29	4.49	253		
		0.71	48.4	-6.80,4	0.396	3.633	3.29	26	10.52	4.14	182		
		0.89	48.0	-6.90,4	0.422	3.446	3.03	22	10.58	3.83	145		
		1.33	46.8	-6.69,4	0.470	3.182	2.67	17.5	10.64	3.43	123		
		1.78	49.1	-5.65,4	0.532	2.905	2.28						
60. Nicoll 2	1965	0.18	78.2	-3.80,4	0.414	3.429	3.01	18.5	10.56	3.50	120		
		0.36	78.2	-3.64,4	0.459	3.196	2.68	14.5	10.41	3.06	81.0		
		0.53	78.1	-3.35,4	0.508	2.991	2.40	13.5	10.29	2.91	53.4		
		0.71	78.1	-3.28,4	0.550	2.839	2.20	11.5	10.31	2.70	35.3		
		0.89	78.0	-3.37,4	0.580	2.736	2.05	10.0	10.45	2.55	25.1		
		1.33	77.9	-3.11,4	0.639	2.568	1.92	8.0	10.58	2.31	24.5		
		1.78	78.0	-2.70,4	0.691	2.444	1.64	6.5	10.30	2.02			
61. Nicoll 3	1965	0.27	12.1	-3.48,5	0.087	13.49	16.5						
		0.36	11.2	-3.75,5	0.090	13.25	16.2						
		0.53	9.21	-4.46,5	0.086	13.77	16.9						
		0.71	8.25	-4.95,5	0.087	13.57	16.6						
		0.89	5.15	-8.15,5	0.060	19.24	24.2						
62. Nicoll 4	1965	0.18	32.2	-1.21,5	0.194	6.442	7.17	105	10.12	8.00	1920		
		0.36	31.6	-1.19,5	0.225	5.706	6.20	85	10.41	7.40	1430		
		0.53	31.8	-1.15,5	0.261	5.055	5.22	68	10.41	6.62	1090		
		0.71	31.2	-1.15,5	0.285	4.717	4.86	58	10.52	6.18	806		
		0.89	30.6	-1.14,5	0.306	4.454	4.49	50	10.61	5.79	590		
		1.33	29.0	-1.19,5	0.340	4.086	3.99	38	10.78	5.12	374		
		1.78	32.5	-8.50,4	0.420	3.454	3.04						
63. Nicoll 5	1965	0.18	23.8	-5.10,3	0.546	2.825	2.17	15.0	8.64	2.58	51.4		
		0.36	23.8	-4.77,3	0.616	2.603	1.865	11.7	8.71	2.30	30.1		

Author(s)	Date	x(ft)	u_G(ft/s)	R_2	H_{12}	H_{32}	ζ	$10^3 s_S$	ℓ'	z_E	$10^3\overline{s}$	$10^3\overline{s}_{eq}$	Comments
63. Nicoll 5 (cont.)	1965	0.53	23.8	-4.22,3	0.677	2.457	1.69	9.5	9.01	2.14	15.8		
		0.71	23.7	-4.58,3	0.707	2.396	1.58	8.5	9.21	2.07	7.45		
		0.89	23.9	-4.22,3	0.736	2.334	1.495	7.3	9.18	1.91	3.75		
		1.33	24.0	-4.20,3	0.789	2.244	1.395	5.7			6.9		
		1.78	24.1	-3.63,3	0.810	2.205	1.30						
64. Nicoll 7	1965	0.18	41.5	-1.52,4	0.460	3.168	2.64	18	9.71	3.18	92.0		
		0.36	41.5	-1.40,4	0.515	2.943	2.335	14.5	9.83	2.89	55.1		
		0.53	41.4	-1.33,4	0.571	2.752	2.06	12	9.57	2.56	36.1		
		0.71	41.5	-1.37,4	0.602	2.652	1.94	10	9.69	2.36	28.8		
		0.89	41.4	-1.20,4	0.644	2.549	1.79	9	9.89	2.29	28.0		
		1.33	40.4	-1.12,4	0.701	2.419	1.60	7	9.94	2.03	24.0		
		1.78	40.5	-1.12,4	0.738	2.344	1.50						
65. Nicoll 8	1965	0.18	30.2	-2.62,4	0.352	3.922	3.68	35	9.31	4.25	335		
		0.36	30.1	-2.35,4	0.409	3.515	3.12	27	9.42	3.77	187		
		0.53	29.9	-2.44,4	0.454	3.259	2.76	22	9.55	3.45	102		
		0.71	30.3	-2.25,4	0.498	3.055	2.50	18	9.62	3.14	60.5		
		0.89	30.2	-2.26,4	0.531	2.920	2.33	15	9.72	2.90	48.9		
		1.33	30.0	-2.12,4	0.585	2.726	2.04	11	9.87	2.52	66.3		
		1.78	29.7	-1.96,4	0.638	2.576	1.83						
66. Nicoll 9	1965	0.18	20.9	-4.14,4	0.261	5.005	5.13						
		0.36	20.6	-4.26,4	0.302	4.481	4.42						
		0.53	20.3	-4.18,4	0.341	4.074	3.88						
		0.71	20.1	-4.04,4	0.372	3.795	3.50						
		0.89	19.8	-4.20,4	0.394	3.638	3.28						
		1.33	19.0	-4.18,4	0.437	3.364	2.91						
		1.78	21.6	-2.99,4	0.528	2.932	2.32						
67. Nicoll 10	1965	0.18	7.47	-1.43,5	0.099	11.87	14.3						
		0.36	7.12	-1.42,5	0.120	10.13	12.0						
		0.53	6.76	-1.47,5	0.134	9.153	10.7						
		0.71	6.37	-1.56,5	0.141	8.708	10.1						
		0.89	5.95	-1.68,5	0.143	8.606	9.95						

Author(s)	Date	R_{max}	$10^3 \sigma_s$	Author(s)	Date	R_{max}	$10^3 \sigma_s$
Myers, Schauer and Eustis	1961	11500	2.91	Bradshaw and Gee	1962	2980	3.67
		13300	2.98			3520	3.57
		14800	2.62			4600	3.45
		15100	2.97			5050	3.34
		16000	2.97			5850	3.27
		18600	2.58			6220	3.11
		17600	2.70			6870	3.14
		19000	2.60			7145	3.13
		18700	3.08			7328	3.10
		20600	2.66			7499	3.12
		3760	3.70			8166	3.08
		3600	3.90			7621	2.91
		6050	3.61			9722	3.05
		6420	3.49			11040	2.92
		7900	3.82			12390	2.84
		8900	3.64			12850	2.84
		10300	3.66			13090	2.83
		10700	3.55			13800	2.78
		11700	3.36				
		13900	3.33				
		15800	3.24				
		17500	3.13				
		19700	2.95				
		20400	3.09				
		23400	3.10				
		25000	2.82				

TABLE 1 (continued): Drag data for wall jets ($R_2 = -\infty$)

Author(s)	Date	Relation	Comments
Wieghardt Rubert and Persh Walz	1945 1951 1960	$H_{32} = \dfrac{4H_{12}/3}{H_{12} - 1/3}$	Derived directly from power-law velocity profile
Wieghardt	1945	$H_{32} = \dfrac{1.269\ H_{12}}{H_{12} - 0.379}$	Modifications of power-law relation
Fernholz	1962	$H_{32} = \dfrac{1.273\ H_{12}}{H_{12} - 0.37} + 5.4\ (\dfrac{H_{12}}{10})^4$	
Fernholz	1964	$H_{12} = 1 + 1.48(2 - H_{32}) + 104(2 - H_{32})^{6.7}$	Empirical
Goldberg	1966	$H_{32} = \dfrac{1.295\ H_{12}}{H_{12} - 0.36}$	Modification of power-law relation
Nicoll and Escudier	1966	$H_{32} = 1.431 - 0.0971/H_{12} + 0.775/H_{12}^2$	Empirical

TABLE 2: Summary of explicit shape-factor relations (H_{12}~H_{32}) for uniform-density turbulent boundary layers ($R_2 > 0$)

Author(s)	Date	Relation	Restrictions
Ludwieg and Tillmann	1949	$s_S = 0.123\ R_2^{-0.268}\ 10^{-0.678H_{12}}$	Conventional boundary layers ($R_2 > 0$)
Ross	1953	$s_S = 0.0245[1 - \frac{2}{3}(H_{12}-1) + 0.043(H_{12}-1)^4]R_2^{-0.268}$	
Uram	1960	$s_S = 0.0075[\log_{10}(8.05H_{12}^{-1.818})]^{2.04}\ R_2^{-0.1155}$	
Fernholz	1964	$s_S = 0.029[\log_{10}(8.05H_{12}^{-1.818})]^{1.705}\ R_2^{-0.268}$	
Mueller, Korst and Chow	1964	$s_S = 0.394H_{12}^{-3.23}\ R_2^{-0.268}$	
Walz	1965	$s_S = (0.0566\ H_{32} - 0.0842)R_2^{-0.268}$	
Felsch	1965	$s_S = 0.029[0.93 - 1.95\ \log_{10}(H_{12})]^{1.705}\ R_2^{-0.268}$	
Escudier, Nicoll and Spalding	1966	$s_S = [0.243\ \zeta^2 + 0.0376\ \zeta - 0.00106 + 0.0914\ \zeta^2/(1 + 65/\zeta)]/\ell^2$ $\ell = \ln[3.389\ R_2\zeta/\{(1-\zeta)(1+2\zeta)\}]$	
Glauert	1956	$\sigma_s = 0.0225\ R_{max}^{-0.25}$	Wall jets ($R_2 = -\infty$)
Sigalla	1958	$\sigma_s = 0.02825\ R_{max}^{-0.25}$	
Bradshaw and Gee	1962	$\sigma_s = 0.01575\ R_{max}^{-0.182}$	

TABLE 3: Summary of explicit drag laws for uniform-density turbulent boundary layers

Author(s)	Date	Expression for G	Comments
Rotta (1)	1950	$\frac{2 + 3\Pi + 4\Pi^2/3}{(1 + \Pi)\kappa}$	Based upon linear wake profile: $w = 2\xi$. Expression for K modified to fit data of Schultz-Grunow (1940) and of Ludwieg and Tillmann (1949). $\kappa = 0.40$, $E = 8.00$.
Rotta (2)	1953	As for Rotta (1)	Expression for s_s modified to: $[8\{\log_{10}(R_2)\}^{0.919} - 0.1 + K + 5.75 \log_{10}(H_{12}]^{-2}$.
Coles	1956	$\frac{2 + 3.2\Pi + 1.522\,\Pi^2}{(1 + \Pi)\kappa}$	Tabulated wake profile deduced from a wide survey of experimental boundary-layer velocity profiles. $\kappa = 0.41$, $E = 7.77$ (values given by Coles, 1962).
Cornish	1960	$\frac{11.1 + 18.35\Pi + 8.93\,\Pi^2}{(1 + \Pi)\kappa}$	Sinusoidal wake profile: $w = [(1 - \cos\pi\xi)]$. Third component added to velocity profile - tabulated 'outer wall function'. $\kappa = 0.412$, $E = 10$.
Moses	1964	$\frac{2 + 3.168\Pi + 1.0448\,\Pi^2}{(1 + \Pi)\kappa}$	Double-power wake profile: $w = 6\xi^2 - 4\xi^3$. $\kappa = 0.40$, $E = 7.69$.
Spalding	1964	$\frac{2 + 3.179\Pi + 1.5\,\Pi^2}{(1 + \Pi)\kappa}$	Sinusoidal wake profile. $\kappa = 0.41$, $E = 7.7$.
Nash	1965	$K = \frac{3}{2}G + \frac{2100}{G^2 + 200} - 20$	$K\{G\}$ relation obtained by correlation of experimental data of Schultz-Grunow (1940), Ludwieg and Tillmann (1949), Clauser (1954) and Bradshaw (see Bradshaw and Ferriss, 1965). $\kappa = 0.40$, $E = 8.00$.
Log-wall plus linear-wake	-	$\frac{2 + 3\Pi + 4\Pi^2/3}{(1 + \Pi)\kappa}$	Unmodified form of Rotta's (1950, 1953) drag laws. $\kappa = 0.41$, $E = 7.7$.

TABLE 4: Summary of implicit drag laws for uniform-density turbulent boundary layers

Author(s)	Date	Type	Root-mean-square deviations (per cent)			
			$R_2>0$	$0 \geq R_2 > -\infty$	$R_2=-\infty$	Overall
Ludwieg and Tillmann	1949	Explicit	19.2			
Ross	1953	"	19.7			
Uram	1960	"	19.4			
Fernholz	1964	"	15.0			
Mueller, Korst and Chow	1964	"	15.8			
Walz	1965	"	20.6			
Felsch	1965	"	14.5			
Glauert	1956	"			29.1	
Sigalla	1958	"			13.2	
Bradshaw and Gee	1962	"			9.6	
Rotta (1)	1950	Implicit	24.1	20.2		
Rotta (2)	1953	"	21.4			
Coles	1956	"	15.4	15.9		
Cornish	1960	"	13.7	16.4		
Moses	1964	"	12.4	15.7	16.8	13.9
Spalding	1964	"	13.8	15.8	14.0	14.2
Nash	1965	"	15.4			
"log-wall plus linear-wake"	-	"	18.5	30.1	9.5	20.0
Escudier, Nicoll and Spalding	1966	Explicit	11.0	12.9	8.0	10.9

Note: Blank areas in the table may be taken as indicating regions of inapplicability of the drag law under consideration.

TABLE 5: Comparison of drag law of Escudier, Nicoll and Spalding (1966) with previous recommendations.

Author(s)	Date	Relation	Comments
Rubert and Persh	1951	$\bar{s} = 2\{H_{12}(3H_{12}-1)s_S+2a.10^{-0.678H_{12}}]$, $a = \{0.0246(H_{12}-1)-F_2[1672(H_{12}-1.25)^{0.535}-35.15] \times [H_{12}(3H_{12}-0.9)-0.1]\}$	Empirical
Rotta	1952	$\bar{s} = s_S(1+a\, s_S^{\frac{1}{2}})$, $a = -5.55 + 1.5\Pi + 1.84\Pi^2$	
Truckenbrodt	1952	$\bar{s} = 0.0056\, R_2^{-1/6}$	Approximation to Rotta's relation
Schuh	1954	$\bar{s} = a-bF_2$, $a = a\{H_{12}\}$, $b = b\{H_{12}\}$	a, b empirical.
Mueller, Korst and Chow	1964	$\bar{s} = 0.01355\{[1+9.4(H_{12}-1.2)]^{\frac{1}{2}}-1\}R_2^{-1/6}$	Based upon data for re-attaching boundary layers.
Walz	1965	$\bar{s} = [0.00481+0.0822(H_{32}-1.5)^{4.81}]R_2^{-0.2317H_{32}+0.2644}$	Based upon Clauser's (1954) data for equilibrium boundary layers.
Felsch	1965	$\bar{s} = s_S[\{1+(1+1/H_{12})\beta\}R_2 dH_{32}/dR_2+\{1+(1-1/H_{12})\beta\}H_{32}]$	(1) Expression for $\bar{s}$ is a re-arranged form of shape-factor equation (2.3-29). (2) Empirical correlation for $R_2 dG/dR_2 = f\{G,\beta\}$.
Tani	1966	$\bar{s} = a-bF_2$, $a = s_S[1.476-0.465H_{12}+0.504(H_{12}-1)^2/H_{12}]$ $b = (H_{12}-1)[1.790-0.675H_{12}+0.742(H_{12}-1)^2/H_{12}]$	Approximation to Rotta's relation.

TABLE 6: Summary of shear-work-integral relations for uniform-density turbulent boundary layers.

Author(s)	Date	Relation	Comments
Goldberg	1966	$R_2 d\bar{s}/dR_x = 0.009(\bar{s}_{eq} - \bar{s})$ $\bar{s}_{eq} = 0.0056(1-2.5\times10^{7}\ F_2{}^{3} - 10^{2}F_2)R_2{}^{-1/6}$	(1) $\bar{s}_{eq}$ = empirical $\bar{s}$-relation for equilibrium boundary layers. (2) Allows for 'history' effects.
Escudier and Spalding	1966	$\bar{s} = 0.547\ s_S + 10^{-3}\ (2.107H_{12} - 2.286)$	Empirical.
Escudier and Nicoll	1966	$\bar{s} = \frac{1}{3}(2\zeta+1)s_S + \begin{cases} 0.00565(1-\zeta)^{2.715}, & \zeta < 1 \\ 0.01(\zeta-1)^{3}, & \zeta > 1 \end{cases}$	Discussed in CHAPTER 4.

TABLE 6 (continued)

Station 1		2		5		7	
Y(IN)	$\bar{U}/U_G$	Y(IN)	$\bar{U}/U_G$	Y(IN)	$\bar{U}/U_G$	Y(IN)	$\bar{U}/U_G$
6.24, -3	0.327	6.24, -3	0.308	6.24, -3	0.269	6.24, -3	0.171
7.24, -3	0.338	7.24, -3	0.314	7.24, -3	0.277	7.24, -3	0.187
9.24, -3	0.398	9.24, -3	0.354	8.24, -3	0.290	9.24, -3	0.205
1.22, -2	0.475	1.22, -2	0.437	1.02, -2	0.316	1.22, -2	0.262
1.52, -2	0.503	1.52, -2	0.478	1.32, -2	0.379	1.62, -2	0.295
1.92, -2	0.523	1.92, -2	0.512	1.62, -2	0.424	2.12, -2	0.309
2.42, -2	0.546	2.42, -2	0.526	1.92, -2	0.443	2.72, -2	0.324
3.12, -2	0.565	3.02, -2	0.541	2.32, -2	0.461	3.52, -2	0.337
4.02, -2	0.587	3.82, -2	0.565	2.92, -2	0.477	4.52, -2	0.347
5.32, -2	0.608	4.82, -2	0.579	3.72, -2	0.493	6.02, -2	0.374
6.82, -2	0.633	6.12, -2	0.600	4.72, -2	0.512	8.02, -2	0.389
8.32, -2	0.652	7.62, -2	0.612	6.02, -2	0.527	1.10, -1	0.419
1.08, -1	0.682	9.62, -2	0.637	8.02, -2	0.545	1.45, -1	0.440
1.33, -1	0.707	1.21, -1	0.660	1.00, -1	0.572	2.05, -1	0.483
1.58, -1	0.730	1.51, -1	0.680	1.25, -1	0.593	2.70, -1	0.518
1.88, -1	0.750	1.91, -1	0.707	1.55, -1	0.616	3.45, -1	0.559
2.28, -1	0.781	2.41, -1	0.738	1.95, -1	0.644	4.20, -1	0.591
2.68, -1	0.804	3.01, -1	0.766	2.45, -1	0.672	5.20, -1	0.641
3.18, -1	0.827	3.61, -1	0.799	3.05, -1	0.702	6.20, -1	0.683
3.68, -1	0.849	4.21, -1	0.825	3.75, -1	0.740	7.20, -1	0.706
4.18, -1	0.871	4.81, -1	0.849	4.55, -1	0.764	8.70, -1	0.762
4.68, -1	0.895	5.46, -1	0.876	5.45, -1	0.816	9.70, -1	0.806
5.18, -1	0.908	5.96, -1	0.890	6.25, -1	0.840	1.07, +0	0.842
5.68, -1	0.922	6.71, -1	0.913	7.25, -1	0.871	1.17, +0	0.875
6.18, -1	0.942	7.71, -1	0.947	8.25, -1	0.901	1.27, +0	0.894
6.68, -1	0.952	8.71, -1	0.965	9.25, -1	0.935	1.37, +0	0.922
7.68, -1	0.973	9.71, -1	0.980	1.03, +0	0.956	1.47, +0	0.940
8.68, -1	0.986	1.07, +0	0.991	1.13, +0	0.970	1.57, +0	0.960
9.68, -1	0.992	1.17, +0	0.994	1.23, +0	0.985	1.77, +0	0.984
1.07, +0	0.995	1.27, +0	0.999	1.33, +0	0.995	1.97, +0	0.993
1.17, +0	0.997	1.37, +0	1.001	1.43, +0	0.999	2.17, +0	0.996
1.27, +0	0.999	1.47, +0	1.002	1.58, +0	1.001	2.37, +0	1.000
1.37, +0	1.000	1.67, +0	1.000	1.78, +0	1.002		
				1.88, +0	1.002		
				2.08, +0	1.000		

TABLE 7(a) Mean-velocity profiles of present writer; measured with pitot tube

(1) No blowing

Station 8		9	
Y(IN)	$\bar{U}$/UG	Y(IN)	$\bar{U}$/UG
6.24, -3	0.102	6.24, -3	-0.089
7.24, -3	0.116	7.24, -3	-0.098
9.24, -3	0.134	9.24, -3	-0.106
1.22, -2	0.140	1.22, -2	-0.055
1.62, -2	0.150	1.62, -2	-0.098
2.12, -2	0.174	2.12, -2	-0.068
3.02, -2	0.195	2.72, -2	-0.068
4.02, -2	0.199	3.42, -2	-0.055
5.52, -2	0.221	5.22, -2	-0.055
7.02, -2	0.224	6.72, -2	-0.054
9.02, -2	0.247	8.72, -2	-0.036
1.20, -1	0.268	1.27, -1	-0.097
1.50, -1	0.274	1.77, -1	-0.078
1.90, -1	0.290	2.77, -1	0.112
2.40, -1	0.328	3.77, -1	0.070
3.20, -1	0.372	4.77, -1	0.144
4.20, -1	0.436	5.77, -1	0.234
5.20, -1	0.475	6.77, -1	0.253
6.70, -1	0.539	8.77, -1	0.342
8.20, -1	0.613	1.08, +0	0.432
9.20, -1	0.644	1.28, +0	0.507
1.02, +0	0.677	1.38, +0	0.568
1.07, +0	0.702	1.48, +0	0.621
1.17, +0	0.746	1.78, +0	0.721
1.22, +0	0.753	1.93, +0	0.779
1.32, +0	0.794	2.08, +0	0.839
1.37, +0	0.823	2.23, +0	0.893
1.47, +0	0.850	2.38, +0	0.927
1.57, +0	0.877	2.58, +0	0.966
1.67, +0	0.905	3.08, +0	1.000
1.77, +0	0.924		
1.87, +0	0.947		
1.97, +0	0.964		
2.07, +0	0.973		
2.17, +0	0.981		
2.27, +0	0.989		
2.37, +0	0.993		
2.47, +0	0.997		
2.57, +0	1.000		

TABLE 7(a) (1) (Cont.)

Station 1		2		3		4	
Y(IN)	$\bar{U}/UG$	Y(IN)	$\bar{U}/UG$	Y(IN)	$\bar{U}/UG$	Y(IN)	$\bar{U}/UG$
6.24, -3	0.256	6.24, -3	0.250	6.24, -3	0.226	6.24, -3	0.232
7.24, -3	0.267	7.24, -3	0.264	7.24, -3	0.240	7.24, -3	0.242
8.24, -3	0.277	9.24, -3	0.298	8.24, -3	0.253	9.24, -3	0.272
1.02, -2	0.305	1.22, -2	0.354	1.02, -2	0.276	1.22, -2	0.323
1.32, -2	0.343	1.62, -2	0.401	1.32, -2	0.313	1.72, -2	0.370
1.72, -2	0.380	2.12, -2	0.420	1.72, -2	0.346	2.42, -2	0.387
2.22, -2	0.402	2.72, -2	0.428	2.22, -2	0.378	3.32, -2	0.417
2.82, -2	0.417	3.62, -2	0.452	2.82, -2	0.397	4.42, -2	0.433
3.52, -2	0.426	4.82, -2	0.468	3.52, -2	0.413	5.72, -2	0.449
4.32, -2	0.441	6.32, -2	0.487	4.32, -2	0.426	7.32, -2	0.459
5.22, -2	0.453	8.22, -2	0.503	5.22, -2	0.435	9.02, -2	0.478
6.22, -2	0.464	1.12, -1	0.535	6.22, -2	0.445	1.10, -1	0.493
7.42, -2	0.480	1.52, -1	0.569	7.32, -2	0.454	1.40, -1	0.506
8.72, -2	0.494	2.02, -1	0.612	8.82, -2	0.466	1.80, -1	0.534
1.02 -1	0.516	2.52, -1	0.654	1.08, -1	0.480	2.40, -1	0.568
1.22, -1	0.537	3.02, -1	0.699	1.33, -1	0.500	3.20, -1	0.616
1.47, -1	0.564	3.52, -1	0.740	1.63, -1	0.520	4.00, -1	0.659
1.77, -1	0.596	4.02, -1	0.773	2.03, -1	0.548	4.80, -1	0.705
2.27, -1	0.653	4.52, -1	0.807	2.53, -1	0.582	5.70, -1	0.760
2.77, -1	0.705	5.02, -1	0.830	3.13, -1	0.630	6.50, -1	0.795
3.47, -1	0.770	5.52, -1	0.853	3.83, -1	0.682	7.30, -1	0.827
4.27, -1	0.822	6.02, -1	0.868	4.53, -1	0.728	8.10, -1	0.866
5.07, -1	0.860	6.72, -1	0.888	5.33, -1	0.776	8.90, -1	0.896
5.87, -1	0.891	7.72, -1	0.917	6.13, -1	0.819	9.70, -1	0.909
6.77, -1	0.927	8.72, -1	0.942	6.93, -1	0.846	1.05, +0	0.938
7.77, -1	0.951	9.72, -1	0.961	7.83, -1	0.885	1.13, +0	0.952
8.77, -1	0.974	1.07, +0	0.976	8.83, -1	0.913	1.21, +0	0.963
9.77, -1	0.987	1.17, +0	0.987	9.83, -1	0.933	1.30, +0	0.974
1.08, +0	0.996	1.27, +0	0.993	1.08, +0	0.955	1.41, +0	0.986
1.18, +0	1.001	1.37, +0	0.996	1.18, +0	0.967	1.52, +0	0.991
1.28, +0	1.004	1.47, +0	0.999	1.28, +0	0.981	1.62, +0	0.995
1.38, +0	1.005	1.57, +0	1.000	1.38, +0	0.986	1.77, +0	0.997
1.58, +0	1.003			1.48, +0	0.992	1.97, +0	1.000
1.78, +0	1.000			1.58, +0	0.993		
				1.78, +0	0.996		
				1.98, +0	1.000		

TABLE 7(a) (2) Porous strip

Station 5		6		7		8		9	
Y(IN)	$\bar{U}$/UG	Y(IN)	$\bar{U}$/UG	Y(IN)	$\bar{U}$/UG	Y(IN)	$\bar{U}$/UG	Y(IN)	$\bar{U}$/UG
6.24, -3	0.196	6.24, -3	0.185	6.24, -3	0.170	6.24, -3	0.129	6.24, -3	0.081
7.24, -3	0.206	7.24, -3	0.188	7.24, -3	0.187	7.24, -3	0.109	7.24, -3	0.081
8.24, -3	0.218	9.24, -3	0.195	8.24, -3	0.187	1.92, -2	0.135	9.24, -3	0.081
9.24, -3	0.229	1.22, -2	0.214	9.24, -3	0.187	2.92, -2	0.140	1.22, -2	0.081
1.12, -2	0.250	1.72, -2	0.259	1.12, -2	0.194	3.92, -2	0.156	1.72, -2	0.090
1.42, -2	0.279	2.42, -2	0.288	1.42, -2	0.202	4.92, -2	0.156	2.72, -2	0.090
1.82, -2	0.299	3.32, -2	0.318	1.92, -2	0.216	5.92, -2	0.156	3.72, -2	0.081
2.32, -2	0.327	4.42, -2	0.334	2.62, -2	0.233	7.42, -2	0.165	5.22, -2	0.081
2.92, -2	0.355	5.72, -2	0.353	3.52, -2	0.236	8.92, -2	0.161	6.72, -2	0.081
3.62, -2	0.367	7.22, -2	0.362	4.62, -2	0.254	1.09, -1	0.179	8.72, -2	0.070
4.52, -2	0.381	9.22, -2	0.385	5.92, -2	0.263	1.34, -1	0.183	1.07, -1	0.070
5.62, -2	0.397	1.27, -1	0.395	7.42, -2	0.274	1.59, -1	0.183	1.37, -1	0.058
7.02, -2	0.409	1.77, -1	0.426	9.42, -2	0.285	1.89, -1	0.183	1.77, -1	0.071
8.22, -2	0.414	2.47, -1	0.450	1.24, -1	0.292	2.19, -1	0.211	2.27, -1	0.059
9.72, -2	0.429	3.37, -1	0.488	1.64, -1	0.310	2.59, -1	0.218	2.77, -1	0.072
1.17, -1	0.439	4.47, -1	0.544	2.14, -1	0.328	3.09, -1	0.232	3.27, -1	0.073
1.47, -1	0.453	5.67, -1	0.597	2.84, -1	0.353	3.59, -1	0.254	3.77, -1	0.047
1.87, -1	0.474	7.17, -1	0.659	3.74, -1	0.387	4.29, -1	0.264	4.77, -1	0.095
2.37, -1	0.499	8.67, -1	0.726	4.74, -1	0.423	5.09, -1	0.297	5.77, -1	0.138
2.87, -1	0.520	1.02, +0	0.801	5.84, -1	0.465	6.09, -1	0.343	6.77, -1	0.180
3.57, -1	0.558	1.17, +0	0.860	7.14, -1	0.519	7.59, -1	0.387	7.77, -1	0.229
4.37, -1	0.596	1.32, +0	0.907	8.64, -1	0.575	9.59, -1	0.469	8.77, -1	0.244
5.37, -1	0.658	1.47, +0	0.945	1.01, +0	0.649	1.16, +0	0.554	9.77, -1	0.279
6.37, -1	0.692	1.62, +0	0.970	1.16, +0	0.708	1.36, +0	0.636	1.08, +0	0.328
7.37, -1	0.756	1.77, +0	0.982	1.31, +0	0.782	1.56, +0	0.729	1.18, +0	0.362
8.37, -1	0.792	1.92, +0	0.991	1.46, +0	0.839	1.66, +0	0.784	1.28, +0	0.401
9.37, -1	0.838	2.07, +0	0.995	1.61, +0	0.891	1.76, +0	0.816	1.38, +0	0.422
1.04, +0	0.877	2.22, +0	1.000	1.76, +0	0.936	1.86, +0	0.862	1.48, +0	0.467
1.14, +0	0.911			1.91, +0	0.966	1.96, +0	0.881	1.58, +0	0.521
1.24, +0	0.928			2.06, +0	0.977	2.06, +0	0.913	1.73, +0	0.570
1.34, +0	0.954			2.21, +0	0.988	2.16, +0	0.935	1.88, +0	0.632
1.44, +0	0.969			2.36, +0	0.993	2.26, +0	0.958	2.03, +0	0.682
1.59, +0	0.980			2.51, +0	0.996	2.36, +0	0.969	2.18, +0	0.752
1.74, +0	0.991			2.61, +0	1.000	2.46, +0	0.978	2.33, +0	0.820
1.89, +0	0.995					2.56, +0	0.985	2.48, +0	0.851
2.04, +0	0.998					2.66, +0	0.991	2.63, +0	0.907
2.19, +0	1.000					2.76, +0	0.993	2.78, +0	0.939
						2.86, +0	0.995	2.98, +0	0.969
						2.96, +0	0.998	3.18, +0	0.988
						3.06, +0	1.000	3.38, +0	0.996
								3.58, +0	1.000

TABLE 7(a) (2) (Cont.)

Station 1		2		3		4	
Y(IN)	Ū/UG	Y(IN)	Ū/UG	Y(IN)	Ū/UG	Y(IN)	Ū/UG
6.24, -3	0.075	6.24, -3	0.132	6.24, -3	0.172	6.24, -3	0.180
7.24, -3	0.075	7.24, -3	0.147	7.24, -3	0.175	7.24, -3	0.180
1.22, -2	0.093	8.24, -3	0.155	8.24, -3	0.178	9.24, -3	0.201
1.92, -2	0.098	1.02, -2	0.168	1.02, -2	0.193	1.22, -2	0.238
2.92, -2	0.103	1.32, -2	0.194	1.42, -2	0.227	1.72, -2	0.277
4.42, -2	0.116	1.72, -2	0.205	2.02, -2	0.276	2.42, -2	0.299
6.42, -2	0.132	2.22, -2	0.215	2.82, -2	0.300	3.32, -2	0.321
9.42, -2	0.163	3.22, -2	0.234	4.02, -2	0.311	4.52, -2	0.344
1.44, -1	0.222	5.22, -2	0.252	5.52, -2	0.325	6.02, -2	0.355
2.04, -1	0.310	8.22, -2	0.273	7.52, -2	0.340	8.02, -2	0.365
2.64, -1	0.414	1.32, -1	0.304	1.05, -1	0.355	1.07, -1	0.379
3.14, -1	0.507	2.02, -1	0.366	1.50, -1	0.384	1.42, -1	0.394
3.54, -1	0.572	2.72, -1	0.436	2.00, -1	0.412	1.92, -1	0.417
3.94, -1	0.646	3.42, -1	0.518	2.60, -1	0.451	2.62, -1	0.456
4.24, -1	0.688	4.02, -1	0.580	3.30, -1	0.502	3.52, -1	0.499
4.54, -1	0.728	4.67, -1	0.654	4.00, -1	0.554	4.32, -1	0.544
4.84, -1	0.773	5.22, -1	0.715	4.70, -1	0.614	5.02, -1	0.589
5.14, -1	0.790	5.82, -1	0.772	5.40, -1	0.668	5.72, -1	0.630
5.49, -1	0.820	6.52, -1	0.836	6.10, -1	0.717	6.52, -1	0.681
5.74, -1	0.839	7.12, -1	0.860	6.80, -1	0.772	7.32, -1	0.736
6.14, -1	0.861	7.72, -1	0.885	7.50, -1	0.822	8.02, -1	0.774
6.64, -1	0.879	8.42, -1	0.917	8.30, -1	0.864	8.72, -1	0.822
7.24, -1	0.901	9.22, -1	0.941	9.10, -1	0.900	9.42, -1	0.848
8.04, -1	0.932	1.02, +0	0.962	9.90, -1	0.930	1.01, +0	0.881
8.84, -1	0.963	1.14, +0	0.983	1.07, +0	0.950	1.08, +0	0.915
9.64, -1	0.977	1.27, +0	0.990	1.16, +0	0.970	1.15, +0	0.937
1.05, +0	0.988	1.41, +0	0.998	1.25, +0	0.979	1.23, +0	0.954
1.15, +0	0.996	1.56, +0	1.000	1.34, +0	0.987	1.31, +0	0.974
1.26, +0	0.998			1.43, +0	0.991	1.39, +0	0.980
1.37, +0	1.001			1.53, +0	0.996	1.47, +0	0.987
				1.63, +0	0.997	1.57, +0	0.992
				1.73, +0	0.998	1.67, +0	0.997
				1.88, +0	1.000	1.77, +0	0.998
						1.87, +0	1.000

TABLE 7(a) (3) Perforated strip

Station 5		6		7		8		9	
Y(IN)	$\bar{U}$/UG	Y(IN)	$\bar{U}$/UG	Y(IN)	$\bar{U}$/UG	Y(IN)	$\bar{U}$/UG	Y(IN)	$\bar{U}$/UG
6.24, -3	0.169	6.24, -3	0.157	6.24, -3	0.126	6.24, -3	0.107	6.24, -3	0.087
7.24, -3	0.172	7.24, -3	0.149	7.24, -3	0.126	7.24, -3	0.107	8.24, -3	0.079
8.24, -3	0.176	8.24, -3	0.153	9.24, -3	0.132	1.22, -2	0.120	1.32, -2	0.069
9.24, -3	0.186	1.02, -2	0.161	1.22, -2	0.146	1.72, -2	0.120	2.32, -2	0.069
1.12, -2	0.198	1.32, -2	0.187	1.82, -2	0.156	2.72, -2	0.126	3.82, -2	0.057
1.42, -2	0.230	1.82, -2	0.204	2.82, -2	0.188	4.22, -2	0.132	6.82, -2	0.018
1.92, -2	0.268	2.62, -2	0.231	4.82, -2	0.205	6.22, -2	0.132	1.13, -1	0.019
2.72, -2	0.296	3.72, -2	0.270	8.32, -2	0.225	1.02, -1	0.148	1.73, -1	-0.032
3.82, -2	0.308	5.02, -2	0.274	1.33, -1	0.248	1.62, -1	0.167	2.43, -1	-0.048
5.12, -2	0.327	7.02, -2	0.291	2.13, -1	0.272	2.42, -1	0.176	3.23, -1	-0.025
7.12, -2	0.349	1.00, -1	0.310	3.23, -1	0.299	3.42, -1	0.196	4.13, -1	0.035
1.01, -1	0.359	1.45, -1	0.326	4.53, -1	0.365	4.72, -1	0.244	5.13, -1	0.095
1.51, -1	0.380	2.05, -1	0.352	6.13, -1	0.415	6.22, -1	0.292	6.23, -1	0.131
2.21, -1	0.421	2.95, -1	0.385	7.63, -1	0.472	7.72, -1	0.338	7.23, -1	0.149
2.91, -1	0.448	4.05, -1	0.424	9.13, -1	0.541	9.72, -1	0.413	8.73, -1	0.188
3.81, -1	0.486	5.65, -1	0.493	1.06, +0	0.601	1.17, +0	0.483	1.02, +0	0.237
4.81, -1	0.540	7.15, -1	0.550	1.21, +0	0.668	1.37, +0	0.565	1.17, +0	0.300
5.81, -1	0.587	8.65, -1	0.625	1.36, +0	0.735	1.57, +0	0.650	1.32, +0	0.346
6.81, -1	0.634	1.02, +0	0.690	1.51, +0	0.801	1.77, +0	0.729	1.47, +0	0.399
7.81, -1	0.691	1.17, +0	0.770	1.61, +0	0.834	1.97, +0	0.810	1.62, +0	0.445
8.81, -1	0.742	1.32, +0	0.842	1.76, +0	0.889	2.17, +0	0.889	1.77, +0	0.498
9.81, -1	0.795	1.47, +0	0.900	1.91, +0	0.934	2.37, +0	0.937	1.97, +0	0.582
1.08, +0	0.843	1.62, +0	0.943	2.06, +0	0.962	2.57, +0	0.971	2.17, +0	0.647
1.18, +0	0.884	1.77, +0	0.970	2.21, +0	0.978	2.77, +0	0.987	2.37, +0	0.735
1.28, +0	0.918	1.97, +0	0.990	2.36, +0	0.985	2.97, +0	0.994	2.57, +0	0.813
1.38, +0	0.949	2.17, +0	0.995	2.56, +0	0.988	3.17, +0	1.000	2.77, +0	0.882
1.48, +0	0.968	2.37, +0	1.000	2.76, +0	0.993			2.97, +0	0.928
1.58, +0	0.982			3.06, +0	1.000			3.17, +0	0.962
1.68, +0	0.987							3.37, +0	0.977
1.78, +0	0.993							3.57, +0	0.984
1.88, +0	0.996							3.77, +0	0.989
1.98, +0	0.998							3.97, +0	0.994
2.08, +0	1.000							4.17, +0	1.000

TABLE 7(a) (3) (Cont.)

Test	Stn.	u_G/u_1	R_2	H_{12}	H_{32}	ζ	$10^3 s_S(C)$	$10^3 s_S(P)$	ℓ'	z_E	$10^3\bar{s}$	Comments
No Blowing	1	1.000	4.28,3	1.367	1.775	0.648	1.44	1.441	9.98	0.908	1.54	1) Width of blowing section = 1 in; station 1 $2\frac{1}{8}$ in downstream of blowing section; distance between adjacent x-stations = $2\frac{1}{4}$ in.
	3	0.957	5.00,3	1.389	1.759	0.623	1.37	1.332	10.10	0.887		
	5	0.902	6.17,3	1.455	1.727	0.570	1.12	1.091	10.16	0.807		
	7	0.828	9.55,3	1.644	1.663	0.456	0.62	0.630	9.89	0.588		
	8	0.790	1.16,4	1.984	1.595	0.322	0.27	0.272	9.51	0.373		
	9	0.764	1.17,4	3.331	1.553	0.227	<0	<0	-	-		
Porous Strip	1	1.000	5.20,3	1.577	1.691	0.507	0.88	0.806	9.88	0.687	2.66	2) $u_1/\nu = 5\times10^5$/ft.
	2	0.979	6.03,3	1.517	1.712	0.542	0.94	0.857	9.78	0.705		
	3	0.955	7.37,3	1.578	1.689	0.503	0.81	0.851	10.18	0.729		3) $v_S/u_G \approx 0.075$ for porous and perforated strips.
	4	0.929	7.68,3	1.574	1.684	0.494	0.85	0.806	9.92	0.683		
	5	0.900	9.17,3	1.672	1.653	0.437	0.69	0.700	10.02	0.643		
	6	0.870	1.04,4	1.760	1.627	0.387	0.57	0.598	9.78	0.551		
	7	0.841	1.24,4	2.013	1.571	0.271	0.35	0.346	9.70	0.433		
	8	0.818	1.41,4	2.423	1.525	0.145	0.14	0.146	9.52	0.279		
	9	0.800	1.55,4	3.210	1.495		0.025	0.031	9.01	0.118		4) $s_S(C)$ from Clauser plot; $s_S(P)$ from Preston tube.
Perforated Strip	1	1.000	5.66,3	2.493	1.578	0.287	0.090	0.130	9.10	0.228	2.15	
	2	0.981	6.88,3	2.071	1.586	0.303	0.33	0.361	9.46	0.417		
	3	0.953	7.96,3	1.882	1.605	0.343	0.49	0.517	9.67	0.511		5) ℓ' and z_E from smoothed s_S (see figure 6.8).
	4	0.926	8.97,3	1.835	1.607	0.348	0.54	0.824	9.73	0.544		
	5	0.897	1.01,4	1.844	1.604	0.341	0.50	0.524	9.92	0.533		
	6	0.870	1.17,4	1.975	1.575	0.279	0.39	0.400	9.75	0.466		
	7	0.843	1.36,4	2.171	1.552	0.223	0.24	0.226	9.96	0.395		
	8	0.818	1.54,4	2.576	1.507	0.072	0.12	0.182	9.78	0.286		
	9	0.814	1.62,4	3.618	1.517	0.118	<0	0.044	8.68	0.114		

TABLE 7(b): Experimental data of present writer (velocity-profile data from pitot-tube measurements).

Station 1			2			3		
Y(IN)	$\bar{U}/UG$	$\tilde{U}'/\bar{U}$	Y(IN)	$\bar{U}/UG$	$\tilde{U}'/\bar{U}$	Y(IN)	$\bar{U}/UG$	$\tilde{U}'/\bar{U}$
1.00, -4	0.119	3.11, -1	1.00, -4	0.077	3.92, -1	1.00, -4	0.108	2.72, -1
1.00, -3	0.158	3.26, -1	1.00, -3	0.120	4.23, -1	1.00, -3	0.127	3.03, -1
3.00, -3	0.235	3.19, -1	3.00, -3	0.238	3.62, -1	3.00, -3	0.207	3.22, -1
6.00, -3	0.340	2.79, -1	6.00, -3	0.381	4.06, -1	6.00, -3	0.315	2.87, -1
1.00, -2	0.427	2.32, -1	1.10, -2	0.468	3.44, -1	1.00, -2	0.412	2.35, -1
1.50, -2	0.491	1.95, -1	1.90, -2	0.512	1.83, -1	1.50, -2	0.464	2.07, -1
2.10, -2	0.518	1.77, -1	2.90, -2	0.572	1.52, -1	2.10, -2	0.498	1.86, -1
2.80, -2	0.561	1.61, -1	4.20, -2	0.593	1.44, -1	2.90, -2	0.533	1.69, -1
3.60, -2	0.587	1.51, -1	5.70, -2	0.622	1.34, -1	3.90, -2	0.566	1.56, -1
4.50, -2	0.602	1.44, -1	7.50, -2	0.660	1.26, -1	5.40, -2	0.590	1.45, -1
5.60, -2	0.618	1.39, -1	9.50, -2	0.683	1.22, -1	6.90, -2	0.620	1.38, -1
6.90, -2	0.639	1.34, -1	1.25, -1	0.715	1.15, -1	8.90, -2	0.641	1.33, -1
8.40, -2	0.651	1.32, -1	1.75, -1	0.757	1.07, -1	1.19, -1	0.673	1.27, -1
1.04, -1	0.679	1.26, -1	2.45, -1	0.809	9.69, -2	1.59, -1	0.695	1.20, -1
1.34, -1	0.708	1.21, -1	3.35, -1	0.836	8.51, -2	2.09, -1	0.724	1.14, -1
1.74, -1	0.738	1.13, -1	4.45, -1	0.891	7.00, -2	2.69, -1	0.765	1.08, -1
2.34, -1	0.781	1.02, -1	5.75, -1	0.929	5.44, -2	3.39, -1	0.788	9.73, -2
3.04, -1	0.832	9.18, -2	7.25, -1	0.958	3.94, -2	4.19, -1	0.832	8.97, -2
3.94, -1	0.865	7.07, -2	8.95, -1	0.979	2.44, -2	5.09, -1	0.857	8.05, -2
4.04, -1	0.907	6.93, -2	1.11, +0	0.989	1.20, -2	6.09, -1	0.897	7.05, -2
6.04, -1	0.935	5.78, -2	1.31, +0	1.000	7.27, -3	7.19, -1	0.923	6.02, -2
7.14, -1	0.971	4.23, -2	1.53, +0	1.000	4.50, -3	8.39, -1	0.965	4.63, -2
8.34, -1	0.985	2.89, -2				9.69, -1	0.979	3.25, -2
9.54, -1	0.993	1.77, -2				1.12, +0	0.993	1.89, -2
1.10, +0	0.992	1.17, -2				1.27, +0	0.993	1.27, -2
1.25, +0	1.000	7.79, -3				1.42, +0	1.000	8.21, -3
1.40, +0	1.000	5.52, -3				1.57, +0	1.000	5.82, -3

TABLE 7(c) Mean-velocity and turbulence-intensity profiles of present writer; measured with single hot wire
(1) No blowing

Station 4			5			6		
Y(IN)	$\bar{U}$/UG	$\widetilde{U'}/\bar{U}$	Y(IN)	$\bar{U}$/UG	$\widetilde{U'}/\bar{U}$	Y(IN)	$\bar{U}$/UG	$\widetilde{U'}/\bar{U}$
1.00, -4	0.084	4.51, -1	1.00, -4	0.172	1.23, -1	1.00, -4	0.043	4.37, -1
1.00, -3	0.105	4.61, -1	1.00, -3	0.076	3.28, -1	1.00, -3	0.055	5.17, -1
3.00, -3	0.167	4.38, -1	2.00, -3	0.096	4.15, -1	3.00, -3	0.122	5.35, -1
6.00, -3	0.254	3.71, -1	4.00, -3	0.169	4.19, -1	6.00, -3	0.208	4.54, -1
1.10, -2	0.333	3.09, -1	7.00, -3	0.249	3.72, -1	1.10, -2	0.326	3.32, -1
1.90, -2	0.442	2.21, -1	1.10, -2	0.324	3.08, -1	1.80, -2	0.354	3.01, -1
2.90, -2	0.502	1.79, -1	1.60, -2	0.396	2.63, -1	2.70, -2	0.412	2.56, -1
4.40, -2	0.562	1.59, -1	2.20, -2	0.435	2.27, -1	3.90, -2	0.439	2.21, -1
6.40, -2	0.598	1.46, -1	2.90, -2	0.472	2.10, -1	5.30, -2	0.463	2.06, -1
8.90, -2	0.620	1.40, -1	3.80, -2	0.487	1.97, -1	6.90, -2	0.494	1.92, -1
1.29, -1	0.682	1.27, -1	4.90, -2	0.512	1.84, -1	8.70, -2	0.513	1.87, -1
1.89, -1	0.706	1.18, -1	6.20, -2	0.543	1.70, -1	1.17, -1	0.553	1.72, -1
2.69, -1	0.774	1.06, -1	7.40, -2	0.565	1.65, -1	1.57, -1	0.575	1.68, -1
3.79, -1	0.800	9.36, -2	8.90, -2	0.576	1.61, -1	2.17, -1	0.618	1.52, -1
5.09, -1	0.864	7.85, -2	1.09, -1	0.599	1.55, -1	2.97, -1	0.671	1.37, -1
6.59, -1	0.922	6.27, -2	1.39, -1	0.628	1.48, -1	3.97, -1	0.736	1.23, -1
8.29, -1	0.962	4.78, -2	1.84, -1	0.652	1.39, -1	5.17, -1	0.787	1.07, -1
1.02, +0	0.993	2.75, -2	2.34, -1	0.702	1.29, -1	6.67, -1	0.832	9.01, -2
1.21, +0	0.994	1.55, -2	2.94, -1	0.735	1.21, -1	8.67, -1	0.926	6.86, -2
1.41, +0	0.996	8.66, -3	3.64, -1	0.755	1.15, -1	1.07, +0	0.936	4.89, -2
1.61, +0	0.997	5.77, -3	4.54, -1	0.782	1.04, -1	1.27, +0	0.966	3.02, -2
1.81, +0	0.999	4.64, -3	5.54, -1	0.832	9.37, -2	1.47, +0	0.987	1.74, -2
1.88, +0	1.000	4.44, -3	6.74, -1	0.868	8.21, -2	1.67, +0	0.998	9.70, -3
			8.04, -1	0.906	7.16, -2	1.87, +0	0.998	6.71, -3
			9.54, -1	0.944	5.73, -2	2.07, +0	0.999	5.06, -3
			1.13, +0	0.984	3.99, -2	2.22, +0	1.000	4.75, -3
			1.33, +0	0.992	2.32, -2			
			1.53, +0	0.992	1.28, -2			
			1.73, +0	1.000	7.86, -3			
			1.88, +0	1.000	5.79, -3			
			2.08, +0	1.000	5.46, -3			

TABLE 7(c) (1) (Cont.)

Station 7			8			9		
Y(IN)	$\bar{U}/U_G$	$\widetilde{U'}/\bar{U}$	Y(IN)	$\bar{U}/U_G$	$\widetilde{U'}/\bar{U}$	Y(IN)	$\bar{U}/U_G$	$\widetilde{U'}/\bar{U}$
1.00, -4	0.094	4.85, -1	1.00, -4	0.053	1.54, -1	1.00, -4	0.013	4.89, -1
1.00, -3	0.102	5.17, -1	1.00, -3	0.034	3.22, -1	1.00, -3	0.011	6.01, -1
3.00, -3	0.145	5.12, -1	3.00, -3	0.033	6.26, -1	2.00, -3	0.012	7.72, -1
6.00, -3	0.187	4.75, -1	6.00, -3	0.052	7.39, -1	4.00, -3	0.017	8.93, -1
1.00, -2	0.231	4.21, -1	1.00, -2	0.084	7.41, -1	7.00, -3	0.027	9.30, -1
1.50, -2	0.254	3.87, -1	1.50, -2	0.121	6.99, -1	1.20, -2	0.044	8.56, -1
2.10, -2	0.298	3.48, -1	2.10, -2	0.142	6.67, -1	2.00, -2	0.052	8.36, -1
2.80, -2	0.318	3.23, -1	2.80, -2	0.164	6.26, -1	3.20, -2	0.068	7.85, -1
3.70, -2	0.336	3.07, -1	3.60, -2	0.177	6.15, -1	4.90, -2	0.078	7.71, -1
4.70, -2	0.370	2.84, -1	4.50, -2	0.189	5.94, -1	7.00, -2	0.088	7.52, -1
6.00, -2	0.386	2.69, -1	5.50, -2	0.202	5.72, -1	1.00, -1	0.098	7.27, -1
7.50, -2	0.390	2.65, -1	6.60, -2	0.215	5.51, -1	1.40, -1	0.111	7.18, -1
9.30, -2	0.406	2.53, -1	7.90, -2	0.230	5.37, -1	1.90, -1	0.123	7.01, -1
1.12, -1	0.428	2.49, -1	9.40, -2	0.245	5.20, -1	2.50, -1	0.136	6.78, -1
1.37, -1	0.450	2.41, -1	1.14, -1	0.259	4.93, -1	3.20, -1	0.182	6.39, -1
1.72, -1	0.473	2.30, -1	1.44, -1	0.274	4.61, -1	4.10, -1	0.216	6.01, -1
2.17, -1	0.502	2.15, -1	1.84, -1	0.292	4.54, -1	5.20, -1	0.273	5.43, -1
2.72, -1	0.547	2.03, -1	2.34, -1	0.316	4.26, -1	6.70, -1	0.315	4.94, -1
3.37, -1	0.584	1.82, -1	3.04, -1	0.346	3.90, -1	8.70, -1	0.410	3.95, -1
4.07, -1	0.611	1.70, -1	3.84, -1	0.407	3.38, -1	1.07, +0	0.523	2.88, -1
4.97, -1	0.663	1.56, -1	4.84, -1	0.475	2.79, -1	1.27, +0	0.661	2.18, -1
6.07, -1	0.718	1.38, -1	6.34, -1	0.551	2.31, -1	1.47, +0	0.736	1.56, -1
7.37, -1	0.776	1.21, -1	7.84, -1	0.625	1.93, -1	1.67, +0	0.777	1.27, -1
8.87, -1	0.830	1.07, -1	9.84, -1	0.698	1.51, -1	1.87, +0	0.865	9.29, -2
1.04, +0	0.851	9.35, -2	1.18, +0	0.779	1.21, -1	2.07, +0	0.911	6.98, -2
1.19, +0	0.894	7.89, -2	1.38, +0	0.829	9.93, -2	2.27, +0	0.939	4.16, -2
1.34, +0	0.923	6.66, -2	1.63, +0	0.904	7.40, -2	2.47, +0	0.969	2.37, -2
1.49, +0	0.961	5.08, -2	1.88, +0	0.951	4.54, -2	2.67, +0	0.989	1.33, -2
1.64, +0	0.977	3.56, -2	2.08, +0	0.975	2.92, -2	2.87, +0	1.000	8.86, -3
1.79, +0	0.984	2.22, -2	2.28, +0	0.992	1.84, -2	3.08, +0	1.000	6.92, -3
1.94, +0	1.000	1.53, -2	2.48, +0	0.992	1.02, -2			
2.09, +0	1.000	1.04, -2	2.68, +0	0.992	7.87, -3			
2.24, +0	1.000	7.79, -3	2.88, +0	1.000	7.01, -3			
2.39, +0	1.000	7.23, -3						

TABLE 7(c) (1) (Cont.)

Station 1			2			3		
Y(IN)	$\bar{U}/U_G$	$\widetilde{U'}/\bar{U}$	Y(IN)	$\bar{U}/U_G$	$\widetilde{U'}/\bar{U}$	Y(IN)	$\bar{U}/U_G$	$\widetilde{U'}/\bar{U}$
1.00, -4	0.067	3.47, -1	1.00, -4	0.070	5.24, -1	1.00, -4	0.100	3.95, -1
1.00, -3	0.080	3.84, -1	1.00, -3	0.079	5.14, -1	1.00, -3	0.127	3.97, -1
3.00, -3	0.132	3.93, -1	2.00, -3	0.097	4.97, -1	3.00, -3	0.173	3.88, -1
6.00, -3	0.201	3.59, -1	4.00, -3	0.158	4.56, -1	6.00, -3	0.246	3.34, -1
1.00, -2	0.263	3.15, -1	7.00, -3	0.250	3.60, -1	1.00, -2	0.283	2.81, -1
1.50, -2	0.314	2.72, -1	1.10, -2	0.306	3.05, -1	1.50, -2	0.326	2.68, -1
2.10, -2	0.359	2.39, -1	1.60, -2	0.346	2.68, -1	2.10, -2	0.364	2.45, -1
2.90, -2	0.397	2.18, -1	2.20, -2	0.370	2.42, -1	2.80, -2	0.387	2.26, -1
3.90, -2	0.419	1.96, -1	3.00, -2	0.406	2.21, -1	3.60, -2	0.406	2.15, -1
5.40, -2	0.453	1.84, -1	4.00, -2	0.439	2.06, -1	4.60, -2	0.427	2.05, -1
6.90, -2	0.478	1.78, -1	5.20, -2	0.456	1.97, -1	5.70, -2	0.440	2.01, -1
8.90, -2	0.500	1.70, -1	6.70, -2	0.474	1.89, -1	7.20, -2	0.457	1.95, -1
1.14, -1	0.539	1.64, -1	8.70, -2	0.505	1.80, -1	8.70, -2	0.462	1.94, -1
1.44, -1	0.575	1.60, -1	1.12, -1	0.530	1.74, -1	1.07, -1	0.489	1.87, -1
1.84, -1	0.625	1.51, -1	1.42, -1	0.564	1.66, -1	1.37, -1	0.503	1.85, -1
2.34, -1	0.692	1.39, -1	1.82, -1	0.598	1.57, -1	1.77, -1	0.542	1.80, -1
2.94, -1	0.756	1.21, -1	2.32, -1	0.648	1.44, -1	2.27, -1	0.593	1.73, -1
3.64, -1	0.810	1.04, -1	3.02, -1	0.724	1.30, -1	2.87, -1	0.630	1.59, -1
4.44, -1	0.852	9.05, -2	3.92, -1	0.797	1.08, -1	3.67, -1	0.691	1.42, -1
5.34, -1	0.904	7.76, -2	5.02, -1	0.841	8.75, -2	4.67, -1	0.763	1.21, -1
6.34, -1	0.942	6.90, -2	6.32, -1	0.895	6.97, -2	5.87, -1	0.833	9.58, -2
7.44, -1	0.973	5.88, -2	7.82, -1	0.942	5.66, -2	7.27, -1	0.894	7.52, -2
8.64, -1	0.997	4.63, -2	9.32, -1	0.981	4.22, -2	8.87, -1	0.929	5.79, -2
1.01, +0	1.011	2.86, -2	1.09, +0	0.992	2.59, -2	1.04, +0	0.973	4.16, -2
1.21, +0	1.017	1.57, -2	1.24, +0	0.994	1.73, -2	1.24, +0	0.981	2.42, -2
1.41, +0	1.015	8.37, -3	1.44, +0	0.996	9.49, -3	1.44, +0	0.989	1.39, -2
1.61, +0	1.012	5.57, -3	1.64, +0	0.998	6.02, -3	1.64, +0	0.990	8.29, -3
1.86, +0	1.000	4.12, -3	1.84, +0	1.000	4.70, -3	1.84, +0	0.999	5.49, -3
						2.04, +0	1.000	4.54, -3

TABLE 7(c) (2) Porous strip

Station 4			5			6		
Y(IN)	$\bar{U}/U_G$	$\widetilde{U'}/\bar{U}$	Y(IN)	$\bar{U}/U_G$	$\widetilde{U'}/\bar{U}$	Y(IN)	$\bar{U}/U_G$	$\widetilde{U'}/\bar{U}$
1.00, -4	0.051	5.26, -1	1.00, -4	0.069	5.20, -1	1.00, -4	0.030	4.65, -1
1.00, -3	0.060	5.36, -1	1.00, -3	0.075	5.19, -1	1.00, -3	0.036	5.36, -1
2.00, -3	0.079	5.25, -1	2.00, -3	0.098	5.05, -1	2.00, -3	0.048	5.84, -1
4.00, -3	0.126	4.97, -1	3.00, -3	0.118	5.02, -1	4.00, -3	0.077	6.09, -1
7.00, -3	0.176	4.42, -1	5.00, -3	0.159	4.68, -1	7.00, -3	0.132	5.46, -1
1.10, -2	0.246	3.69, -1	8.00, -3	0.203	4.15, -1	1.10, -2	0.185	4.61, -1
1.60, -2	0.308	3.08, -1	1.30, -2	0.254	3.45, -1	1.60, -2	0.224	4.10, -1
2.30, -2	0.344	2.74, -1	2.00, -2	0.306	3.03, -1	2.20, -2	0.241	3.83, -1
3.20, -2	0.365	2.55, -1	2.90, -2	0.327	2.78, -1	2.90, -2	0.269	3.56, -1
4.40, -2	0.392	2.37, -1	4.00, -2	0.354	2.57, -1	3.80, -2	0.289	3.34, -1
5.80, -2	0.411	2.26, -1	5.30, -2	0.366	2.49, -1	5.00, -2	0.299	3.14, -1
7.50, -2	0.431	2.19, -1	6.80, -2	0.391	2.36, -1	6.50, -2	0.324	3.01, -1
9.80, -2	0.462	2.06, -1	8.50, -2	0.404	2.32, -1	8.50, -2	0.336	2.92, -1
1.14, -1	0.468	2.04, -1	1.04, -1	0.426	2.26, -1	1.15, -1	0.367	2.78, -1
1.32, -1	0.485	2.02, -1	1.25, -1	0.440	2.24, -1	1.60, -1	0.388	2.67, -1
1.52, -1	0.518	1.95, -1	1.48, -1	0.445	2.22, -1	2.10, -1	0.423	2.58, -1
1.82, -1	0.531	1.92, -1	1.71, -1	0.460	2.16, -1	2.80, -1	0.450	2.48, -1
2.32, -1	0.554	1.86, -1	1.96, -1	0.484	2.10, -1	3.70, -1	0.503	2.34, -1
3.02, -1	0.602	1.76, -1	2.26, -1	0.489	2.08, -1	4.80, -1	0.549	2.16, -1
3.92, -1	0.670	1.61, -1	2.76, -1	0.524	2.04, -1	6.10, -1	0.602	1.95, -1
5.02, -1	0.737	1.40, -1	3.46, -1	0.555	1.94, -1	7.60, -1	0.678	1.70, -1
6.32, -1	0.829	1.13, -1	4.46, -1	0.615	1.81, -1	9.20, -1	0.765	1.40, -1
7.82, -1	0.890	8.48, -2	5.96, -1	0.690	1.54, -1	1.07, +0	0.846	1.08, -1
9.52, -1	0.938	5.79, -2	7.66, -1	0.778	1.21, -1	1.27, +0	0.911	7.43, -2
1.10, +0	0.964	4.34, -2	9.46, -1	0.887	8.89, -2	1.47, +0	0.949	4.68, -2
1.25, +0	0.983	3.19, -2	1.15, +0	0.938	5.77, -2	1.67, +0	0.980	2.65, -2
1.40, +0	1.001	2.04, -2	1.40, +0	0.984	3.28, -2	1.87, +0	0.989	1.63, -2
1.55, +0	1.004	1.32, -2	1.65, +0	0.991	1.68, -2	2.07, +0	0.990	1.14, -2
1.70, +0	0.998	9.41, -3	1.90, +0	0.992	8.96, -3	2.27, +0	0.999	7.93, -3
1.90, +0	1.000	6.32, -3	2.15, +0	1.000	6.19, -3	2.57, +0	1.000	5.94, -3
			2.40, +0	1.000	4.97, -3			

Table 7(c) (2) (Cont.)

Station 7			8			9		
Y(IN)	$\bar{U}$/UG	$\widetilde{U'}/\bar{U}$	Y(IN)	$\bar{U}$/UG	$\widetilde{U'}/\bar{U}$	Y(IN)	$\bar{U}$/UG	$\widetilde{U'}/\bar{U}$
1.00, -4	0.028	6.59, -1	1.00, -4	0.013	4.97, -1	1.00, -4	0.001	1.00, +0
1.00, -3	0.032	6.61, -1	1.00, -3	0.013	5.93, -1	1.00, -3	0.003	1.00, +0
2.00, -3	0.037	7.0[illegible], -1	2.00, -3	0.016	7.04, -1	2.00, -3	0.004	1.00, +0
4.00, -3	0.058	7.13, -1	4.00, -3	0.026	8.34, -1	3.00, -3	0.005	1.00, +0
7.00, -3	0.085	6.89, -1	7.00, -3	0.036	8.40, -1	5.00, -3	0.007	1.00, +0
1.10, -2	0.117	6.35, -1	1.10, -2	0.050	8.05, -1	8.00, -3	0.011	1.00, +0
1.60, -2	0.130	5.96, -1	1.60, -2	0.070	7.66, -1	1.20, -2	0.015	1.00, +0
2.20, -2	0.158	5.47, -1	2.40, -2	0.077	7.53, -1	1.80, -2	0.021	9.81, -1
2.90, -2	0.168	5.3[illegible], -1	3.20, -2	0.084	7.20, -1	2.70, -2	0.028	9.59, -1
3.80, -2	0.187	4.9[illegible], -1	4.10, -2	0.102	6.98, -1	3.80, -2	0.036	9.16, -1
4.90, -2	0.206	4.63, -1	5.10, -2	0.110	6.71, -1	5.10, -2	0.041	8.97, -1
6.30, -2	0.240	4.21, -1	6.60, -2	0.114	6.66, -1	6.60, -2	0.044	8.81, -1
7.90, -2	0.241	4.20, -1	8.60, -2	0.121	6.62, -1	8.60, -2	0.047	8.83, -1
9.90, -2	0.251	4.10, -1	1.16, -1	0.141	6.21, -1	1.08, -1	0.053	8.59, -1
1.24, -1	0.260	3.92, -1	1.56, -1	0.152	6.02, -1	1.33, -1	0.059	8.35, -1
1.54, -1	0.274	3.82, -1	2.06, -1	0.167	5.85, -1	1.63, -1	0.060	8.36, -1
1.94, -1	0.313	3.51, -1	2.66, -1	0.190	5.62, -1	2.13, -1	0.068	8.09, -1
2.44, -1	0.337	3.42, -1	3.46, -1	0.236	5.00, -1	2.83, -1	0.082	7.89, -1
3.14, -1	0.361	3.25, -1	4.46, -1	0.244	4.78, -1	3.83, -1	0.115	7.30, -1
4.04, -1	0.394	3.01, -1	5.66, -1	0.292	4.26, -1	5.13, -1	0.124	7.30, -1
5.14, -1	0.448	2.77, -1	7.16, -1	0.367	3.76, -1	6.63, -1	0.166	6.76, -1
6.44, -1	0.517	2.43, -1	8.66, -1	0.487	3.06, -1	8.63, -1	0.229	6.07, -1
7.94, -1	0.571	2.25, -1	1.07, +0	0.505	2.77, -1	1.01, +0	0.275	5.48, -1
9.44, -1	0.639	1.96, -1	1.27, +0	0.607	2.28, -1	1.16, +0	0.326	4.82, -1
1.09, +0	0.720	1.64, -1	1.47, +0	0.691	1.92, -1	1.31, +0	0.394	4.25, -1
1.24, +0	0.780	1.35, -1	1.67, +0	0.796	1.49, -1	1.46, +0	0.466	3.71, -1
1.39, +0	0.843	1.07, -1	1.87, +0	0.874	1.06, -1	1.61, +0	0.510	3.33, -1
1.54, +0	0.896	8.11, -2	2.07, +0	0.920	7.40, -2	1.76, +0	0.589	2.86, -1
1.69, +0	0.950	5.72, -2	2.27, +0	0.960	4.74, -2	1.91, +0	0.705	2.39, -1
1.84, +0	0.959	3.89, -2	2.47, +0	0.977	2.78, -2	2.11, +0	0.747	1.96, -1
2.04, +0	0.977	2.43, -2	2.67, +0	0.987	1.68, -2	2.31, +0	0.825	1.55, -1
2.24, +0	0.987	1.43, -2	2.87, +0	0.988	1.20, -2	2.61, +0	0.933	8.84, -2
2.44, +0	0.988	1.02, -2	3.07, +0	0.990	9.38, -3	2.91, +0	0.978	4.40, -2
2.64, +0	0.998	7.92, -3	3.37, +0	1.000	7.79, -3	3.21, +0	0.998	2.00, -2
2.89, +0	1.000	6.44, -3				3.51, +0	1.000	5.75, -3

TABLE 7(c) (2) (Cont.)

Station 1			3			5		
Y(IN)	$\bar{U}/U_G$	$\tilde{U}'/\bar{U}$	Y(IN)	$\bar{U}/U_G$	$\tilde{U}'/\bar{U}$	Y(IN)	$\bar{U}/U_G$	$\tilde{U}'/\bar{U}$
1.00, -4	0.013	5.64, -1	1.00, -4	0.035	7.02, -1	1.00, -4	0.026	3.95, -1
1.00, -3	0.012	6.30, -1	1.00, -3	0.046	7.13, -1	1.00, -3	0.029	5.43, -1
3.00, -3	0.013	7.45, -1	2.00, -3	0.067	6.92, -1	2.00, -3	0.033	6.86, -1
6.00, -3	0.022	8.76, -1	4.00, -3	0.101	6.42, -1	4.00, -3	0.070	6.93, -1
9.00, -3	0.032	8.58, -1	7.00, -3	0.141	5.71, -1	7.00, -3	0.119	6.38, -1
1.30, -2	0.040	8.32, -1	1.30, -2	0.184	4.96, -1	1.30, -2	0.193	5.00, -1
1.80, -2	0.049	8.15, -1	2.10, -2	0.225	4.25, -1	2.50, -2	0.250	4.14, -1
2.40, -2	0.064	7.63, -1	3.30, -2	0.262	3.69, -1	3.90, -2	0.310	3.51, -1
3.00, -2	0.073	7.43, -1	5.10, -2	0.290	3.44, -1	5.50, -2	0.309	3.38, -1
3.80, -2	0.080	7.28, -1	7.60, -2	0.317	3.25, -1	7.30, -2	0.331	3.22, -1
4.60, -2	0.090	7.08, -1	1.11, -1	0.341	3.11, -1	9.30, -2	0.336	3.18, -1
5.40, -2	0.102	6.86, -1	1.61, -1	0.366	3.06, -1	1.23, -1	0.359	3.03, -1
6.20, -2	0.108	6.78, -1	2.31, -1	0.424	2.89, -1	1.63, -1	0.389	2.92, -1
7.20, -2	0.116	6.60, -1	3.11, -1	0.494	2.69, -1	2.23, -1	0.416	2.81, -1
8.20, -2	0.127	6.49, -1	4.11, -1	0.569	2.36, -1	3.03, -1	0.465	2.63, -1
9.20, -2	0.141	6.25, -1	5.41, -1	0.659	1.94, -1	4.03, -1	0.507	2.52, -1
1.02, -1	0.151	6.14, -1	6.91, -1	0.806	1.43, -1	5.23, -1	0.564	2.30, -1
1.12, -1	0.155	6.04, -1	8.61, -1	0.909	9.00, -2	6.73, -1	0.659	1.96, -1
1.22, -1	0.174	5.80, -1	1.06, +0	0.965	5.01, -2	8.43, -1	0.757	1.62, -1
1.32, -1	0.190	5.53, -1	1.26, +0	0.985	2.58, -2	9.23, -1	0.764	1.52, -1
1.47, -1	0.205	5.33, -1	1.46, +0	0.996	1.41, -2	1.11, +0	0.890	1.06, -1
1.62, -1	0.234	5.01, -1	1.66, +0	0.998	8.74, -3	1.31, +0	0.933	6.63, -2
1.77, -1	0.254	4.72, -1	1.86, +0	1.000	6.21, -3	1.52, +0	0.989	3.21, -2
1.92, -1	0.275	4.51, -1				1.72, +0	0.999	1.70, -2
2.12, -1	0.305	4.16, -1				1.92, +0	1.000	1.05, -2
2.32, -1	0.351	3.77, -1				2.08, +0	1.000	7.94, -3
2.62, -1	0.396	3.35, -1						
3.02, -1	0.471	2.82, -1						
3.52, -1	0.575	2.25, -1						
4.12, -1	0.680	1.76, -1						
4.82, -1	0.767	1.36, -1						
5.62, -1	0.854	1.05, -1						
6.52, -1	0.895	8.40, -2						
7.52, -1	0.929	6.64, -2						
8.62, -1	0.974	5.08, -2						
1.01, +0	0.992	3.18, -2						
1.16, +0	1.001	1.94, -2						
1.31, +0	1.000	1.17, -2						
1.46, +0	1.000	7.29, -3						
1.61, +0	1.000	5.52, -3						

TABLE 7(c) (3) Perforated strip

Station 7			8			9		
Y(IN)	$\bar{U}/U_G$	$\widetilde{U'}/\bar{U}$	Y(IN)	$\bar{U}/U_G$	$\widetilde{U'}/\bar{U}$	Y(IN)	$\bar{U}/U_G$	$\widetilde{U'}/\bar{U}$
1.00, -4	0.014	4.21, -1	1.00, -4	0.001	1.00, +0	1.00, -4	0.010	3.47, -1
1.00, -3	0.011	6.85, -1	1.00, -3	0.001	1.00, +0	1.00, -3	0.006	4.79, -1
2.00, -3	0.011	8.14, -1	2.00, -3	0.001	1.00, +0	2.00, -3	0.005	6.89, -1
3.00, -3	0.018	8.84, -1	4.00, -3	0.002	1.00, +0	4.00, -3	0.004	9.63, -1
5.00, -3	0.029	9.12, -1	7.00, -3	0.006	1.00, +0	7.00, -3	0.009	9.94, -1
8.00, -3	0.046	9.08, -1	1.20, -2	0.018	1.00, +0	1.20, -2	0.021	9.71, -1
1.30, -2	0.069	8.59, -1	2.70, -2	0.034	9.89, -1	2.00, -2	0.037	9.02, -1
2.10, -2	0.098	7.93, -1	3.70, -2	0.040	9.70, -1	3.20, -2	0.050	8.44, -1
3.10, -2	0.121	7.47, -1	5.20, -2	0.055	9.25, -1	4.70, -2	0.058	8.20, -1
4.30, -2	0.133	7.13, -1	7.20, -2	0.055	9.24, -1	6.70, -2	0.067	7.90, -1
5.80, -2	0.132	7.04, -1	9.70, -2	0.065	9.04, -1	9.00, -2	0.076	7.62, -1
7.80, -2	0.174	6.42, -1	1.32, -1	0.085	8.48, -1	1.15, -1	0.066	7.85, -1
1.03, -1	0.172	6.18, -1	1.77, -1	0.086	8.54, -1	1.50, -1	0.076	7.62, -1
1.38, -1	0.187	5.90, -1	2.37, -1	0.111	8.10, -1	2.00, -1	0.086	7.43, -1
1.83, -1	0.221	5.42, -1	3.17, -1	0.138	7.58, -1	2.70, -1	0.098	7.28, -1
2.43, -1	0.239	5.21, -1	4.17, -1	0.152	7.22, -1	3.60, -1	0.110	7.16, -1
3.23, -1	0.299	4.58, -1	5.47, -1	0.202	6.37, -1	4.80, -1	0.124	7.04, -1
4.23, -1	0.343	4.09, -1	7.07, -1	0.263	5.68, -1	6.30, -1	0.151	6.62, -1
5.53, -1	0.390	3.56, -1	8.97, -1	0.330	4.71, -1	8.30, -1	0.183	6.28, -1
7.13, -1	0.455	3.10, -1	1.13, +0	0.471	3.55, -1	1.08, +0	0.258	5.55, -1
9.23, -1	0.553	2.58, -1	1.33, +0	0.538	3.04, -1	1.33, +0	0.373	4.60, -1
1.07, +0	0.643	2.21, -1	1.53, +0	0.610	2.59, -1	1.63, +0	0.451	3.73, -1
1.27, +0	0.749	1.78, -1	1.73, +0	0.733	2.03, -1	1.93, +0	0.543	2.98, -1
1.47, +0	0.797	1.46, -1	1.93, +0	0.812	1.59, -1	2.28, +0	0.687	2.21, -1
1.67, +0	0.892	1.07, -1	2.13, +0	0.869	1.24, -1	2.68, +0	0.856	1.34, -1
1.87, +0	0.956	6.69, -2	2.33, +0	0.927	8.35, -2	3.18, +0	0.969	4.54, -2
2.07, +0	0.974	3.72, -2	2.53, +0	0.979	5.06, -2	3.68, +0	0.989	1.42, -2
2.27, +0	0.983	2.01, -2	2.73, +0	1.000	2.51, -2	4.18, +0	1.000	9.51, -3
2.47, +0	0.982	1.24, -2	2.93, +0	1.000	1.66, -2			
2.67, +0	0.991	9.18, -3	3.18, +0	1.000	1.07, -2			
2.87, +0	1.001	7.46, -3						
3.07, +0	1.000	6.46, -3						

TABLE 7(c) (3) (Cont.)

Test	Stn.	u_G/u_1	R_2	H_{12}	H_{32}	ζ	Comments
No blowing	1	1.000	4.13,3	1.376	1.778	0.654	1) Width of blowing section = 1in; station 1 $2^1/8$in downstream of blowing section; distance between adjacent x-stations = $2^1/4$ in. 2) u_1/ν= 5×10^5/ft. 3) v_S/u_G =0.07 for porous and perforated strips.
	2	0.980	4.15,3	1.336	1.791	0.675	
	3	0.957	5.04,3	1.383	1.770	0.640	
	4	0.931	4.74,3	1.405	1.764	0.631	
	5	0.902	5.83,3	1.469	1.751	0.609	
	6	0.868	6.51,3	1.489	1.724	0.564	
	7	0.828	8.73,3	1.628	1.678	0.483	
	8	0.790	1.10,4	1.979	1.611	0.357	
	9	0.764	1.25,4	2.658	1.539	0.191	
Porous strip	1	1.000	4.11,3	1.694	1.650	0.431	
	2	0.979	5.51,3	1.560	1.706	0.533	
	3	0.955	6.75,3	1.580	1.696	0.514	
	4	0.929	6.85,3	1.649	1.668	0.466	
	5	0.900	8.44,3	1.713	1.645	0.422	
	6	0.870	9.99,3	1.824	1.618	0.370	
	7	0.841	1.18,4	2.052	1.579	0.288	
	8	0.818	1.36,4	2.535	1.530	0.163	
	9	0.800	1.42,4	3.392	1.476	-	
Perforated strip	1	1.000	5.17,3	2.715	1.569	0.265	
	3	0.953	7.46,3	1.964	1.593	0.318	
	5	0.897	9.47,3	1.876	1.601	0.336	
	7	0.843	1.26,4	2.295	1.553	0.227	
	8	0.818	1.38,4	3.000	1.502	0.039	
	9	0.814	1.74,4	3.233	1.477	-	

TABLE 7(d) Experimental data of present writer: velocity - profile data from hot-wire measurements

No Blowing		Porous Strip		Perforated Strip	
Y(IN)	10^3S	Y(IN)	10^3S	Y(IN)	10^3S
0.137	1.937	0.137	2.788	.137	2.849
0.161	2.005	0.165	3.394	.156	2.942
0.186	1.886	0.190	4.081	.181	3.120
0.236	1.598	0.215	4.438	.206	3.867
0.286	1.562	0.240	4.663	.231	3.807
0.336	1.389	0.265	4.446	.256	3.872
0.386	1.250	0.290	4.274	.281	3.939
0.436	1.123	0.340	4.088	.306	3.711
0.486	0.955	0.390	3.159	.331	3.412
0.536	0.857	0.440	2.197	.356	3.259
0.586	0.715	0.490	1.513	.381	2.968
0.636	0.651	0.540	1.157	.431	2.209
0.686	0.536	0.590	0.996	.481	1.611
0.736	0.337	0.690	0.818	.531	0.563
0.786	0.279	0.790	0.599	.581	0.758
0.836	0.242	0.890	0.424	.631	0.569
0.886	0.179	1.040	0.233	.681	0.523
0.936	0.134	1.190	0.098	.781	0.463
0.986	0.104	1.341	0.051	.881	0.243
1.086	0.062	1.490	0.019	0.981	0.205
1.187	0.040	1.640	0.006	1.081	0.133
1.286	0.026	1.791	0.002	1.182	0.063
1.387	0.011			1.332	0.026
				1.482	0.014
				1.631	0.004
				1.711	0.002

TABLE 7(e) Shear-stress profiles of present writer at station 1

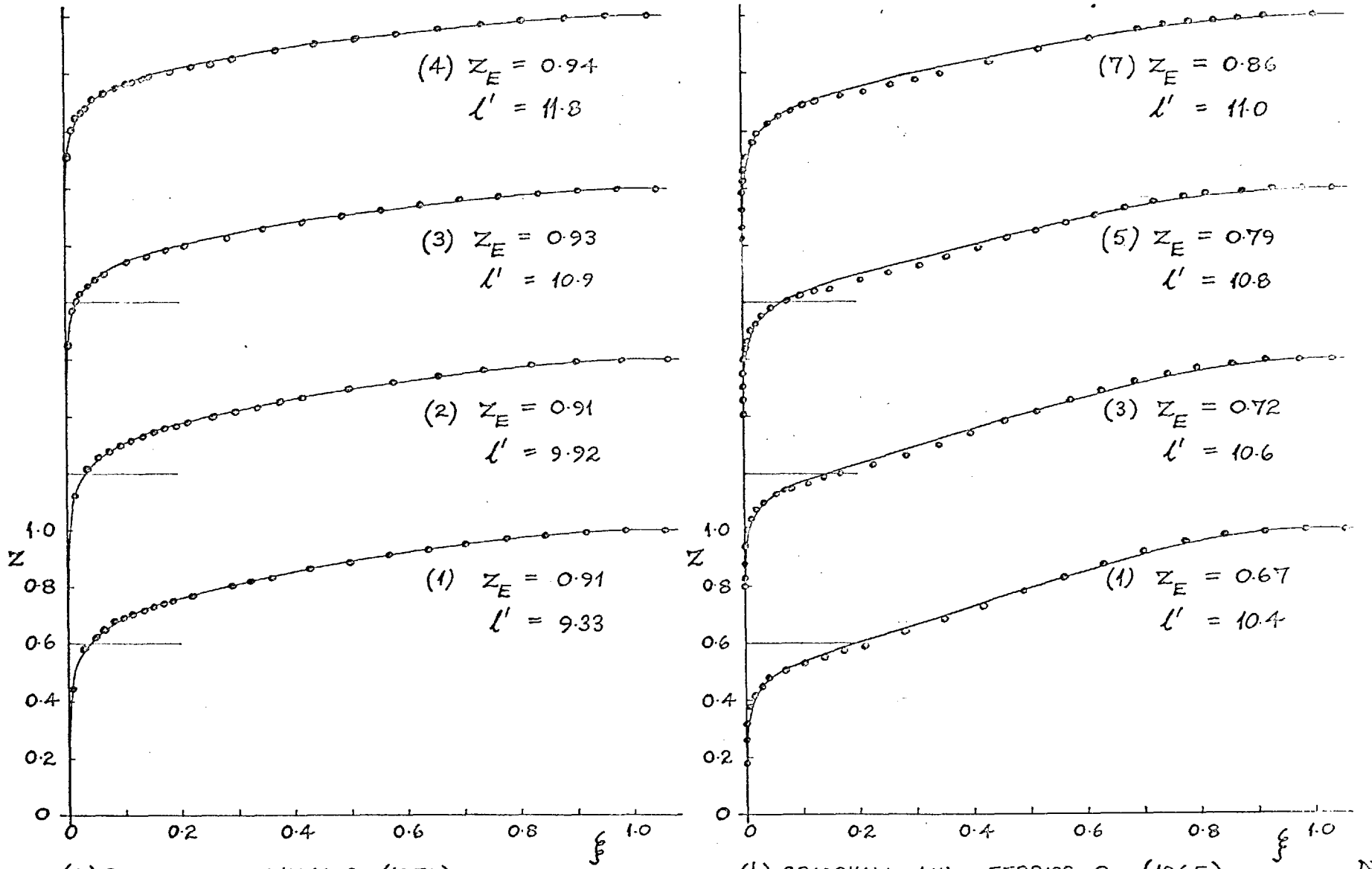


FIGURE 3.1 COMPARISON OF MEASURED VELOCITY PROFILES WITH (3.2-9)

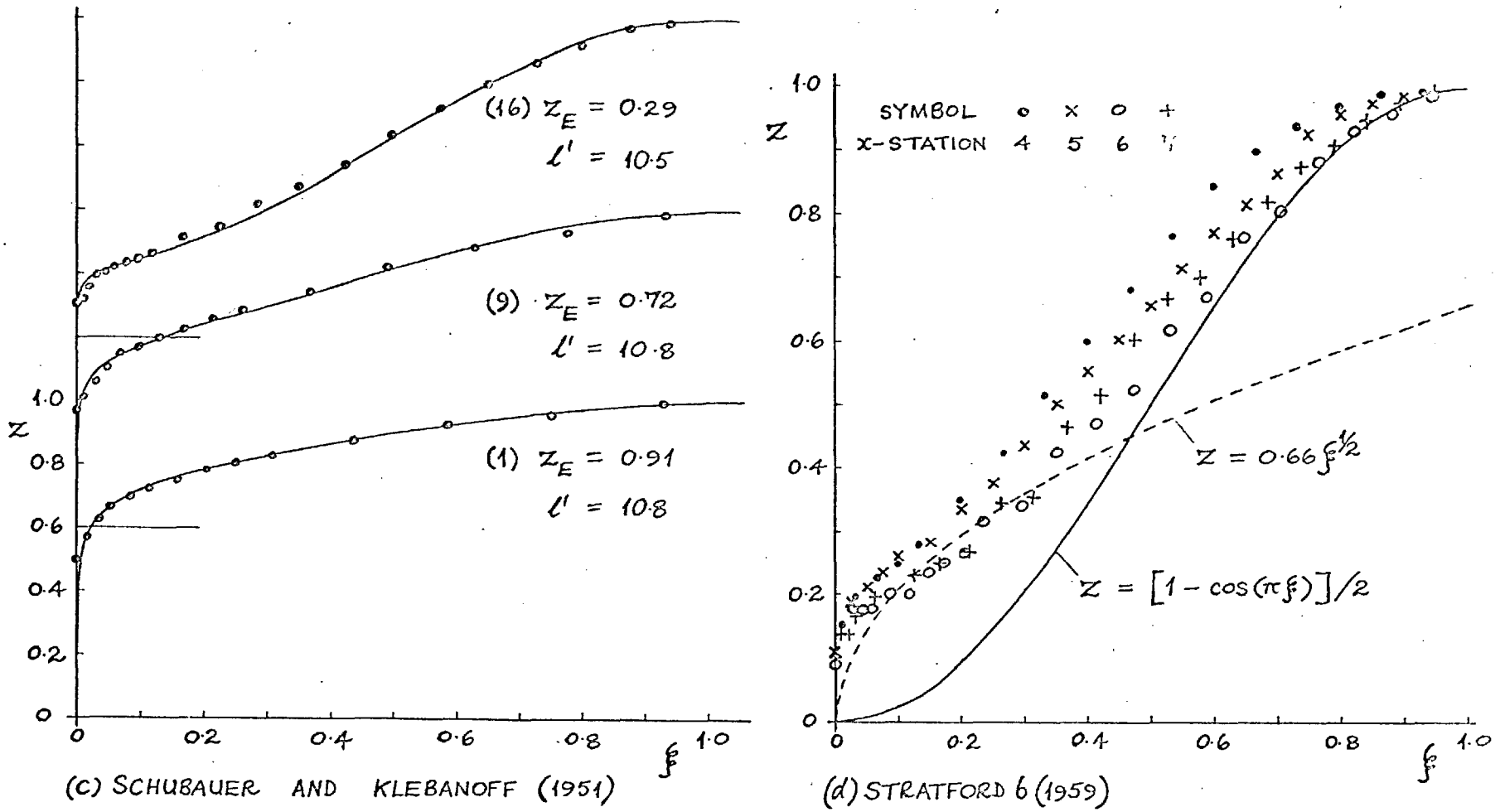
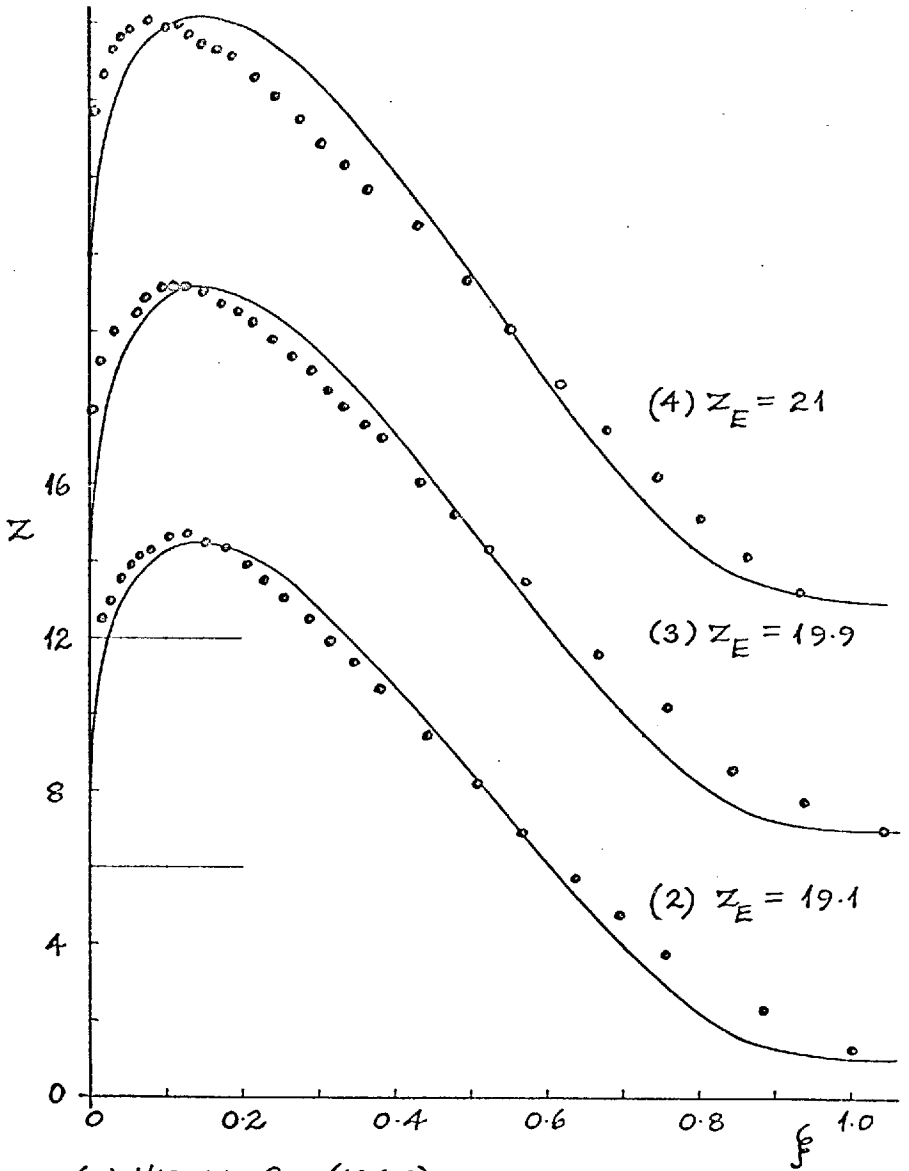
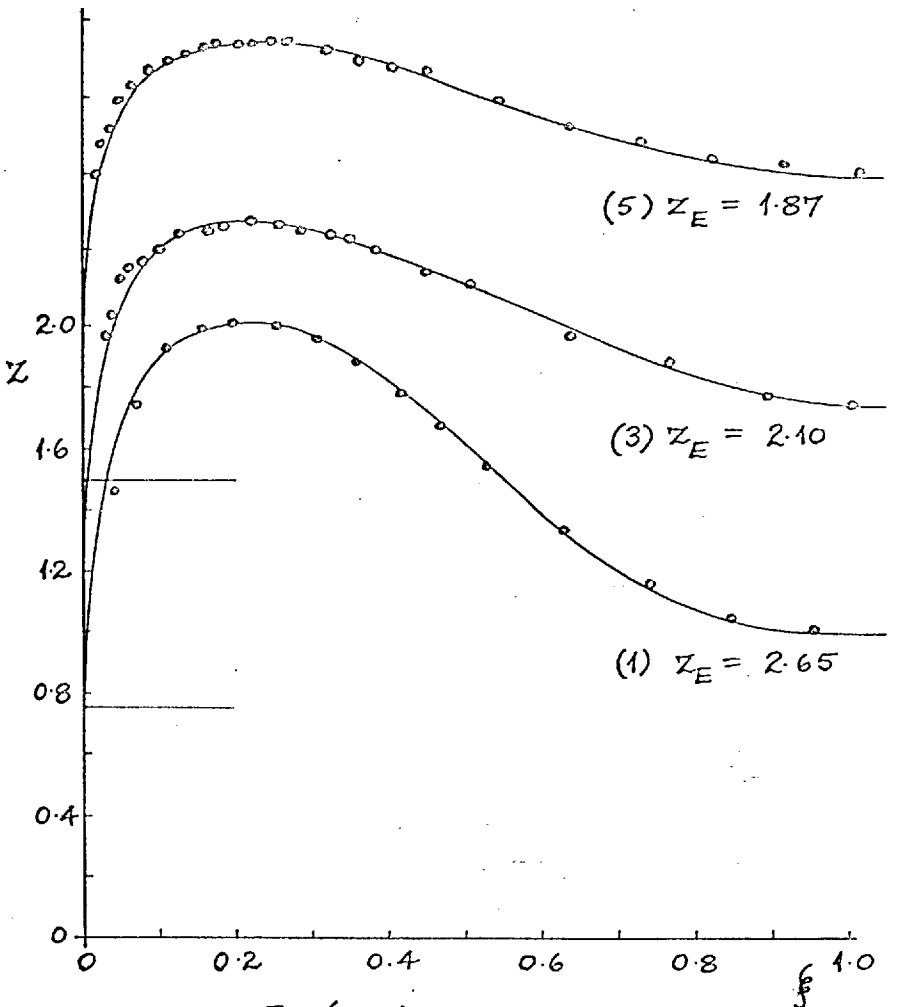


FIGURE 3.1 (CONT.)



(e) NICOLL 3 (1965)



(f) NICOLL 5 (1965)

FIGURE 3.1 (CONCL.)

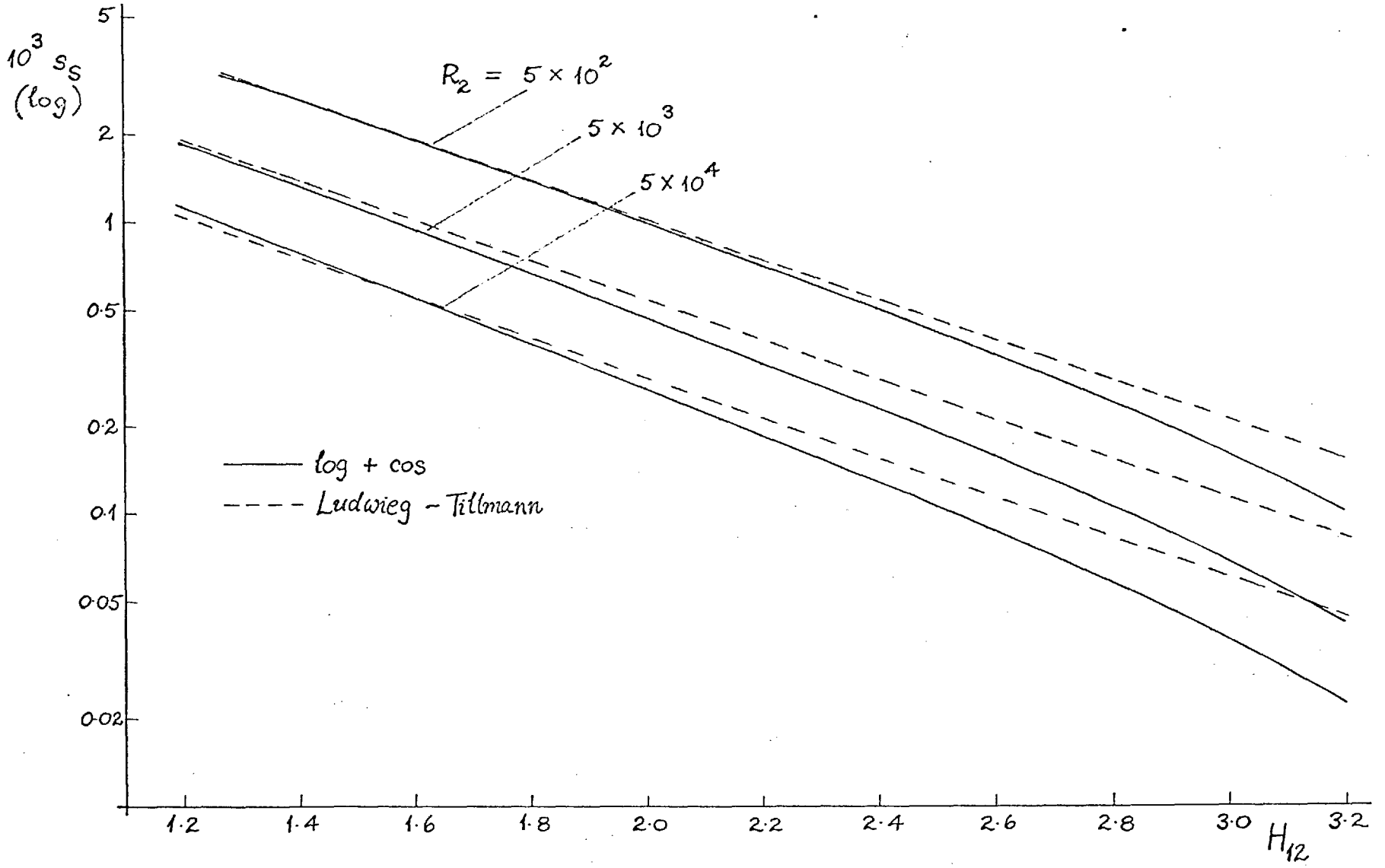


FIGURE 3.2 COMPARISON WITH DRAG LAW OF LUDWIEG AND TILLMANN OF THAT IMPLICIT IN LOG-PLUS-COS VELOCITY-PROFILE EXPRESSION

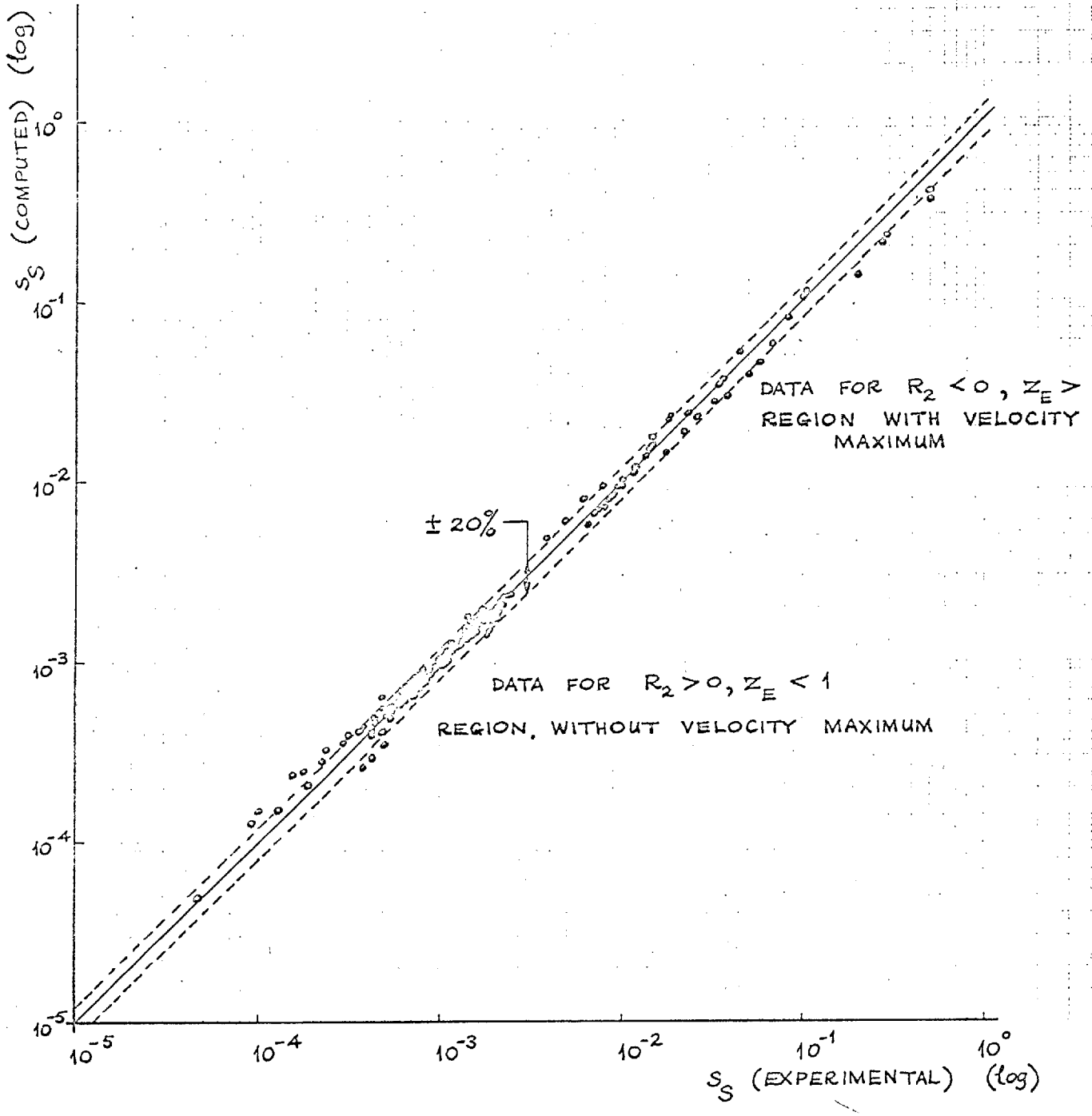


FIGURE 3.3 COMPARISON WITH EXPERIMENTAL DATA OF VALUES OF S_S COMPUTED FROM R_2 AND H_{12} WITH DRAG LAW IMPLICIT IN LOG-PLUS-COS VELOCITY-PROFILE EXPRESSION.

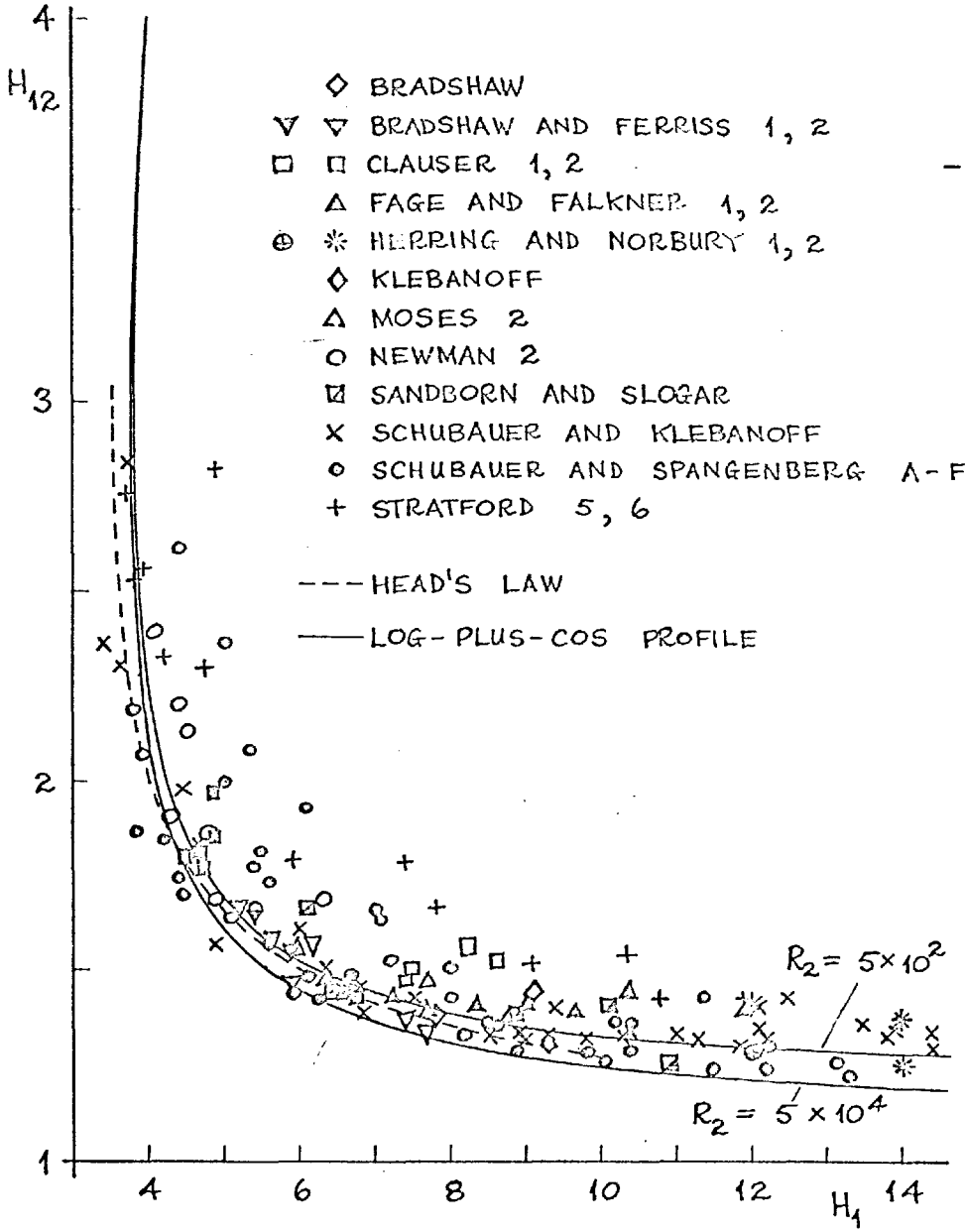


FIGURE 3.4 COMPARISON OF SHAPE-FACTOR RELATIONSHIPS WITH EXPERIMENTAL DATA

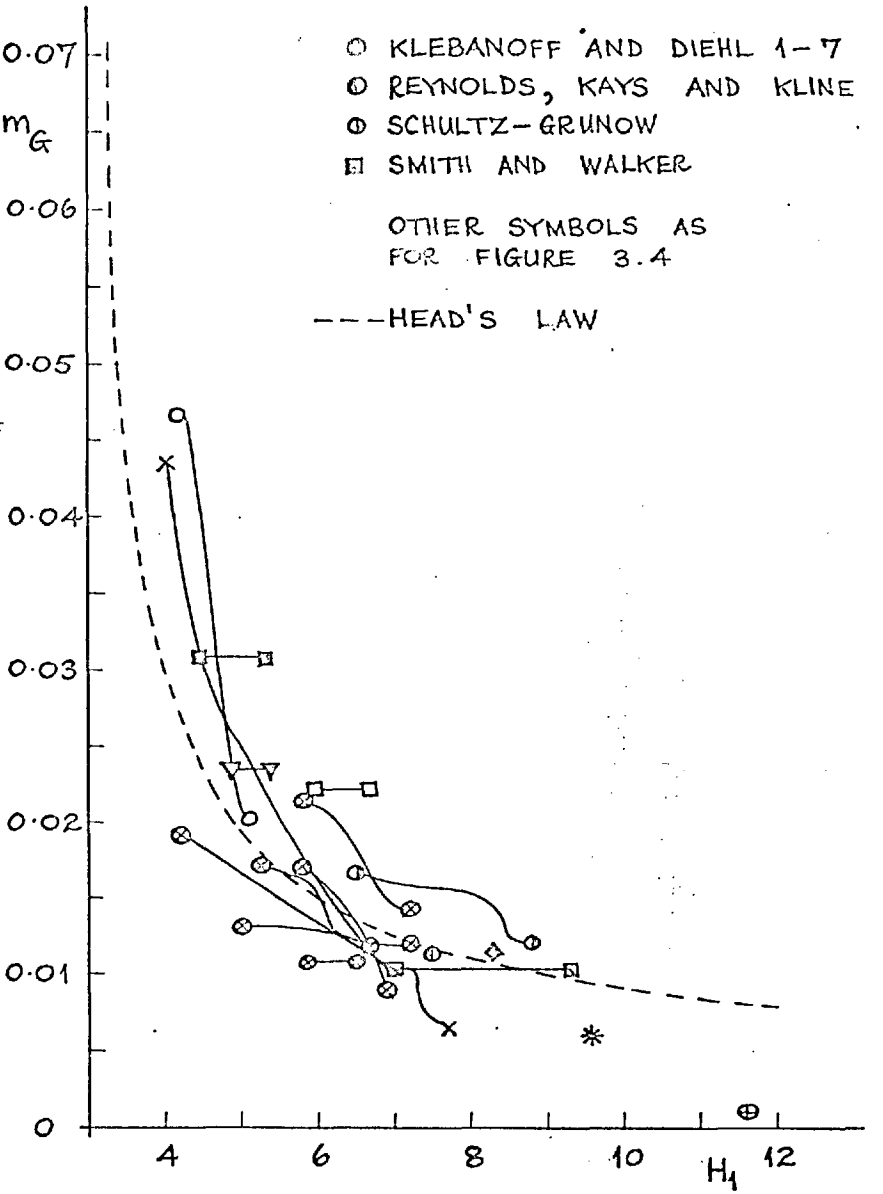


FIGURE 3.5 COMPARISON OF HEAD'S ENTRAINMENT LAW WITH EXPERIMENTAL DATA

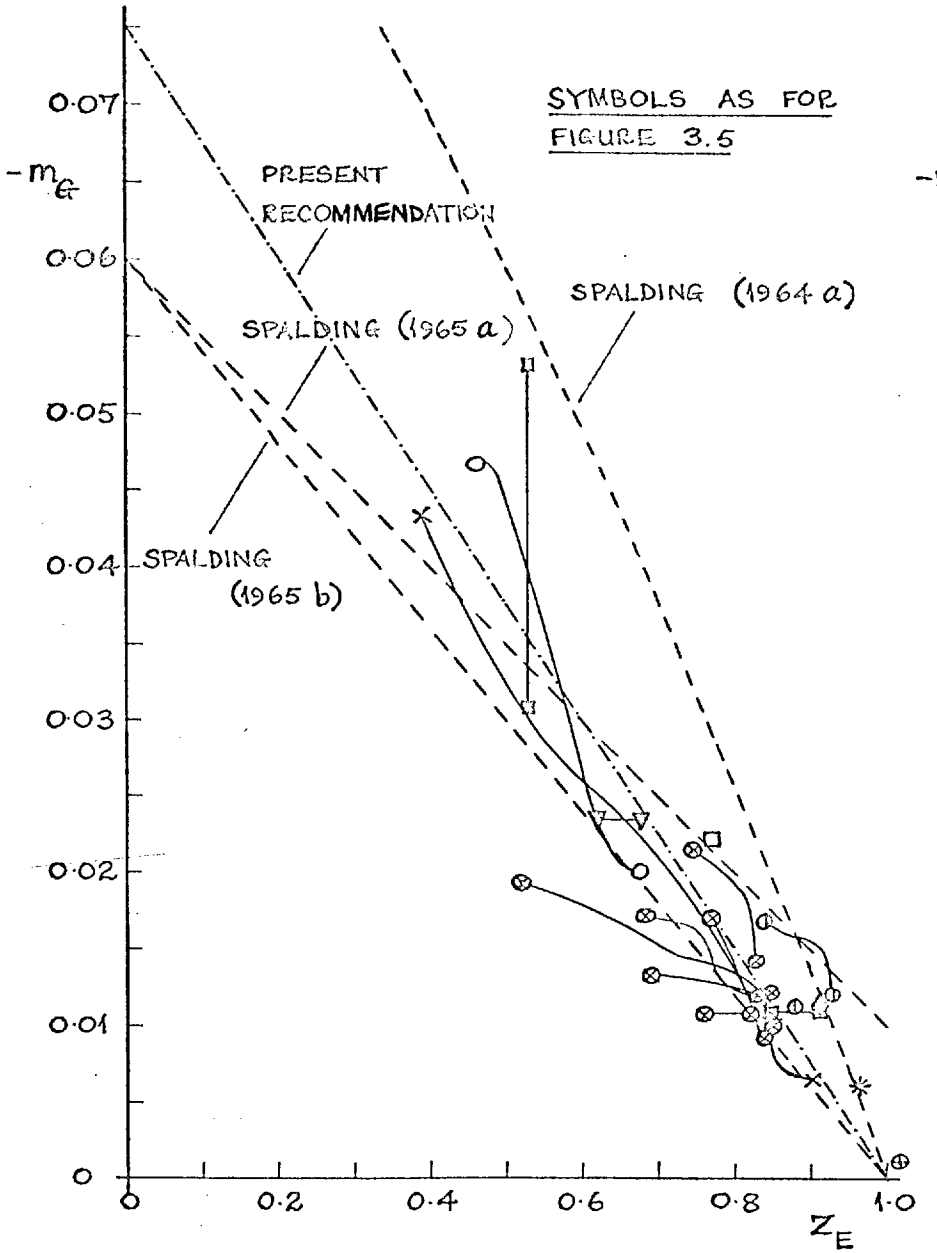


FIGURE 3.6 COMPARISON OF VARIOUS ENTRAINMENT LAWS WITH EXPERIMENTAL DATA

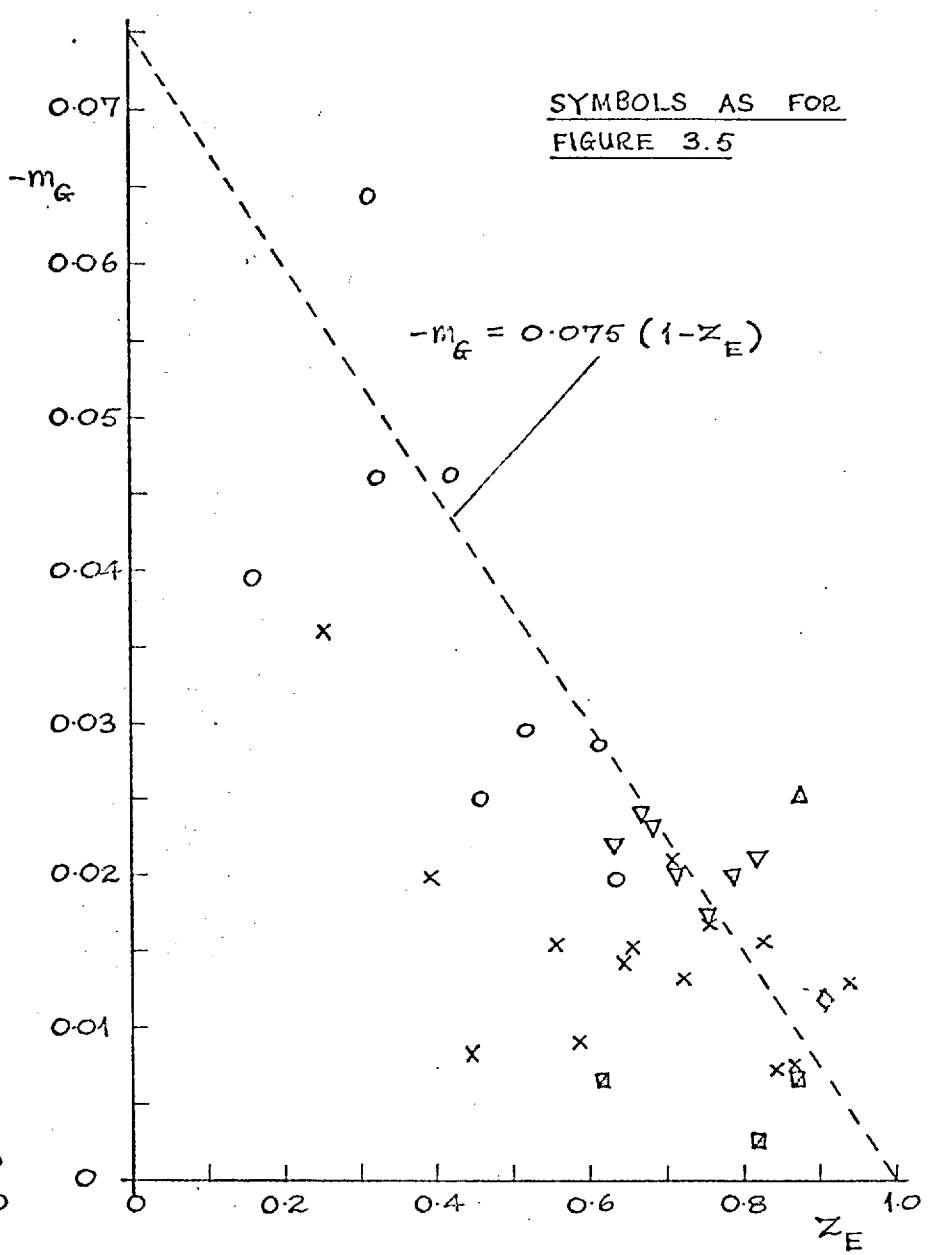


FIGURE 3.7 COMPARISON OF RECOMMENDED ENTRAINMENT LAW WITH VALUES OF $-m_G$ DEDUCED FROM S~Z CURVES; $Z_E < 1$

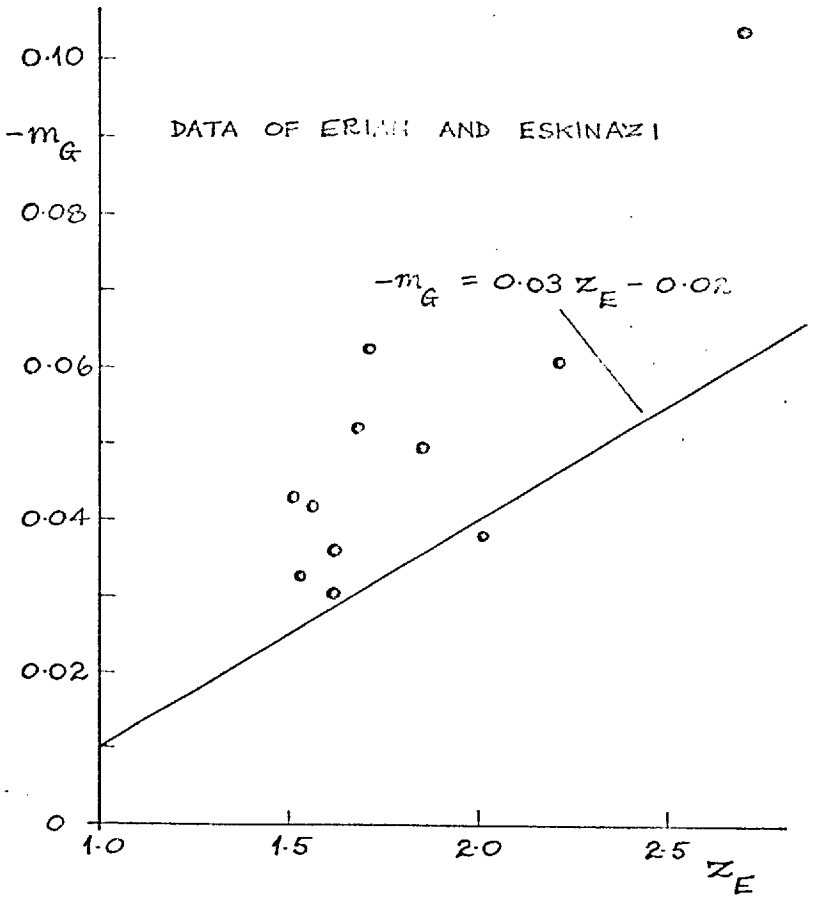


FIGURE 3.8 COMPARISON OF RECOMMENDED ENTRAINMENT LAW WITH VALUES OF $-m_G$ DEDUCED FROM $S \sim z$ CURVES; $z_E > 1$

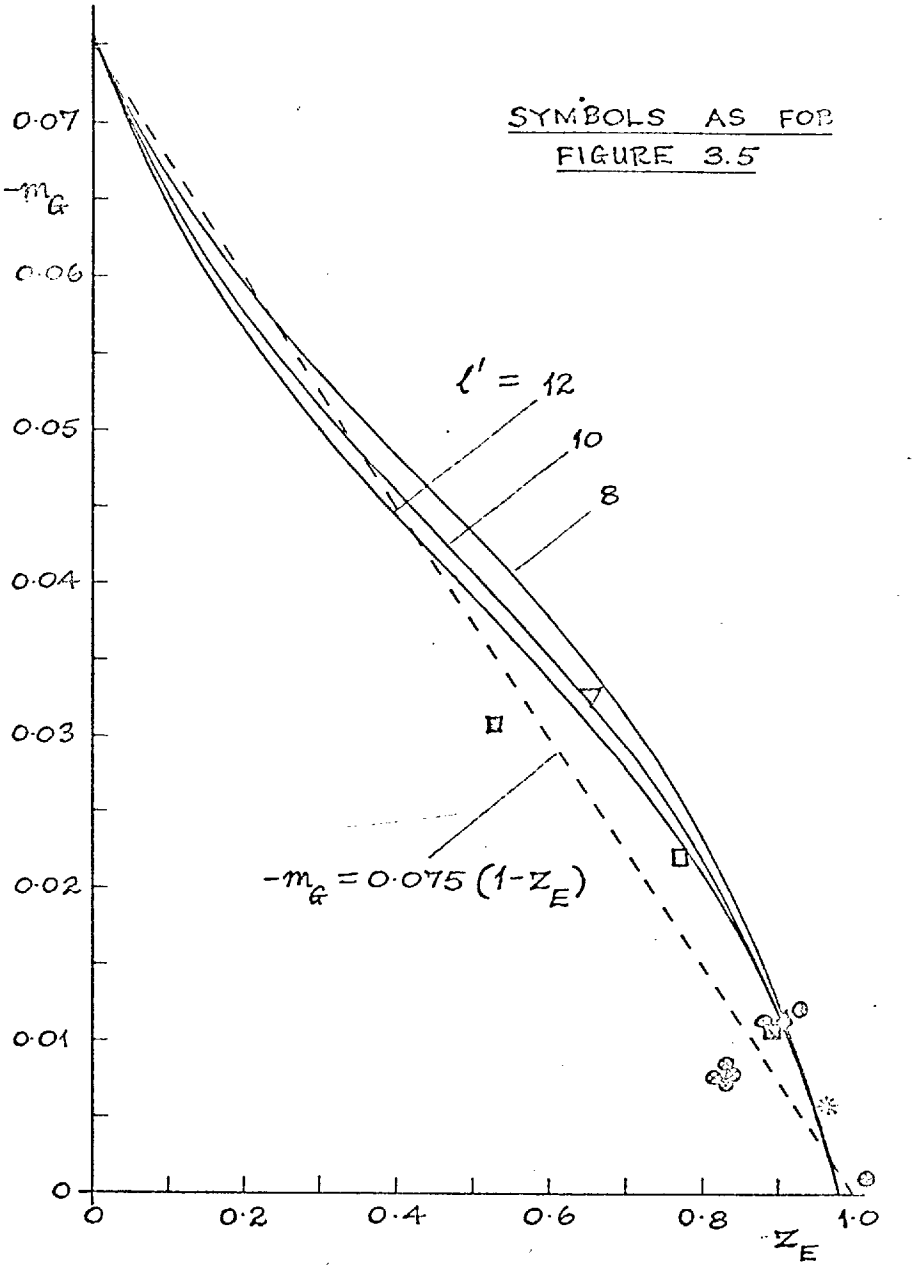


FIGURE 3.9 COMPARISON OF ENTRAINMENT LAW, DEDUCED FOR EQUILIBRIUM BOUNDARY LAYERS, WITH EXPERIMENTAL DATA

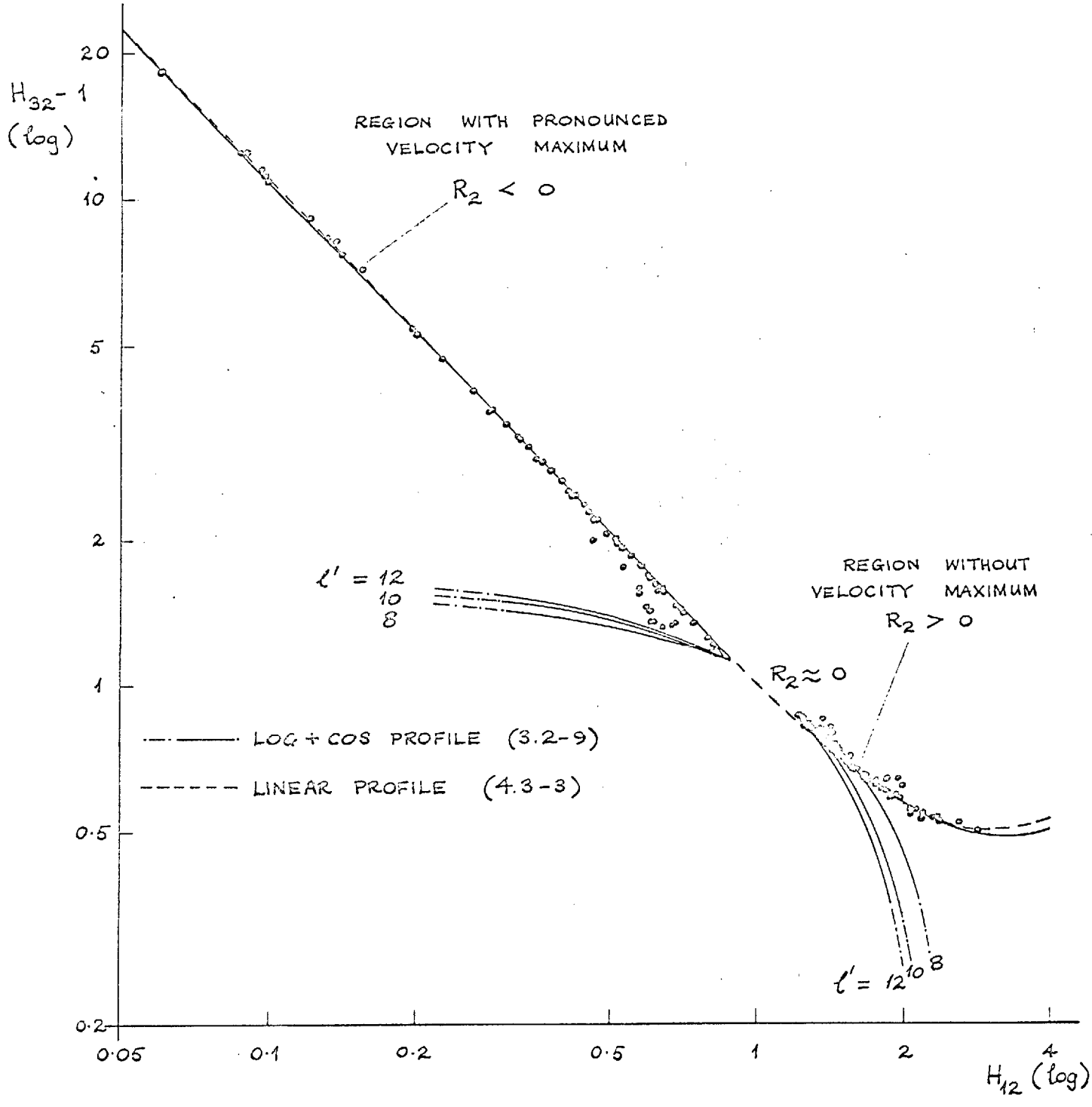


FIGURE 4.1 COMPARISON OF SHAPE-FACTOR RELATIONS, DEDUCED FROM VELOCITY-PROFILE EXPRESSIONS, WITH EXPERIMENTAL DATA

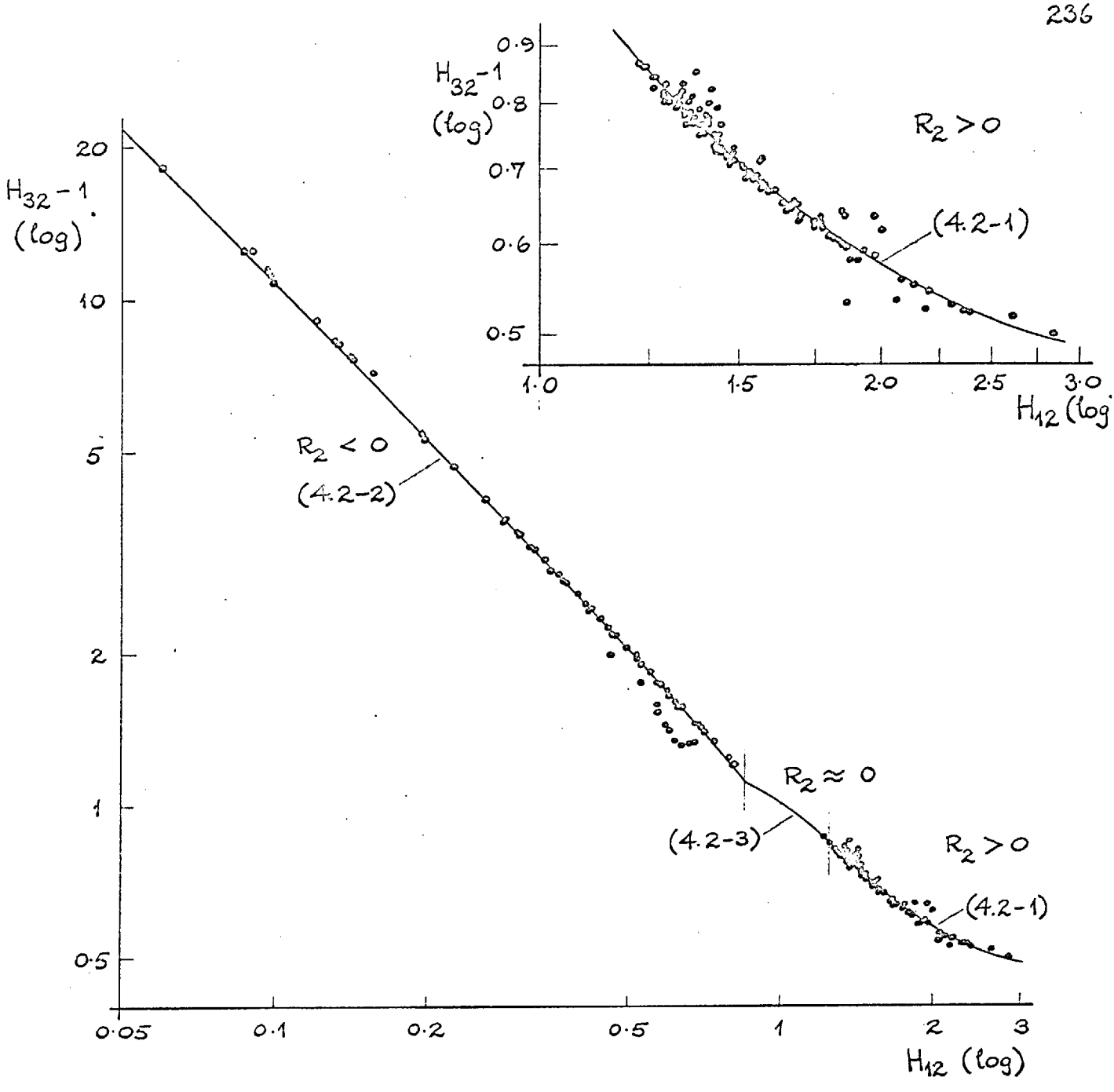


FIGURE 4.2 COMPARISON OF RECOMMENDED SHAPE-FACTOR RELATION WITH EXPERIMENTAL DATA

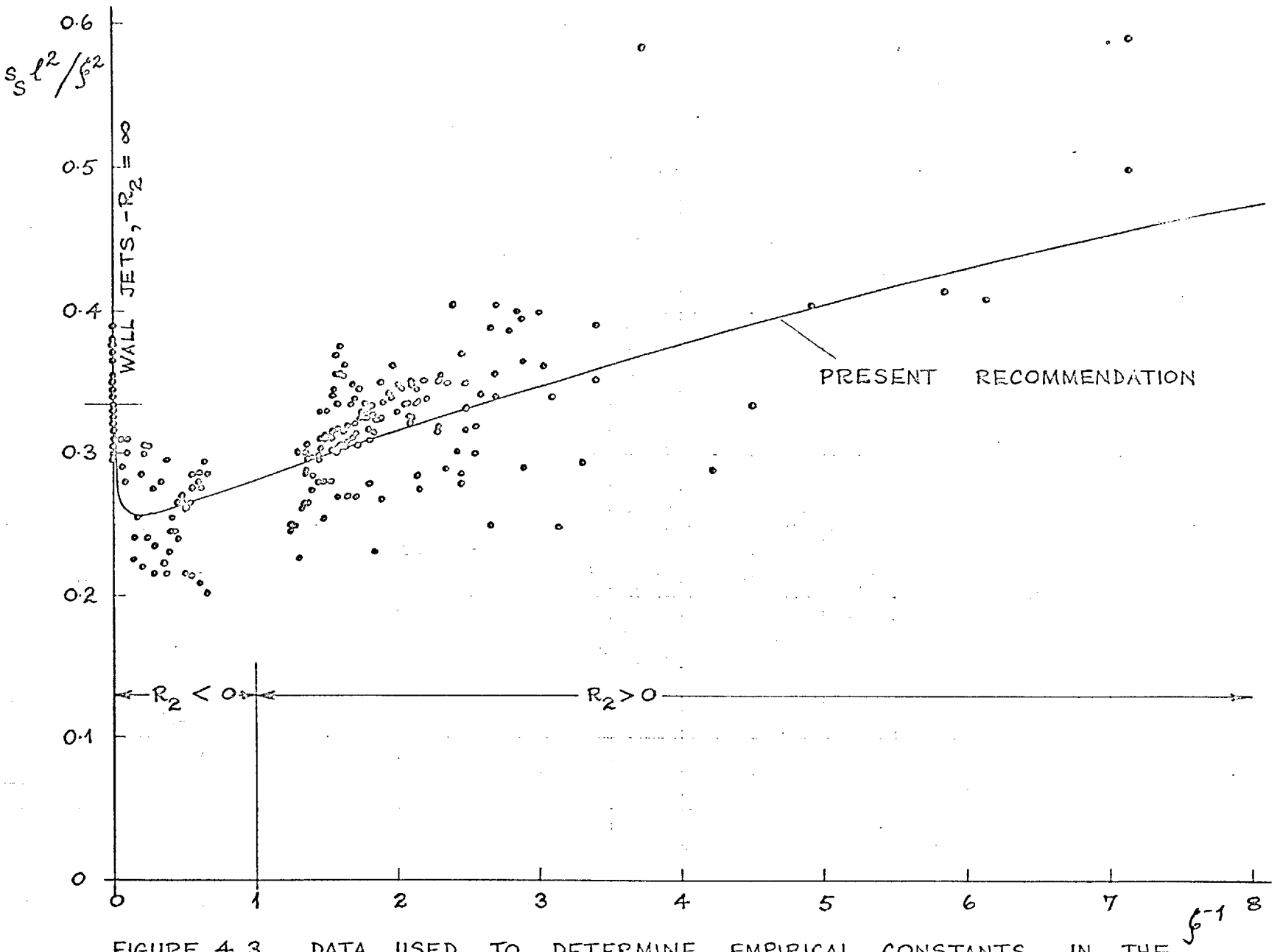


FIGURE 4.3 DATA USED TO DETERMINE EMPIRICAL CONSTANTS IN THE DRAG – LAW RECOMMENDATION

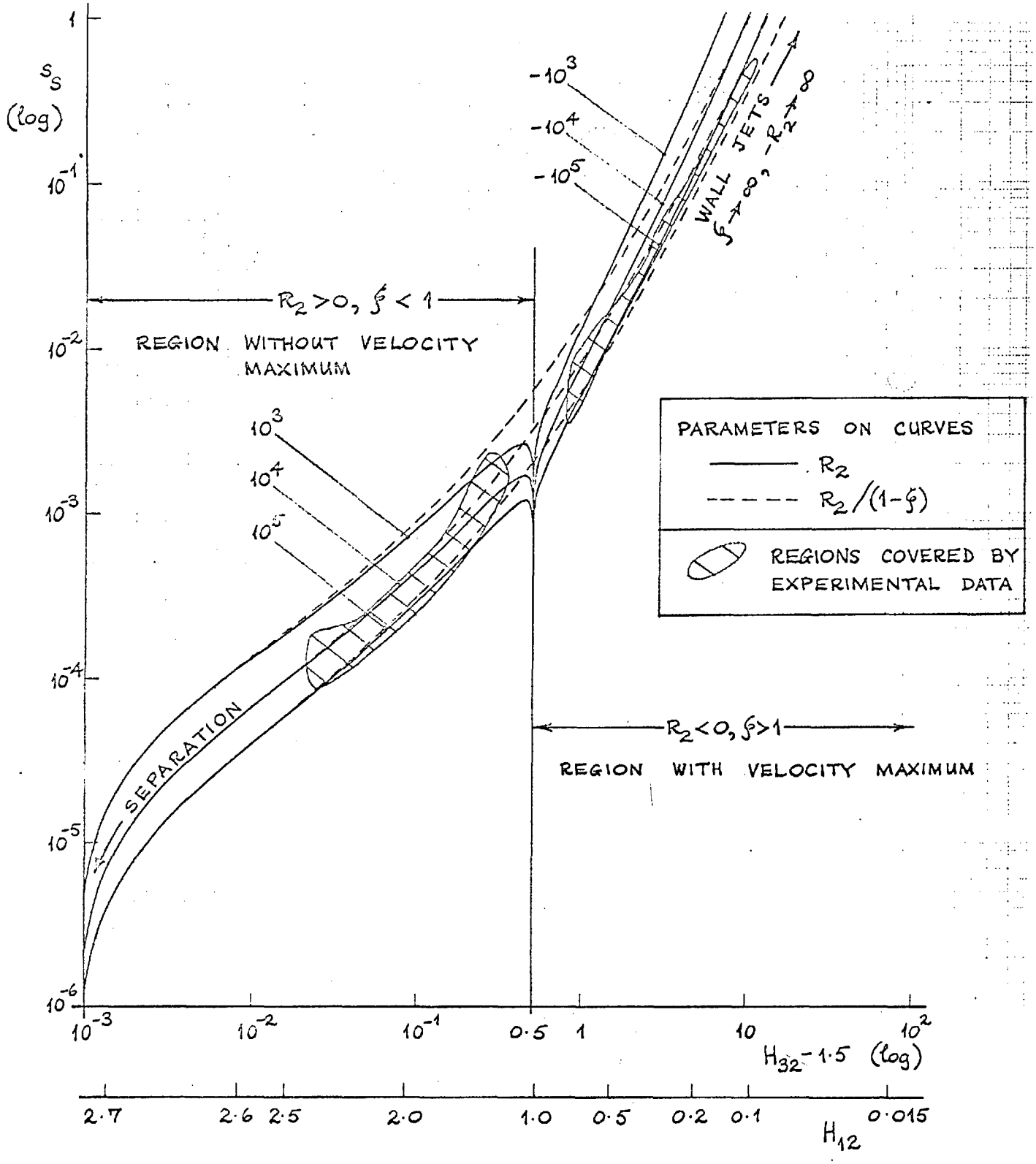


FIGURE 4.4 GRAPHICAL REPRESENTATION OF THE RECOMMENDED DRAG LAW, (4.3-19)

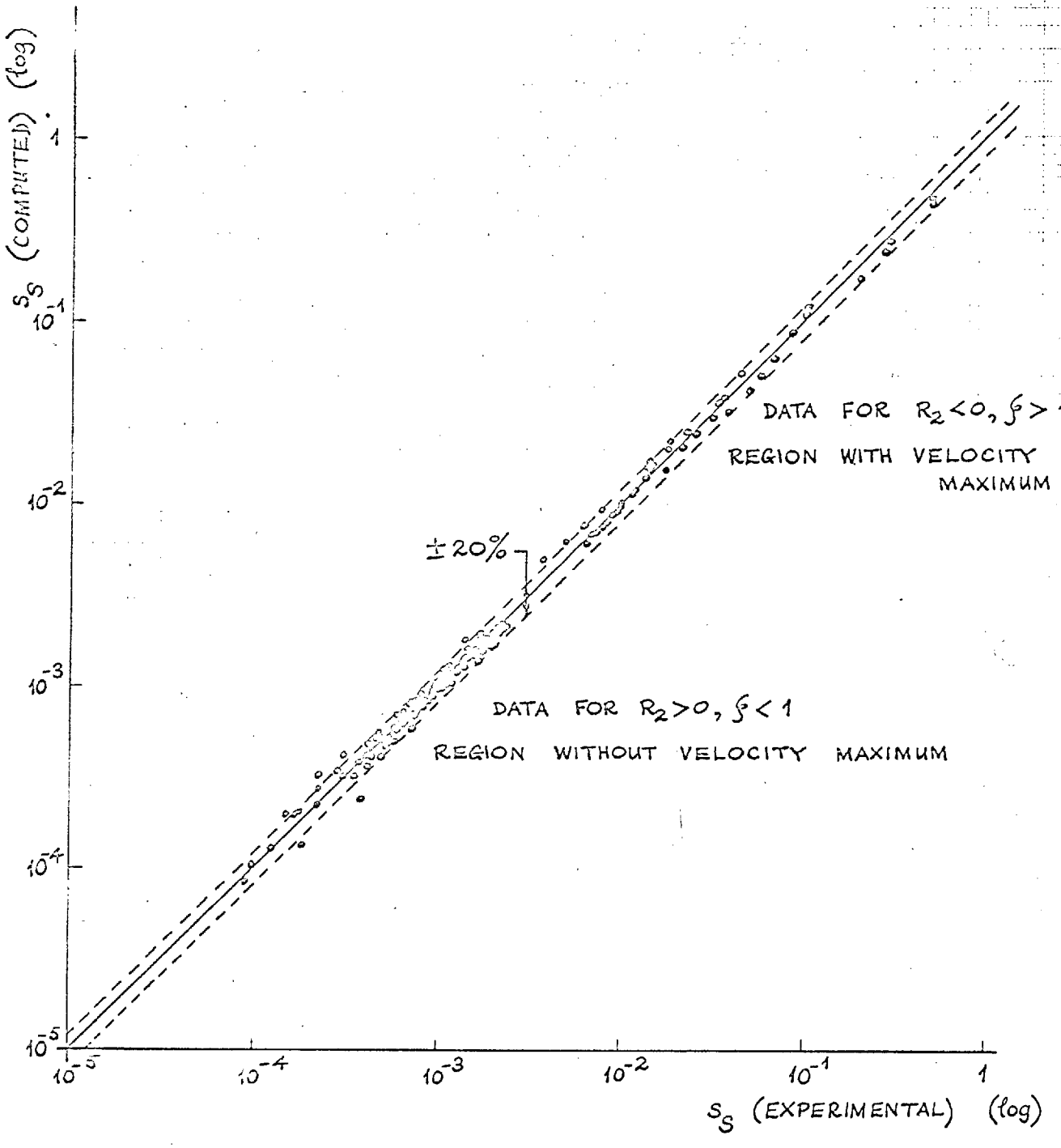


FIGURE 4.5 COMPARISON WITH EXPERIMENTAL DATA OF VALUES OF S_S COMPUTED FROM R_2 AND H_{32} WITH RECOMMENDED DRAG LAW

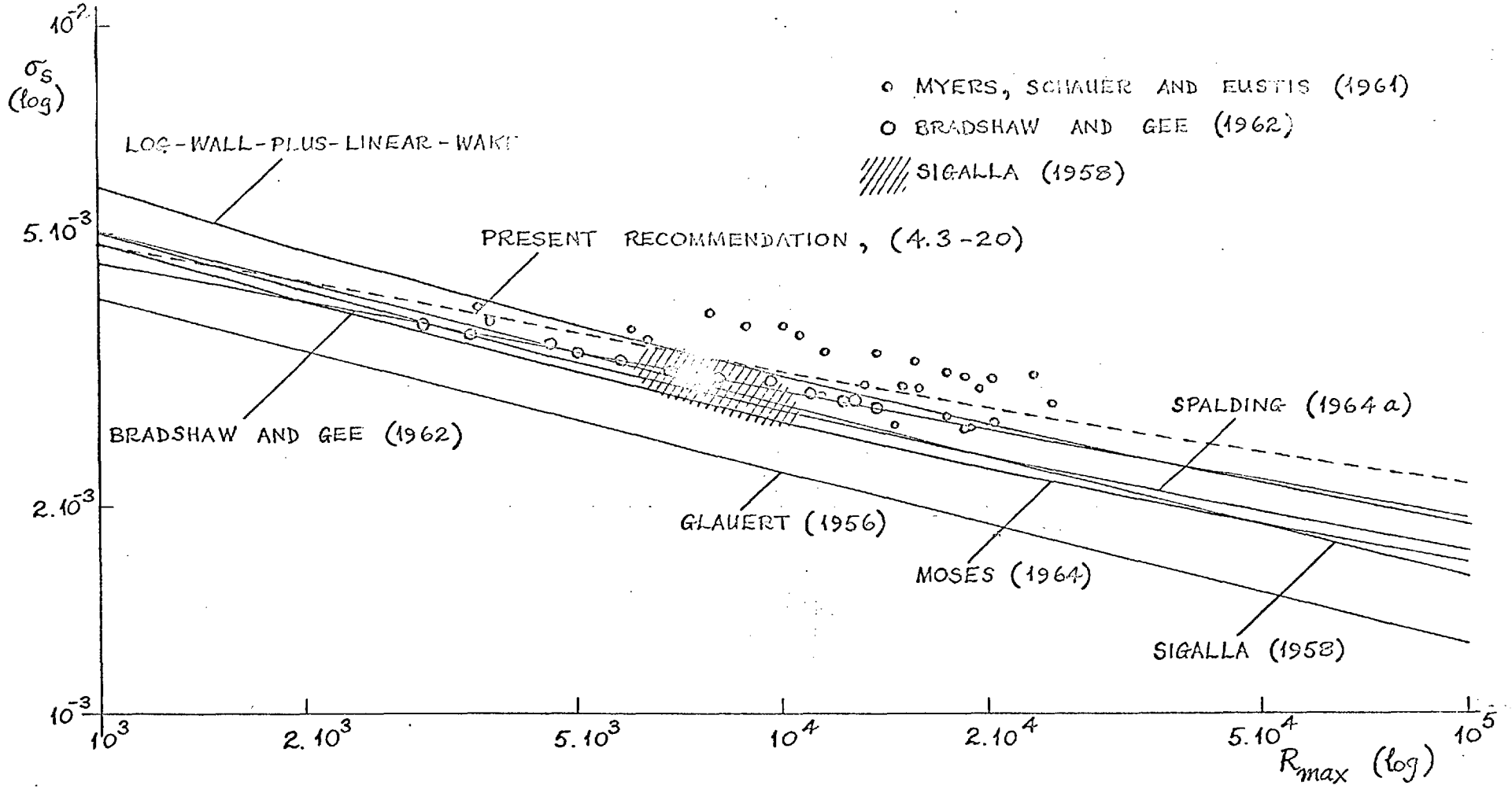


FIGURE 4.6 COMPARISON OF DRAG LAWS WITH EXPERIMENTAL DATA FOR WALL JETS

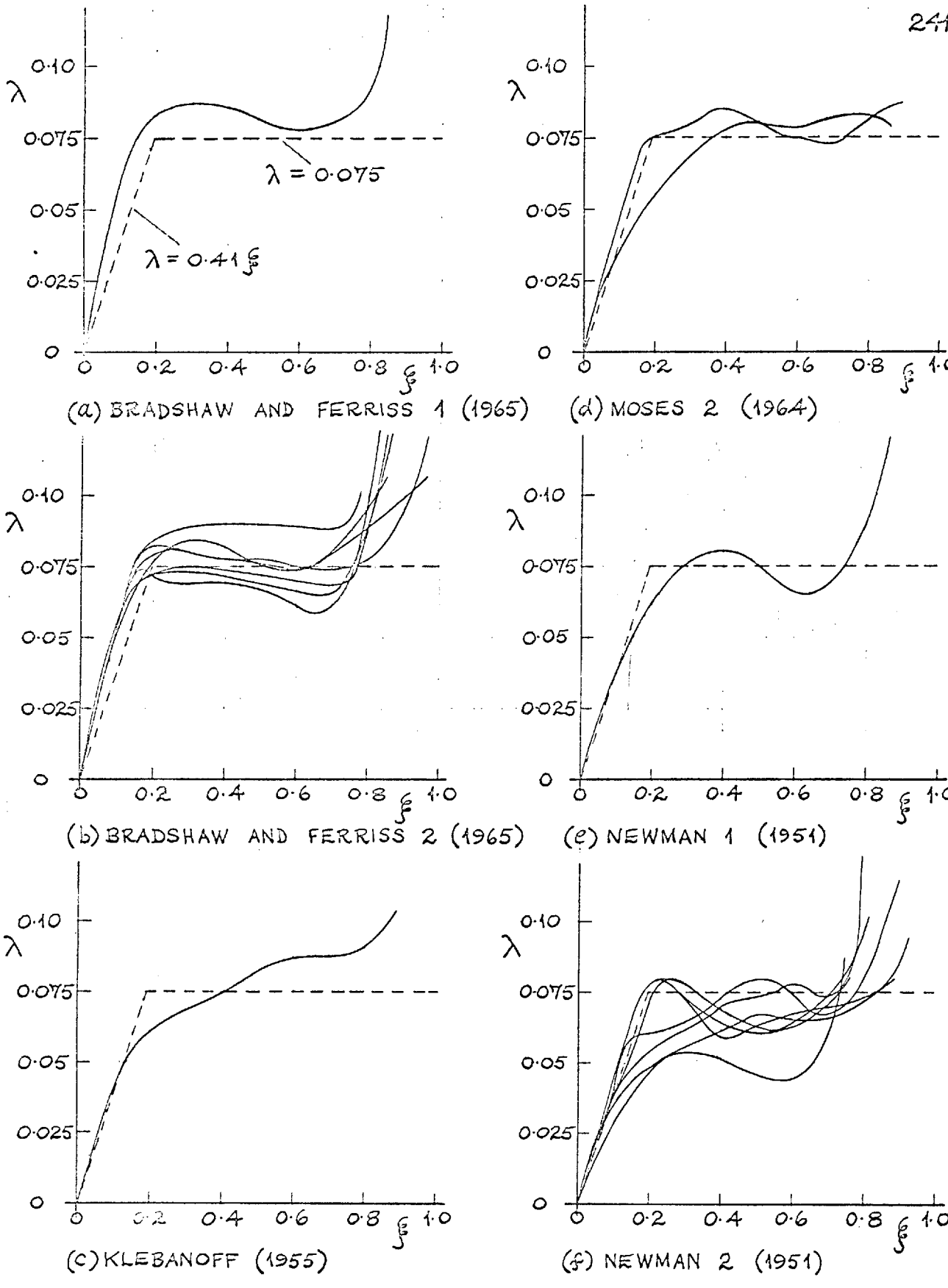
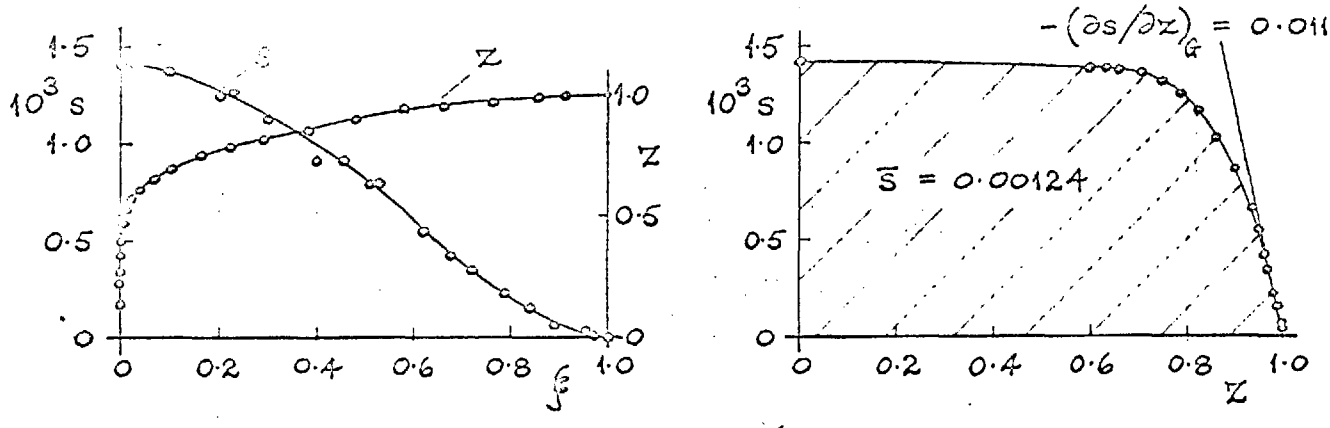
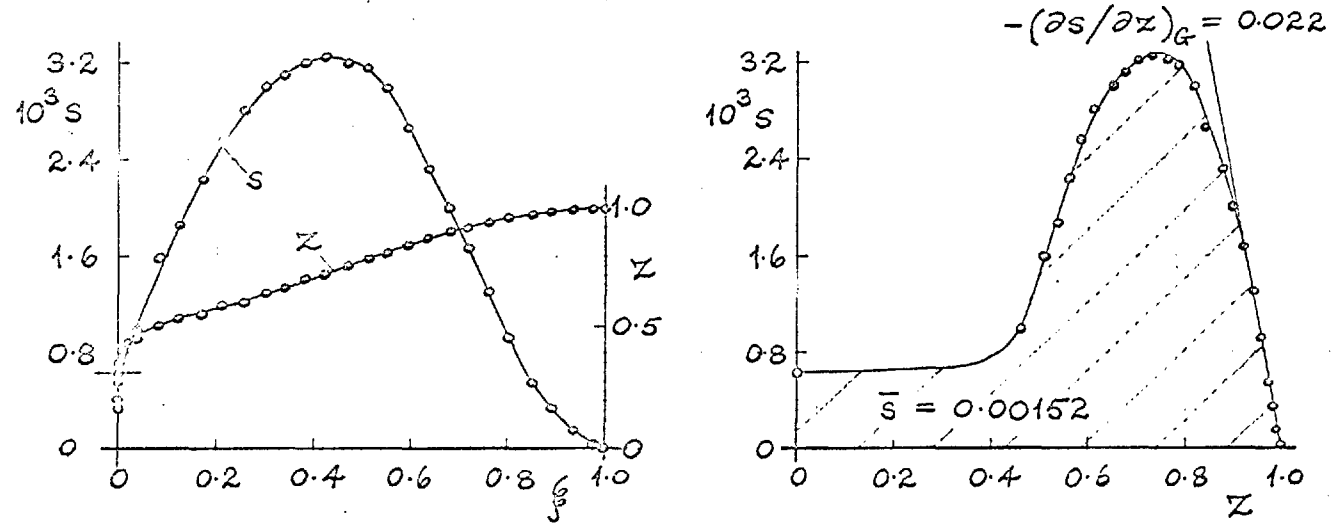


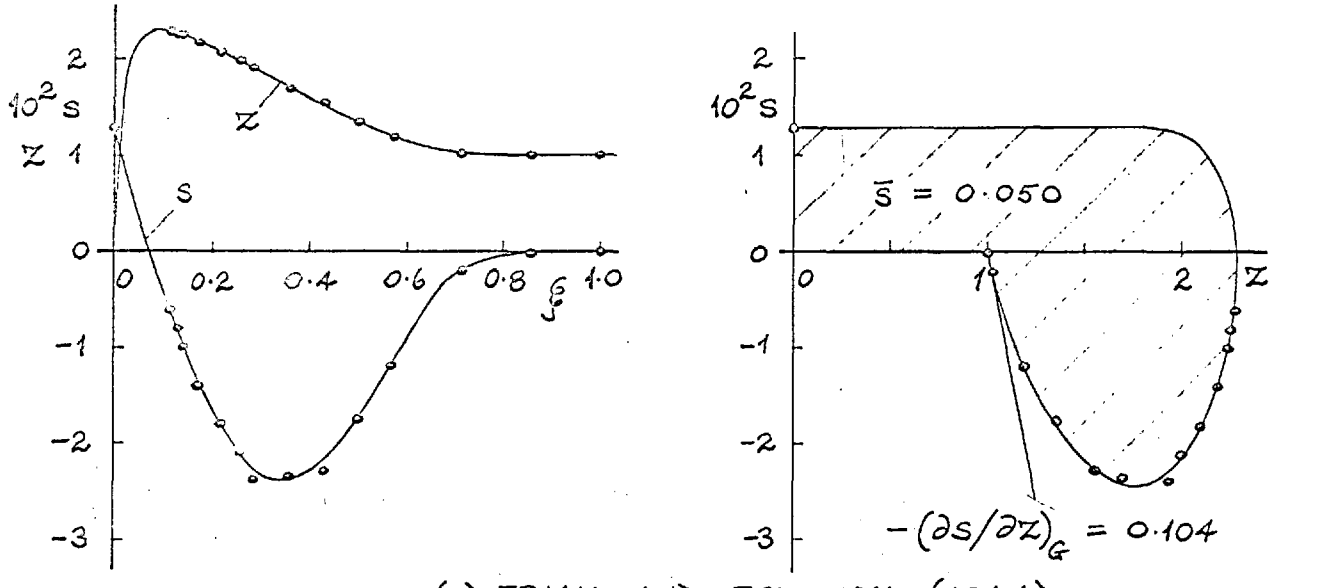
FIGURE 4.7 MIXING-LENGTH PROFILES CALCULATED FROM EXPERIMENTAL DATA FOR BOUNDARY LAYERS WITH $R_2 > 0$



(a) KLEBANOFF (1955)



(b) BRADSHAW AND FERRISS 1 (1965)



(c) ERIAN AND ESKINAZI (1964)

FIGURE 4.8 EXPERIMENTALLY - DETERMINED SHEAR-STRESS AND VELOCITY PROFILES

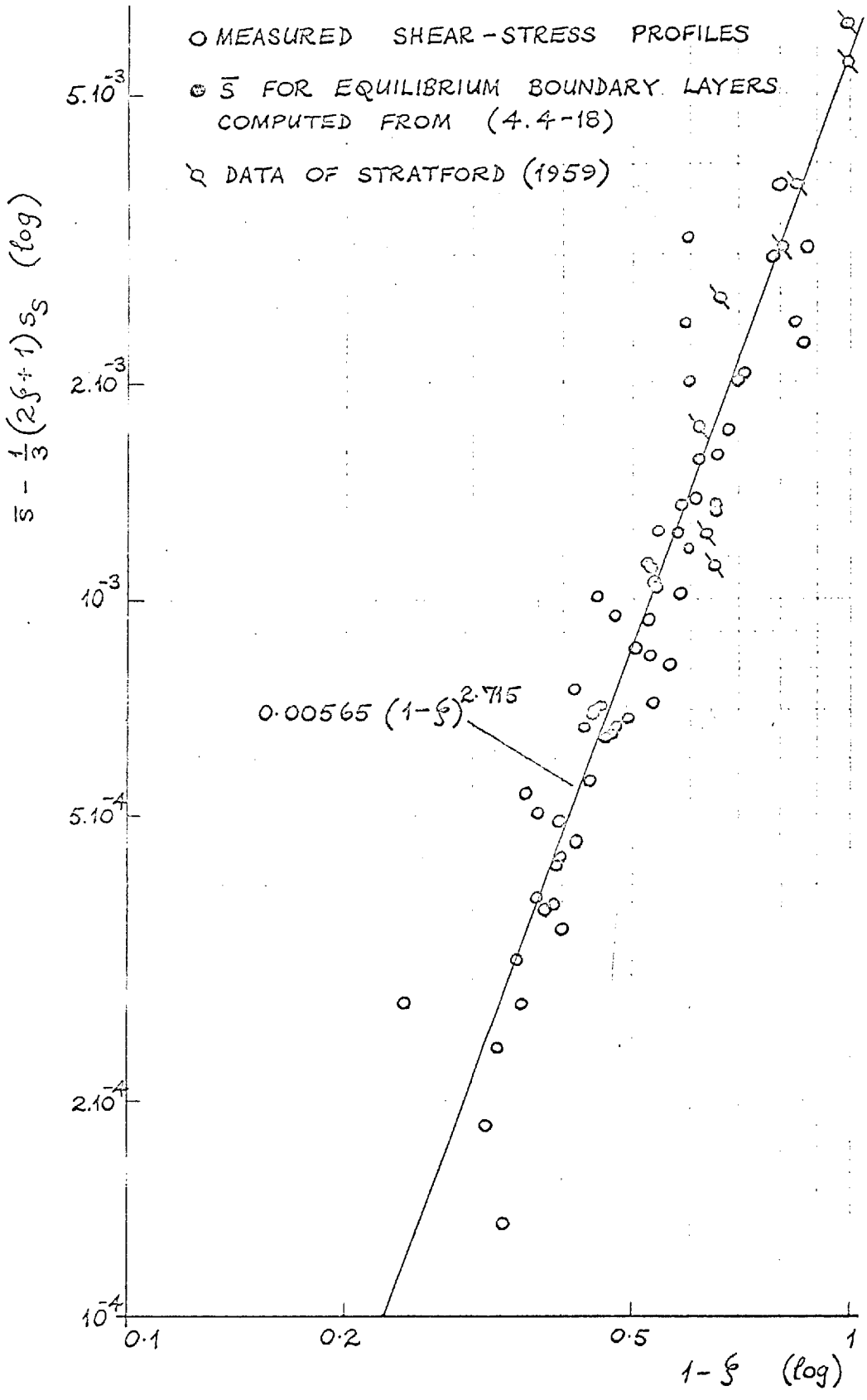


FIGURE 4.9 CORRELATION OF $\bar{S}$ - DATA FOR $\zeta < 1$

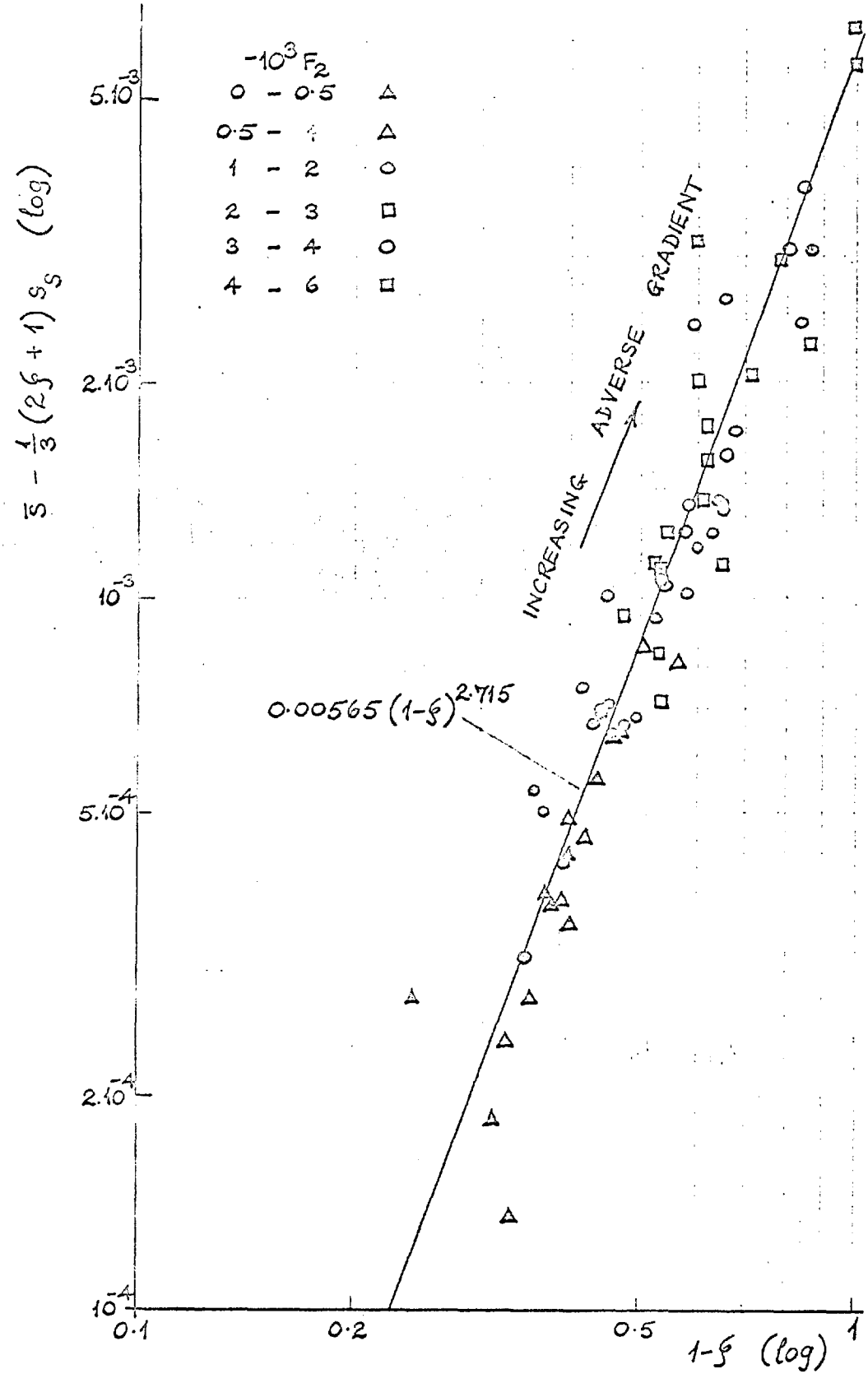


FIGURE 4.10 EXAMINATION OF $\bar{S}$-CORRELATION (FOR $\zeta < 1$) FOR PRESSURE-GRADIENT DEPENDENCE

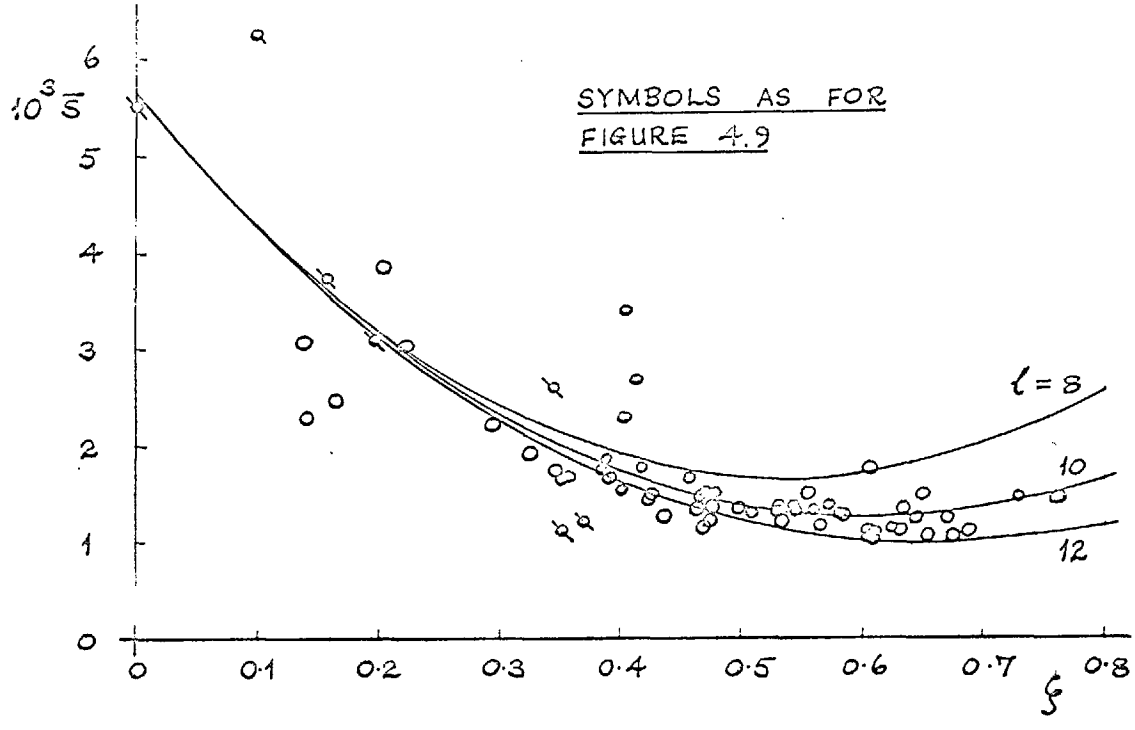


FIGURE 4.11 COMPARISON OF RECOMMENDED $\bar{S}$-RELATION, (4.4-20), WITH EXPERIMENTAL DATA FOR $\zeta < 1$

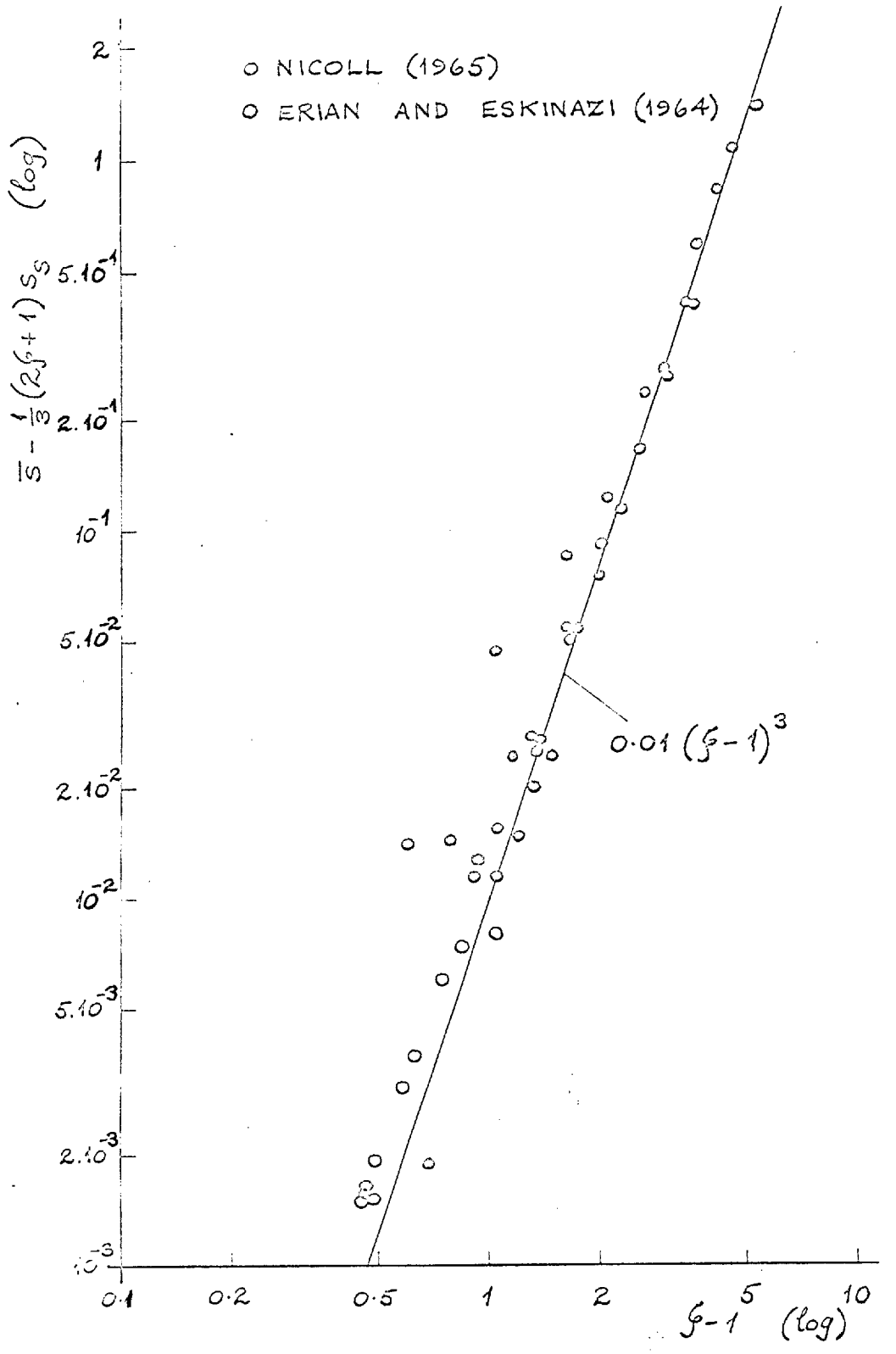


FIGURE 4.12 CORRELATION OF $\bar{S}$-DATA FOR $1 < \zeta < \infty$

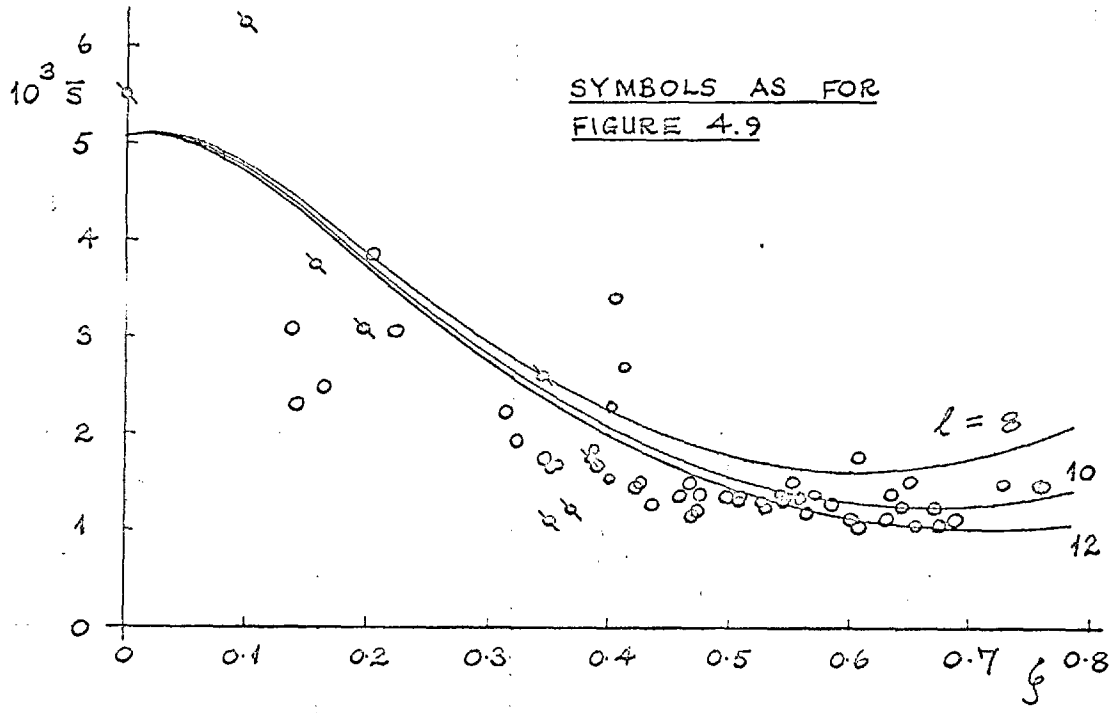


FIGURE 4.13 COMPARISON OF CURVES DERIVED FOR EQUILIBRIUM FLOWS FROM NASH'S $G \sim \beta$ RELATION WITH EXPERIMENTAL DATA FOR $\zeta < 1$

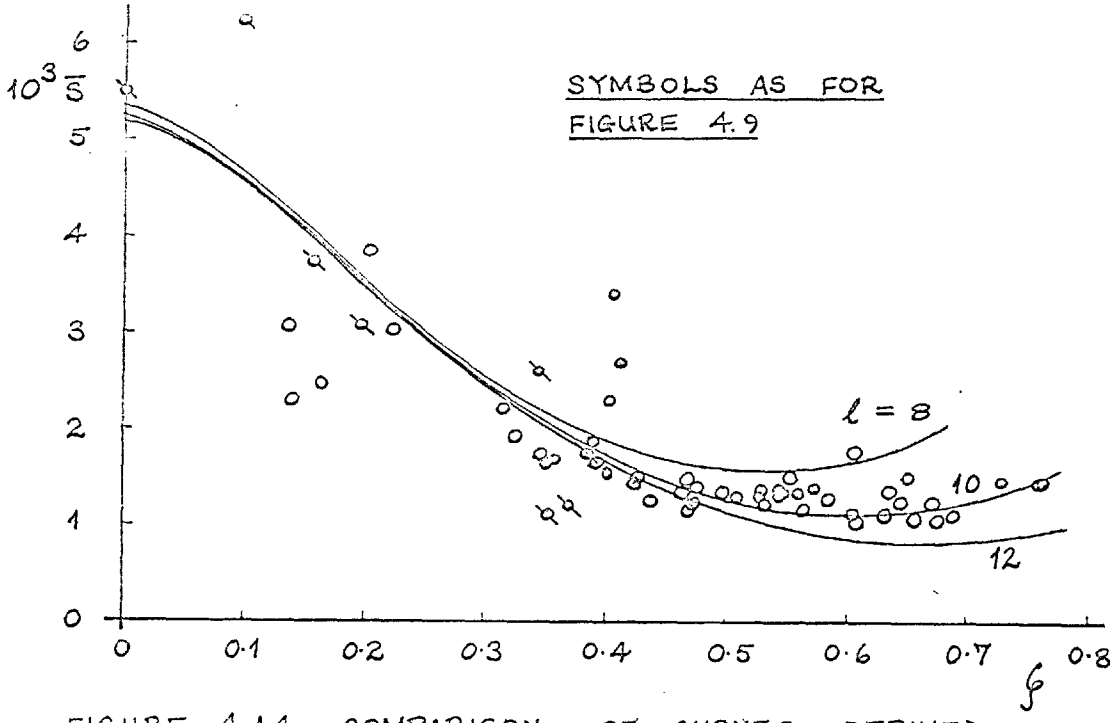


FIGURE 4.14 COMPARISON OF CURVES DERIVED FROM ENTRAINMENT LAW OF ESCUDIER AND NICOLL, (3.3-7), WITH EXPERIMENTAL DATA FOR $\zeta < 1$

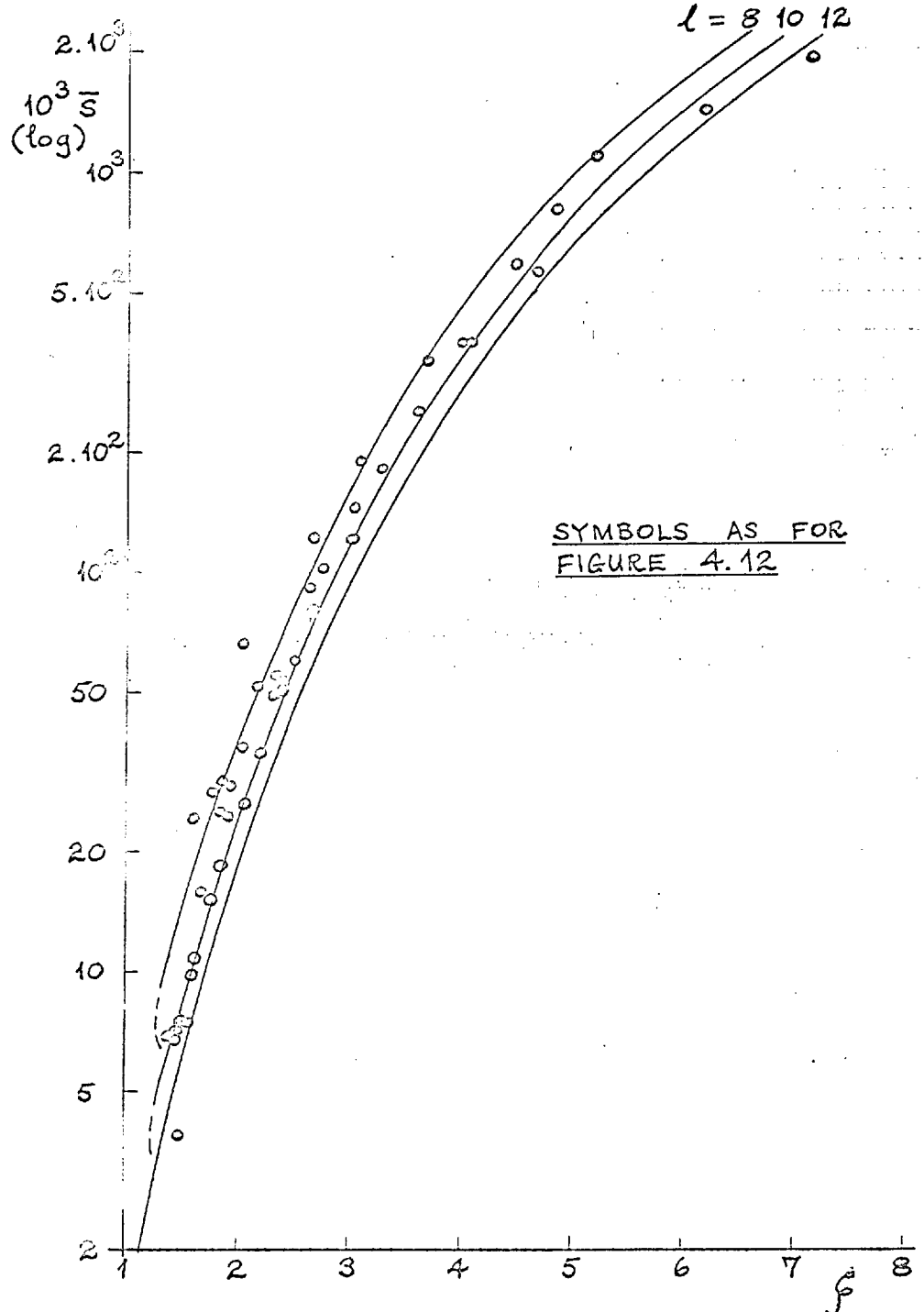


FIGURE 4.15 COMPARISON OF CURVES DERIVED FROM ENTRAINMENT LAW OF ESCUDIER AND NICOLL, (3.3-8), WITH EXPERIMENTAL DATA FOR $\zeta > 1$

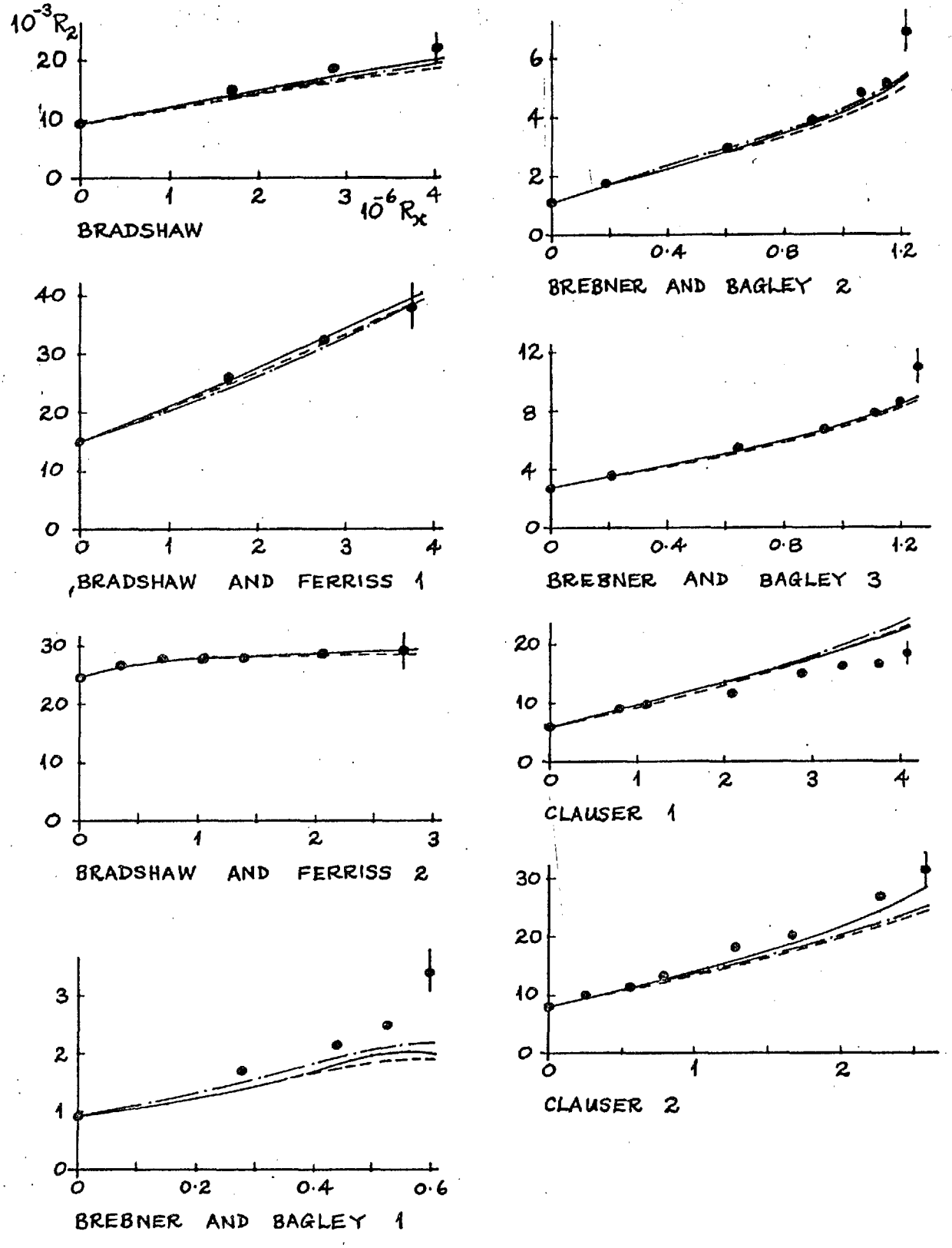
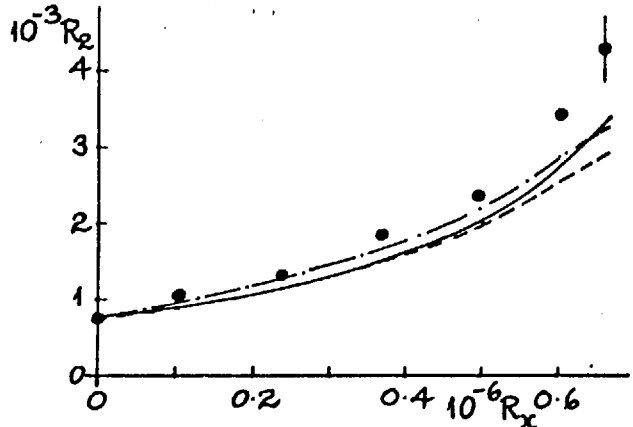
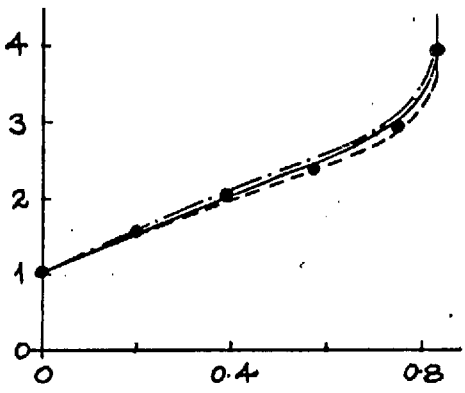


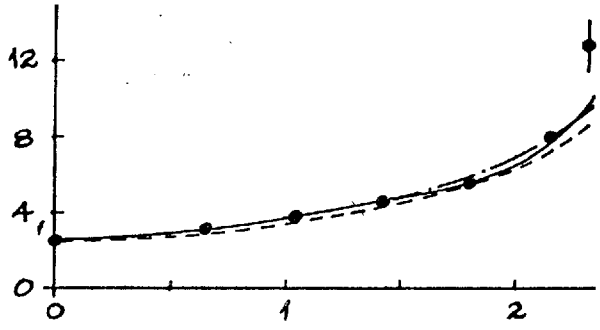
FIGURE 5.1 COMPARISON OF R_2 CALCULATIONS WITH EXPERIMENT
——— TWO-DIMENSIONALITY CHECK; - - - - - ENTRAINMENT METHOD;
—·—·— KINETIC-ENERGY METHOD



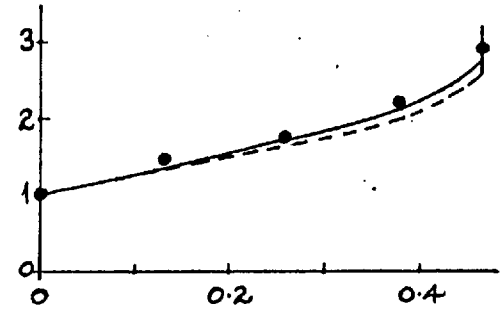
VON DOENHOFF AND TETERVIN 1



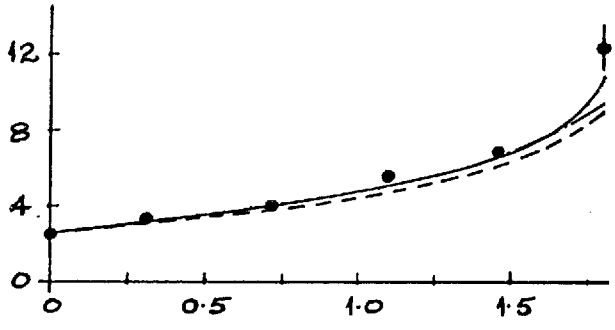
FAGE 1



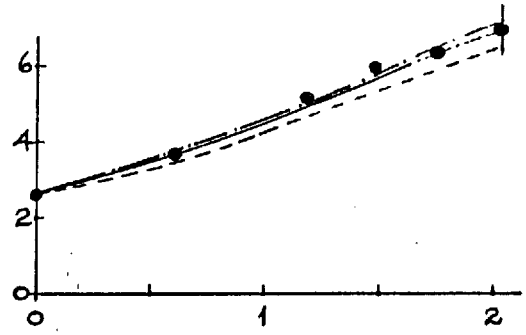
VON DOENHOFF AND TETERVIN 2



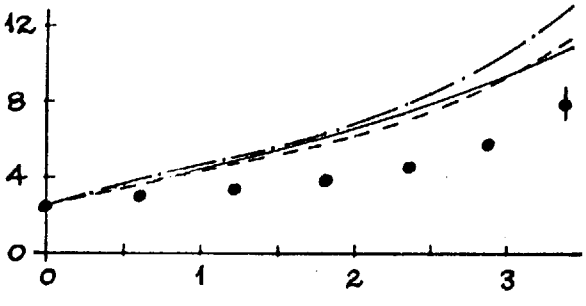
FAGE 2



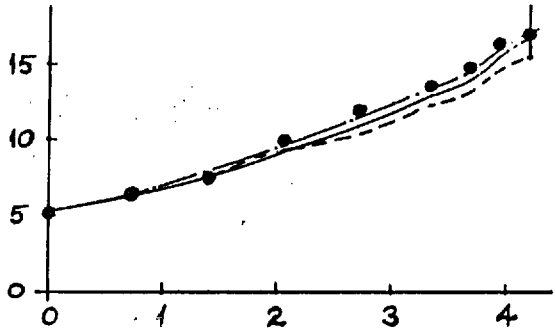
VON DOENHOFF AND TETERVIN 3



GAULT 1

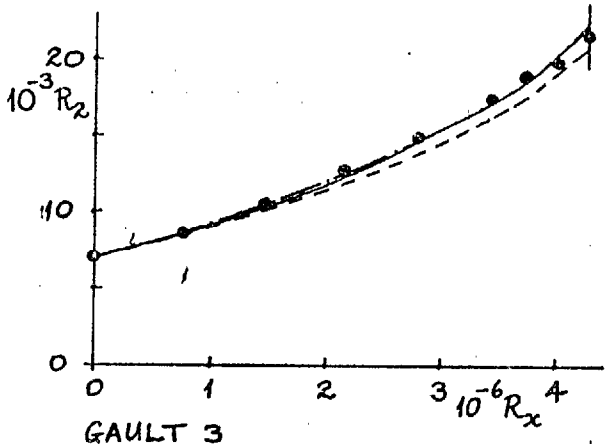


VON DOENHOFF AND TETERVIN 4

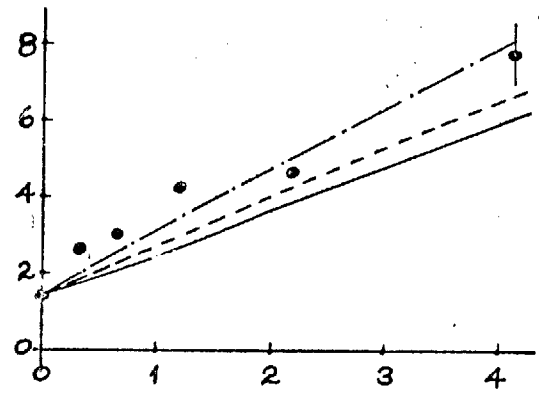


GAULT 2

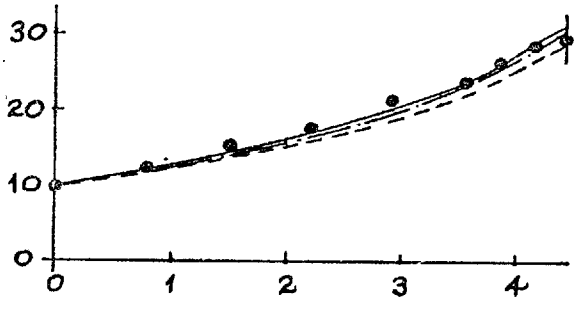
FIGURE 5.1 (CONT.)



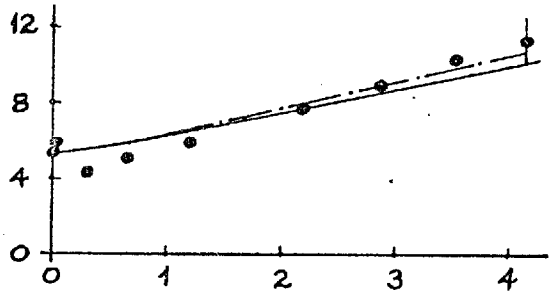
GAULT 3



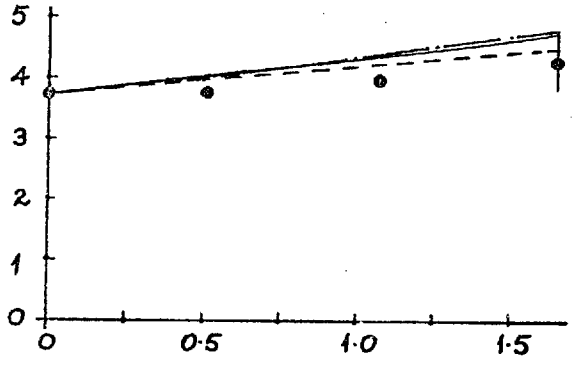
KLEBANOFF AND DIEHL 2



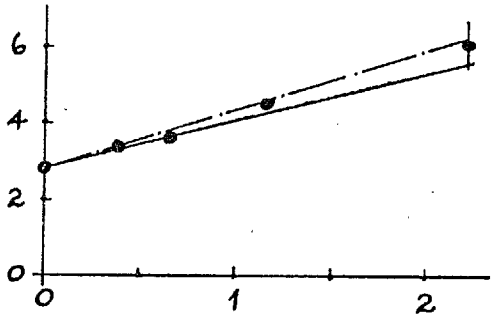
GAULT 4



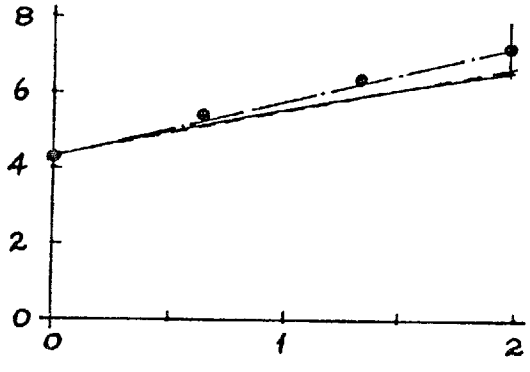
KLEBANOFF AND DIEHL 3



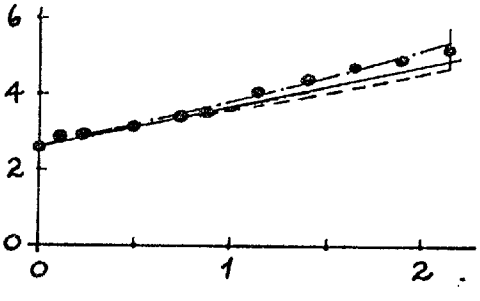
HERRING AND NORBURY



KLEBANOFF AND DIEHL 4

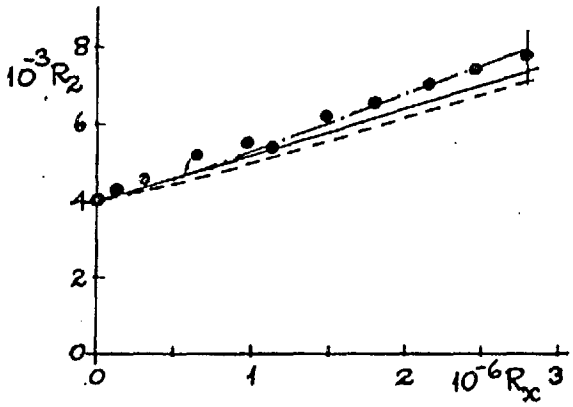


KLEBANOFF AND DIEHL 1

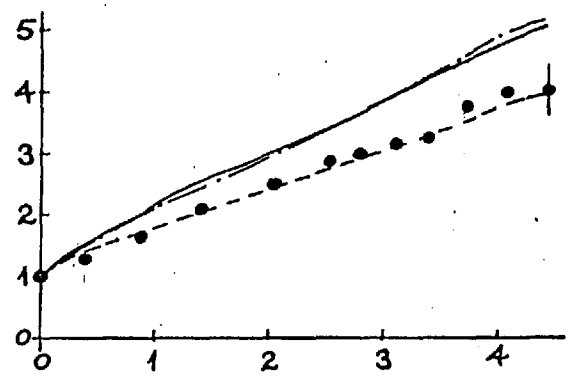


KLEBANOFF AND DIEHL 5

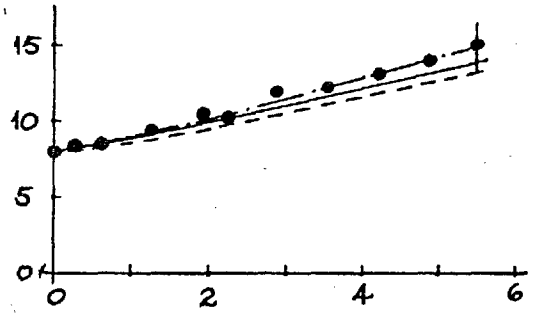
FIGURE 5.1 (CONT.)



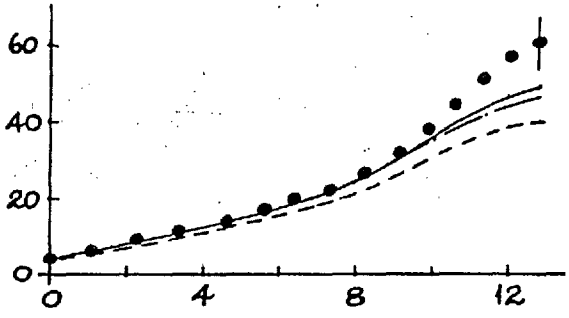
KLEBANOFF AND DIEHL 6



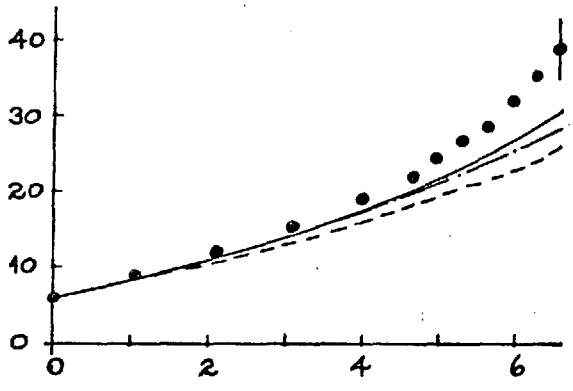
LUDWIEG AND TILLMANN C



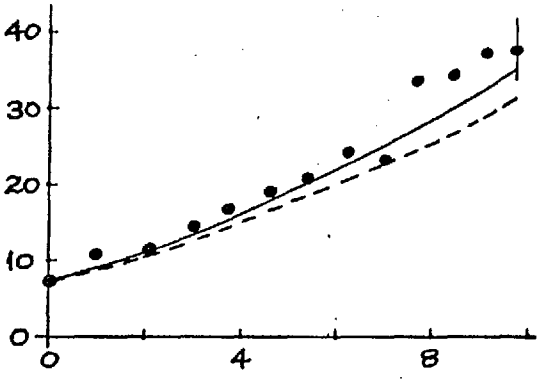
KLEBANOFF AND DIEHL 7



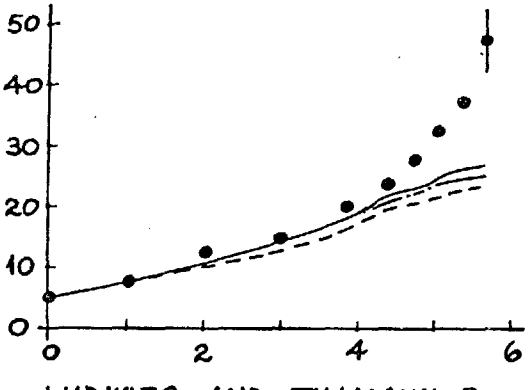
LUDWIEG AND TILLMANN 1



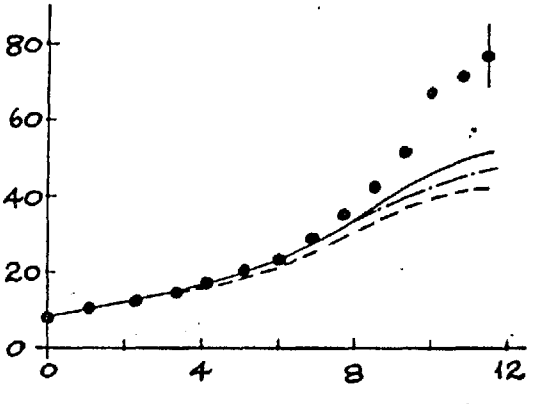
LUDWIEG AND TILLMANN A



LUDWIEG AND TILLMANN 2

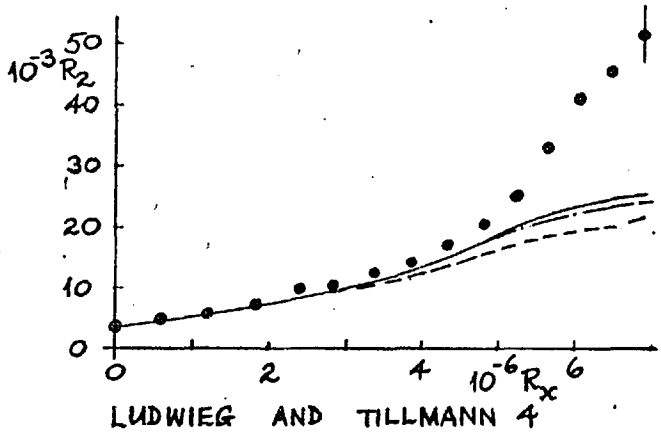


LUDWIEG AND TILLMANN B

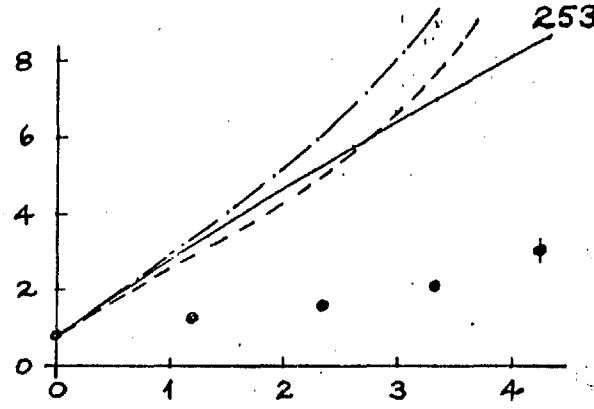


LUDWIEG AND TILLMANN 3

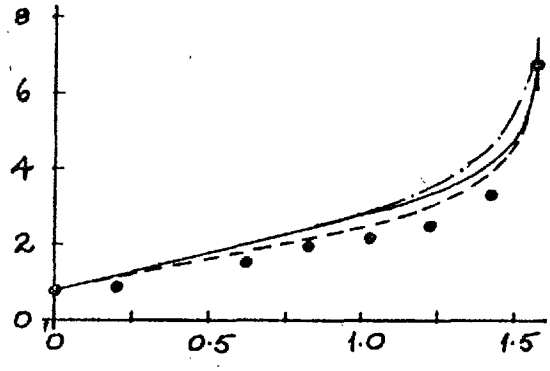
FIGURE 5.1 (CONT.)



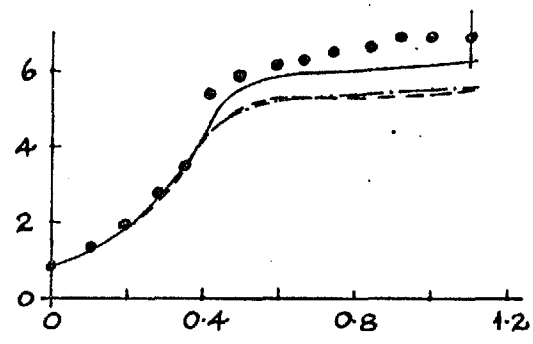
LUDWIEG AND TILLMANN 4



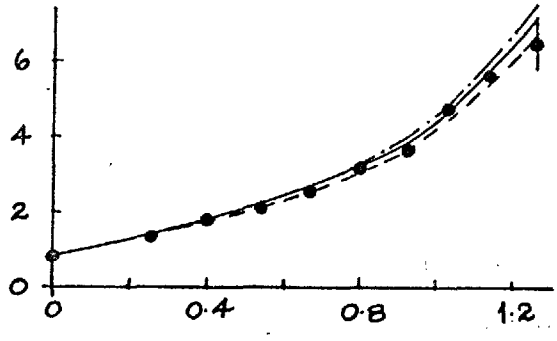
MOSES 4



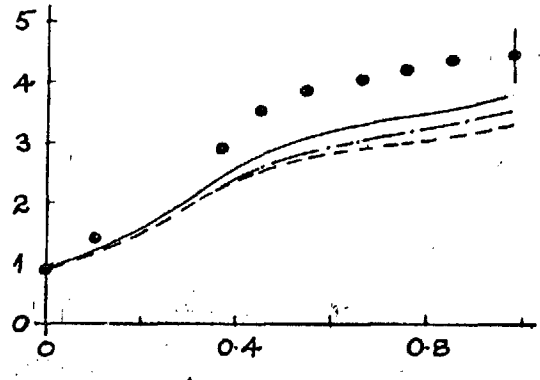
MOSES 1



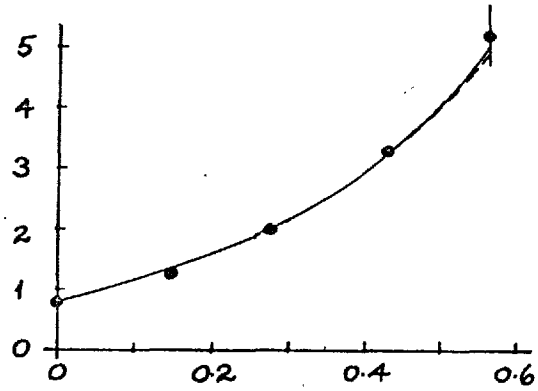
MOSES 5



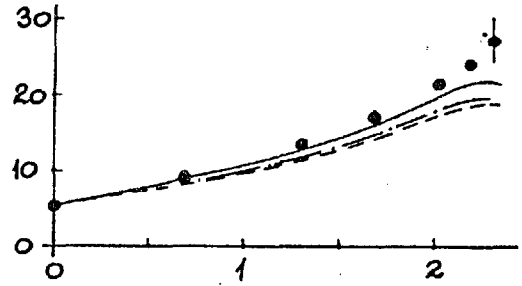
MOSES 2



MOSES 6

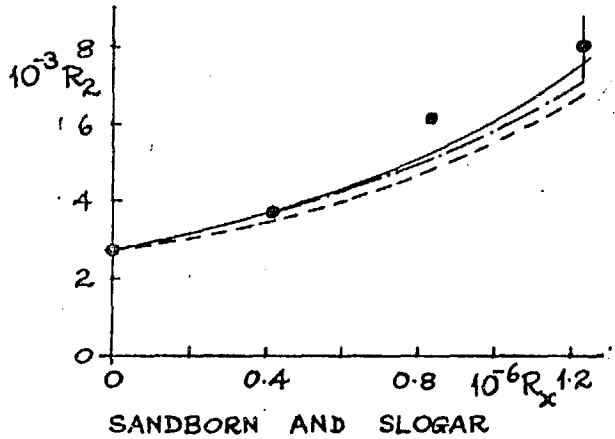


MOSES 3

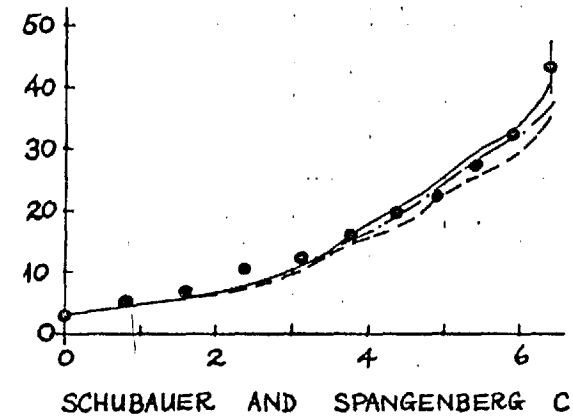


NEWMAN 2

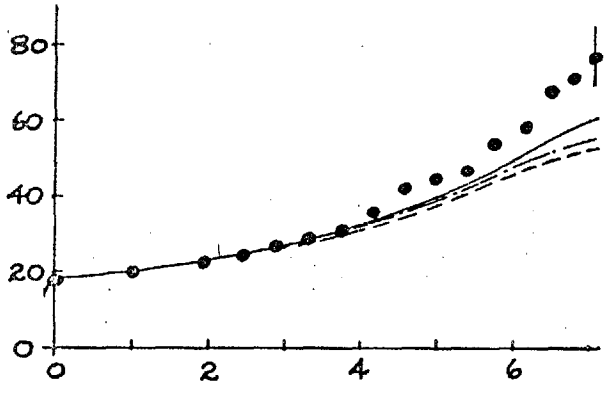
FIGURE 5.1 (CONT.)



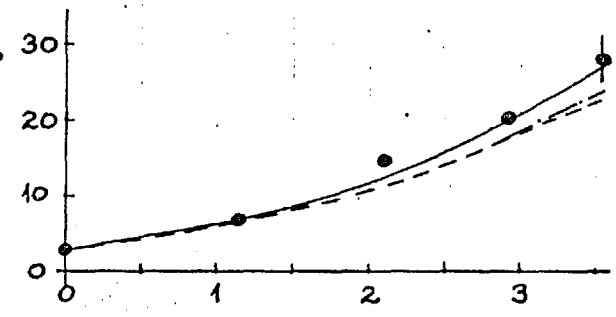
SANDBORN AND SLOGAR



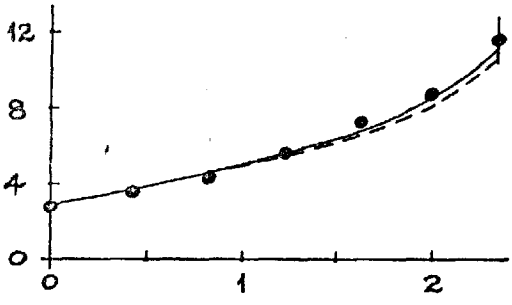
SCHUBAUER AND SPANGENBERG C



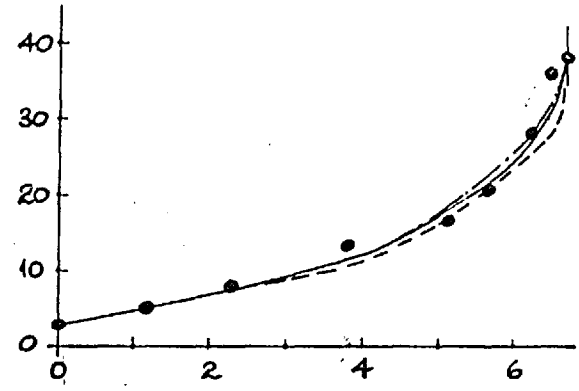
SCHUBAUER AND KLEBANOFF



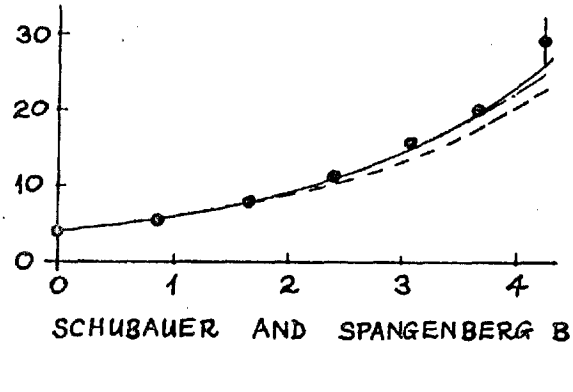
SCHUBAUER AND SPANGENBERG D



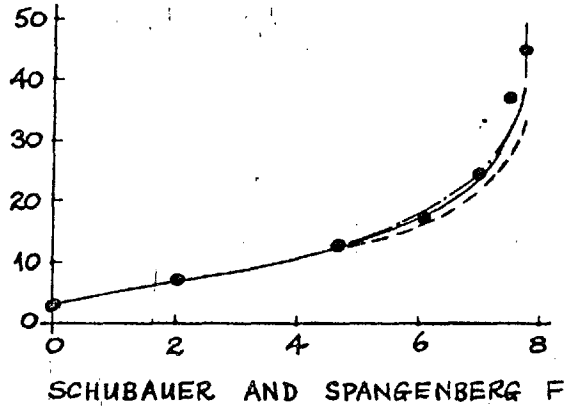
SCHUBAUER AND SPANGENBERG A



SCHUBAUER AND SPANGENBERG E



SCHUBAUER AND SPANGENBERG B



SCHUBAUER AND SPANGENBERG F

FIGURE 5.1 (CONT.)

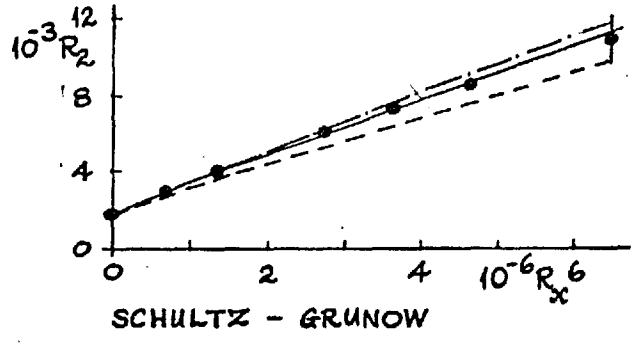


FIGURE 5.1 (CONCL.)

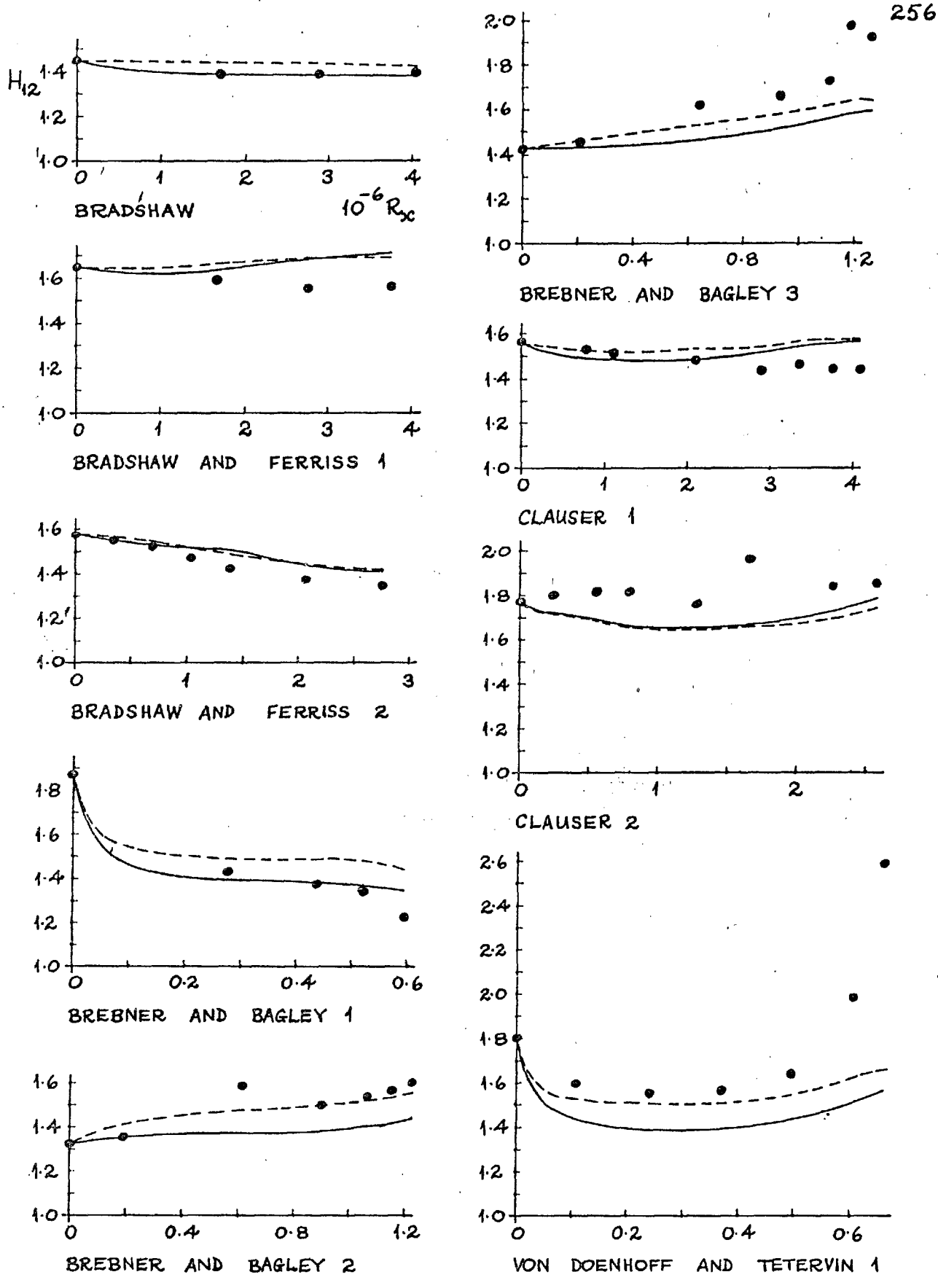
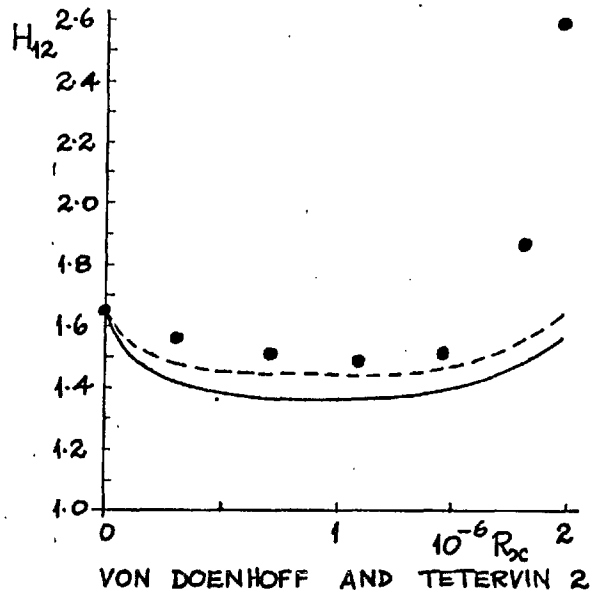
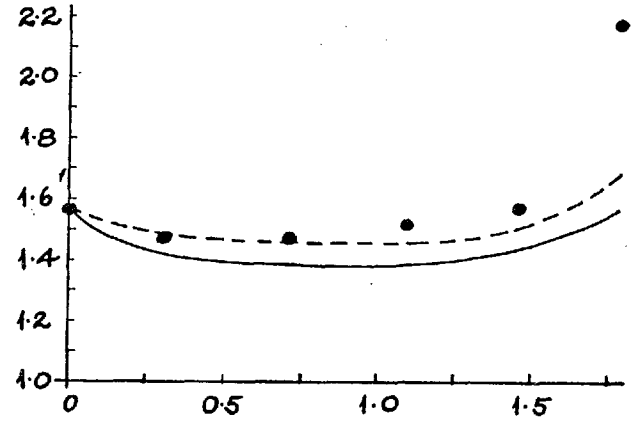


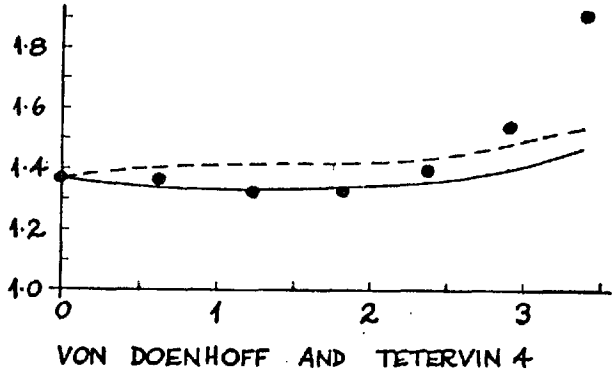
FIGURE 5.2 COMPARISON OF SHAPE-FACTOR CALCULATIONS WITH EXPERIMENT; - - - - - ENTRAINMENT METHOD, ——— KINETIC-ENERGY METHOD



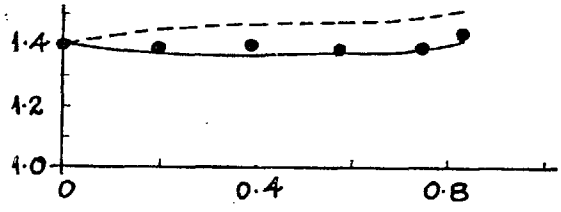
VON DOENHOFF AND TETERVIN 2



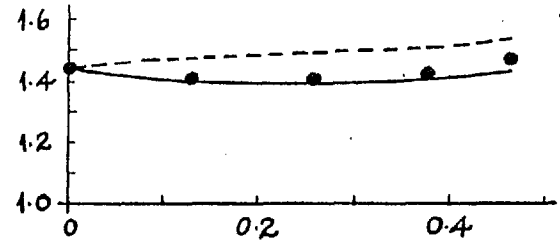
VON DOENHOFF AND TETERVIN 3



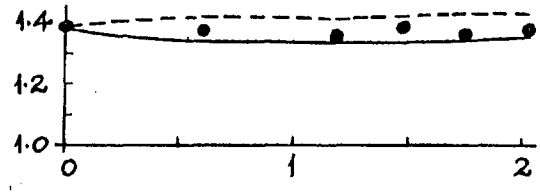
VON DOENHOFF AND TETERVIN 4



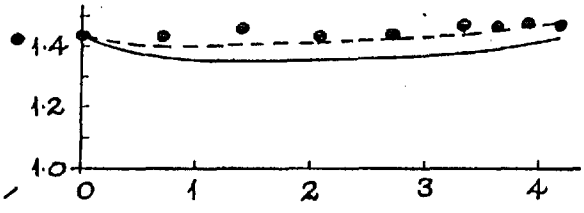
FAGE 1



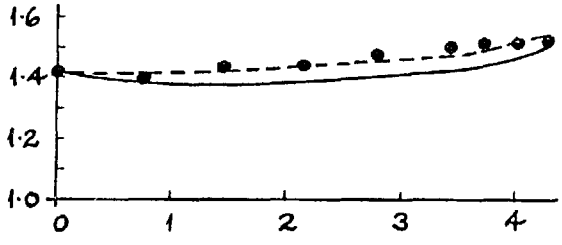
FAGE 2



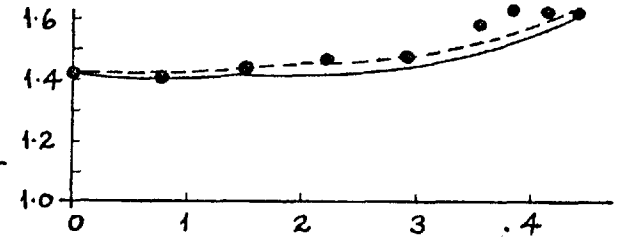
GAULT 1



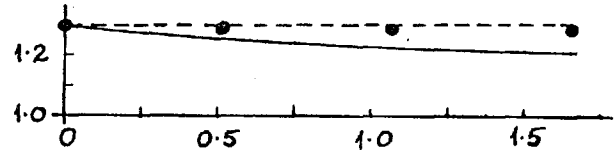
GAULT 2



GAULT 3

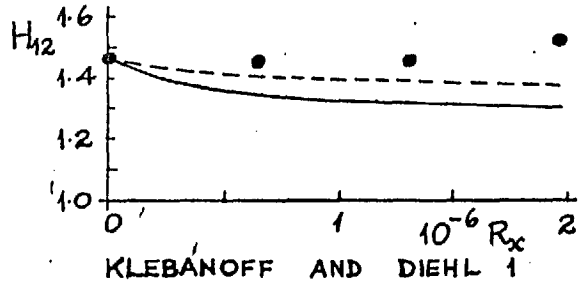


GAULT 4

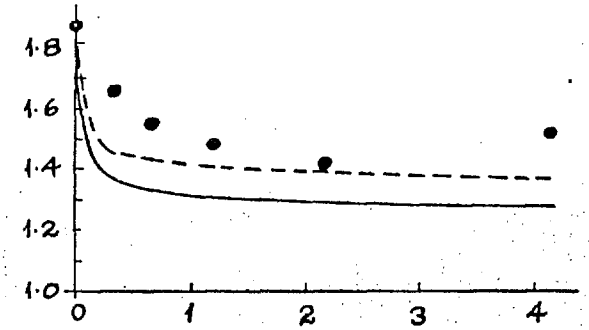


HERRING AND NORBURY

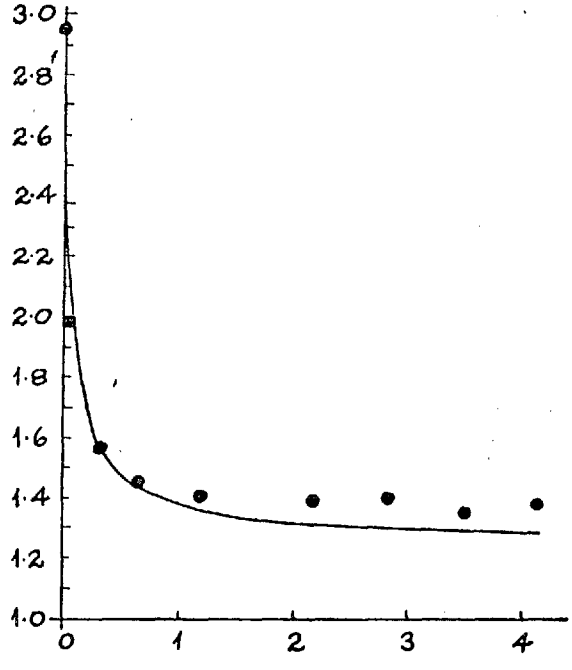
FIGURE 5.2 (CONT.)



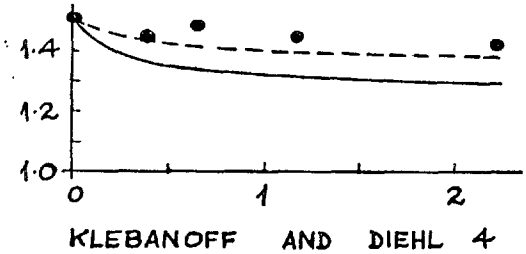
KLEBANOFF AND DIEHL 1



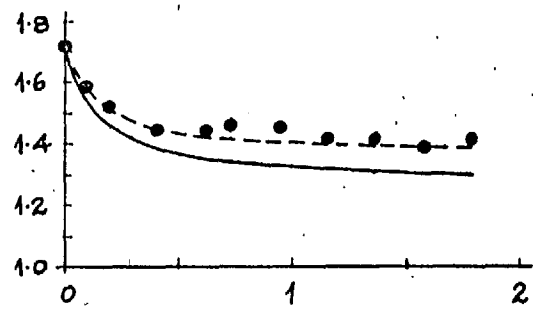
KLEBANOFF AND DIEHL 2



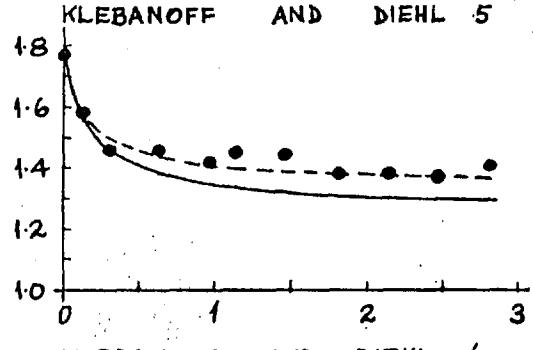
KLEBANOFF AND DIEHL 3



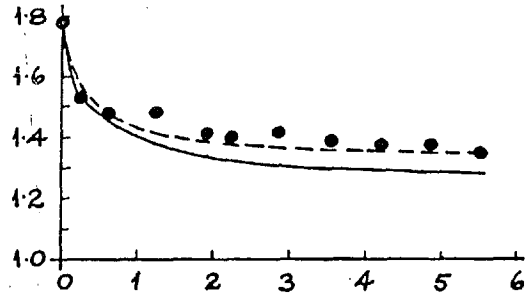
KLEBANOFF AND DIEHL 4



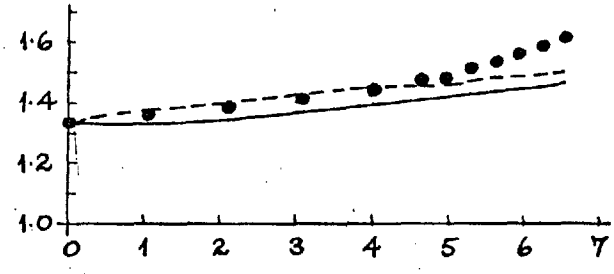
KLEBANOFF AND DIEHL 5



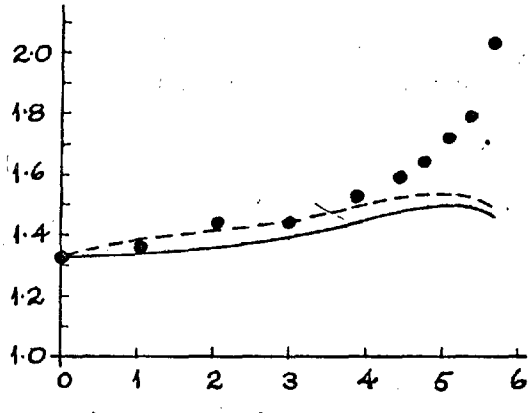
KLEBANOFF AND DIEHL 6



KLEBANOFF AND DIEHL 7

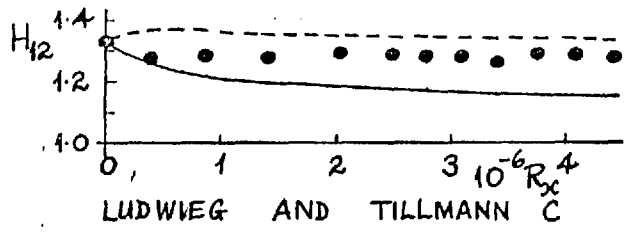


LUDWIEG AND TILLMANN A

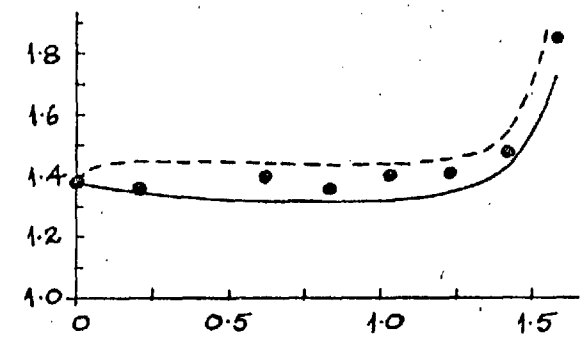


LUDWIEG AND TILLMANN B

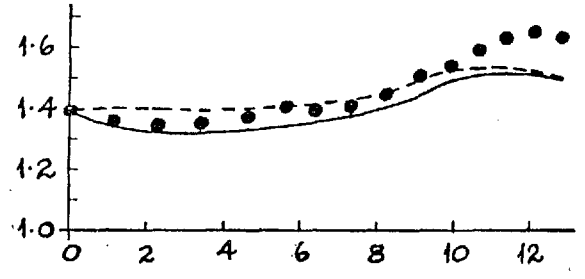
FIGURE 5.2 (CONT.)



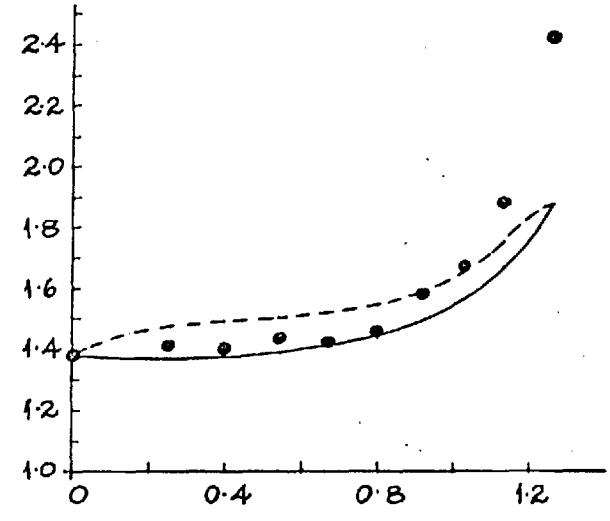
LUDWIEG AND TILLMANN C



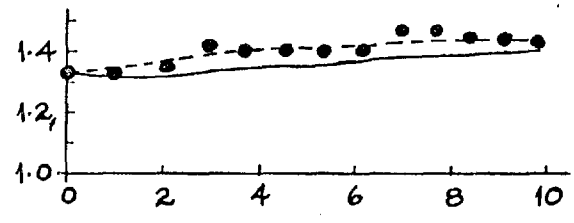
MOSES 1



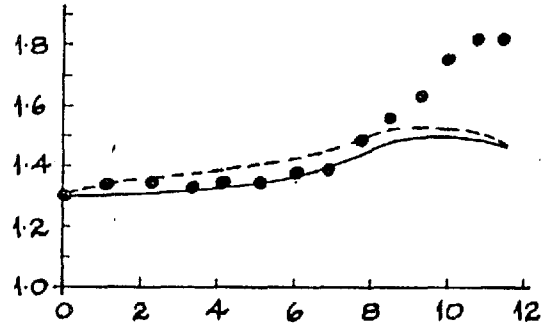
LUDWIEG AND TILLMANN 1



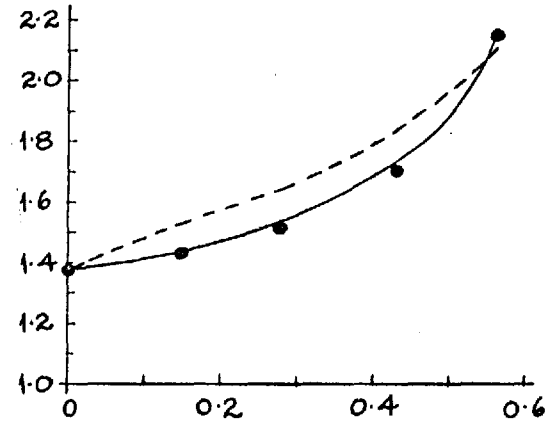
MOSES 2



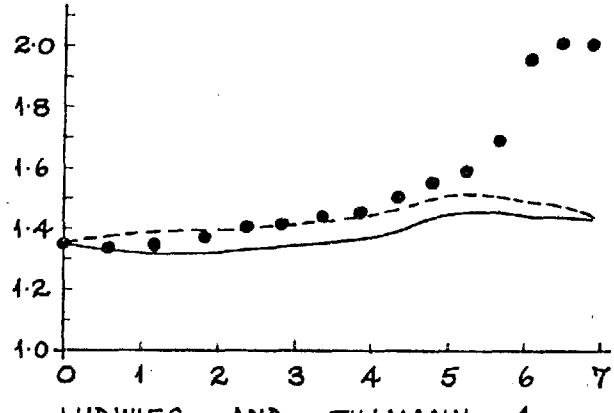
LUDWIEG AND TILLMANN 2



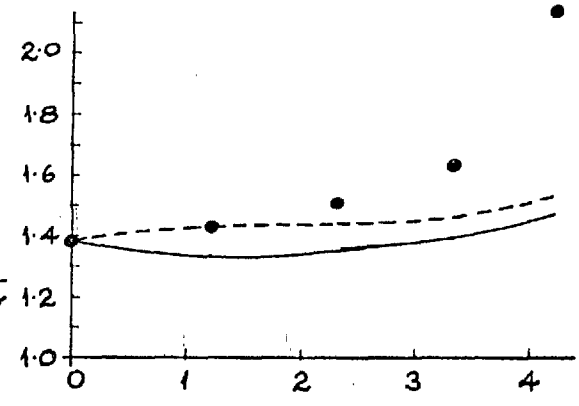
LUDWIEG AND TILLMANN 3



MOSES 3

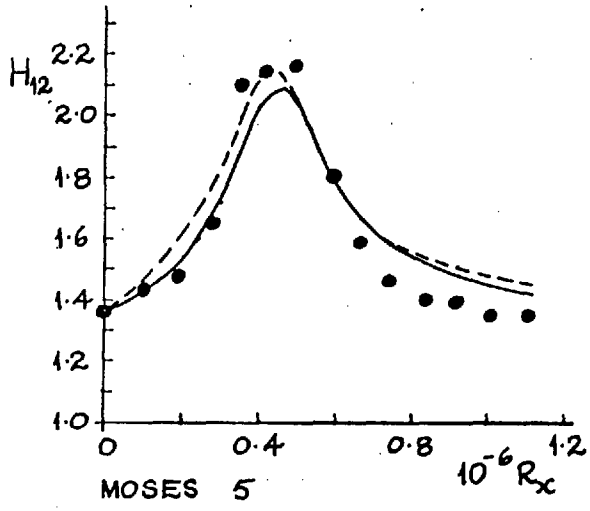


LUDWIEG AND TILLMANN 4

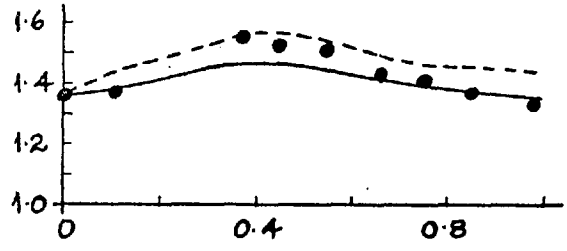


MOSES 4

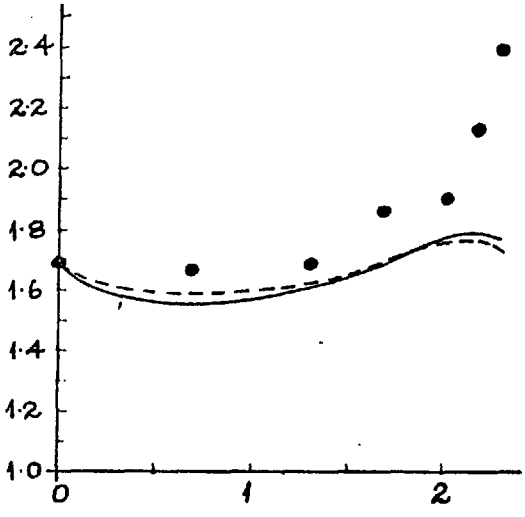
FIGURE 5.2 (CONT.)



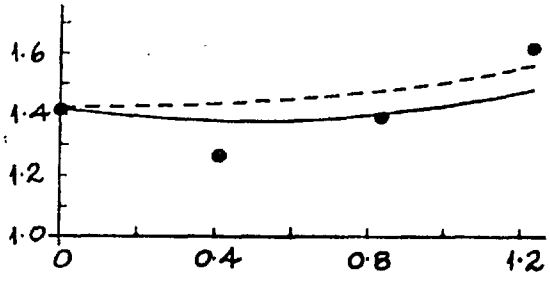
MOSES 5



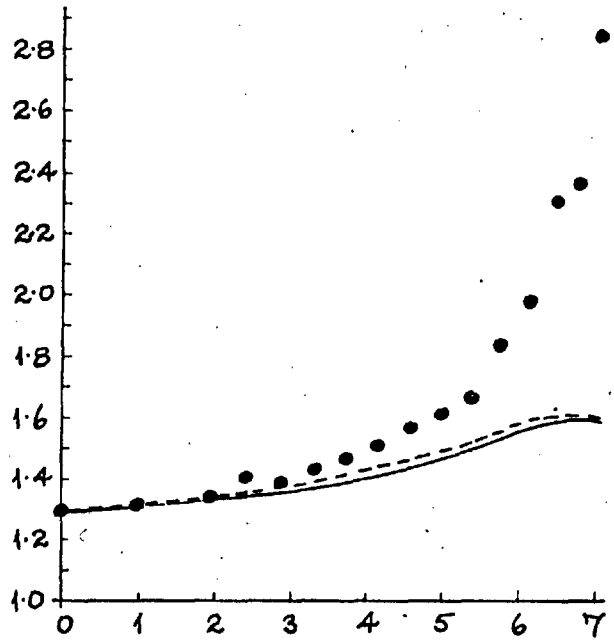
MOSES 6



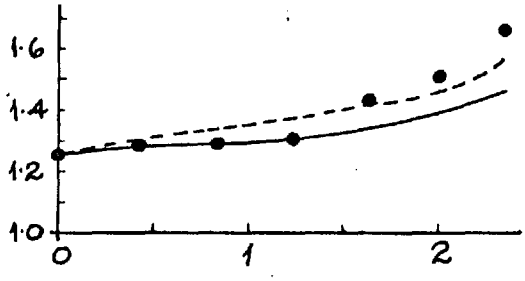
NEWMAN



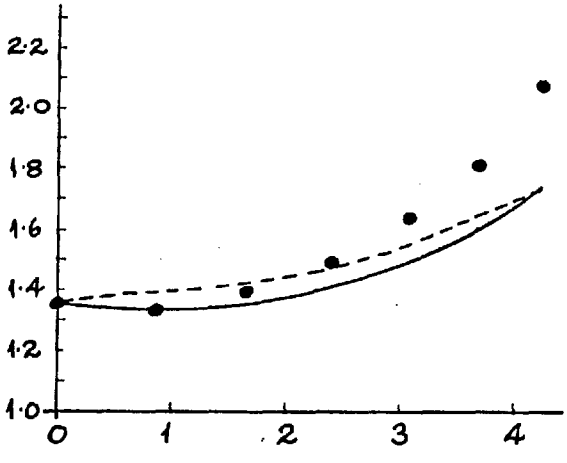
SANDBORN AND SLOGAR



SCHUBAUER AND KLEBANOFF

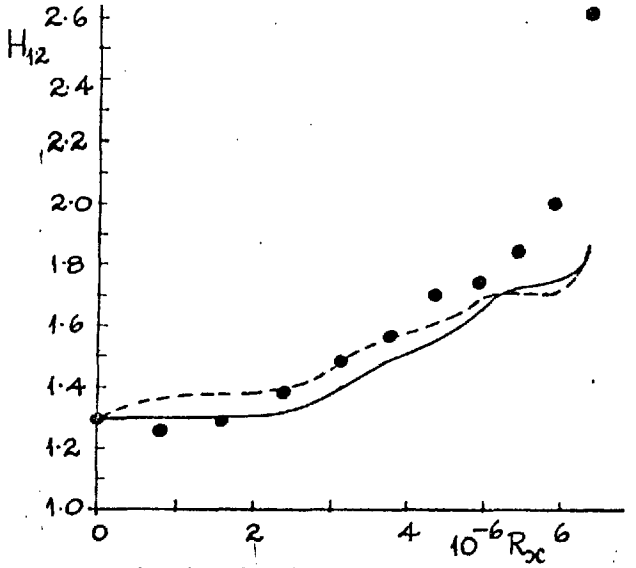


SCHUBAUER AND SPANGENBERG A

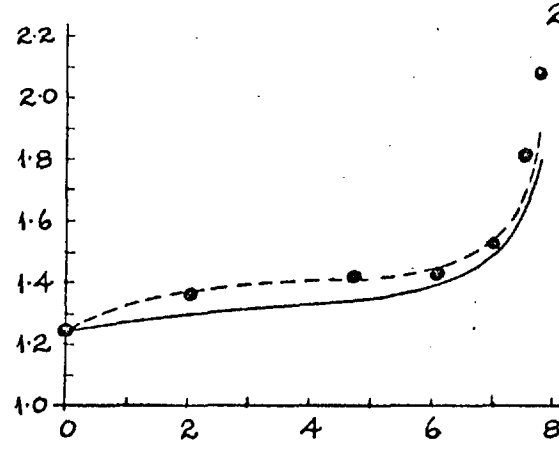


SCHUBAUER AND SPANGENBERG B

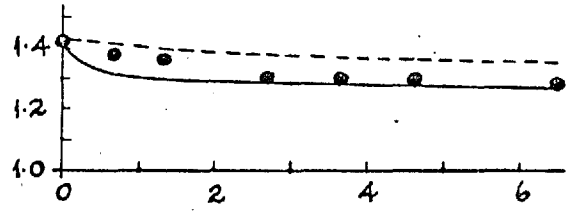
FIGURE 5.2 (CONT.)



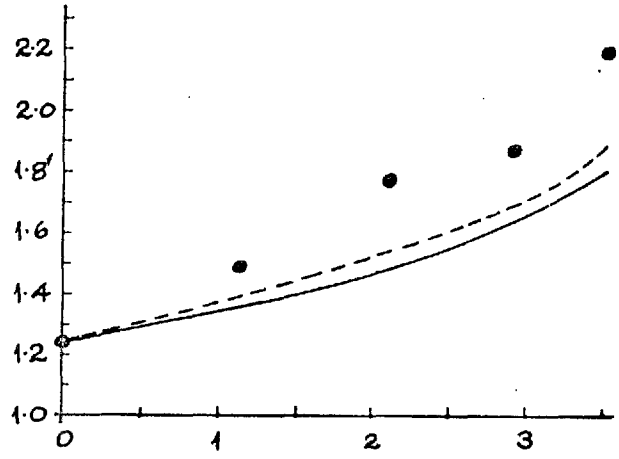
SCHUBAUER AND SPANGENBERG C



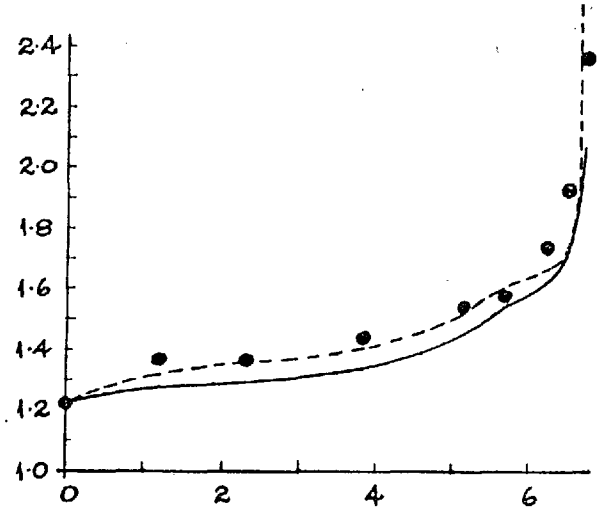
SCHUBAUER AND SPANGENBERG F



SCHULTZ - GRUNOW



SCHUBAUER AND SPANGENBERG D



SCHUBAUER AND SPANGENBERG E

FIGURE 5.2 (CONCL.)

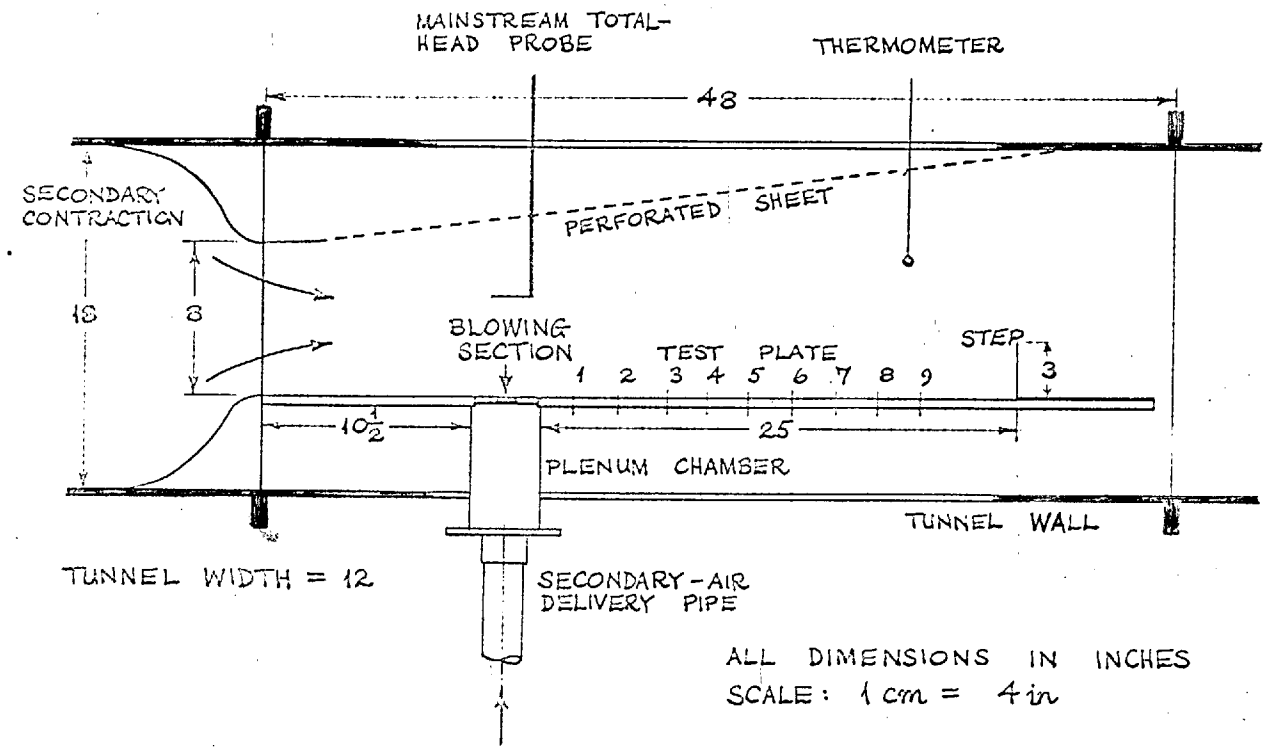


FIGURE 6.1 LAYOUT AND MAIN DIMENSIONS OF WORKING SECTION

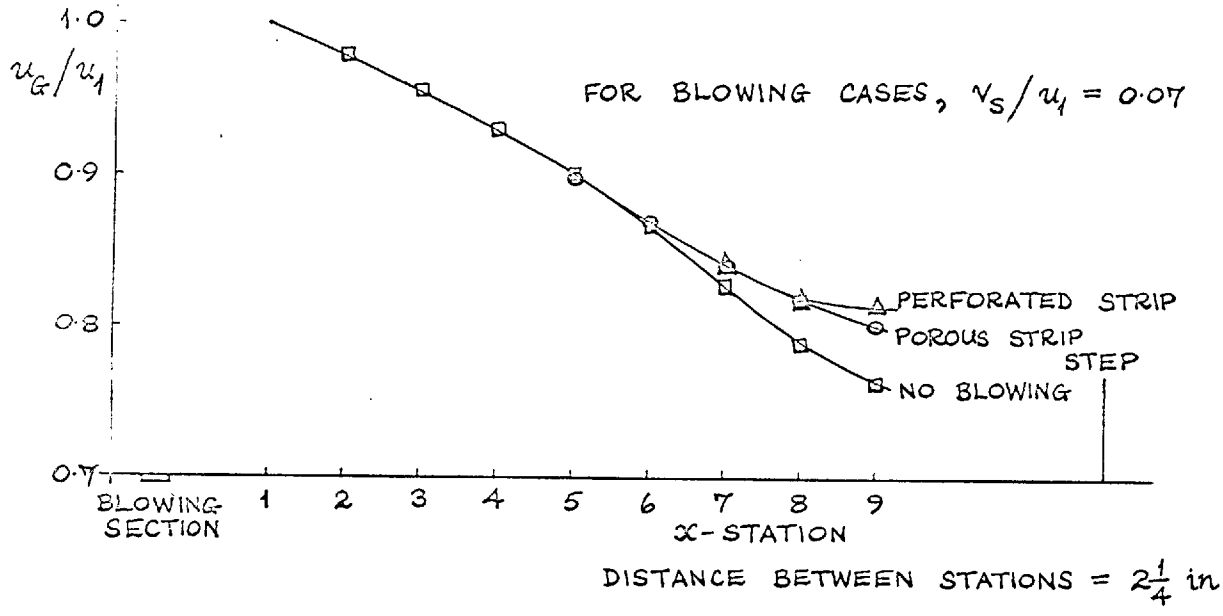
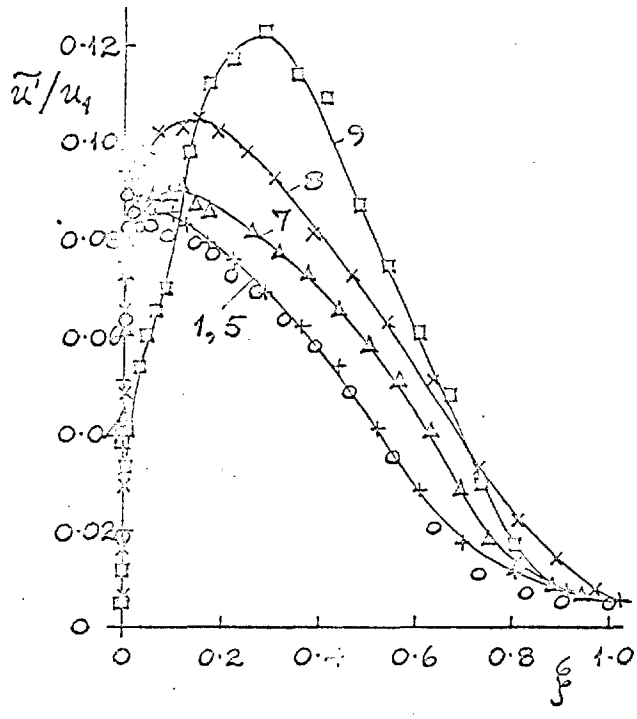
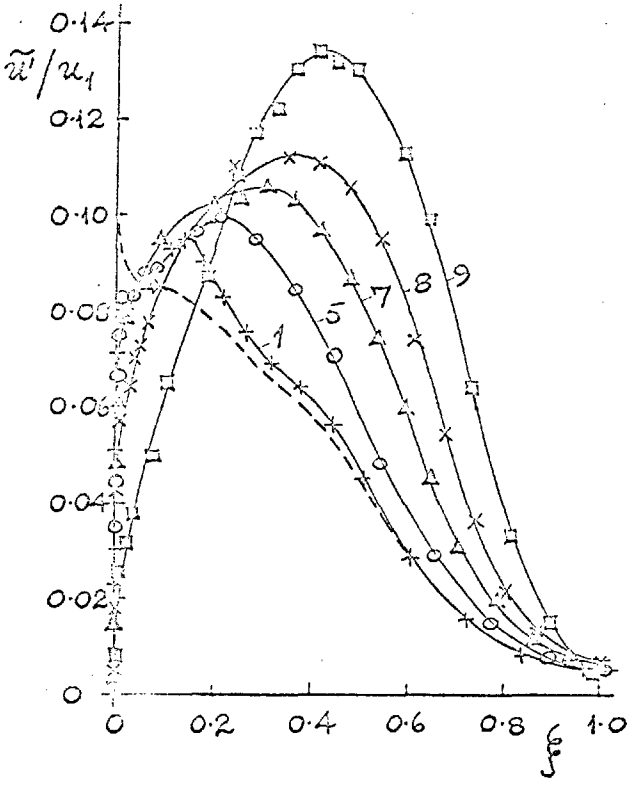


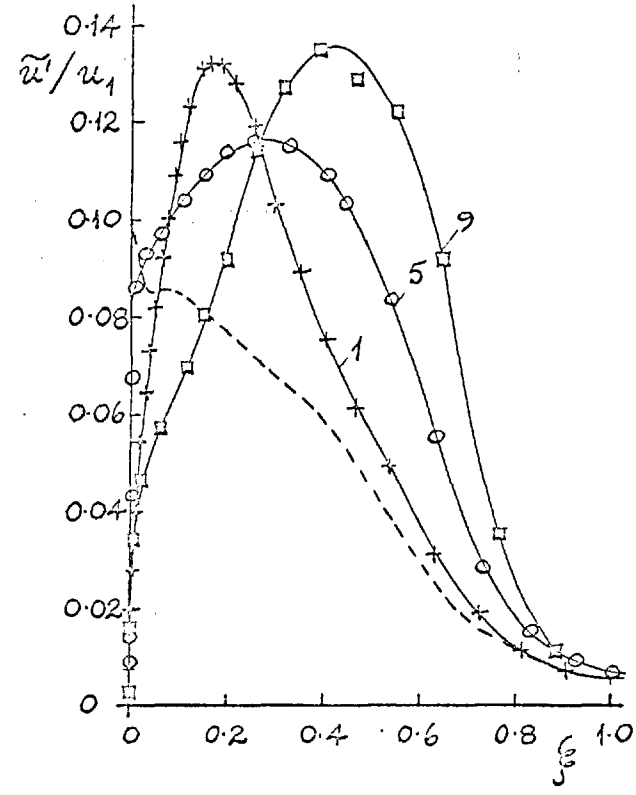
FIGURE 6.2 MAINSTREAM-VELOCITY VARIATION



(a) NO BLOWING



(b) POROUS STRIP

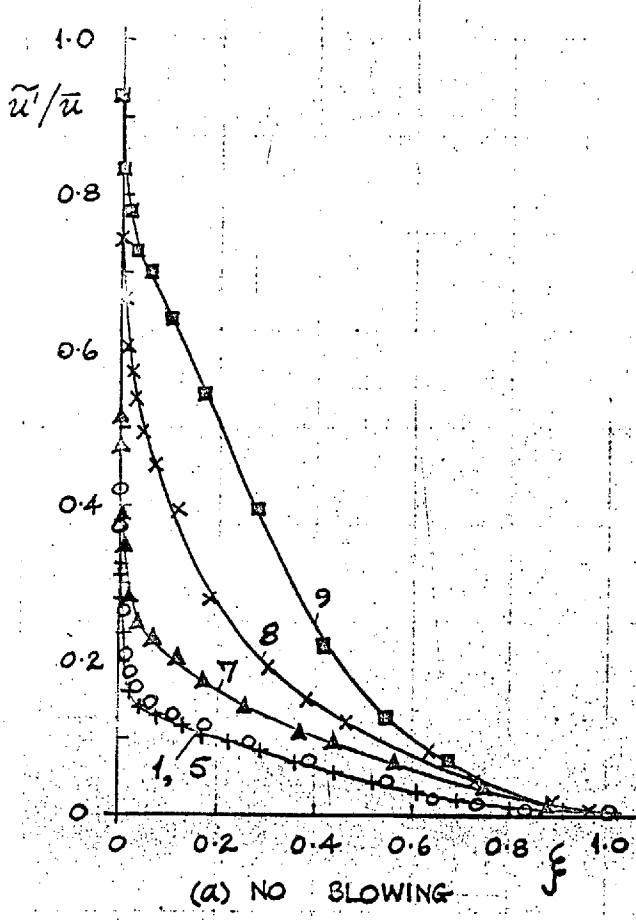


(c) PERFORATED STRIP

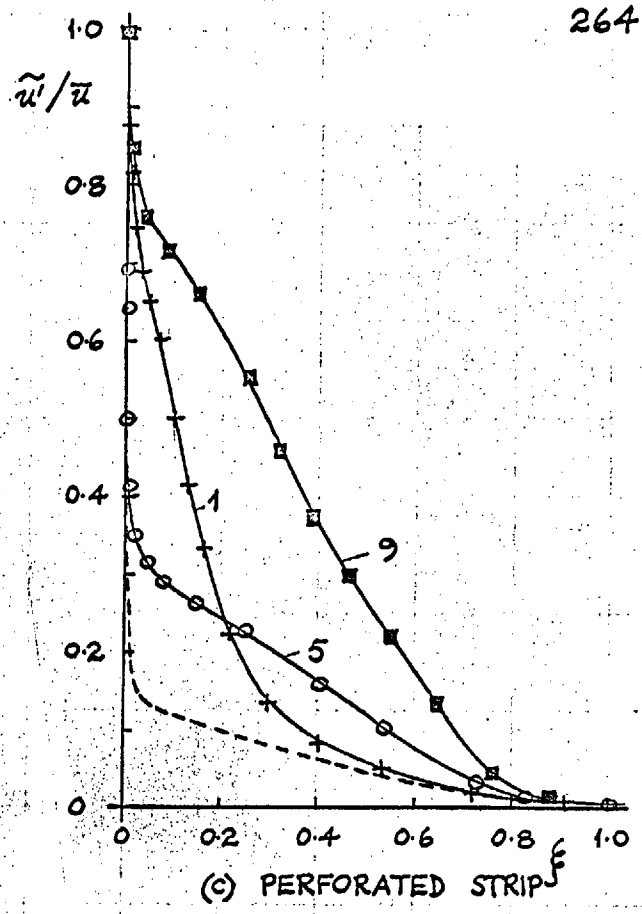
SYMBOL	+	o	Δ	x	□
x-STATION	1	5	7	8	9

--------- NO BLOWING, STATION 1

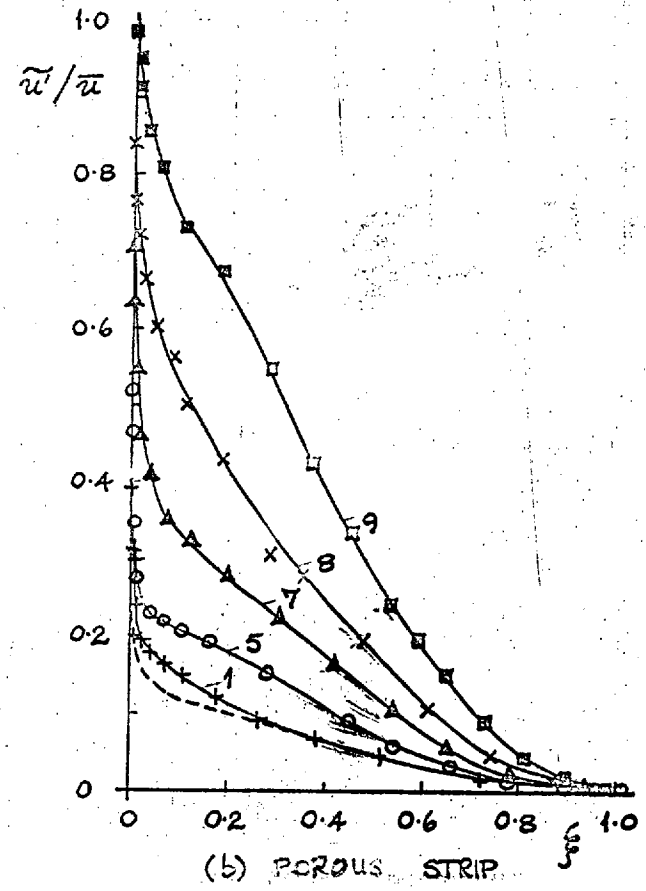
FIGURE 6.3 RMS u-COMPONENT INTENSITY PROFILES



(a) NO BLOWING



(c) PERFORATED STRIP



(b) POROUS STRIP

SYMBOL	+	o	▲	x	■
x-STATION	1	5	7	8	9

-------- NO BLOWING, STATION 1

FIGURE 6.4 RMS u-COMPONENT INTENSITY PROFILES

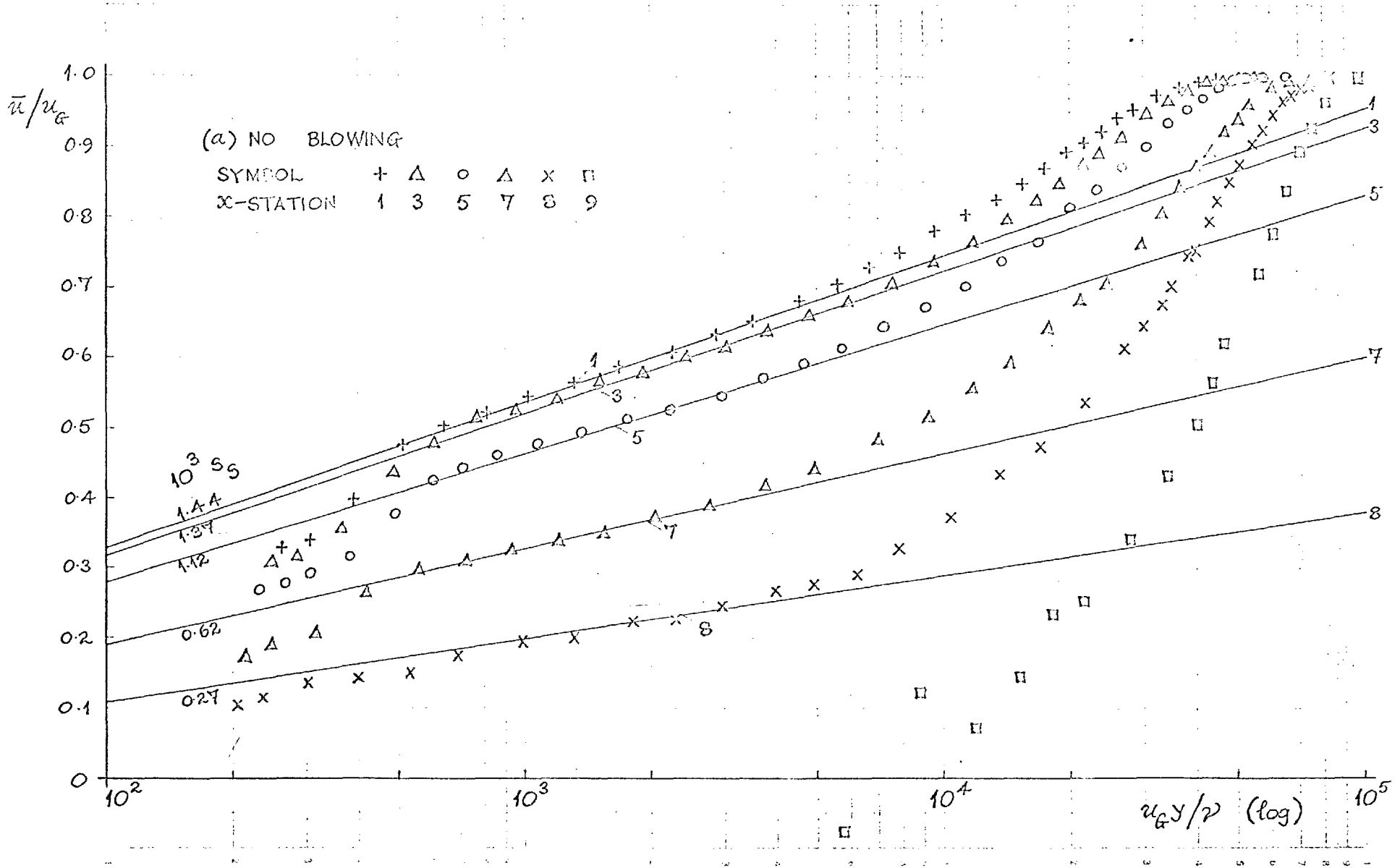


FIGURE 6.5 SEMILOGARITHMIC (CLAUSER) PLOT OF MEAN-VELOCITY PROFILES

(a) NO BLOWING

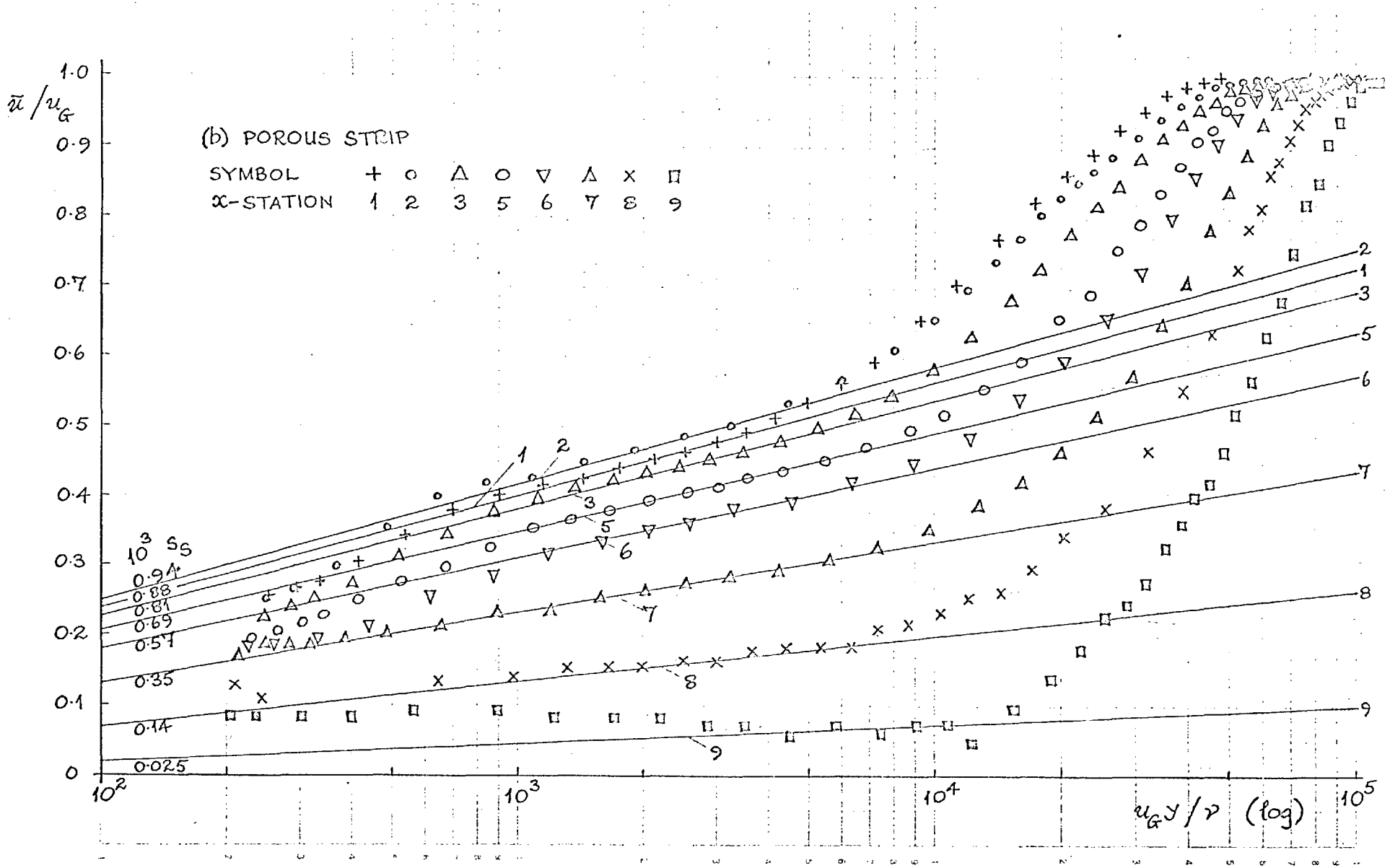


FIGURE 6.5 (b) POROUS STRIP, $v_s/u_1 = 0.07$

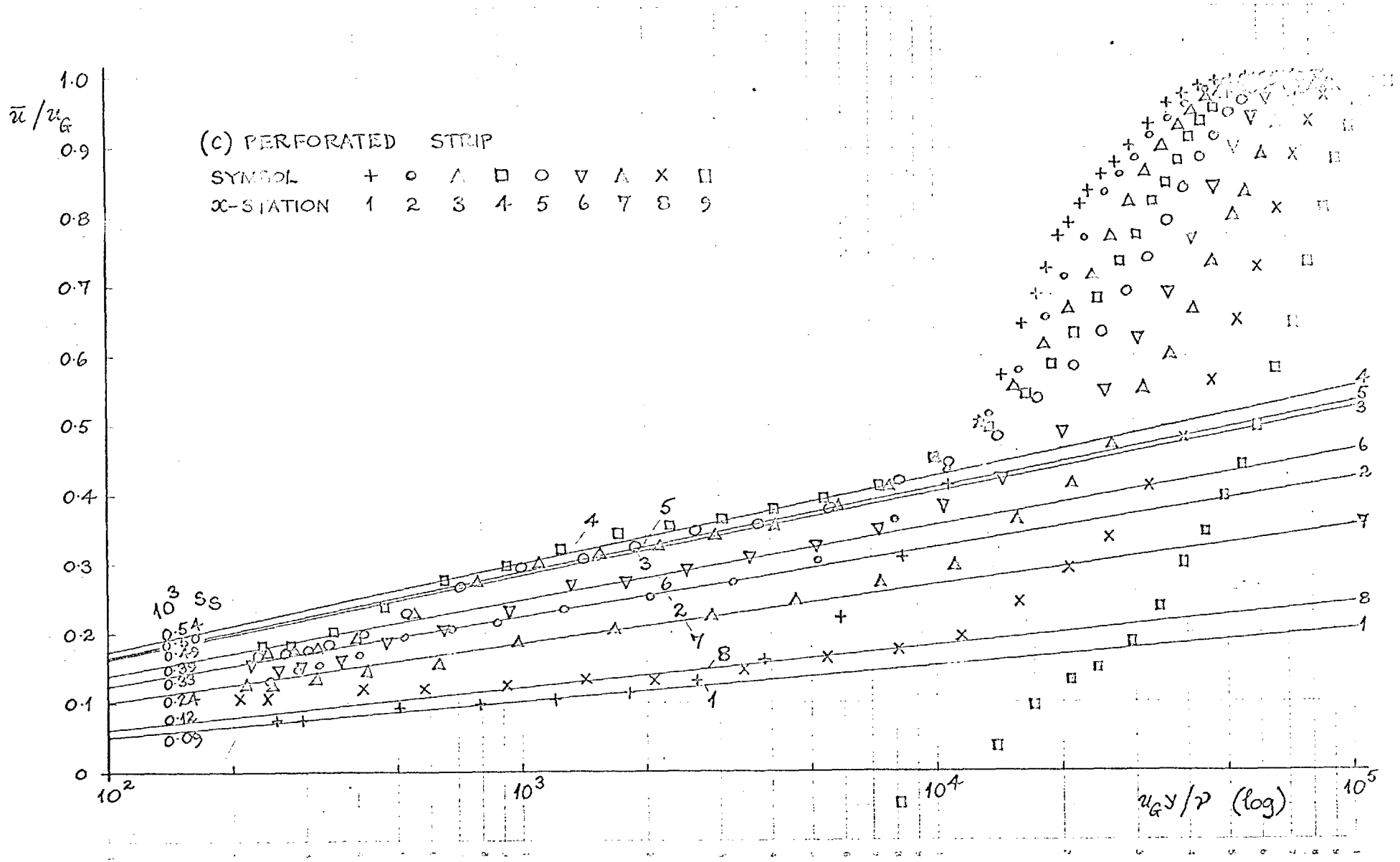
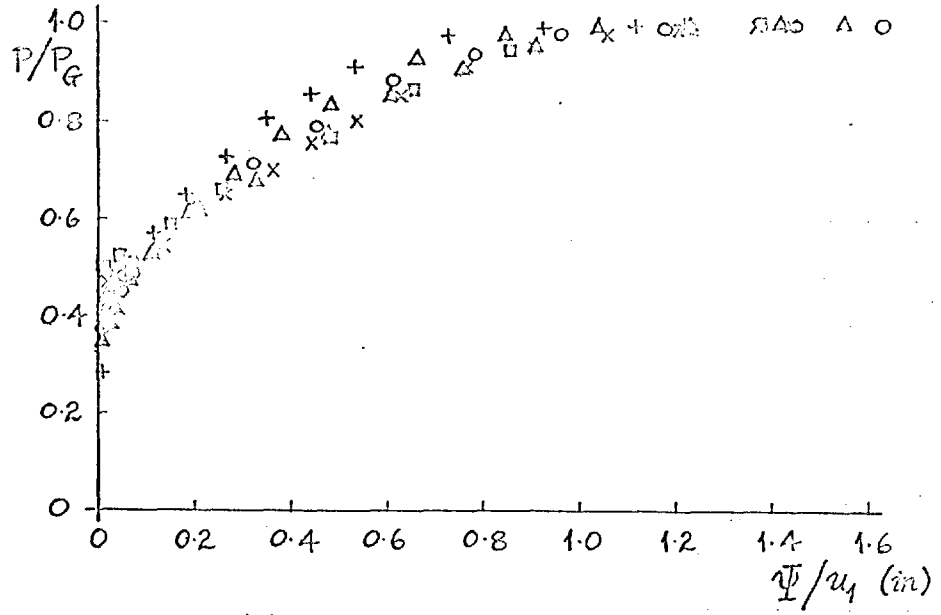
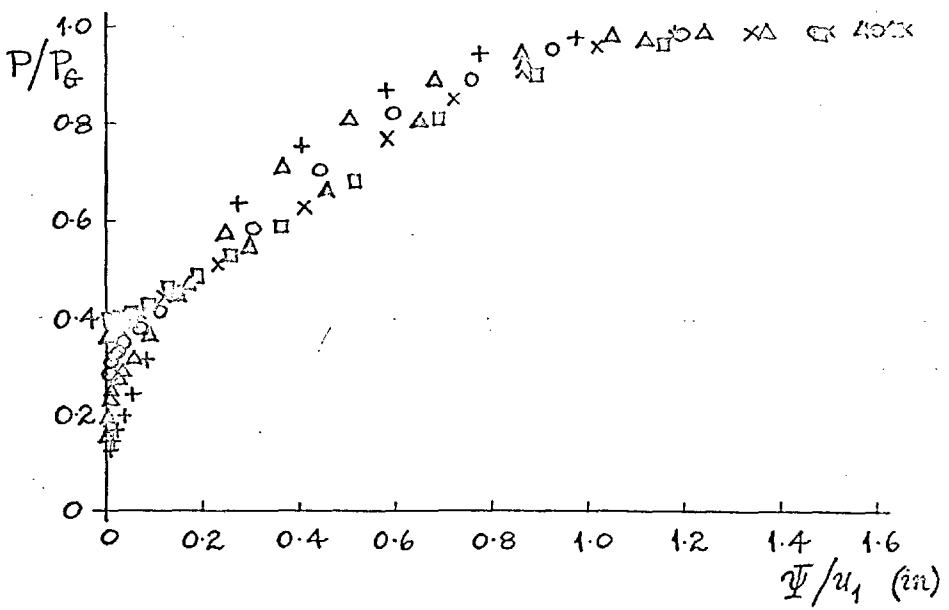


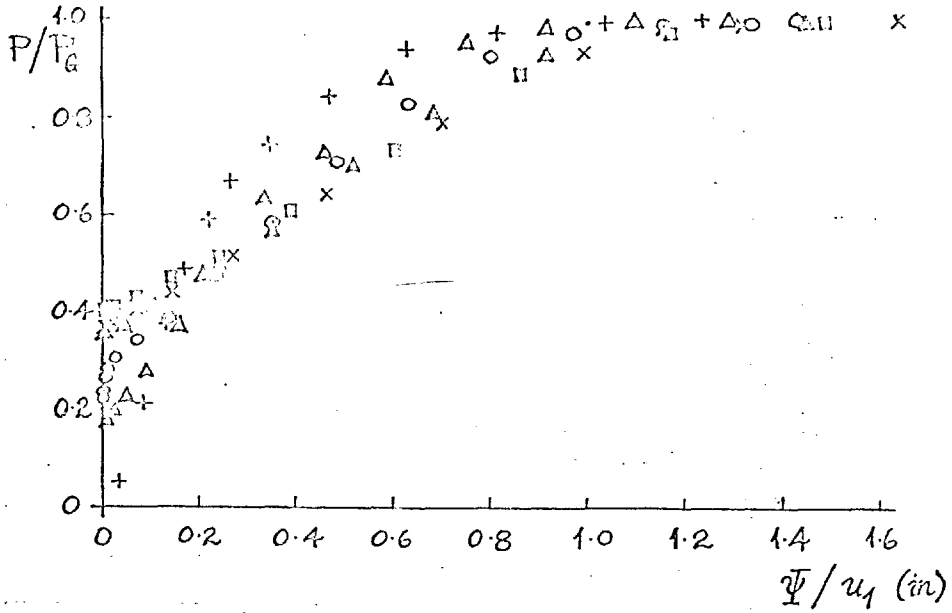
FIGURE 6.5 (c) PERFORATED STRIP, $v_s/u_1 = 0{\cdot}07$



(a) NO BLOWING



(b) POROUS STRIP



(c) PERFORATED STRIP

SYMBOL	+	Δ	o	Δ	×	□
x-STATION	1	3	5	7	8	9

FIGURE 6.6 TOTAL PRESSURE PLOTTED AGAINST Ψ/u_1

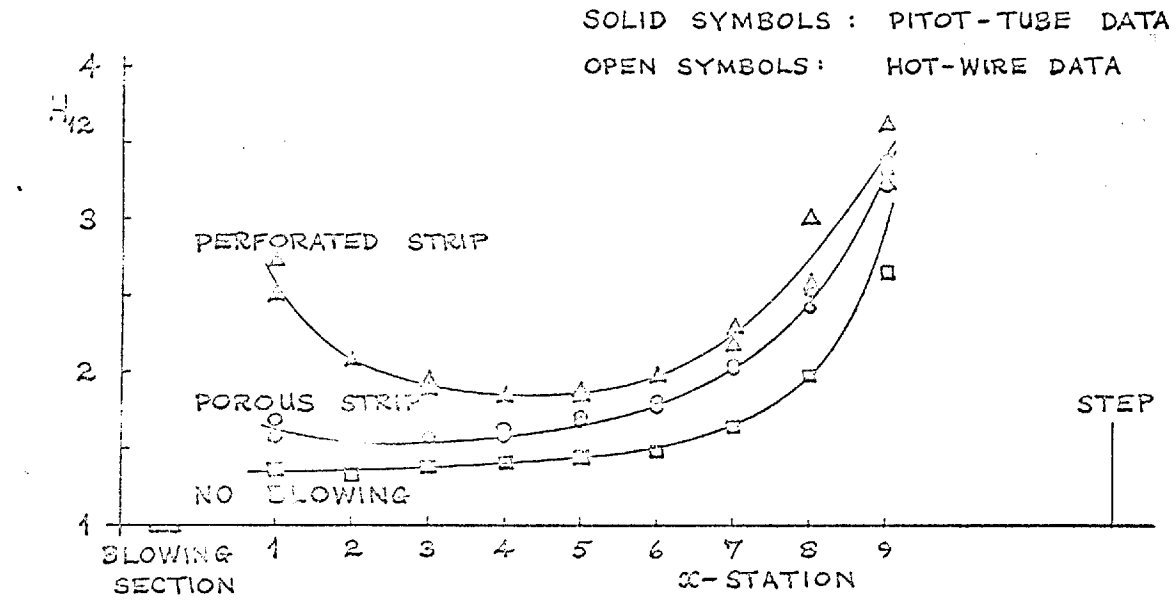


FIGURE 6.7 SHAPE-FACTOR VARIATION

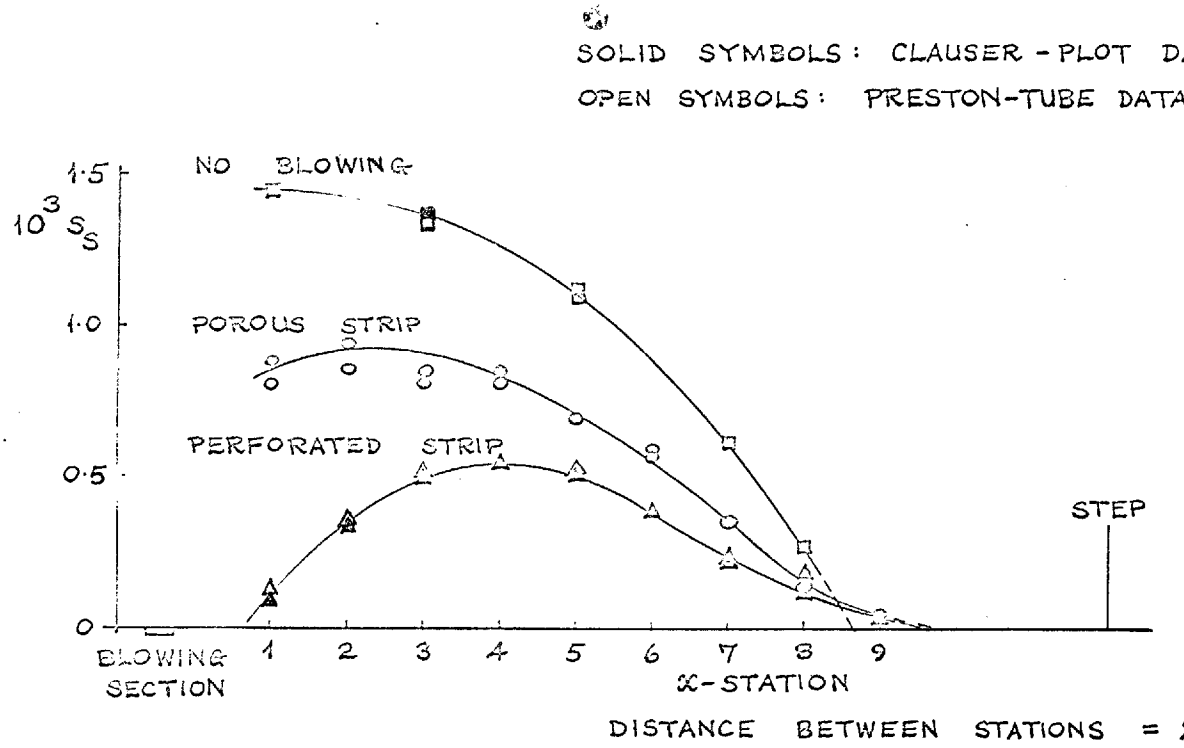
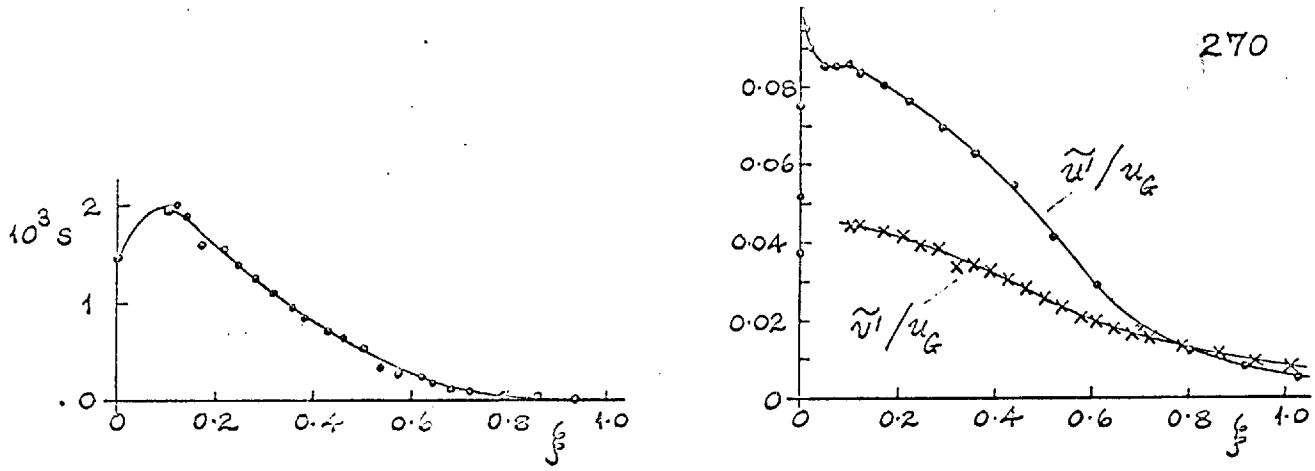
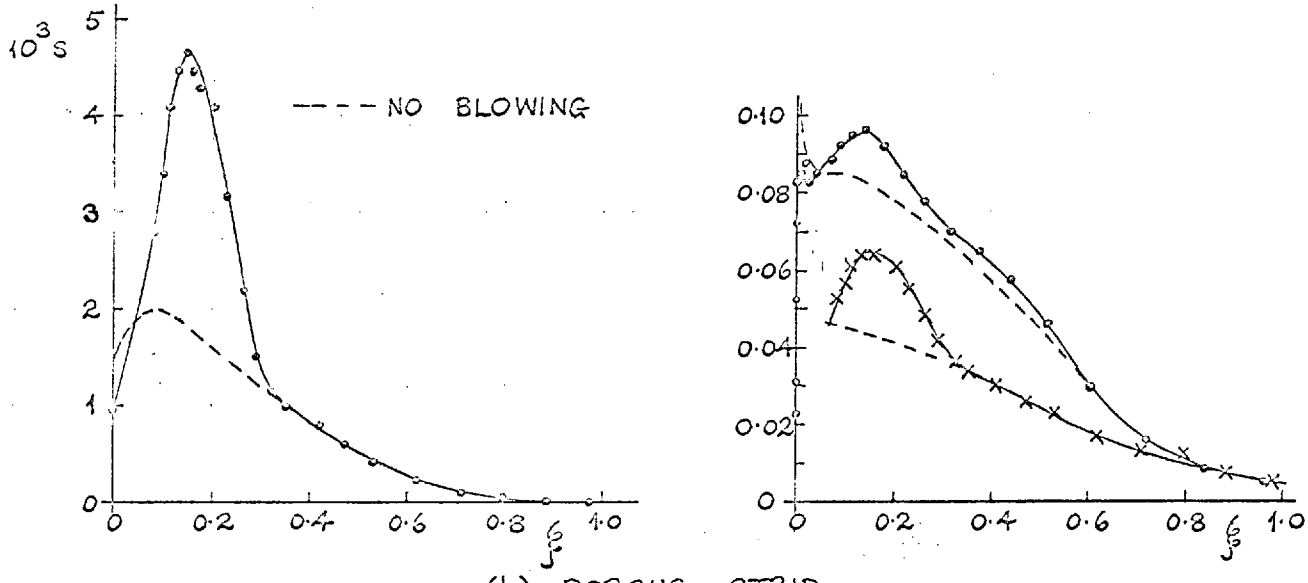


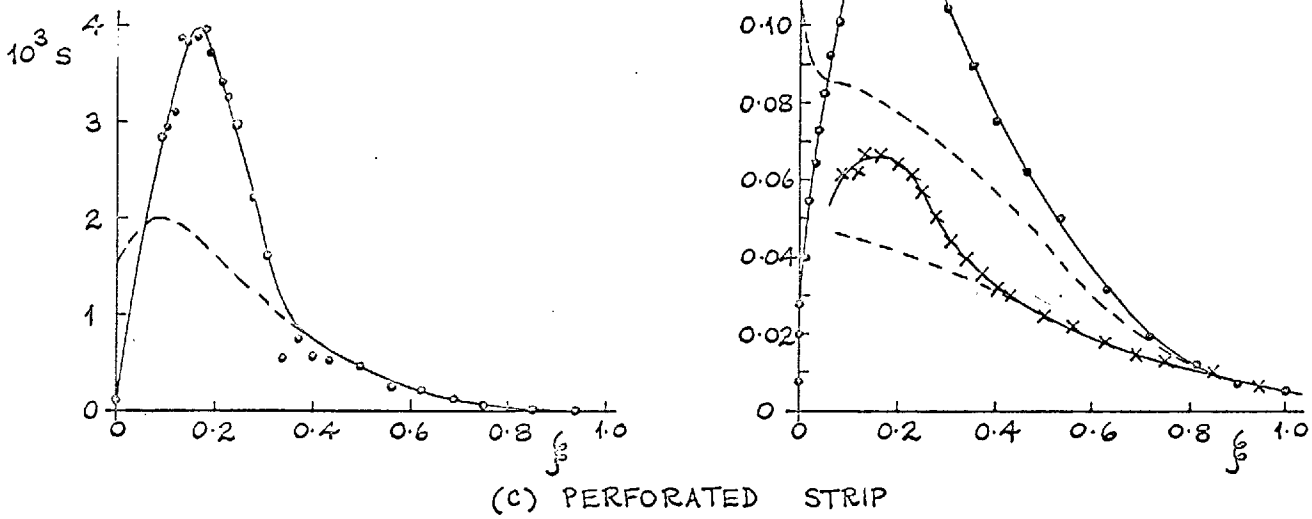
FIGURE 6.8 WALL SHEAR-STRESS VARIATION



(a) NO BLOWING

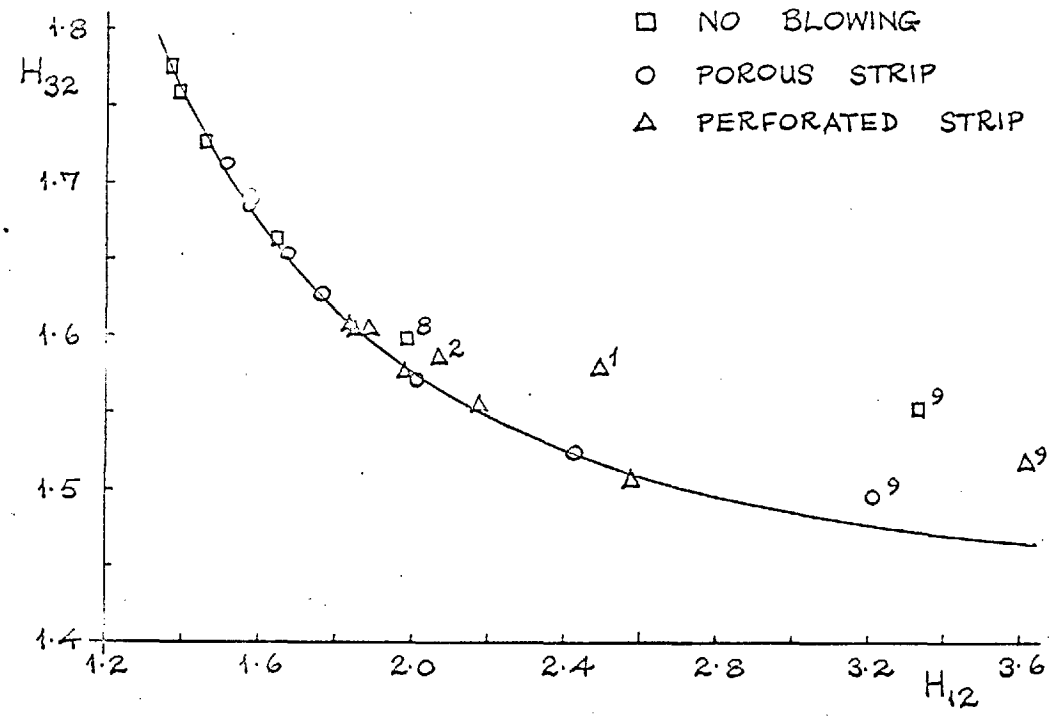


(b) POROUS STRIP

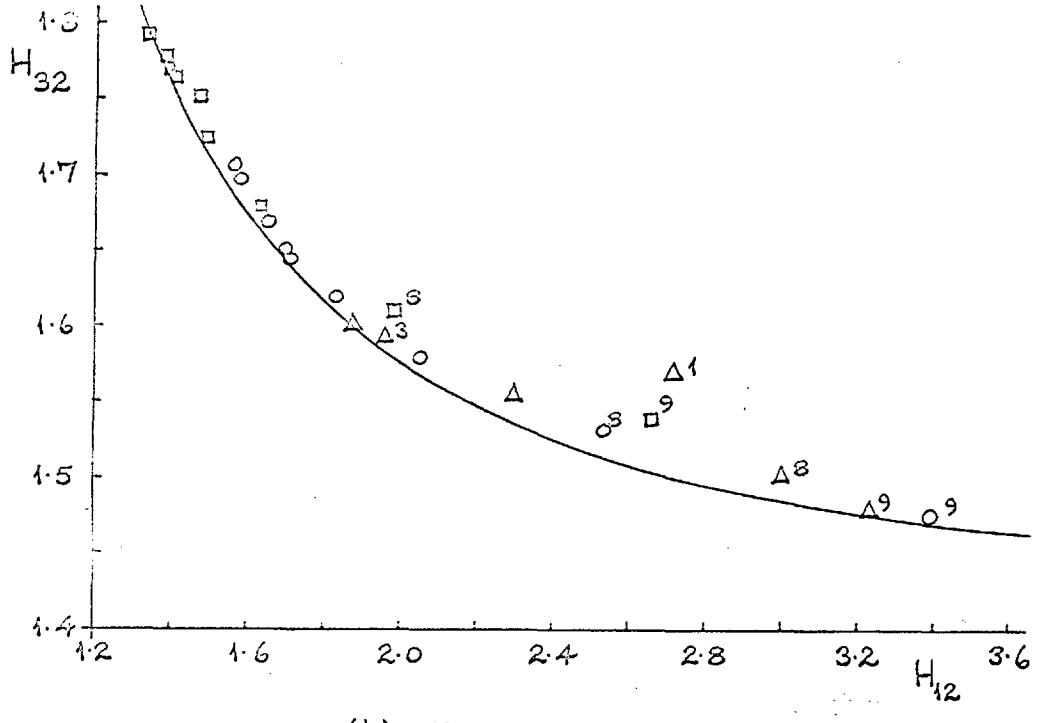


(c) PERFORATED STRIP

FIGURE 6.9 SHEAR-STRESS AND TURBULENCE-INTENSITY PROFILES AT STATION 1



(a) PITOT-TUBE DATA



(b) HOT-WIRE DATA

FIGURE 6.10 COMPARISON OF SHAPE-FACTOR DATA WITH EMPIRICAL RELATION OF CHAPTER 4, (4.2-1).

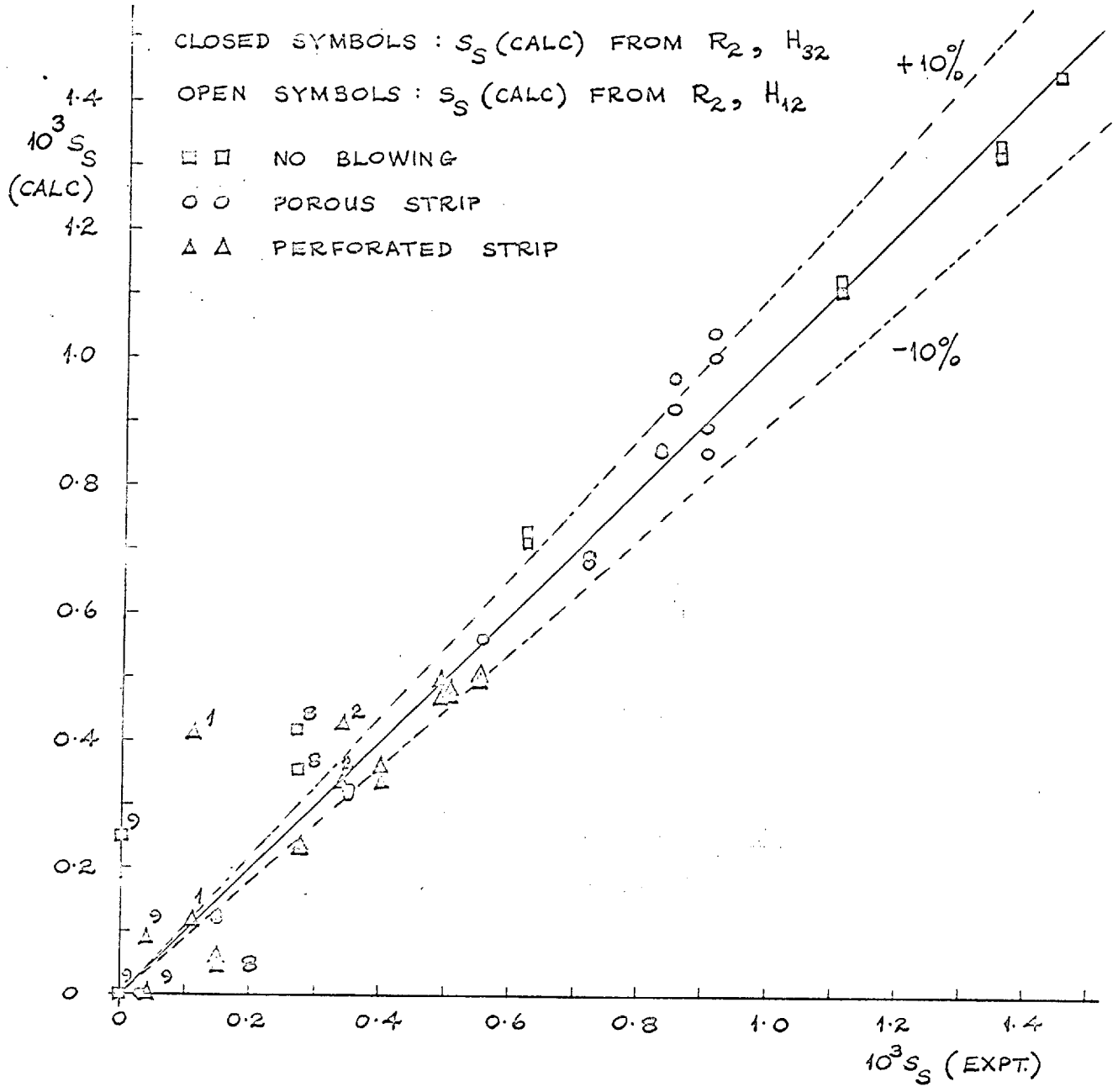


FIGURE 6.11 COMPARISON OF EXPERIMENTAL VALUES OF S_S WITH VALUES CALCULATED FROM DRAG LAW, (4.3-19)

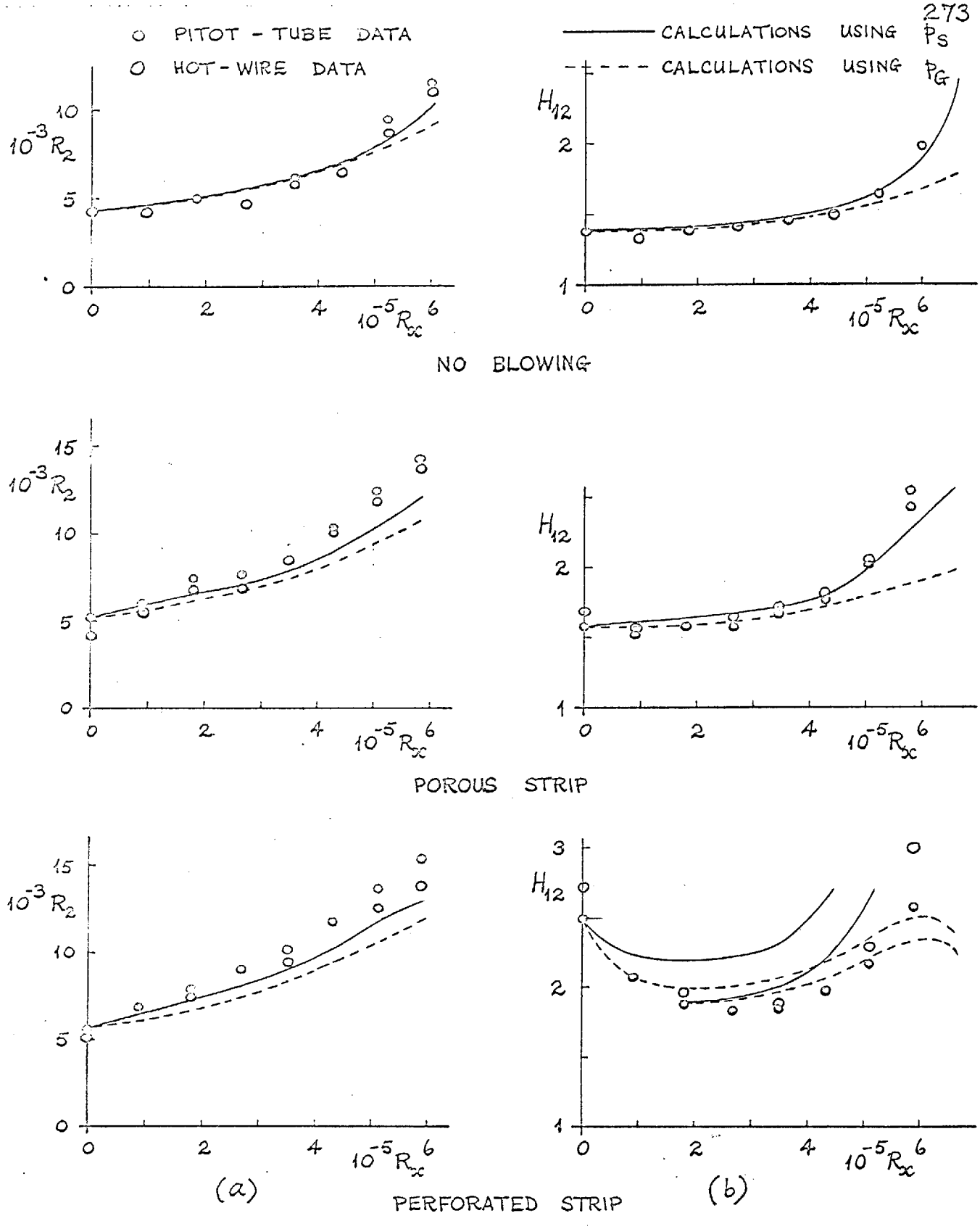


FIGURE 6.12 (a) COMPARISONS BETWEEN EXPERIMENTAL AND TWO-DIMENSIONAL (CALCULATED) VALUES OF R_2

FIGURE 6.12 (b) COMPARISONS BETWEEN EXPERIMENTAL AND PREDICTED (KINETIC-ENERGY METHOD) VALUES OF H_{12}

APPENDIX 1. Differential equations for the entrainment method

Complete expressions for dz_E/dR_x and $d\ell'/dR_x$

The definitions of H_1 and R_2 are

$$R_2 \equiv (I_1-I_2)R_G \qquad (2.3\text{-}15)$$

and

$$H_1 \equiv R_m/R_2 = I_1/(I_1-I_2) \qquad (2.3\text{-}18)$$

and, from the definitions of ℓ' (3.2-10) and z_E (3.2-11), R_G may be written as

$$R_G = \ell' \exp(\ell')/(E\kappa z_E) \qquad (A.1\text{-}1).$$

The integral quantities I_1 and I_2 can be evaluated by use of the log-plus-cos velocity-profile expression (3.2-9) as

$$I_1 = 0.5+(0.5-1/\ell')z_E \qquad (A.1\text{-}2)$$

and

$$I_2 = 0.375+[0.25-(I+1)/\ell']z_E + [0.375+(I-1)/\ell'+2/\ell'^2]z_E^2 \qquad (A.1\text{-}3),$$

where

$$I \equiv \int_0^1 \cos(\pi\xi)\ln(\xi)d\xi = -\mathrm{Si}(\pi)/\pi = -0.589$$

(values of the Si-function are tabulated by Dwight, 1958). Thus H_1 and R_2 can be written explicitly in terms of z_E and ℓ' alone, and it is seen that

$$\frac{dR_2}{dR_x} = \frac{\partial R_2}{\partial z_E}\frac{dz_E}{dR_x} + \frac{\partial R_2}{\partial \ell'}\frac{d\ell'}{dR_x} \qquad (A.1\text{-}4)$$

and $$\frac{dH_1}{dR_x} = \frac{\partial H_1}{\partial z_E}\frac{dz_E}{dR_x} + \frac{\partial H_1}{\partial \ell'}\frac{d\ell'}{dR_x} \qquad (A.1\text{-}5).$$

So that

$$\frac{dz_E}{dR_x} = \frac{\frac{\partial R_2}{\partial \ell'}\frac{dH_1}{dR_x} - \frac{\partial H_1}{\partial \ell'}\frac{dR_2}{dR_x}}{\frac{\partial R_2}{\partial \ell'}\frac{\partial H_1}{\partial z_E} - \frac{\partial H_1}{\partial \ell'}\frac{\partial R_2}{\partial z_E}} \qquad (A.1\text{-}6)$$

and $$\frac{d\ell'}{dR_x} = \frac{-\frac{\partial R_2}{\partial z_E}\frac{dH_1}{dR_x} + \frac{\partial H_1}{\partial z_E}\frac{dR_2}{dR_x}}{\frac{\partial R_2}{\partial \ell'}\frac{\partial H_1}{\partial z_E} - \frac{\partial H_1}{\partial \ell'}\frac{\partial R_2}{\partial z_E}} \qquad (A.1\text{-}7).$$

The quantities $\partial H_1/\partial \ell'$, $\partial H_1/\partial z_E$, $\partial R_2/\partial \ell'$ and $\partial R_2/\partial z_E$ can be evaluated from the expressions given at the beginning of this appendix; and dR_2/dR_x and dH_1/dR_x are given by (2.3-25) and (2.3-28).

Approximate expressions for dz_E/dR_x

Spalding (1964a) noted that ℓ' is a slowly-varying quantity, so that the neglect of $d\ell'/dR_x$ in (A.1-5) seemed to be a justifiable means of obtaining a simpler expression for dz_E/dR_x than (A.1-6),

i.e. $$dz_E/dR_x = \frac{dH_1/dR_x}{\partial H_1/\partial z_E} \qquad (A.1\text{-}8).$$

It was this equation, together with the integral mass-conservation equation (2.3-24), for which Escudier and Nicoll (1966a) reported solutions. But, neither Spalding nor Escudier and Nicoll actually checked that the neglect of $d\ell'/dR_x$ was entirely justified. Moreover, Patankar and Wolfshtein (1966) report that a similar procedure applied to a parametric-profile type of kinetic-energy method in fact does give rise to appreciable inaccuracies in the predictions. However, the writer has now carried out extensive checks which show that the errors introduced by this procedure into the entrainment method are indeed negligible. Nevertheless, the simplification brought about by the neglect of $d\ell'/dR_x$ in equation (A.1-6) is minimal, so that the solutions reported in CHAPTER 5 are based upon the complete equations, (A.1-6) and (A.1-7).

APPENDIX 2: Estimation of the normal-stress terms

To be considered here are the integral momentum equation (2.3-25), with the ω-term omitted, and the two shape-factor equations (2.3-28) and (2.3-29),

$$\text{i.e.}\quad \frac{dR_2}{dR_x} = s_S - (H_{12}+1)F_2 + \frac{1}{u_G^2}\frac{d}{dx}\int_o^{y_G}(\overline{u'^2}-\overline{v'^2})dy \qquad (2.3\text{-}25)$$

$$R_2\frac{dH_1}{dR_x} = -m_G - H_1 s_S + (H_{12}+1)H_1F_2 - \frac{H_1}{u_G^2}\frac{d}{dx}\int_o^{y_G}(\overline{u'^2}-\overline{v'^2})dx \qquad (2.3\text{-}28)$$

$$R_2\frac{dH_{32}}{dR_x} = 2\overline{s} - H_{32}s_S + (H_{12}-1)H_{32}F_2 - \frac{H_{32}}{u_G^2}\frac{d}{dx}\int_o^{y_G}(\overline{u'^2}-\overline{v'^2})dy + \frac{2}{u_G^2}\int_o^{y_G}\frac{\overline{u}}{u_G}\frac{\partial}{\partial x}(\overline{u'^2}-\overline{v'^2})dy \qquad (2.3\text{-}29).$$

The final (integral) terms of each of these equations are those which require evaluation. For this to be possible, it is evidently necessary to relate $(\overline{u'^2}-\overline{v'^2})$ to known quantities. The assumption made here appears first to have been used by Ross (1953a, b); it is based upon the observation of Dryden (1947) that the angle, α, which the principal axis of the turbulent stress tensor makes with the direction of the mean flow is almost a constant,

$$\text{i.e.}\qquad \tan(2\alpha) = \frac{-2\overline{u'v'}}{\overline{u'^2}-\overline{v'^2}} = \text{constant}.$$

Ross took the value of the constant to be 0.74; more recently Trezek and Robertson (1965) adopted a value of unity. The latter is the value used here,

$$\text{i.e.} \qquad \overline{u'^2}-\overline{v'^2} = -2\overline{u'v'} \approx 2su_G^2 \qquad \text{(A.2-1)}.$$

For the shear stress, the Prandtl mixing-length hypothesis discussed in CHAPTER 4 is again made use of. But, the ramp-function mixing-length distribution adopted earlier leads to algebra more tedious to work than is warranted by either the crudity of the other assumptions or the purpose of the analysis (which is to give an order-of-magnitude estimate, of the effect on the boundary-layer calculations of CHAPTER 5, of including the cross-flow pressure gradient). Therefore, the mixing-length assumption is simplified further to $\lambda = \lambda_G$ for all values of ξ. If the linear velocity profile (4.3-3) is also used, the final expression for the normal-stress term becomes

$$\boxed{\overline{u'^2}-\overline{v'^2} = 2\lambda_G^2(1-\zeta)^2u_G^2} \qquad \text{(A.2-2)}.$$

The result of evaluating the first of the two integrals is then

$$\frac{1}{u_G^2}\frac{d}{dx}\int_o^{y_G}(\overline{u'^2}-\overline{v'^2})dy = 2\lambda_G^2(1-\zeta)\left[(1-\zeta)\frac{dy_G}{dx}+2(1-\zeta)\frac{y_G}{u_G}\frac{du_G}{dx}-2y_G\frac{d\zeta}{dx}\right].$$

The evaluation of the second integral proceeds as follows*,

$$\frac{1}{u_G^2}\int_o^{y_G} \frac{\bar{u}}{u_G}\frac{\partial}{\partial x}(\overline{u'^2}-\overline{v'^2})dy \approx \frac{1}{u_G^3}\frac{d}{dx}\int_o^{y_G}\bar{u}(\overline{u'^2}-\overline{v'^2})dy$$

$$= \lambda_G^2(1-\zeta)(1+\zeta)\Big[(1-\zeta)\frac{dy_G}{dx} +$$

$$+3(1-\zeta)\frac{y_G}{u_G}\frac{du_G}{dx} - \frac{(1+3\zeta)}{(1+\zeta)}\,y_G\,\frac{d\zeta}{dx}\Big].$$

It is convenient to substitute for y_G in terms of δ_2 and ζ through the relation derivable from the linear velocity profile,

i.e. $$\delta_2/y_G = (1-\zeta)(1-2\zeta)/6 \qquad (4.3\text{-}6).$$

Then the two integral expressions may be written (after some algebra) as follows

$$\frac{1}{u_G^2}\frac{d}{dx}\int_o^{y_G}(\overline{u'^2}-\overline{v'^2})dy = 12\lambda_G^2\frac{(1-\zeta)}{(1+2\zeta)}\Big[\frac{dR_2}{dR_x}+F_2-\frac{3}{(1-\zeta)(1+2\zeta)}R_2\frac{d\zeta}{dR_x}\Big]$$

and (A.2-3)

$$\frac{1}{u_G^2}\int_o^{y_G}\frac{\bar{u}}{u_G}\frac{\partial}{\partial x}(\overline{u'^2}-\overline{v'^2})dy = 6\lambda_G^2\frac{(1-\zeta)(1+\zeta)}{(1+2\zeta)}\Big[\frac{dR_2}{dR_x}+2F_2\frac{2(1+\zeta+\zeta^2)}{(1-\zeta^2)(1+2\zeta)}R_2\frac{d\zeta}{dR_x}\Big]$$

(A.2-4).

*The additional assumption here is a convenience not a necessity.

When the kinetic-energy method is under consideration, the equations to be solved are (2.3-25) and (2.3-29). The equation derived in CHAPTER 4 may be used to relate H_{32} with ζ and also $d\zeta/dR_x$ with dH_{32}/dR_x,

i.e. $$H_{32} = \frac{3(1+\zeta)^2}{2(1+2\zeta)} \qquad (4.3\text{-}5)$$

and $$\frac{d\zeta}{dR_x} = \frac{(1+2\zeta)^2}{3\zeta(1+\zeta)} \frac{dH_{32}}{dR_x} \qquad (A.2\text{-}5).$$

Then if (A.2-3) and (A.2-4) are used to replace the integrals in (2.3-25) and (2.3-29), these two equations constitute a soluble set with either R_2 and H_{32} or R_2 and ζ as dependent variables.

When the entrainment method is under consideration the equations to be solved are (2.3-25) and (2.3-28). It is then provident to make use of an equation similar to (4.3-5), also derived from the linear velocity profile, to relate H_1 with ζ,

i.e. $$H_1 = \frac{3(1+\zeta)}{(1-\zeta)(1+2\zeta)} \qquad (A.2\text{-}6)$$

and so $$\frac{d\zeta}{dR_x} = \frac{(1-\zeta)^2(1+2\zeta)^2}{6\zeta(2+\zeta)} \frac{dH_1}{dR_x} \qquad (A.2\text{-}7).$$

And, again, if (A.2-3) is used to replace the integrals in (2.3-25) and (2.3-28), the two equations constitute a soluble set with, now, either R_2 and H_1 or R_2 and ζ as dependent variables.

The final equations in both cases are straightforward to obtain, but quite complex in form, and so are not given here.

APPENDIX 3: Analysis of the electrical signals obtained from a hot-wire anemometer

A.3.1 Introduction

Newman (1951), Sandborn and Slogar (1955), Hinze (1959), Patel (1963) and others have presented methods for the analysis of the electrical signals which are obtained from a hot-wire anemometer. So far as the writer is aware, all previous writers have presented similar analyses valid only for turbulence in which the fluctuating components u' and v' and w' are small compared with the mean velocity $\overline{u}$ (rms values less than about 10% of $\overline{u}$). Some authors, however, have attempted to estimate the errors involved in using the conventional method in the analysis of signals for intensities up to about 20%. Nevertheless, Newman, Schubauer and Klebanoff (1951), Spangenberg, Rowland and Mease (1966) and others have used the analysis, without correction, in the calculation of (indicated) intensities up to 60 or 70%. In the writer's own experiments, intensities of this order, and even greater, were again involved. Consequently, it was decided to undertake a re-examination of the method of analysis, to see if the conventional assumptions are in fact necessary, and if not to suggest an alternative method of analysis, valid even for the very high intensities which are encountered in practice.

A new procedure has evolved from the re-examination and is set out below. The conventional method is also outlined, to indicate where and why highly-restrictive assumptions have in the past been made.

A.3.2 Features common to both analyses

The starting point of both the present and previous analyses is the empirical law which governs the cooling of a hot wire,

i.e. $$E^2 = A + B\, u_N^{\,n} \qquad (A.3\text{-}1).$$

E is the voltage drop across the wire, u_N the velocity normal to the wire, A and B are constants (determined by calibration) which depend upon the wire resistance, geometry, temperature, etc. and n is a universal constant. Various recommendations have been made for n, including the best-known value of 0.5 (King, 1914) and that currently in favour (Patel, Bradshaw and Johnson, 1963, etc.) of 0.45 (Collis and Williams, 1959). It is important to note that although the validity of (A.3-1) has been established only in steady flow, when used in the analysis of hot-wire measurements for turbulent flows it is assumed to hold instantaneously.

The other starting assumptions, which are again conventional but not particularly restrictive, are that the

constants A and B are known, from calibration in a steady flow, and that n is known. It is also assumed that the quantities measured are the mean (D.C.) voltage, $\overline{E}$, and the root-mean-square value, $\tilde{E}'$, of the fluctuating component of the instantaneous voltage, E,

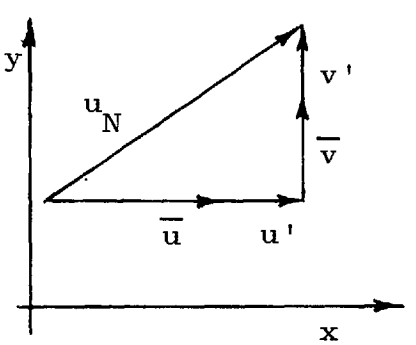
i.e. $$E = \overline{E} + E',$$

so $$\tilde{E}' \equiv \overline{(E'^2)}^{\frac{1}{2}} = \overline{[(E-\overline{E})^2]}^{\frac{1}{2}} \qquad (A.3\text{-}2).$$

The analyses presented here apply specifically to wires operated at constant temperature. Similar analyses could be given for constant-current operation.

A.3.3 Single wire with axis in z-direction (used to measure $\overline{u}$ and $\overline{u'^2}$)

Conventional method of analysis



The vector diagram on the left shows the velocity components in the x-y plane. It is only these components which contribute to the cooling velocity, u_N, for a wire with its axis in the z-direction. From the diagram it is seen that u_N is given by

$$u_N^2 = (\overline{u} + u')^2 + (\overline{v} + v')^2 \qquad (A.3\text{-}3).$$

Also, from (A.3-1), it is seen that

$$\overline{E} = \overline{(A + Bu_N^{\,n})^{\frac{1}{2}}} ,$$

so $$\overline{E} = \overline{[A+B(\overline{u}^2+2u'\overline{u}+u'^2+\overline{v}^2+2v'\overline{v}+v'^2)^{n/2}]^{\frac{1}{2}}} \qquad (A.3\text{-}4).$$

If the value of n is taken as $\frac{1}{2}$ and the binomial theorem applied to (A.3-4) twice, it is found that

$$\overline{E} = (A+B\overline{u}^2)^{\frac{1}{2}}\left[1+\frac{C}{8}\left(-\tfrac{1}{2}\frac{\overline{u'^2}}{\overline{u}^2}+\frac{\overline{v}^2}{\overline{u}^2}+\frac{\overline{v'^2}}{\overline{u}^2}-3\frac{\overline{u'v'}\,\overline{v}}{\overline{u}^3}\right)\right.$$
$$\left.-\frac{C^2}{32}\left(\frac{\overline{u'^2}}{\overline{u}^2}+2\frac{\overline{u'v'}\,\overline{v}}{\overline{u}^3}\right)+O\left(\frac{\overline{u'^3}}{\overline{u}^3}\right)\right] \qquad (A.3\text{-}5),$$

wherein C is defined as

$$C \equiv B\overline{u}^2/(A+B\overline{u}^2) \qquad (A.3\text{-}6)$$

(the value of C is usually close to 0.5 for the wires and velocities encountered in the present work).

An expression for $\overline{E^2}$ also can be deduced from (A.3-1) and (A.3-3), again making use of the binomial theorem; it is

$$\overline{E^2} = (A+B\overline{u}^2)\left[1+\frac{C}{4}\left(-\tfrac{1}{2}\frac{\overline{u'^2}}{\overline{u}^2}+\frac{\overline{v}^2}{\overline{u}^2}+\frac{\overline{v'^2}}{\overline{u}^2}-3\frac{\overline{u'v'}\,\overline{v}}{\overline{u}^3}\right)\right.$$
$$\left.-\frac{C^2}{32}\left(\frac{\overline{u'^2}}{\overline{u}^2}+2\frac{\overline{u'v'}\,\overline{v}}{\overline{u}^3}\right)+O\left(\frac{\overline{u'^3}}{\overline{u}^3}\right)\right] .$$

Now, from (A.3-2), $\overline{E'^2}$ is given by

$$\overline{E'^2} = \overline{E^2} - \overline{E}^2$$

so $$\boxed{\overline{E'^2} = \frac{B^2\overline{u}}{16(A+B\overline{u^{\frac{1}{2}}})}\left[\frac{\overline{u'^2}}{\overline{u}^2} + 2\,\frac{\overline{u'v'}\ \overline{v}}{\overline{u}^3} + O\left(\frac{\overline{u'^3}}{\overline{u}^3}\right)\right]} \qquad \text{(A.3-7)}.$$

Clearly, however, in the absence of further information, (A.3-5) and (A.3-7) can only be used in general circumstances, to determine $\overline{u}$ and $\overline{u'^2}$ from $\overline{E}$ and $\widetilde{E'}$, if the following assumptions are made:

either

$$1 \gg \frac{C}{8}\left(-\tfrac{1}{2}\,\frac{\overline{u'^2}}{\overline{u}^2} + \frac{\overline{v}^2}{\overline{u}^2} + \frac{\overline{v'^2}}{\overline{u}^2} - 3\,\frac{\overline{u'v'}\ \overline{v}}{\overline{u}^3}\right) - \frac{C^2}{32}\left(\frac{\overline{u'^2}}{\overline{u}^2} + 2\,\frac{\overline{u'v'}\ \overline{v}}{\overline{u}^3}\right) \qquad \text{(A.3-8)}$$

and $$\frac{\overline{u'^2}}{\overline{u}^2} \gg 2\,\frac{\overline{u'v'}\ \overline{v}}{\overline{u}^3} \qquad \text{(A.3-9)},$$

when (A.3-5) reduces to

$$\boxed{\overline{E} = (A+B\overline{u^{\frac{1}{2}}})^{\frac{1}{2}}} \qquad \text{(A.3-10)}$$

and (A.3-7) to

$$\boxed{\overline{E'^2} = \frac{B^2\overline{u}}{16(A+B\overline{u^{\frac{1}{2}}})}\ \frac{\overline{u'^2}}{\overline{u}^2}} \qquad \text{(A.3-11)};$$

or $$\frac{\overline{u'^2}}{\overline{u}^2} \gg 2\left(\frac{\overline{v}^2}{\overline{u}^2} + \frac{\overline{v'^2}}{\overline{u}^2} - 3\,\frac{\overline{u'v'}\ \overline{v}}{\overline{u}^3}\right) \qquad \text{(A.3-12)}$$

and $\dfrac{\overline{u'^2}}{\overline{u}^2} \gg 2\,\dfrac{\overline{u'v'}\;\overline{v}}{\overline{u}^3}$ (A.3-13),

when (A.3-5) reduces to

$$\overline{E} = (A+B\overline{u}^2)^{\frac{1}{2}}\left[1 - \frac{C}{16}\left(1+\frac{C}{2}\right)\frac{\overline{u'^2}}{\overline{u}^2}\right] \qquad \text{(A.3-14)}$$

and (A.3-7) again to (A.3-11). Also, of course, the terms of order $\overline{u'^3}/\overline{u}^3$ must be negligible.

However, (A.3-5) and (A.3-7) themselves are subject to conditions even more restrictive than the above. These stem from the necessity to use the binomial theorem in their derivation, for this imposes the following limitation on the terms in (A.3-4):

$$\overline{u}^2 > (2u'\overline{u} + u'^2) + (\overline{v} + v')^2 \qquad \text{(A.3-15)}.$$

Thus the validity of (A.3-5) and (A.3-7) is limited to flows in which (A.3-15) is satisfied, so that even when $\overline{v}$ and v' are negligible, the <u>peak instantaneous</u> intensity is limited to about 40%* and the rms intensity to an appreciably lower figure (probably less than 30%).

<u>New method of analysis</u>

The major flaw in the conventional method of analysis

---

*Since, if $\overline{u}^2 = 2u'\overline{u} + u'^2$, $u'/\overline{u} = \pm\sqrt{2} - 1$.

stems from the necessity to make use of the binomial theorem. The new procedure, which is outlined below, is considerably simpler than the other analysis, primarily because it partially avoids the need to use the binomial theorem, and includes some allowance for terms usually neglected. Although the new method suffers from limitations, they are appreciably less restrictive than those indicated in the previous section.

The first step in the new analysis is to write (A.3-1) as

$$[(E^2 - A)/B]^{1/n} = u_N \qquad \text{(A.3-16)}.$$

Then $\overline{E'^4}$ is set equal to $(\overline{E'^2})^2$, $\overline{E'^6}$ to $(\overline{E'^2})^3$, etc., and $\overline{E'^3}$, $\overline{E'^5}$, etc. are neglected.* Application of these assumptions is greatly simplified when it is realised that they correspond exactly with the assumption that $E'\{t\}$ has the form of a square wave, for then

$$\overline{u}_N = \tfrac{1}{2}\left\{\left[\frac{(\overline{E} + \tilde{E}')^2 - A}{B}\right]^{\frac{1}{n}} + \left[\frac{(\overline{E} - \tilde{E}')^2 - A}{B}\right]^{\frac{1}{n}}\right\} \qquad \text{(A.3-17)}$$

where $\tilde{E}' \equiv (\overline{E'^2})^{\frac{1}{2}}$. A similar expression can be written

---

*It is easily shown as follows that in fact $\overline{E'^4} \geq (\overline{E'^2})^2$, etc. Let $E'^2 = \overline{E'^2} + f\{t\}$, where $t \equiv$ time; then $E'^4 = (\overline{E'^2})^2 + f^2$, $E'^6 = (\overline{E'^2})^3 + 3\overline{E'^2}f^2 + f^3$, etc.; and for any normal distribution $\overline{f^3} = \overline{f^5} = \ldots = 0$.

for $\overline{u_N^2}$; it is

$$\overline{u_N^2} = \tfrac{1}{2}\left\{\left[\frac{(\overline{E} + \tilde{E}')^2 - A}{B}\right]^{\frac{2}{n}} + \left[\frac{(\overline{E} - \tilde{E}')^2 - A}{B}\right]^{\frac{2}{n}}\right\} \qquad \text{(A.3-18)}.$$

Now, for 'simple' turbulence where $u_N = u = \overline{u} + u'$, (A.3-17) is no more than an expression for $\overline{u}$ and (A.3-18) one for $\overline{u}^2 + \overline{u'^2}$, from which $\overline{u'^2}$ is easily determined, no matter how great its value.

In general, of course, u_N is given by (A.3-3),

i.e. $$u_N^2 = \overline{u}^2\left(1 + 2\,\frac{u'}{\overline{u}} + \frac{u'^2}{\overline{u}^2} + \frac{v'^2}{\overline{u}^2} + \frac{\overline{v}^2}{\overline{u}^2} + 2\,\frac{v'\overline{v}}{\overline{u}^2}\right).$$

From this equation it is seen that

$$\overline{u_N^2} = \overline{u}^2\left(1 + \frac{\overline{u'^2}}{\overline{u}^2} + \frac{\overline{v'^2}}{\overline{u}^2} + \frac{\overline{v}^2}{\overline{u}^2}\right),$$

and also, when u', v' and $\overline{v}$ satisfy the inequality (A.3-15),

$$\overline{u}_N = \overline{u}\left[1 + \tfrac{1}{2}\,\frac{\overline{v}^2}{\overline{u}^2} + \tfrac{1}{2}\,\frac{\overline{v'^2}}{\overline{u}^2} + O\left(\frac{\overline{u'^3}}{\overline{u}'^3}\right)\right].$$

Then $\overline{u}$ and $\overline{u'^2}$ are given by

$$\boxed{\overline{u}_N = \overline{u} + O(\overline{v'^2}/\overline{u}^2)} \qquad \text{(A.3-19)}$$

and

$$\boxed{\overline{u_N^2} - \overline{u}^2 = \overline{u'^2} + O(\overline{u'^3}/\overline{u}^3)} \qquad \text{(A.3-20)}.$$

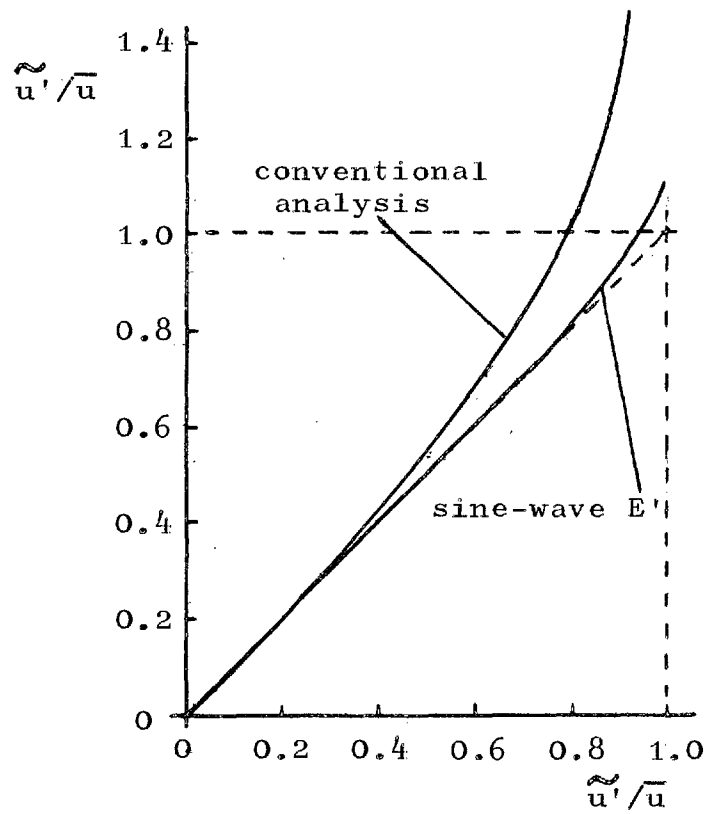
However, when (A.3-15) is not satisfied, other assumptions are necessary. For example, in boundary-layer situations it is commonly found that $\overline{u}^2 >> \overline{v}^2$, and also $\overline{u'^2} > \overline{v'^2}$, when both these latter quantities are large. Then, v^2 may be neglected in comparison with u^2, and (A.3-19) and (A.30-20) may again be used to calculate $\overline{u}$ and $\overline{u'^2}$.

Comparison between results obtained from new and old analyses

A comparison between values of $\tilde{u}'/\overline{u}$ obtained from the conventional and new analyses is shown in the diagram below. An additional comparison is made with results obtained with a sinusoidal, rather than square, waveform for $E'\{t\}$. The figures used to plot the curves shown are based upon the data obtained in the writer's experiments with a single hot-wire probe.

The results show that for intensities up to about 20%, the three analyses give results within 1% of each other. For higher intensities, the conventional analysis gives values considerably in excess of either of the new ones. Also, the use of the sinusoidal waveform for E' makes no significant difference to the results given by the new analysis. Therefore it seems safe to assume that if it were possible to use the true $E'\{t\}$ variation, the results

would be little different from those given by the square wave.



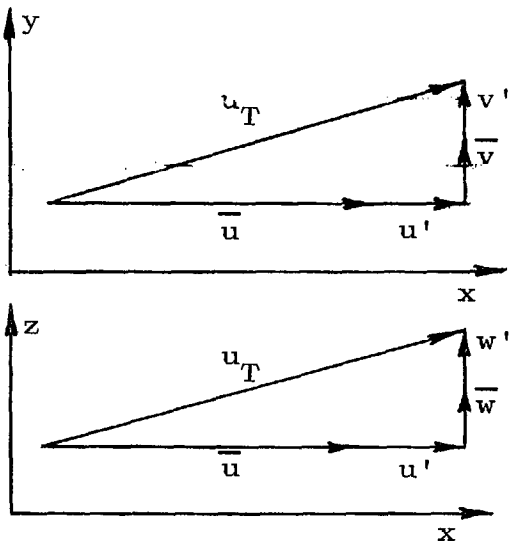
(from square-wave E').

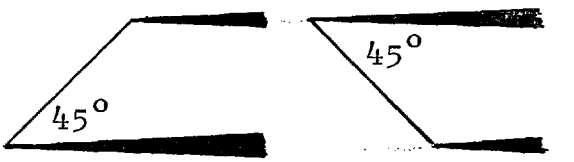
Calculations have also been carried out with a square waveform for u'. The results are insignificantly different from those obtained with a square waveform for E', but the equations to be solved cease to be explicit.

A.3.4 Crossed wires in x-y plane, with wire axes at $\pm 45^{o}$

(used to measure $\overline{v'^2}$ and $\overline{u'v'}$)

Conventional method of analysis





The vector diagram above left shows the velocity components in the x-y plane, and that on the immediate left those in the x-z plane. From these it is seen that the component of the total instantaneous velocity, u_T, normal to wire 1, u_{N_1}, is given by

$$u_{N_1}^2 = \left[\frac{(\bar{u}+u')-(\bar{v}+v')}{\sqrt{2}}\right]^2 + (\bar{w}+w')^2 \qquad \text{(A.3-21)},$$

and the corresponding expression for u_{N_2} is

$$u_{N_2}^2 = \left[\frac{(\bar{u}+u')+(\bar{v}+v')}{\sqrt{2}}\right]^2 + (\bar{w}+w')^2 \qquad \text{(A.3-22)}.$$

Then from (A.3-1) it is seen that

$$\overline{E}_1 = \left\{A_1+B_1\left(\frac{\bar{u}-\bar{v}}{\sqrt{2}}\right)^{\frac{1}{2}}\left[1 + \frac{2u'\bar{u}+u'^2+2v'\bar{v}+v'^2-2v'\bar{u}-2u'\bar{v}}{(\bar{u}-\bar{v})^2} - \frac{-2u'v'+2w'^2}{(\bar{u}-\bar{v})^2}\right]^{\frac{1}{4}}\right\}^{\frac{1}{2}} \qquad \text{(A.3-23)},$$

with a similar expression for $\overline{E}_2$ (terms involving $\overline{w}$ are zero in two-dimensional flow and have been dropped from (A.3-23)).

The binomial theorem must again be used to put (A.3-23) into a practically-useful form. The resulting expression is

$$\overline{E}_1 = \left[A_1+B_1\left(\frac{\overline{u}-\overline{v}}{\sqrt{2}}\right)^{\frac{1}{2}}\right]^{\frac{1}{2}}\left[1+\frac{C_1}{8}\left(1-\frac{3}{2}\frac{\overline{u}^2}{w_1^2}+3\frac{\overline{v}\,\overline{u}}{w_1^2}-\frac{C_1}{4}\frac{\overline{u}^2}{w_1^2}+\frac{C_1}{2}\frac{\overline{v}\,\overline{u}}{w_1^2}\right)\right.$$
$$\left.\left(\frac{\overline{u'^2}+\overline{v'^2}-2\overline{u'v'}}{w_1^2}\right)+\frac{C_1}{4}\frac{\overline{w'^2}}{w_1^2}+O\left(\frac{\overline{u'^3}}{\overline{u}^3}\right)\right] \qquad \text{(A.3-24)}$$

where $C_1 \equiv B_1\left(\frac{\overline{u}-\overline{v}}{\sqrt{2}}\right)^{\frac{1}{2}} \Big/ \left[A_1+B_1\left(\frac{\overline{u}-\overline{v}}{\sqrt{2}}\right)^{\frac{1}{2}}\right]$

and $w_1 \equiv \overline{u} - \overline{v}$.

A similar expression can be deduced for $\overline{E}_2$.

(A.3-1) and (A.3-21) may also be combined, to give

$$\overline{E_1^2} = \left[A_1+B_1\left(\frac{\overline{u}-\overline{v}}{\sqrt{2}}\right)^{\frac{1}{2}}\right]\left[1+\frac{C_1}{4}\left(1-\frac{3}{2}\frac{\overline{u}^2}{w_1^2}+3\frac{\overline{v}\,\overline{u}}{w_1^2}-\frac{C_1}{4}\frac{\overline{u}^2}{w_1^2}+\frac{C_1}{2}\frac{\overline{v}\,\overline{u}}{w_1^2}\right)\right.$$
$$\left.\left(\frac{\overline{u'^2}+\overline{v'^2}-\overline{2u'v'}}{w_1^2}\right)+\frac{C_1}{2}\frac{\overline{w'^2}}{w_1^2}+O\left(\frac{\overline{u'^3}}{\overline{u}^3}\right)\right]$$

with, again, a similar expression for $\overline{E_2^2}$.

Then, the expressions for $\overline{E}_1$ and $\overline{E_1^2}$ can be combined to give

$$\overline{E_1'^2} = \left[A_1+B_1\left(\frac{\overline{u}-\overline{v}}{\sqrt{2}}\right)^{\frac{1}{2}}\right]\frac{C_1^2}{16}\left(\frac{\overline{u}}{w_1}\right)^2\left[\left(\frac{\overline{u'^2}+\overline{v'^2}-2\overline{u'v'}}{w_1^2}\right)\left(1-2\frac{\overline{v}}{\overline{u}}\right)+O\left(\frac{\overline{u'^3}}{\overline{w}_1^3}\right)\right] \qquad \text{(A.3-25)}$$

and the corresponding result for $\overline{E_2'^2}$ is

$$\overline{E_2'^2} = \left[A_2+B_2\left(\frac{\overline{u}+\overline{v}}{\sqrt{2}}\right)^{\frac{1}{2}}\right]\frac{C_2^2}{16}\left(\frac{\overline{u}}{w_2}\right)^2\left[\left(\frac{\overline{u'^2}+\overline{v'^2}+2\overline{u'v'}}{w_2^2}\right)\left(1+2\frac{\overline{v}}{\overline{u}}\right)+O\left(\frac{\overline{u'^3}}{\overline{w}_2^3}\right)\right] \qquad \text{(A.3-26)}$$

(A.3-25) and (A.3-26) may be combined to eliminate $\overline{u'^2}$ and $\overline{v'^2}$ and give an equation for $\overline{u'v'}$. $\overline{u}$ and $\overline{v}$ can be determined from (A.3-24) and its counterpart for $\overline{E}_2$, provided that either the whole of the second square bracket in (A.3-24) is taken as unity (the usual assumption) or the $\overline{w'^2}$ neglected, though the latter assumption is less easy to justify in general circumstances than the former. To determine $\overline{v'^2}$ a fifth equation is required; this may be obtained in a similar way to (A.3-25) and (A.3-26) by deducing an expression for the rms value of either

$(E_1' + E_2')$ or $(E_1' - E_2')$. The result in the latter case is

$$\overline{(E_1'-E_2')^2} = \overline{E_1'^2}+\overline{E_2'^2}-2\left[A_1+B_1\left(\frac{\bar{u}-\bar{v}}{\sqrt{2}}\right)^{\frac{1}{2}}\right]^{\frac{1}{2}}\left[A_2+B_2\left(\frac{\bar{u}+\bar{v}}{\sqrt{2}}\right)^{\frac{1}{2}}\right]^{\frac{1}{2}} \times \frac{C_1C_2}{16}\left(\frac{\bar{u}}{w_1}\frac{\bar{u}}{w_2}\right)^2\left(\frac{\overline{u'^2}\,\overline{-v'^2}}{\bar{u}^2}\right) \qquad (A.3\text{-}27).$$

However, severe limitations have been placed on the generality of all the expressions which have been deduced, again because of the necessity to apply the binomial theorem to (A.3-23). The condition to be satisfied is

$$1 > [(2u'\bar{u}+u'^2)+(2v'\bar{v}+v'^2)-2(v'\bar{u}+u'\bar{v}+u'v')+2w'^2]/(\bar{u}-\bar{v})^2$$

i.e.

$$1 > [(u'^2+v'^2+2w'^2)-2u'v'+2(u'-v')\bar{u}-2(u'-v')\bar{v}]/(\bar{u}-\bar{v})^2$$

The upper limit on the turbulence intensities for which this is satisfied is less easy to specify than was the case with (A.3-15). However, since u' and v' must generally be of opposite sign, when u' is positive all the terms in the last condition-equation are positive and additive, except for the last one which contains $\bar{v}$ and is ~~thus~~ likely to be of lower order than the rest in any case. Thus the likelihood is that the upper limit on the turbulence intensities for which the derivation of the

above equations is valid is again of the order of 30%.

New method of analysis

A procedure similar to that outlined in section (A.3.3) above leads to expressions for $\overline{u_{N_1}^2}$ and $\overline{u_{N_2}^2}$ in terms of $\overline{E}_1$, $\overline{E}_2$, $\overline{E_1'^2}$ and $\overline{E_2'^2}$. As before $u_{N_1}^2$ and $u_{N_2}^2$ are related to $\overline{u}$, $\overline{u'^2}$ etc. by (A.3-21) and (A.3-22),

i.e. $$\overline{u_{N_1}^2} = \tfrac{1}{2}(\overline{u}^2+\overline{u'^2}+\overline{v}^2+\overline{v'^2}-2\overline{u}\,\overline{v}-2\overline{u'v'}+\overline{w'^2}) \qquad \text{(A.3-28)}$$

and $$\overline{u_{N_2}^2} = \tfrac{1}{2}(\overline{u}^2+\overline{u'^2}+\overline{v}^2+\overline{v'^2}+2\overline{u}\,\overline{v}+2\overline{u'v'}+\overline{w'^2}) \qquad \text{(A.3-29).}$$

From these two equations it is seen that

$$\overline{u_{N_1}^2} - \overline{u_{N_2}^2} = -2\overline{u}\,\overline{v} - 2\overline{u'v'} \qquad \text{(A.3-30)}$$

and $$\overline{u_{N_1}^2} - \overline{u_{N_2}^2} = \overline{u}^2+\overline{u'^2}+\overline{v}^2+\overline{v'^2}+2\overline{w'^2} \qquad \text{(A.3-31).}$$

When the turbulence intensities are small compared with $\overline{v}^2$, as may be the case near the edge of a near-separting boundary layer, (A.3-28) and (A.3-29) can be used to obtain $\overline{u}$ and $\overline{v}$ separately. When $\overline{u'^2}$, $\overline{v}^2$, etc. are of the same order, but small compared with $\overline{u}^2$, it is possible to calculate $\overline{u}$ from (A.3-31). Also, when $\overline{u}\,\overline{v}$ is small compared with $\overline{u'v'}$, (A.3-30) can be used to calculate $\overline{u'v'}$.

Unfortunately it is not the case, even for boundary layers, that $\overline{u}\,\overline{v}$ is small compared with $\overline{u'v'}$. Consequently the application of (A.3-30) to the present writer's results led to values of $-\overline{u}\,\overline{v} - \overline{u'v'}$ which were negative over much of the boundary layer. Although the new analysis gives the same results as the conventional one for low-intensity turbulence, in general it is impossible to separate $\overline{u}\,\overline{v}$ from $\overline{u'v'}$. And the same is true of $\overline{v'^2}$ and $\overline{v}^2$.

Similar analyses to the above can be carried out for crossed wires, in the x-z plane, which are used in the measurement of $\overline{w'^2}$. The analyses are subject to similar limitations to those for wires in the x-y plane.

A.3.5 Concluding remarks

1. The conventional method of analysis loses its validity for values of $\tilde{u}'/\overline{u}$ greater than about 0.3 (30% turbulence). The reason is that the conditions which permit the use of the binomial theorem in the derivation of the analysis are then violated.

2. The new analysis essentially results in a linearisation of the output from the anemometer. This analytic linearisation has a twofold advantage over electronic linearisation: first of all it permits a direct comparison to the made between the results of linearised and unlinearised operation, and secondly it is infinitely cheaper than the electronic method which is very expensive.

3. For intensities up to 20% the new and conventional analyses give results within 1% of each other. For higher intensities the conventional analysis gives values of $\widetilde{u'}/\overline{u}$ considerably in excess of those given by the new method (about 50% higher for $\widetilde{u'}/\overline{u} = 0.9$).

4. The use of a sinusoidal, rather than square, waveform for E' makes no significant difference to the results given by the new method. Consequently it is concluded that, if it were possible to use the true $E'\{t\}$ variation, the results would be little different from those given by the square wave.

5. For turbulence intensities greater than about 20% there seems to be no way at present of measuring the turbulent shear stress. The conventional analysis ceases to be valid, and the new one cannot be used to separate $\overline{u}\,\overline{v}$ from $\overline{u'v'}$.

6. Whether the electrical signals obtained from an anemometer correspond to the true magnitude of u, when u' (instantaneously) exceeds $\overline{u}$, depends upon the distance over which the flow reversal occurs. This distance is likely to be small compared with any characteristic probe dimension, so it is probable that the signals do correspond to $|u|$.

Escudier, M.P., Ph.D

The entrainment function in turbulent boundary-layer and wall-jet calculations

By M. P. ESCUDIER AND W. B. NICOLL

J. Fluid Mech. (1966), *vol.* 25, *part* 2, *pp.* 337–366
Printed in Great Britain

The entrainment function in turbulent boundary-layer and wall-jet calculations

By M. P. ESCUDIER AND W. B. NICOLL

Imperial College of Science and Technology, Department of Mechanical Engineering, Exhibition Road, London, S.W. 7

(Received 30 September 1965)

Some of the proposals made by Spalding (1964*a*) in his 'Unified theory of friction, heat transfer, and mass transfer' are examined. The two-component velocity-profile family proposed by Spalding is compared with measured boundary-layer and wall-jet velocity profiles and is shown to be adequate for flows with moderate wake components. The drag law implicit in the velocity-profile family is shown to be in good agreement with experimental data.

Recommendations are provided for entrainment functions for both boundary layers and wall jets.

Predictions of boundary-layer and wall-jet development, based on the recommended entrainment functions, are presented and compared with experiment. The predictions are in good agreement with experiment except in the vicinity of separation.

1. Introduction

1.1. *Spalding's unified theory*

A general theoretical framework has been developed by Spalding (1964*a*) for the prediction of friction, heat transfer and mass transfer in turbulent boundary layers and wall jets. The calculation of the development of the hydrodynamic boundary layer† is based upon the ordinary differential equations for the integral conservation of mass and momentum and employs two auxiliary functions. These are:

(i) A two-parameter velocity profile having two components; one accounting for the effects of mass and momentum transfer to the wall, and the other for interactions with the mainstream.

(ii) A function which relates the rate of mass-entrainment by the boundary layer from the mainstream to the profile and flow parameters.

The utility of the theory depends upon the range of flows for which adequate auxiliary functions can be determined.

1.2. *Object of the present paper*

The present work has three main tasks. These are:

(i) To compare with experimental profiles the velocity profile proposed by Spalding (1964*a*).

† Unless otherwise stated, the term 'boundary layer' may be taken to include wall-jet flows.

(ii) To present the results of a survey of the experimental data which have been analysed for information about entrainment and to recommend entrainment functions for boundary layers and wall jets.

(iii) To compare with experiment the predictions of the 'unified theory', using the entrainment functions determined in (ii) above.

1.3. *Restrictions*

The restrictions to which the flows considered in the the present paper are subject are: (i) uniform fluid properties; (ii) hydrodynamically smooth wall; (iii) impermeable wall; (iv) two-dimensional flow.

2. Mathematical theory

The object of this section is to derive the equations used for the prediction of boundary-layer development and to illustrate the role of the velocity-profile and entrainment assumptions in the theoretical structure of the 'unified theory'.

The first of the two differential equations to be used is that expressing the integral conservation of mass in the boundary layer. This may be written as

$$\frac{d}{dx}\left(\int_0^{y_G}\rho u\,dy\right) = -\rho v_G + \rho u_G \frac{dy_G}{dx}, \tag{2.1}$$

where v_G is the velocity at the outer edge of the boundary layer normal to the surface, and y_G is the boundary-layer thickness. The right-hand side of equation (2.1) represents the total rate of entrainment of mass from the mainstream into the boundary layer. Equation (2.1) can be re-written

$$\frac{d}{dx}\left(\int_0^{y_G}\rho u\,dy\right) = -\dot{m}''_G, \tag{2.2}$$

where the entrainment rate $-\dot{m}''_G$ is defined as

$$-\dot{m}''_G \equiv -\rho v_G + \rho u_G\, dy_G/dx. \tag{2.3}$$

The other differential equation used is the von Kármán momentum integral equation,

$$\frac{d\delta_2}{dx} + (2+H)\frac{\delta_2}{u_G}\frac{du_G}{dx} = \tfrac{1}{2}c_f, \tag{2.4}$$

where δ_2 is the momentum thickness of the boundary layer, H the ratio of the displacement thickness δ_1 to the momentum thickness and $\frac{1}{2}c_f$ the local drag coefficient, defined by

$$\tfrac{1}{2}c_f \equiv \tau/(\rho u_G^2), \tag{2.5}$$

where τ is the local shear stress at the wall.

We follow Spalding (1964*a*) in defining the following non-dimensional quantities:

$$\mathrm{R}_m \equiv \int_0^{y_G}\frac{u}{\nu}dy, \qquad \mathrm{R}_x \equiv \int_0^{x}\frac{u_G}{\nu}dx, \tag{2.6), (2.7}$$

$$\mathrm{R}_2 \equiv u_G\delta_2/\nu, \qquad s \equiv \tfrac{1}{2}c_f, \tag{2.8), (2.9}$$

and

$$-m_G \equiv -\dot{m}''_G/(\rho u_G). \tag{2.10}$$

Equation (2.2) may then be re-written as

$$d\mathrm{R}_m/d\mathrm{R}_x = -m_G, \tag{2.11}$$

and equation (2.4) as

$$\frac{d\mathrm{R}_2}{d\mathrm{R}_x} + (1+H)\,\mathrm{R}_2 \frac{d(\ln u_G)}{d\mathrm{R}_x} = s. \tag{2.12}$$

Equations (2.11) and (2.12) would constitute a soluble set if all the quantities except R_x could be expressed as functions of any two (independent) dependent variables, either explicitly or implicitly through auxiliary relationships. We again follow Spalding in obtaining the required relationships through velocity-profile and entrainment assumptions.

The velocity profile is assumed to be a member of the two-parameter family

$$z = s^{\frac{1}{2}} f\{y^+\} + (1-z_E)\, g\{\xi\}, \tag{2.13}$$

where $z \equiv u/u_G$, $\xi \equiv y/y_G$ and $y^+ \equiv \sqrt{(\tau/\rho)}\, y/\nu$. The quantity z_E is a profile parameter and f and g are universal functions. The physical basis for this assumption and specific forms for f and g will be discussed in § 3. The boundary condition $\xi = 1 : z = 1$, together with the fact that $g\{\xi\}$ is so normalized that $g\{1\} = 1$, yields the local drag law

$$s^{\frac{1}{2}} = z_E/f\{y_G^+\} = z_E/f_G. \tag{2.14}$$

For a wall jet, where $z_E > 1$, the momentum-thickness Reynolds number R_2 passes through zero and the shape factor H through infinity. For the purposes of the numerical integration of equations (2.11) and (2.12), therefore, it is convenient to eliminate R_2 and H. To do this the quantities I_1 and I_2 are introduced, defined by

$$I_1 \equiv \int_0^1 z\, d\xi, \tag{2·15}$$

and

$$I_2 \equiv \int_0^1 z^2\, d\xi. \tag{2·16}$$

Then we have

$$\mathrm{R}_m = \mathrm{R}_2\left(1 - \frac{I_1}{I_2}\right), \qquad H = \frac{1-I_1}{I_1 - I_2}, \tag{2.17), (2.18}$$

and equation (2.12) may be written

$$\mathrm{R}_m \frac{d}{d\mathrm{R}_x}\left(\frac{I_2}{I_1}\right) = \left(\frac{1-I_2}{I_1}\right) \mathrm{R}_m \frac{d(\ln u_G)}{d\mathrm{R}_x} - s + \left(\frac{I_1 - I_2}{I_1}\right)(-m_G). \tag{2.19}$$

We can expand $d(I_2/I_1)/d\mathrm{R}_x$ as

$$\frac{d}{d\mathrm{R}_x}\left(\frac{I_2}{I_1}\right) = \frac{1}{I_1}\left(\frac{\partial I_2}{\partial z_E}\frac{dz_E}{d\mathrm{R}_x} + \frac{\partial I_2}{\partial f_G}\frac{df_G}{d\mathrm{R}_x}\right) - \frac{I_2}{I_1^2}\left(\frac{\partial I_1}{\partial z_E}\frac{dz_E}{d\mathrm{R}_x} + \frac{\partial I_2}{\partial f_G}\frac{df_G}{d\mathrm{R}_x}\right). \tag{2.20}$$

However, the quantity f_G which appears in the drag law and, through the drag law, in the expressions for I_1 and I_2 is found to be slowly varying, so the terms in equation (2.20) containing $df_G/d\mathrm{R}_x$ can be neglected. Equation (2.19) thus becomes, after some re-arrangement,

$$\mathrm{R}_m \frac{dz_E}{d\mathrm{R}_x} = \frac{(1-I_2)\,\mathrm{R}_m\, d(\ln u_G)/d\mathrm{R}_x - I_1 s + (I_1 - I_2)(-m_G)}{(\partial I_2/\partial z_E - I_2/I_1\, \partial I_1/\partial z_E)_{f_G}}. \tag{2.21}$$

With the exception of $-m_G$, all the quantities appearing in equations (2.11) and (2.21) may be related to the main dependent variables R_m and z_E. Thus, once the entrainment function $-m_G$ has been determined, the development of hydrodynamic boundary layers may be predicted, all that is required being the solution of two simultaneous, non-linear, ordinary differential equations.

3. Velocity profile

3.1. *Previous recommendations*

Coles (1956), after an extensive review of low-speed boundary-layer data, proposed the velocity profile

$$u^+ = f\{y^+\} + \frac{2\Pi}{\kappa} g\{\xi\}, \tag{3.1.1}$$

where both $f\{y^+\}$ and $g\{\xi\}$ are functions supposed common to all two-dimensional turbulent boundary layers, Π is a profile parameter and κ a constant. The function $f\{y^+\}$ is termed 'the law of the wall' and, following Coles, $g\{\xi\}$ 'the law of the wake'.

Experiment shows that the law of the wall has the form

$$f\{y^+\} = \frac{1}{\kappa} \ln (Ey^+), \tag{3.1.2}$$

where κ and E are constants. Coles (1956) recommended the values

$$\kappa = 0{\cdot}40, \quad E = 7{\cdot}691;$$

and later (1962)

$$\kappa = 0{\cdot}41, \quad E = 7{\cdot}768.$$

Chi (1962) found that boundary-layer drag data indicate

$$\kappa = 0{\cdot}40, \quad E = 12.$$

Other authors (e.g. Clauser 1954; Spalding 1964*a*, 1965; etc.) have recommended various other values for κ and E. The present authors have followed Spalding (1964*a*) in using

$$\kappa = 0{\cdot}40, \quad E = 6{\cdot}542.$$

Coles (1956) expressed his recommendation for the law of the wake in tabular form and, as was noted by Hinze (1959), this differs only slightly from

$$g\{\xi\} = \tfrac{1}{2}(1 - \cos \pi\xi). \tag{3.1.3}$$

Equation (3.1.3) is compared with Coles' $g\{\xi\}$ relation in figure 1.

Spalding (1964*a*, 1965) used a slightly different profile parameter from Coles' Π and wrote equation (3.1.1) as

$$u^+ = \frac{1}{\kappa} \ln (Ey^+) + (1 - z_E)\, \tfrac{1}{2}(1 - \cos \pi\xi)\, u_G^+, \tag{3.1.4}$$

where the specific forms mentioned above have been utilized for the wall and wake components. The profile parameter z_E can be interpreted physically as the ratio of the law-of-the-wall velocity at the outer edge of the boundary layer to the mainstream velocity. The quantity $(1 - z_E)$ is a measure of the relative magnitude

of the wake-component of the velocity profile. Typical wall and wake components and total velocity profiles are shown in figure 2 for $z_E < 1$ and $z_E > 1$.

Coles (1956), in his determination of the law of the wake, examined only 'conventional' boundary-layer profiles where $z_E < 1$, whereas Spalding (1964*a*) assumed that the same $g\{\xi\}$ function could be used for all boundary layers with $z_E > 0$, including wall-jet flows where $z_E > 1$. One of the aims of the present work

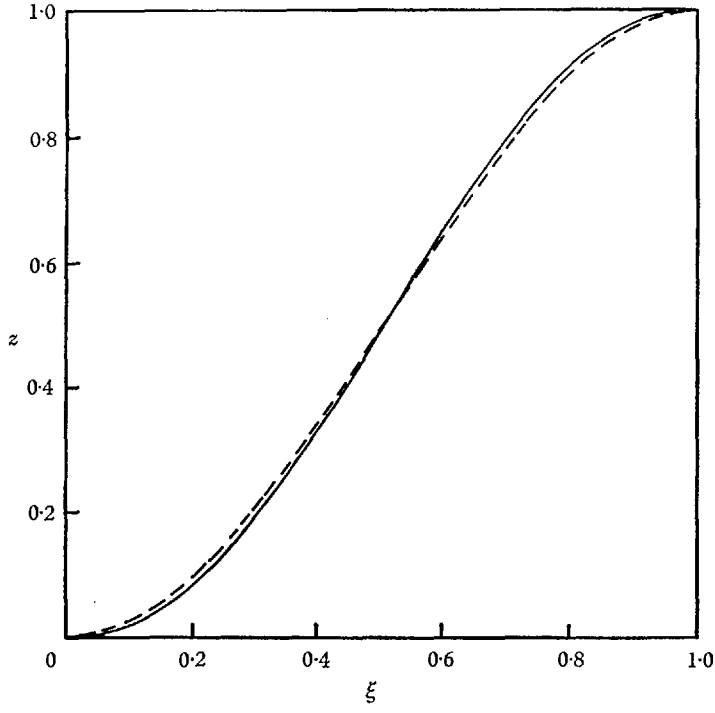


FIGURE 1. Comparison of $z = \frac{1}{2}(1-\cos \pi\xi)$ with Coles's law of the wake. ——, Coles's law of the wake; — — —, $z = \frac{1}{2}(1-\cos \pi\xi)$.

is to examine velocity profiles covering the whole range of z_E values to see if Spalding's assumption is justifiable. Coles himself noted that it was not possible to find satisfactory values for the parameters Π, u_τ ($\equiv \sqrt{(\tau/\rho)}$) and y_G such that equation (3.1.1) would fit a profile, measured by Klebanoff & Diehl (1952), downstream of a point of reattachment. Coles also remarked that experiments performed by Wieghardt (1944) indicated that there is a definite change in the shape, as well as in the amplitude, of the wake component in flow at constant pressure when the level of free-stream turbulence is varied.

3.2. *Drag law*

As shown in § 2, equation (3.1.1) implies a drag law. If we use the form for $f\{y^+\}$ given in equation (3.1.2), the drag law, equation (2.14), becomes

$$s = (\kappa z_E/l)^2, \tag{3.2.1}$$

where

$$l \equiv \ln(Ey_G^+) = \ln(E\mathrm{R}_G s^{\frac{1}{2}}). \tag{3.2.2}$$

It is worth pointing out, perhaps, that the drag law represented by equation (3.2.1) is independent of the specific form of the wake profile assumed.

The drag law deduced from the velocity profile adopted here is compared, in figure 3, with the proposal of Ludwieg & Tillmann (1949) that

$$s = 0{\cdot}123 \times 10^{-0{\cdot}678H} \mathrm{R}_2^{-0{\cdot}268}. \tag{3.2.3}$$

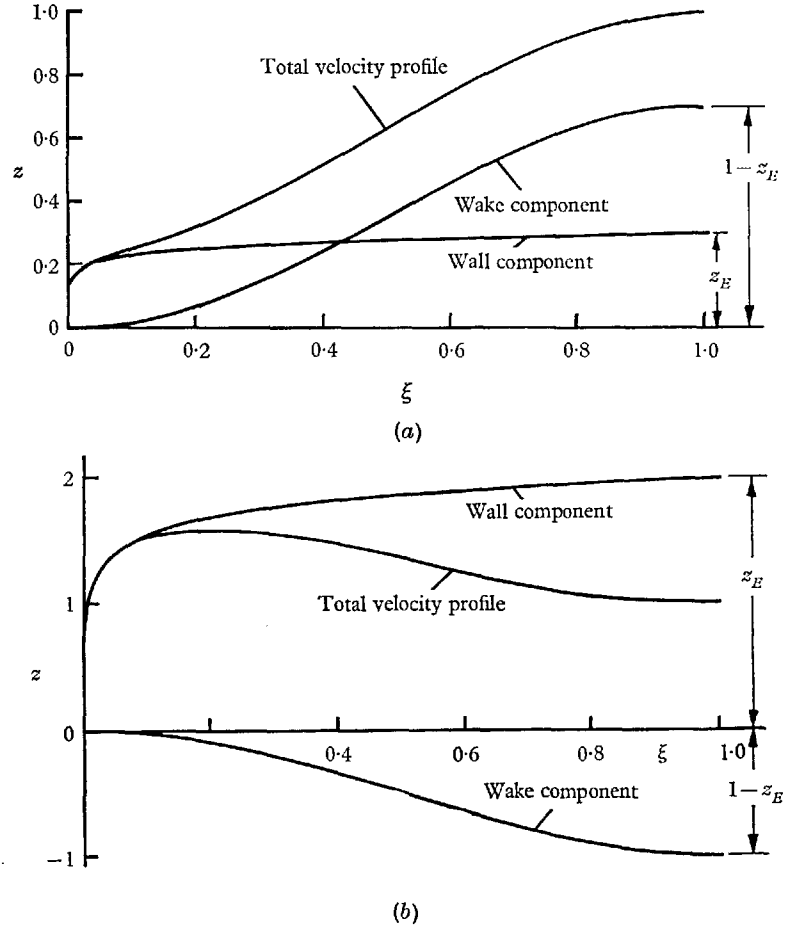


FIGURE 2. Typical velocity profiles according to equation (3.2.4).
(*a*) Boundary-layer profile, $z_E < 1$. (*b*) Wall-jet profile, $z_E > 1$.

The present law clearly yields values for s which are lower than those given by equation (3.2.3); in this connexion it is worth mentioning that Newman (1951) showed the Ludwieg–Tillmann law to overestimate drag, particularly when H is large.

The present drag law is compared directly with experimental data in figure 4. There is considerable scatter, and it is seen that in many cases the wall shear stress is underestimated. Nevertheless, equation (3.2.1) is an improvement on the Ludwieg–Tillmann law for large H values and is the only available drag law which has been recommended for both wall jets and boundary layers. It will be retained, therefore, until a better law becomes available.

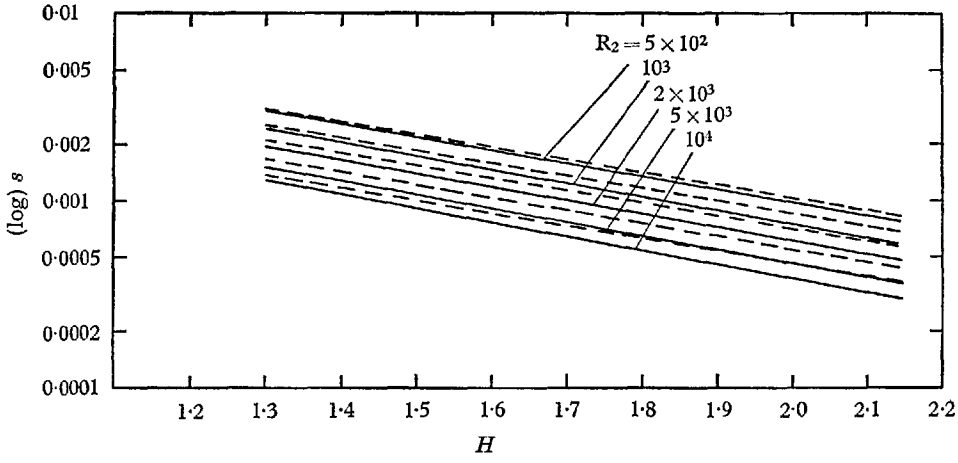


FIGURE 3. Comparison of drag law of Ludwieg & Tillmann (1949) with that derived from the velocity-profile equation (3.2.4). — — —, Ludwieg & Tillmann.

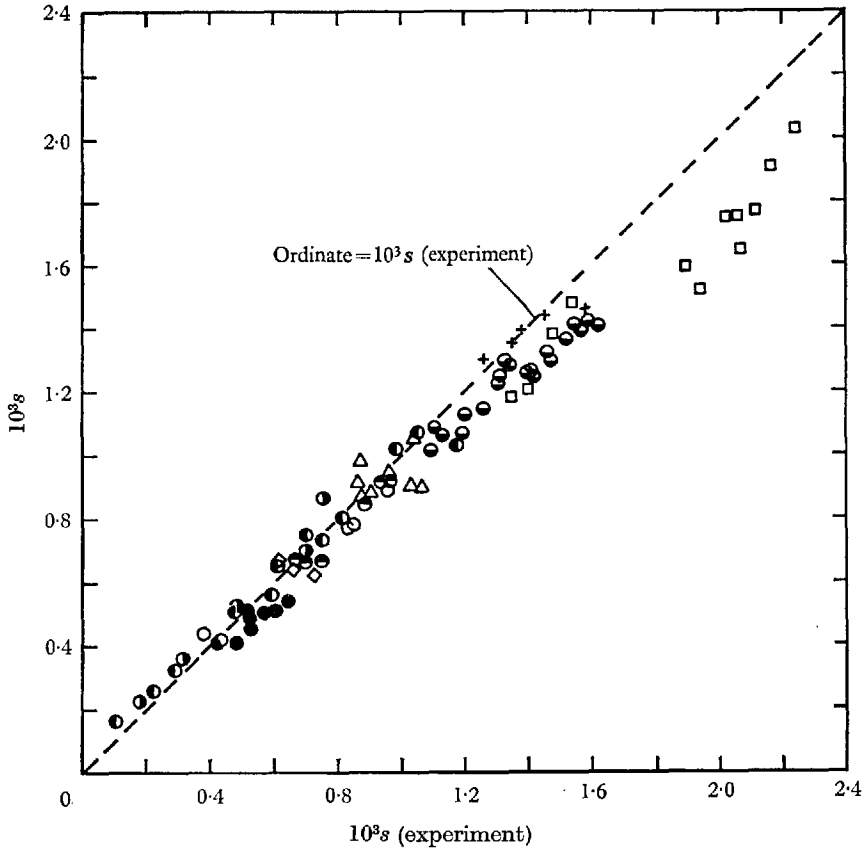


FIGURE 4. Drag coefficients computed from R_2 and H using present drag law compared with experimental data. ◒, Smith & Walker; +, Schultz-Grunow; ◓, recovering layer, ◇, equilibrium layer, Bradshaw & Ferriss; □, Fage & Falkner and Fage; ◐, Schubauer & Klebanoff; ◑, Newman; △, run 1, ●, run 2, Clauser.

Substitution of equation (3.2.1) into the definitions of u^+ and y^+ and substitution of the latter into equation (3.1.4) yields a form of the velocity profile more convenient for later work, it is

$$z = z_E[1 + (\ln \xi/l)] + (1 - z_E)\tfrac{1}{2}(1 - \cos \pi\xi). \tag{3.2.4}$$

3.3. *Comparison with experiment*

Values of the profile parameters have been determined for a number of experimental velocity profiles by the method of least-squares fitting. This procedure gives the values of z_E and y_G which minimize the square deviation R, defined by

$$R \equiv \sum_i [z\{y_i\} - z_i]^2,$$

z_i being the experimental velocity ratio at y_i, and $z\{y_i\}$ the value given by equation (3.2.4) at y_i. The measured and fitted profiles are shown in figures 5–11.

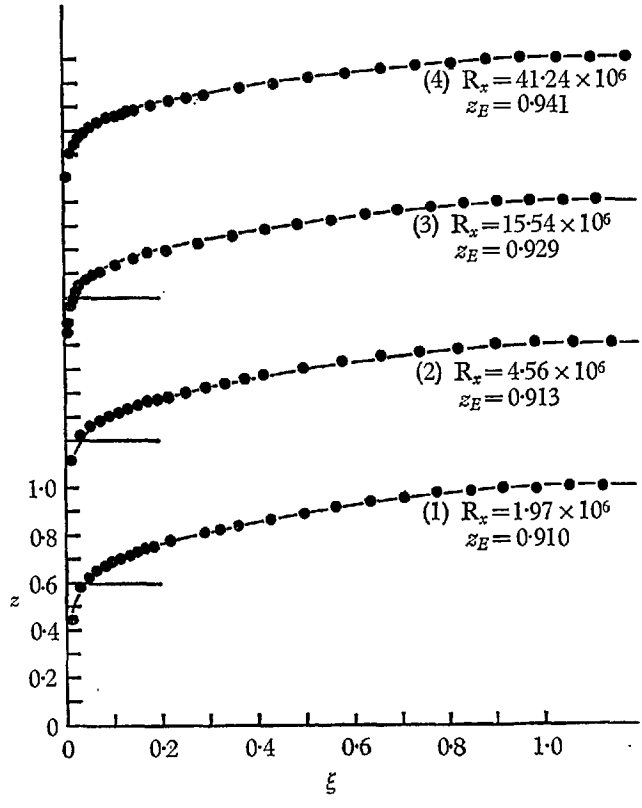


FIGURE 5. Comparison of equation (3.2.4) with experimental velocity profiles Smith & Walker (1959) for flat-plate boundary layers.

In figure 5, four profiles measured by Smith & Walker (1959) in boundary layers developing along a smooth, flat plate under zero pressure gradient are shown. The fitted profiles are evidently fairly good representations of the measured ones, although there is evidence of a small, but systematic, deviation from the fitted profile in the region of $\xi = 0{\cdot}3$. Values of the shape factor H

calculated from the fitted profiles differ by up to 4% from the reported experimental values.

Similar remarks to those in the preceding paragraph can be made about the profiles of Bradshaw & Ferriss (1965) shown in figure 6. These data were obtained for a boundary layer recovering from the effects of an adverse pressure gradient—hence the relatively large wake-component at $x = 47$ in., where $z_E \approx 0{\cdot}67$.

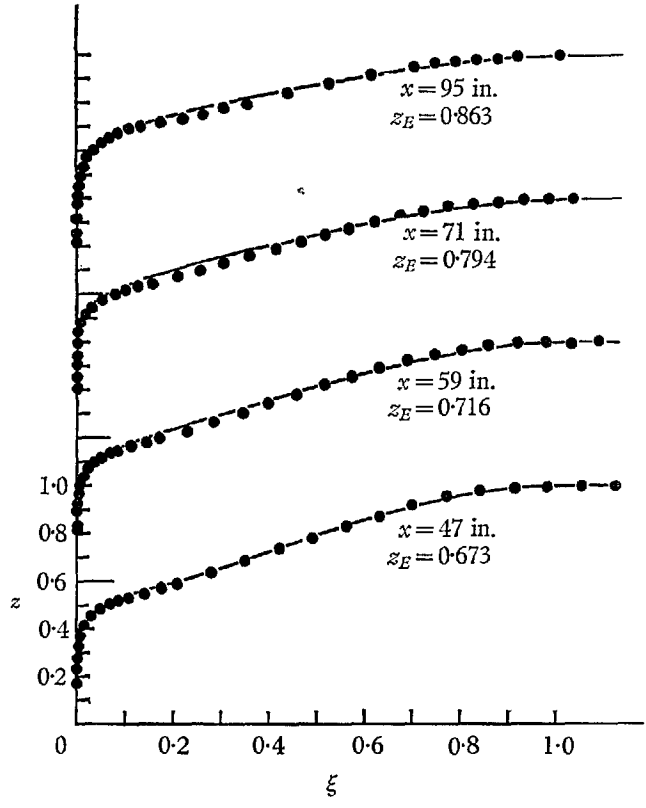


FIGURE 6. Comparison of equation (3.2.4) with experimental velocity profiles of Bradshaw & Ferriss (1965) for a boundary layer recovering from the effects of an adverse pressure gradient.

A purely cursory examination would indicate that equation (3.2.4) is a poorer fit to these data than to those of Smith & Walker, yet in this case the maximum difference between the reported experimental and computed values of H is less than 3%. Clearly, careful thought must be given to deciding what constitutes 'a good fit'.

The profiles of Schubauer & Klebanoff (1951), shown in figure 7, were obtained for a boundary layer subjected to an adverse pressure gradient which eventually caused the layer to separate (a little beyond $x = 25$ ft.) Here again the profiles *appear* to be reasonably well-fitted by equation (3.2.4), although for the two downstream profiles shown, the theoretical profile is inadequate near the wall. The profile at $x = 25$ ft. has a large wake-component, the value of z_E being about

0·29, and in this case the shape factor calculated from the fitted profile is about 2·38, compared with the reported experimental value of 1·99.

The final set of velocity profiles for $z_E < 1$ are those of Stratford (1959), obtained for a boundary layer reported as having zero wall shear. In this case $z_E = 0$ and equation (3.2.4) reduces to the pure wake form

$$z = \tfrac{1}{2}(1 - \cos \pi \xi).$$

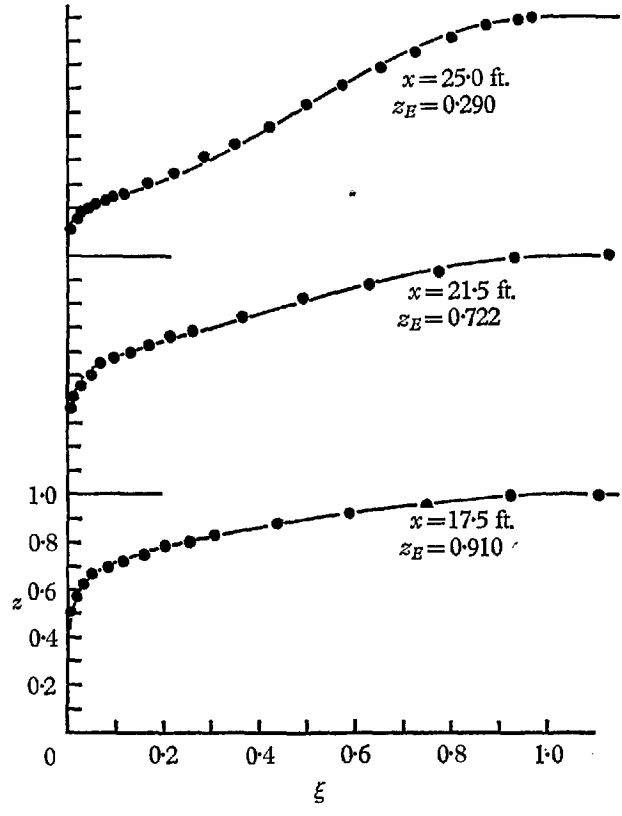


FIGURE 7. Comparison of equation (3.2.4) with experimental velocity profiles of Schubauer & Klebanoff (1951) for a boundary layer with an adverse pressure gradient.

It is seen, in figure 8, that this expression is a very poor representation of Stratford's data. Also, for $z_E = 0$, our profile gives the unique result $H = 4$, whereas Stratford's experiments gave values for H which varied from about 1·8 to 2·6.

All the cases considered above related to boundary layers with $1 > z_E \geqslant 0$. The remaining profiles, shown in figures 9–11, were obtained for boundary layers where $z_E > 1$, that is, for wall-jet flows. In all these cases the assumed profile deviates from the measured one in the same way, being too low near the edge of the layer and near the wall, and too high in the middle of the layer. The deviations are seen to increase in magnitude as z_E increases, that is, as the wake component becomes dominant. Also, the assumed profile gives roughly the correct value for the velocity maximum, but this always occurs further from the wall than the measured maximum.

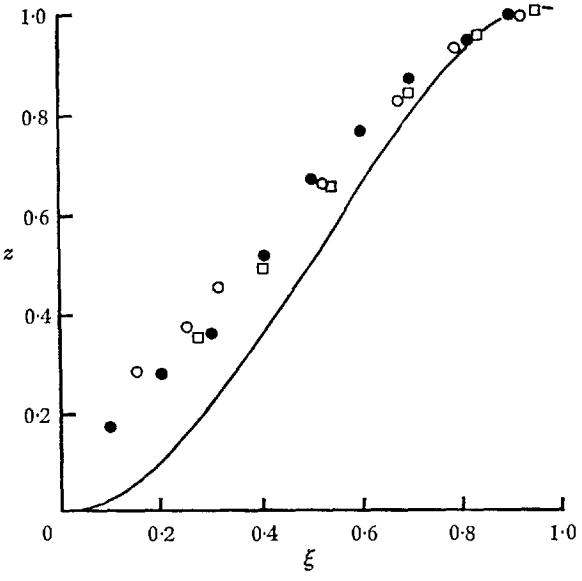


FIGURE 8. Comparison of $z = \frac{1}{2}(1-\cos\pi\xi)$ with experimental velocity profiles of Stratford (1959) for boundary layers with zero wall-shear stress.

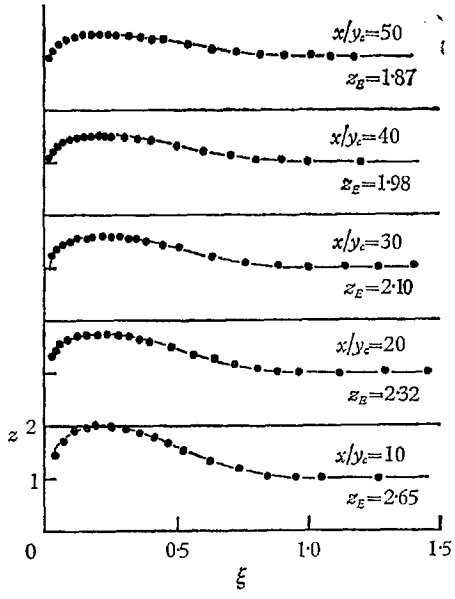


FIGURE 9. Comparison of equation (3.2.4) with experimental wall-jet velocity profiles of Nicoll (1965).

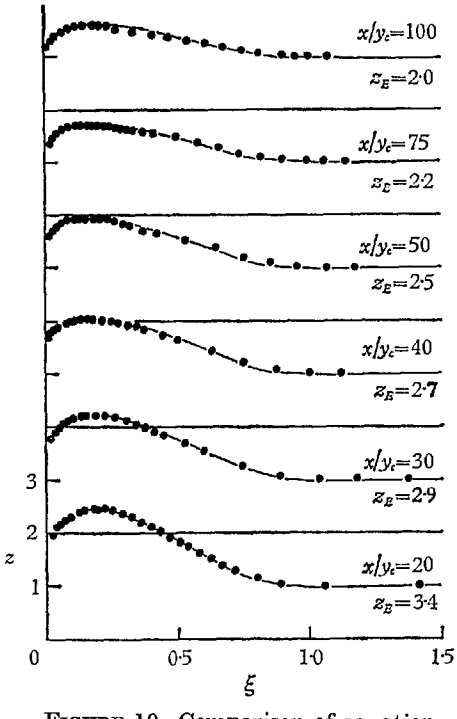


FIGURE 10. Comparison of equation (3.2.4) with experimental wall-jet velocity profiles of Nicoll (1965).

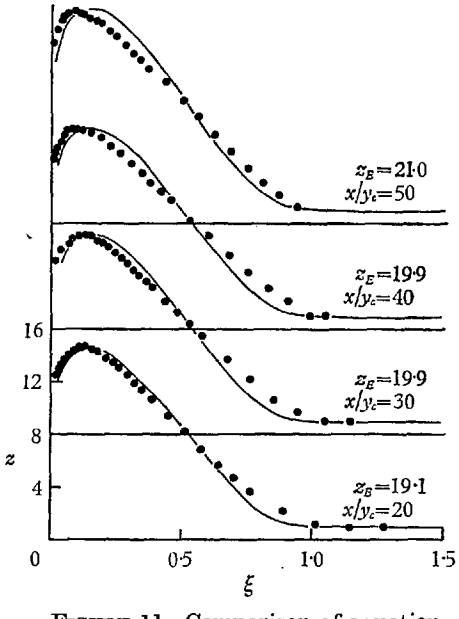


FIGURE 11. Comparison of equation (3.2.4) with experimental wall-jet velocity profiles of Nicoll (1965).

Clearly, for both $z_E > 1$ and $z_E < 1$ there is a need for improvement in the assumed velocity profile. The most obvious deficiency is probably the absence of a term to account for the effects of pressure gradient; current work is aimed at remedying this. For the time being, however, equation (3.2.4) will be retained as the velocity-profile assumption.

4. Entrainment function

4.1. *Review of previous recommendations*

The idea of using an entrainment function as the auxiliary equation in turbulent-boundary-layer calculations came from Head (1960). Head's entrainment function may be written, formally, as

$$-m_G = -m_G\{H_1\}, \tag{4.1.1}$$

where H_1 is a shape factor of the velocity profile, defined by

$$H_1 \equiv (y_G - \delta_1)/\delta_2 \tag{4.1.2}$$

(in terms of I_1 and I_2, $H_1 = I_1/(I_1 - I_2)$). Head made no recommendation for a velocity-profile family and therefore required, in addition to his entrainment function, a relation between the shape factors H and H_1 and also a drag law. The $H \sim H_1$ relation was deduced from experimental data, and the drag law assumed was that proposed by Ludwieg & Tillmann (1949). Head carried out calculations on a number of boundary layers and, in spite of his entrainment law being based upon only two sets of experimental data, those of Newman (1951) and Schubauer & Klebanoff (1951), obtained fairly satisfactory agreement with experiment. In all the cases considered, Head used the measured values of δ_2 in his calculations of H instead of calculating simultaneously δ_2 and H. Only in the case of the experiment of Newman was there poor agreement between the predicted and measured H values. This comparison was improved when δ_2 and H were simultaneously predicted.

Head's entrainment law is shown in figure 12.

The only other author to make recommendations for the entrainment function is Spalding (1964*a*, *b*, 1965). Spalding's first proposal (1964*a*) was

$$\left.\begin{aligned} z_E \leqslant 1: \quad & -m_G = 0{\cdot}1023(1-z_E)\,(1+\tfrac{1}{3}z_E), \\ z_E > 1: \quad & -m_G = 0{\cdot}09(z_E-1)\,(1+\tfrac{1}{3}z_E)/(1+z_E). \end{aligned}\right\} \tag{4.1.3}$$

The basic form for these relations was arrived at by consideration of information relating to free mixing layers. The constants were determined from analyses of the equilibrium flat-plate boundary layer and of the spread and velocity-decay information available for wall jets.

In an annotated version of the paper cited above, Spalding (1964*b*) noted that equations (4.1.3) considerably over-estimate entrainment rates and remarked that these relations were over-elaborate. The following, simpler, relations were then proposed

$$\left.\begin{aligned} z_E \leqslant 1: \quad & -m_G = 0{\cdot}06(1-z_E), \\ z_E > 1: \quad & -m_G = 0{\cdot}03(z_E-1). \end{aligned}\right\} \tag{4.1.4}$$

The entrainment function was modified further in a more recent paper, Spalding (1965), to

$$\left.\begin{aligned} z_E \leqslant 1: \quad & -m_G = 0{\cdot}06 - 0{\cdot}05 z_E, \\ z_E > 1: \quad & -m_G = 0{\cdot}03 z_E - 0{\cdot}02. \end{aligned}\right\} \tag{4.1.5}$$

In figure 12 curves of $-m_G$ plotted against H_1, are drawn representing the proposals of Head (1960), of Spalding (1964*a*, *b*, 1965) and of the present authors, for the entrainment function for $z_E \leqslant 1$.

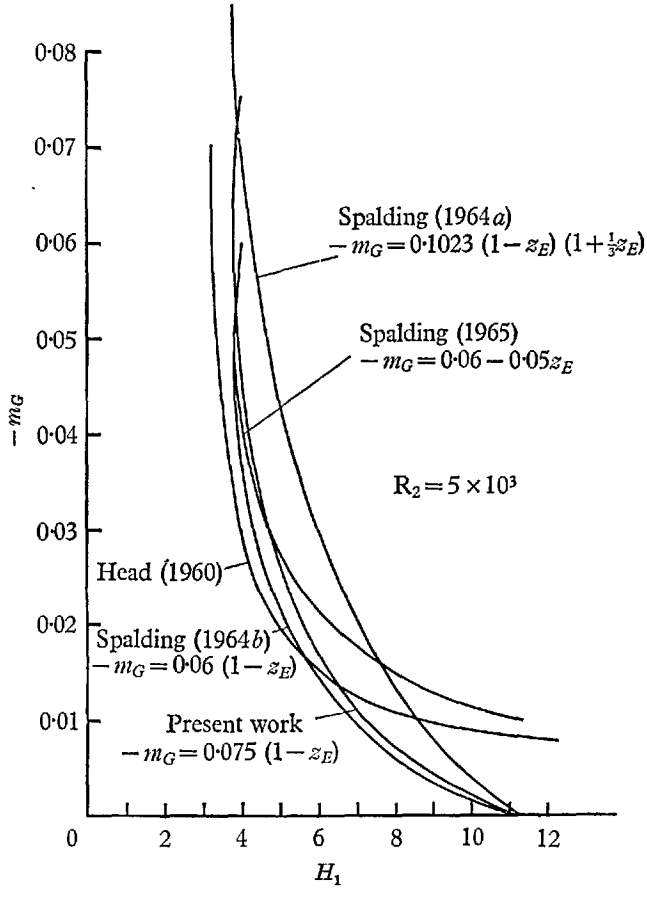


FIGURE 12. Comparison of various recommendations for the entrainment function for $z_E < 1$.

An entrainment law can be deduced from the hypothesis of Mellor & Gibson (1963) that the effective kinematic viscosity in the wake region of a boundary layer is equal to a constant times $u_G.\delta_1$ (the value of the constant was taken as 0·016). It is

$$z_E \leqslant 1: \quad -m_G \approx 0{\cdot}07(1-z_E). \tag{4.1.6}$$

This is not far different from Spalding's proposal, equation (4.1.4).

4.2. *Determination of entrainment rates from experimental data*

The basic information required in the determination of entrainment rates is the variation of R_m with R_x, the value of $-m_G$ being determined by differentiation of R_m with respect to R_x. To deduce R_m from experimental velocity-profile data, it is necessary first to know the boundary-layer thickness y_G and it is evidently desirable to use a consistent method for determining this somewhat arbitrarily-defined quantity. One such method is to adopt a velocity-profile family, such as that represented by equation (3.2.4), and to determine the values of the profile-parameters which give the best fit to the experimental profile. Alternatively, properties of experimental velocity profiles, such as R_2 and H, can be matched with those given by the adopted profile and the profile-parameters determined in this way. With only a few exceptions, the data for wall jets ($z_E > 1$) and boundary layers ($z_E < 1$) have been analysed by different methods. The reasons for this are outlined below and the procedures then described.

One of the authors (W.B.N.) has been concerned exclusively with boundary layers where $z_E > 1$, and the other with flows for which $z_E < 1$. In the latter case, all the data examined were extracted from the literature, whereas many of the wall-jet data were obtained (by W.B.N.) in the authors' own laboratory. Experimental data are almost invariably published in the form of small-scale graphs and the retrieval of complete velocity-profile data is usually extremely difficult and time consuming. For this reason it was felt that, so far as boundary layers with $z_E < 1$ were concerned, best use could be made of the time available by deducing the profile parameters from integral properties of the velocity profiles. For wall jets, of course, most of the experimental data were at hand and, in the main, actual profiles could be analysed.

Naturally, the methods of analysis are complementary and, if the theoretical profile is a good representation of measured profiles, only small differences should arise in the final results.

4.2.1. *Analysis generally used for boundary-layer data where $z_E < 1$*

The velocity-profile expression assumed was that represented by equation (3.2.4). This is a two-parameter profile, so the parameters z_E and y_G, and all quantities associated with velocity profiles, such as R_m, R_G, H, s, etc., can be deduced from any two independent properties of a measured profile, together with the appropriate fluid properties (ρ and μ) and the mainstream velocity u_G.

The two quantities most commonly reported by boundary-layer experimenters are the momentum thickness δ_2 and shape factor H. These were the quantities from which most of the information concerning boundary layers was deduced. A computer program was developed to perform the computations and data from over five hundred profiles were analysed.

4.2.2. *Analysis generally used for wall-jet data*

The velocity profile adopted was again that represented by equation (3.2.1) and the fitting procedure the least-squares method described in § 3.3.

4.2.3. *Analysis occasionally used for wall-jet data*

When the detailed information required for the least-squares-fitting procedure was not available, the profile parameters were determined from the reported experimental values of $z_{\max}$ and $y_{\frac{1}{2}}$, where $z_{\max}$ is defined as the ratio of the maximum velocity in the wall jet to the mainstream velocity, and $y_{\frac{1}{2}}$ is the value of y at which $z = z_{\frac{1}{2}} = \frac{1}{2}(z_{\max}+1)$.

It may be seen from figures 9 to 11 that the least-squares-fitting procedure results in values for $z_{\max}$ and $y_{\frac{1}{2}}$ which agree well with the experimental values.

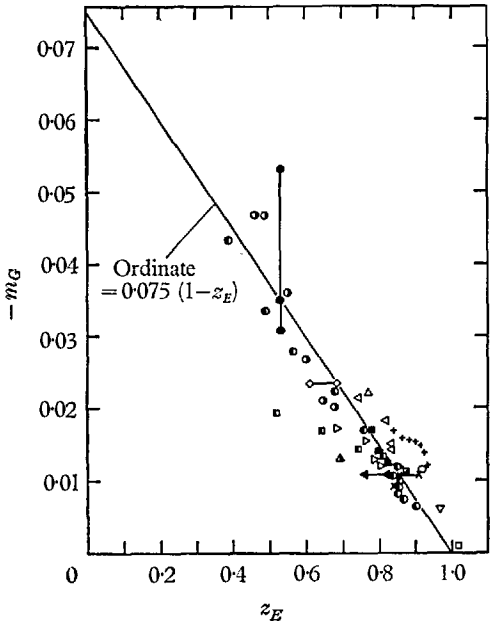


FIGURE 13

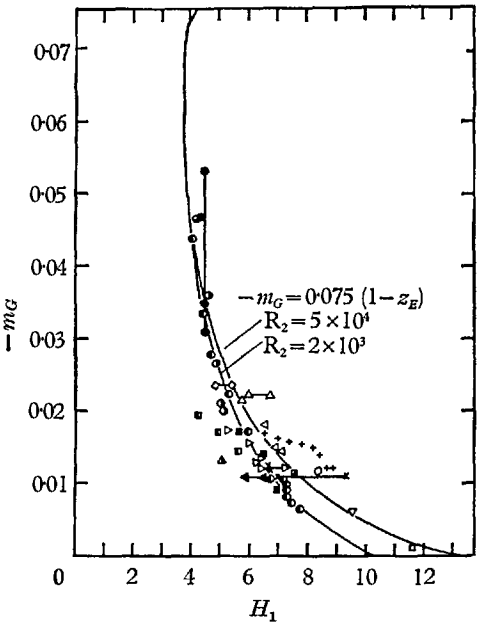


FIGURE 14

FIGURE 13. Entrainment rates deduced from experimental data for $z_E < 1$. ◪, Reynolds, Kays & Kline; ×, Smith & Walker; +, Schultz-Grunow, ○, Klebanoff; ◧ ◁ ◀ ◭ ■ ▷, Klebanoff & Diehl; △ run 1, ● run 2, Clauser; ◇, Bradshaw & Ferriss; ▽ □, Herring & Norbury; ◑, Newman; ◐, Schubauer & Klebanoff.

FIGURE 14. Entrainment rates deduced from experimental data for $z_E < 1$ plotted against Head's shape factor. Symbols as for figure 13.

4.3. *Discussion of entrainment data*

One of the attractive features of the entrainment function lies in the availability of data from which information about it can be obtained. A complete survey of velocity-profile data, of course, would be impossible, and in the present work a certain amount of selection has been necessary. An attempt has been made to include those data which are the most completely reported and, in the opinion of the present authors, the most reliable.

Entrainment rates deduced from all the data considered for boundary layers with $z_E < 1$ have been plotted against z_E and H_1 in figures 13 and 14 respectively.

Although the plot of $-m_G$ against z_E shows considerable scatter, the bulk of the data lends some support to an entrainment law of the form

$$-m_G = \text{const.}\,(1-z_E). \tag{4.3.1}$$

As was mentioned earlier, such a form was proposed by Spalding (1964*b*), the value for the constant being given as 0·06. The present investigation indicates 0·075 to be a better value, i.e.

$$-m_G = 0{\cdot}075(1-z_E). \tag{4.3.2}$$

This result is close to that deducible from the work of Mellor & Gibson (1963) (see § 4.1) and is the present authors' recommendation for $z_E < 1$.

Unfortunately, however, the data obtained for flat-plate boundary layers are irreconcilable with equation (4.3.2). The value of z_E appropriate to such boundary layers is about 0·92 and the corresponding value of $-m_G$, according to equation (4.3.2), is 0·006. The data of Klebanoff (1955), Reynolds, Kays & Kline (1958), Schultz-Grunow (1940) and Smith & Walker (1959) indicate $-m_G \approx 0{\cdot}011$, a value almost double that given above. The value of the constant in equation (4.3.1) would have to be 0·1375 to give $-m_G = 0{\cdot}011$ for $z_E = 0{\cdot}92$, and this would conflict with the data for $z_E < 0{\cdot}92$. This suggests that equation (4.3.1) may not be the best form for an entrainment function and perhaps indicates why Spalding (1965) was lead to propose the relation

$$-m_G = 0{\cdot}06 - 0{\cdot}05 z_E,$$

which gives $-m_G = 0{\cdot}014$ for $z_E = 0{\cdot}92$, a value more in keeping with the flat-plate data. Even so, this equation considerably overestimates entrainment rates for other boundary layers where $z_E \approx 0{\cdot}9$. It is not clear whether this apparent discrepancy in the data is due to scatter, which results from the difficulty of determining $-m_G$, or to the effect of some parameter, other than z_E, which influences the entrainment process.

The $-m_G \sim H_1$ plot in figure 14 shows that the assumption made by Head (1960), that $-m_G$ could be taken as a function of H_1 alone, was quite a reasonable one. Indeed the data so far examined show that the hypothesis of Spalding and of the present authors, that $-m_G = -m_G\{z_E\}$, is only a little better than Head's.

The entrainment data for $z_E > 1$ are shown in figure 15. As for $z_E < 1$, the data display considerable scatter, again probably due to the method of determination of $-m_G$ rather than to any real physical effect. This view is supported by the comparisons of predicted with experimental wall-jet development given in § 5.

The straight line shown in figure 15 represents the equation

$$-m_G = 0{\cdot}03 z_E - 0{\cdot}02, \tag{4.3.3}$$

and is the present authors' recommended entrainment relation for $z_E > 1$.

4.4. *Entrainment function for equilibrium flows*

For an equilibrium boundary layer, Spalding (1964*a*) intimated that the parameter z_E is nearly constant. For such flows, therefore, $dz_E/d\mathrm{R}_x$ can be regarded as negligible and equation (2.21) reduces to

$$(1-I_2)\,\mathrm{R}_m \frac{d(\ln u_G)}{d\mathrm{R}_x} - I_1 s + (I_1 - I_2)\,(-m_G) = 0. \tag{4.4.1}$$

We follow Clauser (1954, 1956) in defining a pressure-gradient parameter β:

$$\beta \equiv \frac{\delta_1}{\tau}\frac{dp}{dx} = -\frac{\mathrm{R}_1}{s}\frac{d(\ln u_G)}{d\mathrm{R}_x}, \tag{4.4.2}$$

which, as Clauser observed, should be constant for equilibrium flows. Equation (4.4.1) may then be re-arranged as

$$-m_G = H_1 s[1+\beta(1+1/H)], \tag{4.4.3}$$

where $H_1 \equiv (y_G-\delta_1)/\delta_2 = I_1/(I_1-I_2)$,

and $H \equiv \delta_1/\delta_2 = (1-I_1)/(I_1-I_2)$.

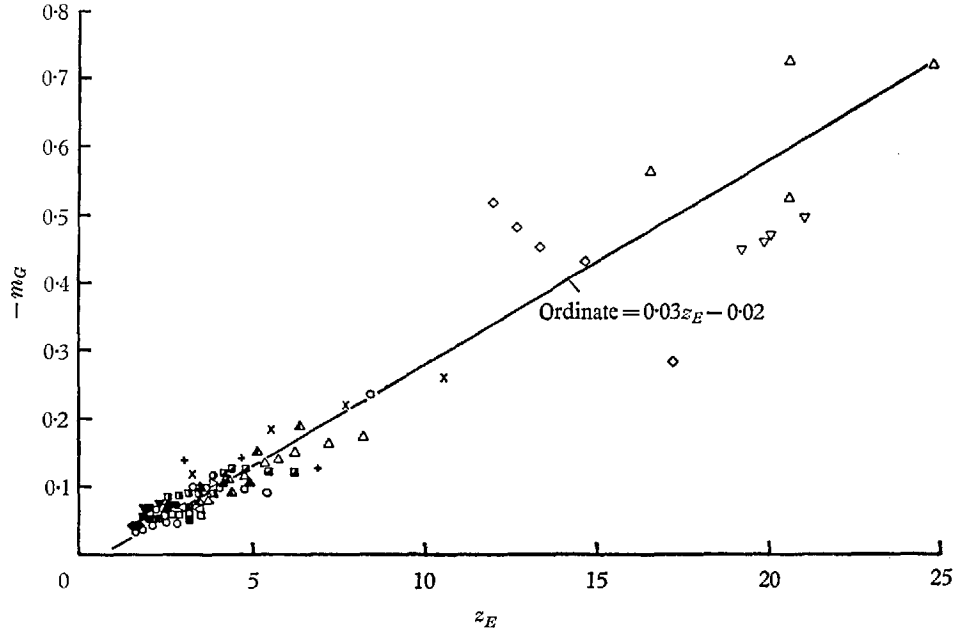


FIGURE 15. Entrainment rates deduced from experimental data for $z_E > 1$. ◁ ▲, Gartshore; ● ▲, Kruka & Eskinazi; ○ ◆ ■ ▼ □ △ ▽ ◇ ◪ ◧, Nicol; ▷ ◑, Patel & Newman; + ×, Seban & Back.

Clauser also showed that an appropriate shape factor for equilibrium flows is G, where

$$G \equiv \left(\int_0^1 F^2\,d\xi\right)\Big/\left(\int_0^1 F\,d\xi\right), \tag{4.4.4}$$

and $$F = (u_G-u)/u_\tau, \quad \text{the velocity defect.} \tag{4.4.5}$$

For a particular value of β, the velocity-defect profiles are independent of Reynolds number and therefore G is constant. Thus, for equilibrium boundary layers, there must be a unique relation between G and β. An empirical relation proposed by Nash (1965) for boundary layers with $z_E < 1$ is

$$G = 6{\cdot}1(\beta+1{\cdot}81)^{\frac{1}{2}} - 1{\cdot}7. \tag{4.4.6}$$

The parameter G is related to the more usual shape factor (H) as follows:

$$G = s^{-\frac{1}{2}}(1-1/H), \tag{4.4.7}$$

$$[\text{or} \quad G = s^{-\frac{1}{2}}(1-2I_1+I_2)/(1-I_1)].$$

Equations (4.4.3), (4.4.6), (4.4.7) and the velocity-profile assumption have been used to determine the curves of $-m_G$ against z_E plotted in figure 16. These curves again indicate that the effects of Reynolds number, measured through the parameter l, are comparatively unimportant and that the hypothesis $-m_G = -m_G\{z_E\}$ is a reasonable one. The curves clearly show the same trends as the experimental data and, perhaps, suggest that the data for flat-plate flows, flows with $z_E \to 0$ and flows with $z_E \approx 1$ will not be well represented by a single straight line (see § 4.3).

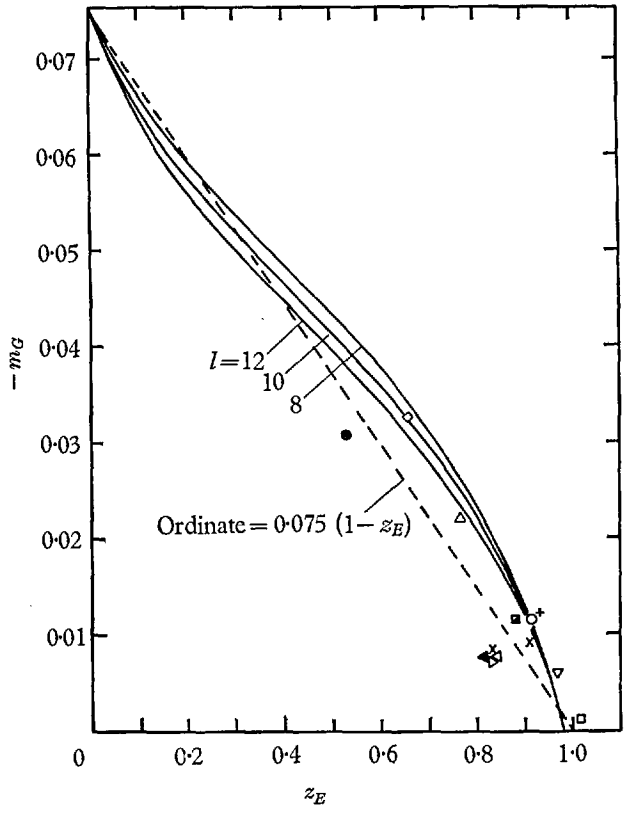


FIGURE 16. Comparison of theoretical entrainment rates for equilibrium boundary layers with experimental data. Symbols as for figure 13.

An interesting result deducible from the equilibrium-boundary-layer analysis is the value of $-m_G$ for $z_E = 0$. In this case, $s = 0$, $\beta = \infty$ and Nash's relation gives

$$G/\beta^{\frac{1}{2}} = 6{\cdot}1. \tag{4.4.8}$$

(N.B. Mellor & Gibson (1963) gave $G/\beta^{\frac{1}{2}} \to 5{\cdot}9$ for $\beta \to \infty$.) Thus, from equation (4.4.6)

$$\beta s = [1/(6{\cdot}1)^2]\,(1 - 1/H)^2$$

and, from equation (4.4.3)

$$-m_G = H_1(\beta s)\,(1 + 1/H),$$

i.e.

$$-m_G = [H_1/(6{\cdot}1)^2]\,(1 - 1/H)^2\,(1 + 1/H). \tag{4.4.9}$$

The assumed velocity profile then gives $z_E = 0$: $H = 4$, $H_1 = 4$, and equation (4.4.9) $-m_G = 0{\cdot}0756$. This result is in excellent agreement with the value for $-m_G$ obtained by extrapolation of the experimental data to $z_E = 0$.

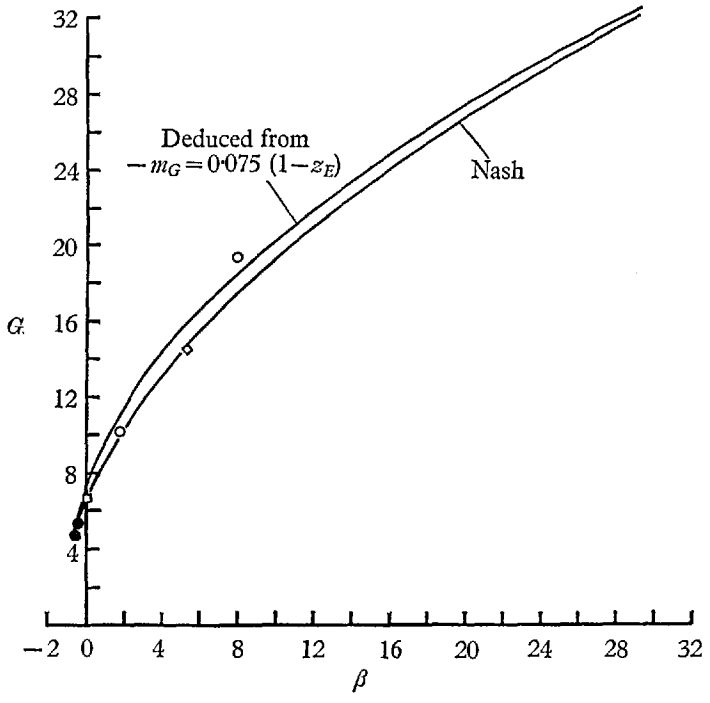


FIGURE 17. Comparison of the $G \sim \beta$ relation of Nash (1965) with the relation deduced from the entrainment function for $z_E < 1$ and with experimental data for equilibrium boundary layers. ●, Favourable pressure gradient, Herring & Norbury; □, zero pressure gradient, Klebanoff; ○, adverse pressure gradient, Clauser; ◇, adverse pressure gradient, Bradshaw & Ferriss.

The equilibrium analysis cannot, at present, be applied to wall-jet flows because Nash's $G \sim \beta$ relation is not valid for such flows. It is of some interest, however, to perform the inverse analysis and determine $G \sim \beta$ relations from the recommended entrainment functions for $z_E < 1$ and $z_E > 1$. The results of this analysis for $z_E < 1$ are shown in figure 17 together with Nash's relation and the available experimental data. The curves for $l = 8, 10$ and 12 are indistinguishable, and the differences between the curves deduced from $-m_G = 0{\cdot}075(1-z_E)$ and Nash's formula are slight. Although the available experimental data for equilibrium boundary layers are sparse, it would seem that there is little to choose between Nash's formula and a $G \sim \beta$ relation deduced via the entrainment function. Also, an entrainment function based upon a $G \sim \beta$ relation is clearly sensitive to the relation adopted.

For equilibrium wall jets, the $G \sim \beta$ relation implied by the entrainment law $-m_G = 0{\cdot}03z_E - 0{\cdot}02$ is shown in figure 18. The practical limitations of experimental apparatus limit accessible values of l to the vicinity of 10 and the spread

with l is thus rather unrealistic (to change l by 10% would require a change of roughly 250% in R_G). The experimental data of Patel & Newman (1961) are shown in figure 18 and are consistent with the $G \sim \beta$ relation deduced for $l = 10$.

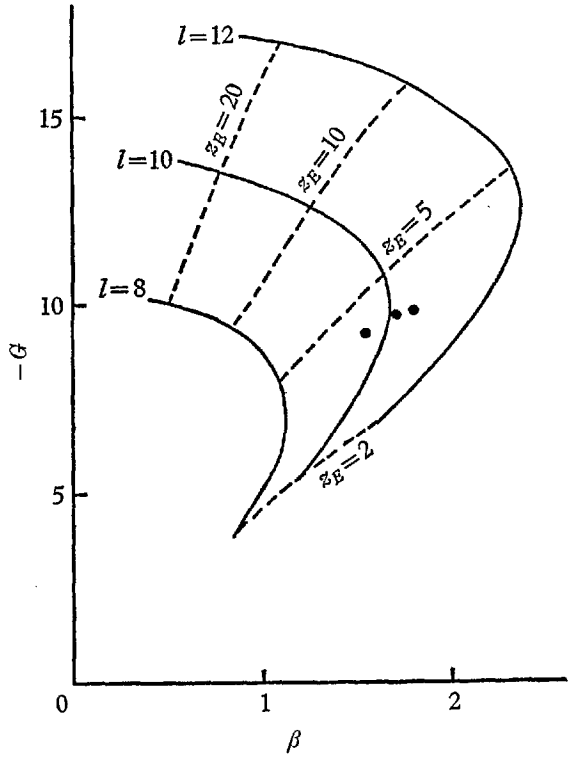


FIGURE 18. The $G \sim \beta$ relation for equilibrium wall jets deduced from the entrainment function for $z_E > 1$. ●, Patel & Newman.

4.5. *Conclusions and recommendations regarding the entrainment function*

The main obstacle in the determination of entrainment rates is the difficulty of specifying the boundary-layer thickness. To a certain extent this has been overcome and some degree of consistency achieved by adopting a velocity-profile family, the thickness and other profile-parameters being determined by fitting this to the experimental profiles or quantities derived from the profiles.

Analysis of a large amount of data has indicated that the hypothesis

$$-m_G = -m_G\{z_E\}$$

is a little better than that of Head (1960), $-m_G = -m_G\{H_1\}$, although there is considerable scatter in both the $-m_G \sim z_E$ and $-m_G \sim H_1$ plots. The difficulties and inherent inaccuracies involved in the determination of $-m_G$ preclude the inclusion of parameters other than z_E in an entrainment function, although the possible importance of other parameters (such as l, $dz_E/d\mathrm{R}_x$, etc.) cannot be ruled out.

The following entrainment functions appear to fit the experimental data as well as any; they will be used, for the time being at least, as auxiliary equations in the prediction of boundary-layer flows.

$$0 \leqslant z_E \leqslant 1: \quad -m_G = 0{\cdot}075(1-z_E),$$

$$1 < z_E: \quad -m_G = 0{\cdot}03z_E - 0{\cdot}02.$$

These relations imply a discontinuity at $z_E = 1$, a result of fitting 'best' straight lines to the data for $z_E < 1$ and $z_E > 1$.

In the following section a brief examination will be made of the sensitivity of the predictions to the entrainment function adopted.

For $z_E < 1$, an entrainment function deduced from the $G \sim \beta$ relation of Nash (1965) for equilibrium boundary layers is in qualitative agreement with the recommendation made above for $z_E < 1$. It is shown, however, that the entrainment function so derived is sensitive to small changes in the $G \sim \beta$ relation.

5. Comparison of the predictions of the present method with experimental data

5.1. *Methods of calculation*

The general prediction procedure involves the simultaneous solution of the differential equations derived in § 2 from the integral mass-conservation equation and the momentum integral equation. The required input is the variation of u_G with R_x and two initial conditions. In the case of boundary layers with $z_E < 1$, these initial conditions were taken as the values of R_m and z_E computed from the reported measured value of R_2 and H at the starting-point. For wall jets the initial values of z_E and R_m were deduced from the measured velocity profile at the starting-point using the least-squares-fitting method.

The quantities predicted were the values of R_2, H and s. In addition, for wall-jet flows the values of the more usual wall-jet variables $u_{\max}/u_G$ and $y_{\frac{1}{2}}/y_c$ were computed with the aid of the assumed velocity profile, equation (3.2.4). As well as this general procedure, calculations for flows with $z_E < 1$ have been carried out using measured values of R_2 as data, the integral mass-conservation equation only being solved. Thompson (1964) came to the conclusion that experimental values of R_2 provide the best basis for comparing the calculated with the measured shape-factor development. This, it was argued, allows some account to be taken of the three-dimensional character of most real flows. Whilst this *may* be true, in completely new circumstances two-dimensional conditions have to be assumed and the prediction of both R_2 and H is necessary.

For equilibrium flows an alternative method of calculation was also used. The value of z_E was taken as the mean of the values deduced from the experimental values of R_2 and H. The prediction procedure again reduces to the integration of a single differential equation. In this case, however, we have an analytical expression for the entrainment law, equation (4.4.3),

$$-m_G = H_1 s(1+\beta+\beta/H).$$

5.2. *Discussion of predictions for flows with* $z_E < 1$

In figures 19–26 are shown reported measured values of R_2 and H plotted against R_x. Also shown are experimental values of skin-friction coefficients s, the method by which these were obtained being noted on the relevant graphs. On each of

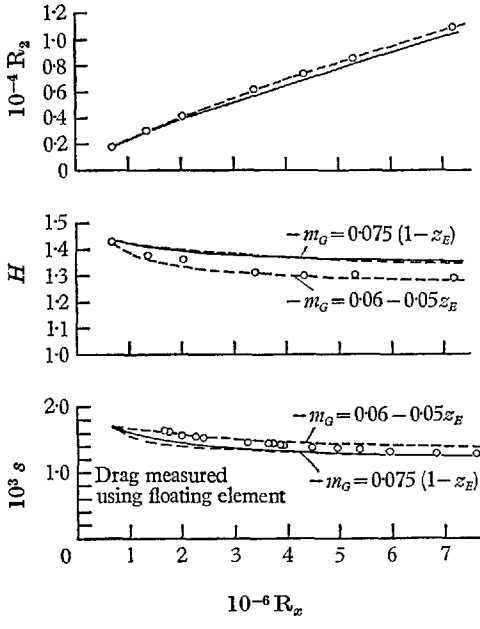


FIGURE 19

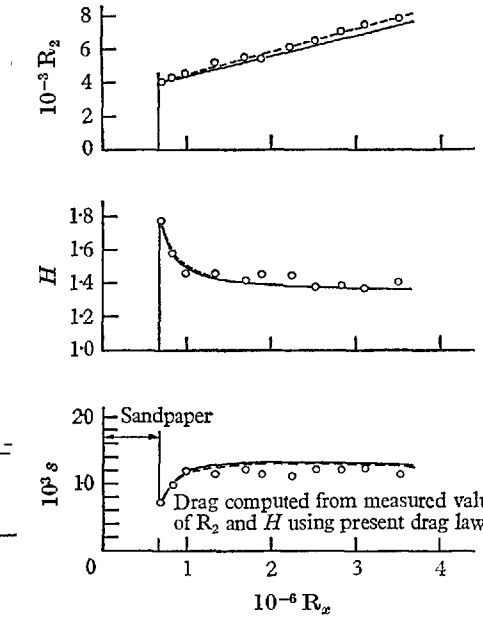


FIGURE 20

FIGURE 19. Comparison of predicted boundary-layer development with experimental data of Schultz-Grunow (1940). Flat-plate boundary layer.

FIGURE 20. Comparison of predicted boundary-layer development with experimental data of Klebanoff & Diehl (1952). Flat-plate boundary layer recovering from the effects of an upstream disturbance, $u_G = 35$ ft./sec.

these figures there appears a number of lines; those drawn full were obtained by the general prediction method (i.e. using as data only $u_G\{R_x\}$ and initial conditions). The chain-dashed lines on the H and s plots were computed using the dashed lines drawn through the plotted R_2 values as data. The additional lines appearing in the figures displaying data for equilibrium boundary layers were obtained assuming a constant value for z_E as outlined in § 5.1.

The following conclusions may be drawn from the comparisons:

(*a*) In the majority of the cases examined, agreement between the predictions and the experimental data is fairly good. Failure to predict R_2 accurately, however, leads to poor predictions of H and s.

(*b*) Predictions of H and s using measured R_2 values are generally better than those obtained when R_2 is computed simultaneously with H. The only exception to this generalization is the prediction of Clauser's second equilibrium boundary layer. The reason for the behaviour of this exceptional case is not yet known.

(*c*) The best predictions of the equilibrium boundary layers of Clauser are obtained when the appropriate constant value of z_E is assumed; this is hardly surprising since z_E and H are very strongly related to one another.

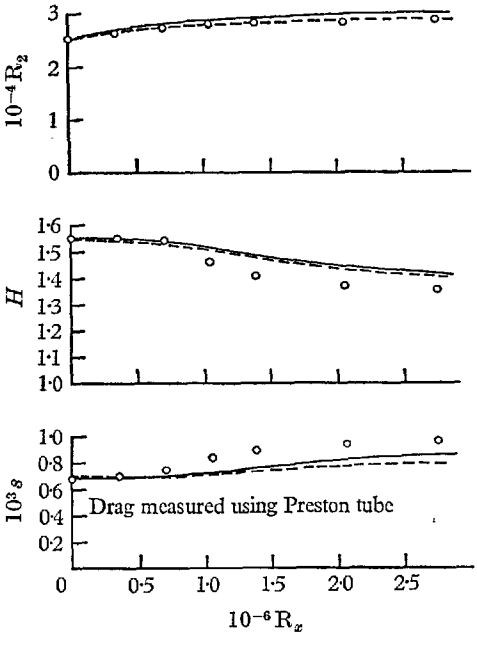


FIGURE 21

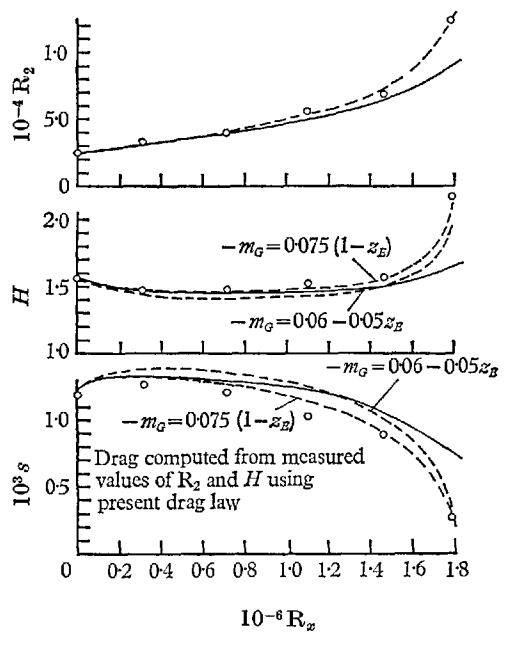


FIGURE 22

FIGURE 21. Comparison of predicted boundary-layer development with experimental data of Bradshaw & Ferriss (1965). Boundary layer recovering from the effects of an adverse pressure gradient.

FIGURE 22. Comparison of predicted boundary-layer development with experimental data of von Doenhoff & Tetervin (1943). Boundary layer on an aerofoil, *NACA* 65 (216) 222 (approx.), $R = 3{\cdot}64 \times 10^6$, $\alpha = 10{\cdot}1°$.

For the boundary layers of Schultz-Grunow (1940) and of von Doenhoff & Tetervin (1943) additional predictions of H and s were made using an entrainment equation differing from that recommended here. The equation used was that recommended by Spalding (1965)

$$-m_G = 0{\cdot}06 - 0{\cdot}05 z_E.$$

In the discussion in § 4.3 it was shown that this entrainment function is a better fit to the experimental data for the flat-plate boundary layer than is equation (4.3.2), the present recommendation. This view is supported by the graphs shown in figure 19, where it is seen that the prediction of Schultz-Grunow's boundary layer is considerably improved using this equation.

Figure 22, however, indicates that Spalding's entrainment equation leads to poorer predictions in the case of the flow reported by von Doenhoff & Tetervin than does the present authors' recommendation.

5.3. *Discussion of predictions of flows with* $z_E > 1$

Comparisons of measured with predicted wall-jet development are shown in figures 27–36. The data shown were reported by Kruka & Eskinazi (1953) and Nicoll (1965) and cover the following ranges of slot Reynolds numbers

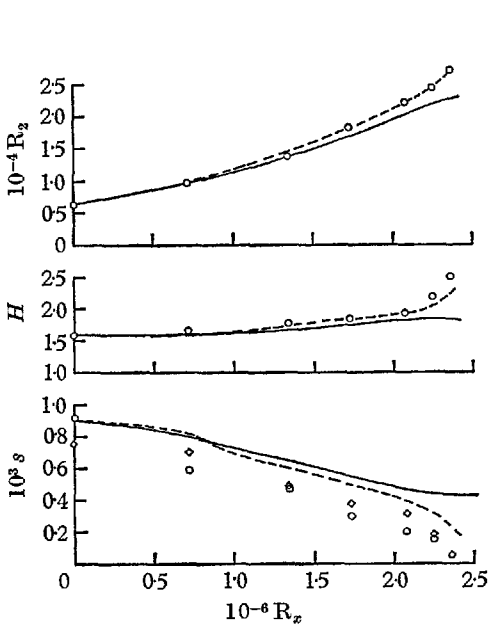


FIGURE 23

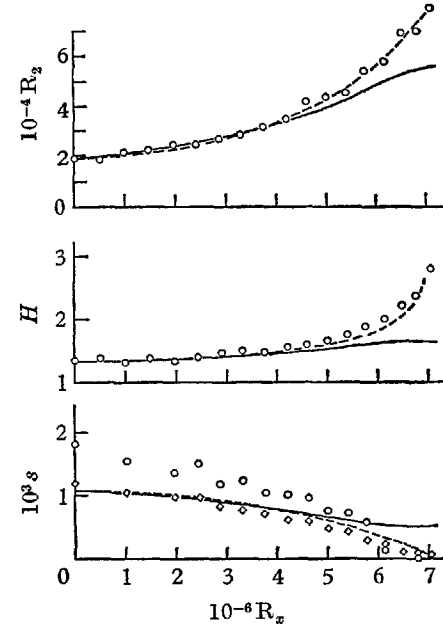


FIGURE 24

FIGURE 23. Comparison of predicted boundary-layer development with experimental data of Newman (1951). Boundary layer on a symmetrical rear-stalling aerofoil. ○, Drag obtained by extrapolating measured shear-stress profiles to wall. ◇, Drag obtained from velocity profiles by Clauser's method.

FIGURE 24. Comparison of predicted boundary-layer development with experimental data of Schubauer & Klebanoff (1951). Boundary layer on a convex wall with an adverse pressure gradient. ○, Drag obtained by extrapolating measured shear-stress profiles to wall. ◇, Drag obtained from velocity profiles by Clauser's method.

$R_c(\equiv u_c y_c/\nu)$ and velocity ratios $(u_c/u_{G,0})$,

$$3{,}000 \leqslant R_c \leqslant 24{,}000,$$

$$1{\cdot}55 \leqslant u_c/u_{G,0} \leqslant 18.$$

In general the predictions follow the experimental results quite closely and it may be concluded that the present method satisfactorily predicts wall-jet development over the range of pressure gradients and velocity ratios examined.

6. Conclusions

6.1. *Velocity profiles*

The velocity profile assumed in the present work, equation (3.2.4), appears to fit experimental velocity profiles adequately for the range

$$0{\cdot}5 < z_E < 5 \quad \text{(approx.)}.$$

At lower z_E the values of the shape factor, H, and the momentum thickness, δ_2, deduced from the least-squares-fitted profile differ significantly from the experi-

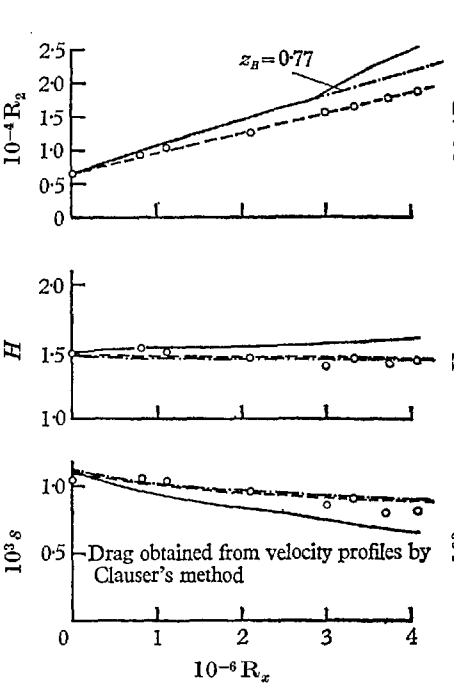


FIGURE 25

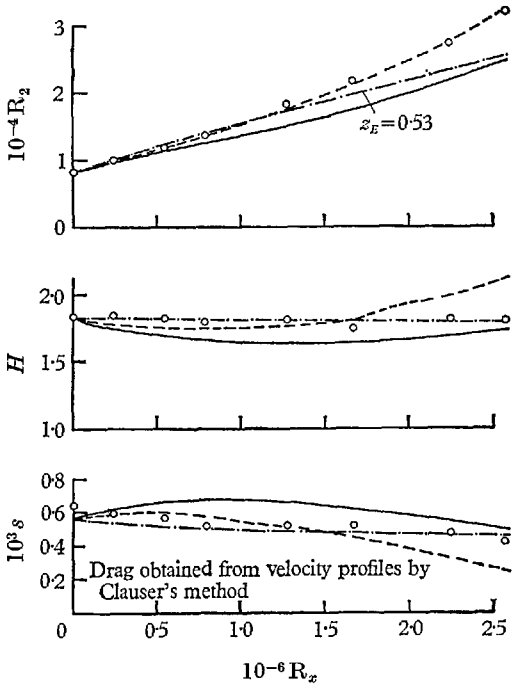


FIGURE 26

FIGURE 25. Comparison of predicted boundary-layer development with experimental data of Clauser (1954), pressure distribution 1. Equilibrium boundary layer with an adverse pressure gradient, $\beta \approx 1{\cdot}8$, $z_E \approx 0{\cdot}77$.

FIGURE 26. Comparison of predicted boundary-layer development with experimental data of Clauser (1954), pressure distribution 2. Equilibrium boundary layer with an adverse pressure gradient, $\beta \approx 8{\cdot}0$, $z_E \approx 0{\cdot}53$.

mental values. At higher z_E, the shape of the experimental profiles differs in a consistent manner from that of the assumed profile. The values of H, δ_2, $y_{\frac{1}{2}}$ and $u_{\max}$ obtained from the least-squares-fitted profile agree closely with the experimental values, although the value of $y_{\max}$ so obtained does not.

The drag law implicit in the assumed profile is an improvement over the Ludwieg–Tillmann drag law at high values of the shape factor H and has the advantage of being applicable to wall-jet flows.

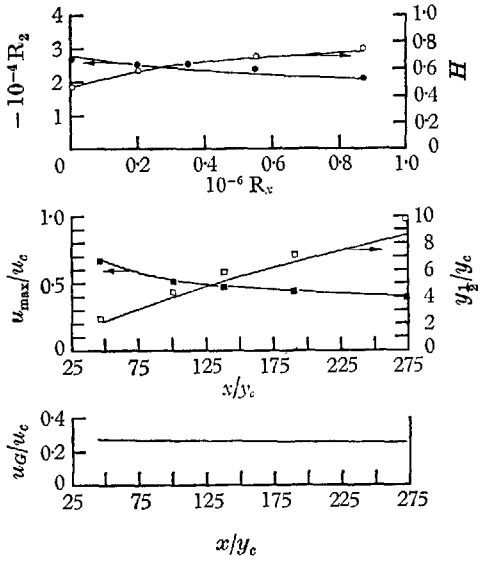


FIGURE 27

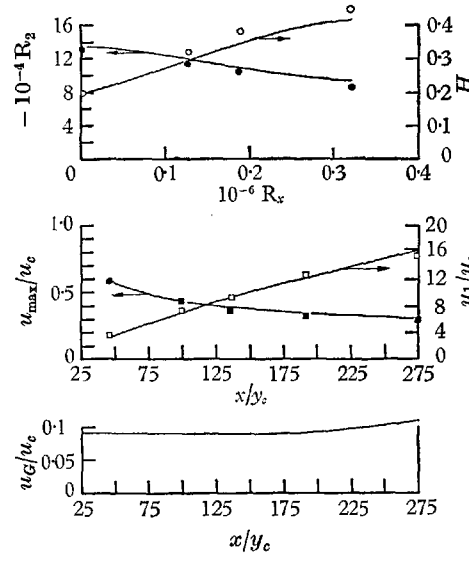


FIGURE 28

FIGURE 27. Comparison of predicted wall-jet development with experimental data of Kruka & Eskinazi (1963), run 1. $u_c/u_{G,0} = 3{\cdot}8$, $R_c = 1{\cdot}07 \times 10^4$. ●, R_2; ○, H; ■, u_{max}/u_c; □, $y_{\frac{1}{2}}/y_c$.

FIGURE 28. Comparison of predicted wall-jet development with experimental data of Kruka & Eskinazi (1963), run 2. $u_c/u_{G,0} = 10$, $R_c = 1{\cdot}31 \times 10^4$. Symbols as for figure 27.

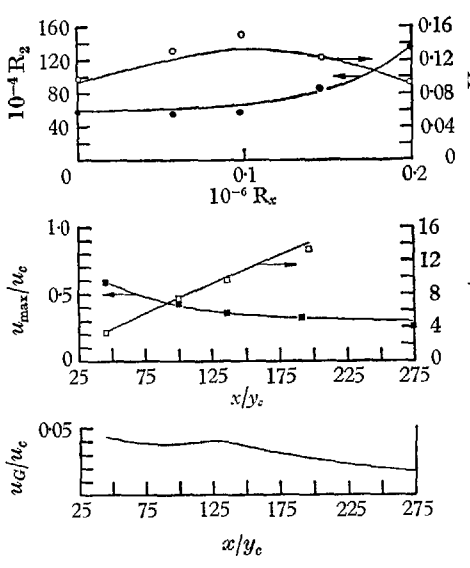


FIGURE 29

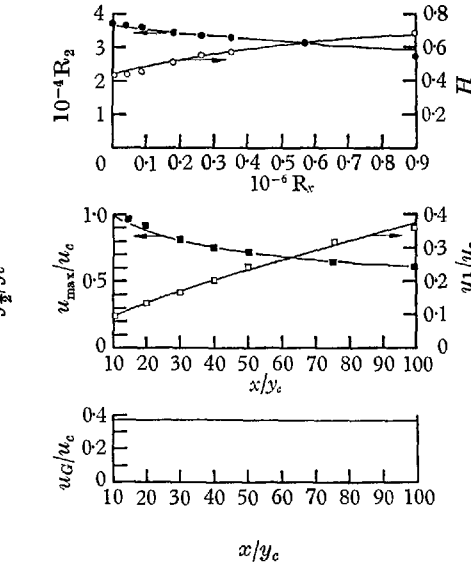


FIGURE 30

FIGURE 29. Comparison of predicted wall-jet development with experimental data of Kruka & Eskinazi (1963), run 3. $u_c/u_{G,0} = 18$, $R_c = 2{\cdot}63 \times 10^4$. Symbols as for figure 27.

FIGURE 30. Comparison of predicted wall-jet development with experimental data of Nicoll (1965), run 2. $u_c/u_{G,0} = 2{\cdot}71$, R $= 2{\cdot}37 \times 10^4$. Symbols as for figure 27.

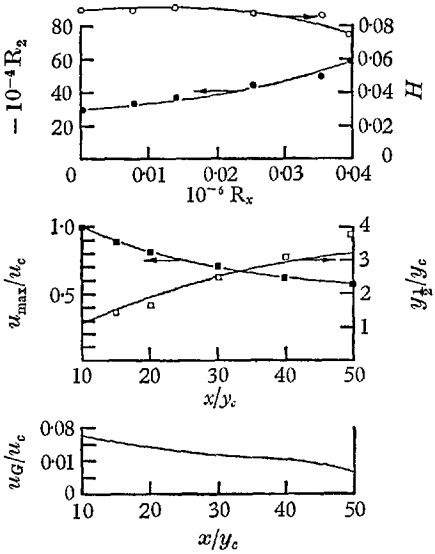


FIGURE 31

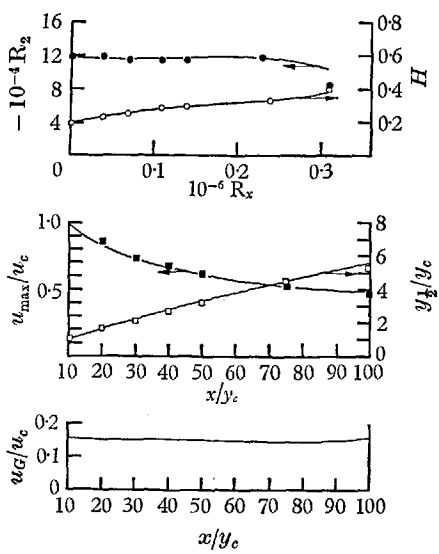


FIGURE 32

FIGURE 31. Comparison of predicted wall-jet development with experimental data of Nicoll (1965), run 3. $u_c/u_{G,0} = 13{\cdot}2$, $R_c = 2{\cdot}31 \times 10^4$. Symbols as for figure 27.

FIGURE 32. Comparison of predicted wall-jet development with experimental data of Nicoll (1965), run 4. $u_c/u_{G,0} = 6{\cdot}22$, $R_c = 2{\cdot}28 \times 10^4$. Symbols as for figure 27.

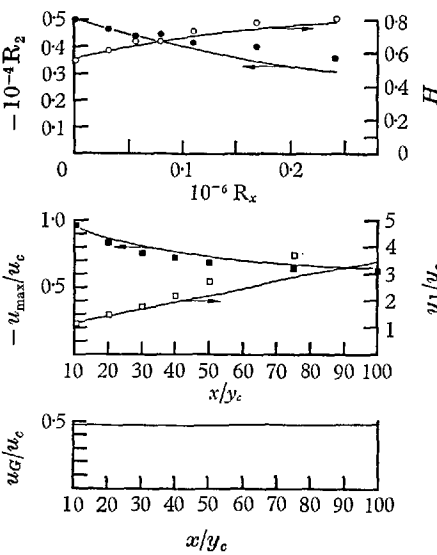


FIGURE 33

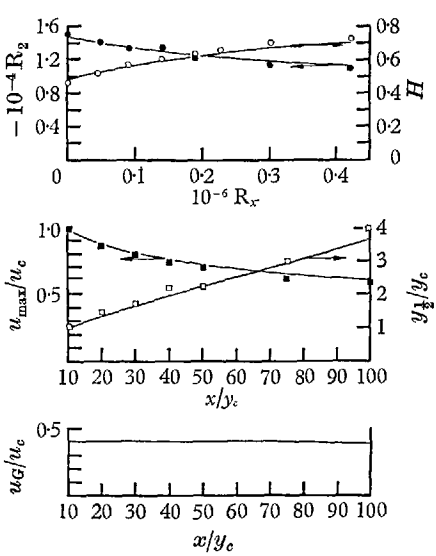


FIGURE 34

FIGURE 33. Comparison of predicted wall-jet development with experimental data of Nicoll (1965), run 5. $u_c/u_{G,0} = 2{\cdot}10$, $R_c = 5{\cdot}59 \times 10^3$. Symbols as for figure 27.

FIGURE 34. Comparison of predicted wall-jet development with experimental data of Nicoll (1965), run 7. $u_c/u_{G,0} = 2{\cdot}43$, $R_c = 1{\cdot}14 \times 10^4$. Symbols as for figure 27.

6.2. *Entrainment function*

Dimensionless entrainment rates are shown to correlate reasonably well with the parameter z_E. The following formulae fit the data as well as any and are the present authors' recommendations

$$0 \leqslant z_E \leqslant 1, \quad -m_G = 0{\cdot}075(1-z_E),$$

$$z_E > 1, \quad -m_G = 0{\cdot}03z_E - 0{\cdot}02.$$

The determination of entrainment requires both the specification of the outer edge of the boundary layer (for the determination of the flow within the boundary

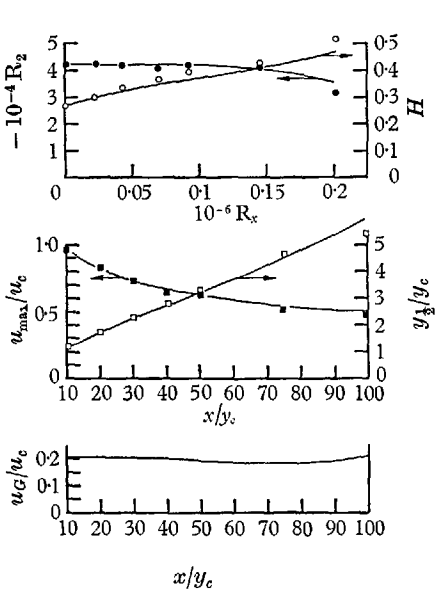


FIGURE 35

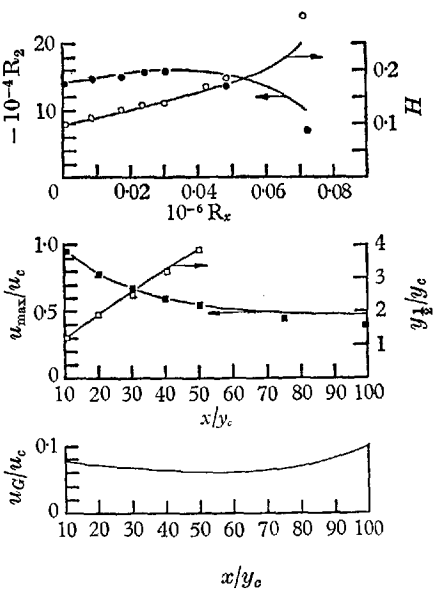


FIGURE 36

FIGURE 35. Comparison of predicted wall-jet development with experimental data of Nicoll (1965), run 9. $u_c/u_{G,0} = 4{\cdot}81$, $R_c = 1{\cdot}14 \times 10^4$. Symbols as for figure 27.

FIGURE 36. Comparison of predicted wall-jet development with experimental data of Nicoll (1965), run 10. $u_c/u_{G,0} = 12{\cdot}9$, $R_c = 1{\cdot}12 \times 10^4$. Symbols as for figure 27.

layer) and the differentiation of the flow so obtained. This gives rise to considerable scatter in the experimental entrainment rates and thus precludes the determination of any weaker dependence of entrainment on quantities other than z_E.

6.3. *Predictions*

Predictions have been made, using the recommended entrainment functions, of the shape factor H, momentum-thickness Reynolds number R_2 and drag coefficient s, and also, in the case of wall-jet flows, of the half-thickness $y_{\frac{1}{2}}$ and the velocity maximum u_{max}. The boundary-layer predictions are in reasonable agreement with experiment, except when separation conditions are approached.

Since the present form of the 'unified theory' applies only to two-dimensional flows, this failure may be due to lack of two-dimensionality in the reported separation experiments. Certainly the predictions based upon experimental values of R_2 are in good agreement with experiment, even when separation occurs. However, since the assumed velocity profile does not fit experimental profiles near separation conditions, the authors reserve their opinion as to the exact cause of the failure to predict separation.

The wall-jet predictions are good, both for zero pressure gradients and for adverse pressure gradients.

The authors would like to express their appreciation to Prof. D.B. Spalding for his help and advice in all stages of their work, which forms part of a programme of research, co-ordinated by Prof. Spalding, into turbulent flows near walls.

Thanks are also due to Mr P. Bradshaw, Prof. F. H. Clauser, Prof. S. Eskinazi, Dr V. Kruka and to Dr B. S. Stratford for making available to the authors unpublished details of their experimental work.

The support of the Ministry of Aviation (Contract no. PD/37/27) is gratefully acknowledged by W. B. Nicoll.

REFERENCES

Bradshaw, P. & Ferriss, D. H. 1965 The response of a retarded equilibrium turbulent boundary layer to the sudden removal of pressure gradient. *NPL Aero. Rep.* no. 1145.

Chi, S. W. 1962 Unpublished work at Imperial College.

Clauser, F. H. 1954 Turbulent boundary layers in adverse pressure gradients. *J. Aero. Sci.* **21**, 91.

Clauser, F. H. 1956 The turbulent boundary layer. *Advances in Applied Mechanics*, iv, no. 1. New York: Academic Press.

Coles, D. 1956 The law of the wake in the turbulent boundary layer. *J. Fluid Mech.* **1**, 191.

Coles, D. E. 1962 The turbulent boundary layer in a compressible fluid. *Rand Corp. Rep.* no. R–403–PR.

Doenhoff, A. E. von & Tetervin, N. 1943 Determination of general relations for the behaviour of turbulent boundary layers. *NACA TR*, no. 772.

Fage, A. 1938 Profile and skin-friction aerofoil drags. *Aero. Res. Counc. R. & M.* no. 1852.

Fage, A. & Falkner, V. M. 1930 An experimental determination of the intensity of friction on the surface of an aerofoil. *Aero. Res. Counc. R. & M.* no. 1315.

Gartshore, I. S. 1964 Jets and wall jets in uniform streaming flow. *McGill Univ., Mech. Eng. Res. Lab. Rep.* no. 64–4.

Head, M. R. 1960 Entrainment in the turbulent boundary layer. *Aero. Res. Counc. R. & M.* no. 3152.

Herring, H. J. & Norbury, J. F. 1963 Some experiments on equilibrium turbulent boundary layers in favourable pressure gradients. *Princeton Univ., Dept. Aerospace & Mech. Sci. FLD*, no. 15.

Hinze, J. O. 1959 *Turbulence.* New York: McGraw Hill.

Klebanoff, P. S. 1955 Characteristics of turbulence in a boundary layer with zero pressure gradient. *NACA Rep.* no. 1247.

Klebanoff, P. S. & Diehl, Z. W. 1952 Some features of artificially thickened fully developed turbulent boundary layers with zero pressure gradient. *NACA Rep.* no. 1110.

Kruka, V. & Eskinazi, S. 1964 The wall-jet in a moving stream. *J. Fluid Mech.* **20**, 555.

LUDWIEG, H. & TILLMANN, W. 1949 Untersuchungen über die Wandschubspannung in turbulenten Reibungsschichten. *Ing.-Arch.* **17**, 288. (Trans. 1950 Investigations of the wall shearing stress in turbulent boundary layers. *NACA TM*, no. 1285.)

MELLOR, G. J. & GIBSON, D. M. 1963. Equilibrium turbulent boundary layers. *Princeton Univ., Dept. Aerospace & Mech. Sci. FLD*, no. 13.

NASH, J. F. 1965 Turbulent-boundary-layer behaviour and the auxiliary equation. *AGARDograph*, no. 97, part 1, 245.

NEWMAN, B. G. 1951 Some contributions to the study of the turbulent boundary layer near separation. *Aust. Dept. Supply Rep.* no. ACA–53.

NICOLL, W. B. 1965 Wall jet velocity profiles and entrainment. *Imperial College, Mech. Eng. Dept. Rep.* no. IC/HRJ/23.

PATEL, R. P. & NEWMAN, B. G. 1961 Self-preserving, two-dimensional turbulent jets and wall jets in a moving stream. *McGill Univ., Mech. Eng. Res. Lab. Rep.* no. Ae 5.

REYNOLDS, W. C., KAYS, W. M. & KLINE, S. J. 1958 Heat transfer in the turbulent incompressible boundary layer. I Constant wall temperature. *NASA Memo*, no. 12–1–58 W.

SCHUBAUER, G. B. & KLEBANOFF, P. S. 1951 Investigation of separation of the turbulent boundary layer. *NACA Rep.* no. 1030.

SCHULTZ-GRUNOW, F. 1940 Neues Reibungswiderstandsgesetz für glatte Platten. *Luftfahrtforschung*, **17**, 239. (Trans. 1941 New frictional resistance law for smooth plates. *NACA TM* no. 986.)

SEBAN, R. A. & BACK, L. H. 1961 Velocity and temperature profiles in a wall jet. *Int. J. Heat & Mass Trans.* **3**, 255.

SMITH, D. W. & WALKER, J. H. 1959 Skin-friction measurements in incompressible flow. *NASA TR*, no. R–26.

SPALDING, D. B. 1964*a* A unified theory of friction, heat transfer and mass transfer in the turbulent boundary layer and wall jet. *Aero. Res. Counc. Rep.* no. 25,925.

SPALDING, D. B. 1964*b* A unified theory of friction, heat transfer and mass transfer in the turbulent boundary layer and wall jet. *Imperial College, Mech. Eng. Dep. Rep.* (Annotated version of previous reference.)

SPALDING, D. B. 1965 The kinetic-energy-deficit equation of the turbulent boundary layer. *AGARDograph*, no. 97, part 1, 191.

STRATFORD, B. S. 1959 An experimental flow with zero skin friction throughout its region of pressure rise. *J. Fluid Mech.* **5**, 17.

THOMPSON, B. G. J. 1964 A critical review of existing methods of calculating the turbulent boundary layer. *Aero. Res. Coun. Rep.* no. 26,109.

WIEGHARDT, K. 1944 Zum Reibungswiderstand rauher Platten. *ZWB KWI U & M*, 6612.

[*Reprinted from* THE AERONAUTICAL QUARTERLY Vol. XVIII, *May 1967*]

Published by THE ROYAL AERONAUTICAL SOCIETY

Escudier, M.P., Ph.D.

Decay of a Velocity Maximum in a Turbulent Boundary Layer

M. P. Escudier, W. B. Nicoll, D. B. Spalding and J. H. Whitelaw

(Mechanical Engineering Department, Imperial College of Science and Technology)

Printed by the Lewes Press Wightman & Co. Ltd., Friars Walk, Lewes, Sussex.

Decay of a Velocity Maximum in a Turbulent Boundary Layer

M. P. Escudier, W. B. Nicoll, D. B. Spalding and J. H. Whitelaw

(Mechanical Engineering Department, Imperial College of Science and Technology)

Summary: The paper describes an "explicit" method of predicting the flow properties of a turbulent boundary layer; particular attention is paid to the region in which the growth of the layer is characterised by the decay of a velocity maximum. The validity of the method is tested against the data of Wieghardt and against new data of the present authors; it is shown to be satisfactory. The integral flow properties predicted by the method are used, together with a further assumption, to predict velocity profiles; these closely resemble the measured ones.

1. Introduction

1.1. THE PROCESS UNDER CONSIDERATION

There are several practical circumstances in which the profile of velocity, in a turbulent boundary layer, exhibits a maximum. This occurs, for example, downstream of a film-cooling slot, when the coolant air is injected at a velocity exceeding that of the main stream (Fig. 1 illustrates the system in question; it is commonly used for the protection of combustion-chamber walls from the action of a hot-gas stream). Velocity maxima may also occur downstream of injection slots provided for the energisation of boundary layer fluid, when this might otherwise separate from the wall*.

Usually the ratio of the maximum velocity to that of the nearby main stream falls towards unity with increase in the distance from the slot; and after it has reached unity the velocity maximum disappears. It is this gradual modification of the velocity profile, the disappearance of the maximum, that is considered in the present paper. A method is provided for predicting the variation of major boundary layer properties (momentum thickness, displacement thickness, drag coefficient) which the disappearance process entails; the method is tested by comparison with experimental data, some of which are new.

1.2. REASONS FOR INTEREST

The special feature of the maximum decay process is that, during its course, the values of the momentum and displacement thicknesses change from negative to positive. Most methods of predicting the development of turbulent boundary layers,

*Such flows are often called "wall jets with external flow".

Received June 1966.

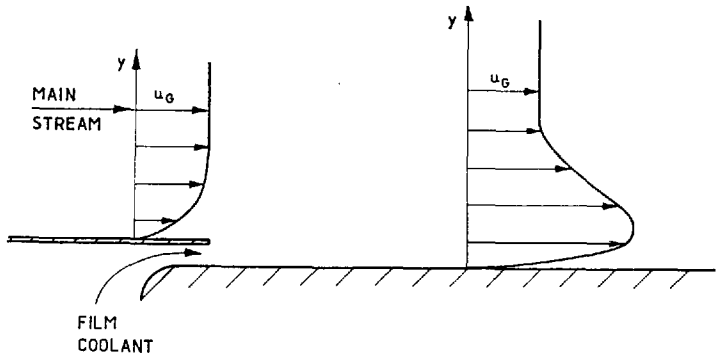


Figure 1. Example of the process which is considered.

for example those of Truckenbrodt[1], Spence[2], Head[3], Thompson[4] and Walz[5], are valid only for the region of positive values of these thicknesses. Other methods of prediction, for example those of Glauert[6] and Myers, Schauer and Eustis[7], are valid only for negative values.

It is true that some prediction methods exist which are capable of application not only to boundary layers with thicknesses of either sign, but also to those for which the sign changes during the course of the development; methods with this capability include those of Gartshore[8], Harris[9], Spalding[10] and Patankar and Spalding[11]. The last-named of these references however has disclosed the existence of a special mathematical difficulty which assails methods relying on the momentum-integral and kinetic-energy-integral equations; this difficulty, which is manifested as a matrix singularity, at one time was a serious bar to progress.

At this point it is necessary to distinguish between what will be called "explicit" and "parametric" methods. In methods of the first kind, explicit formulae are used for the drag coefficient, and for other auxiliary quantities, in terms of the momentum and kinetic-energy thicknesses, the quantities which are the dependent variables of the differential equations. In methods of the second kind, both the boundary layer thicknesses and the auxiliary quantities are expressed in terms, not of each other, but of certain "parameters"; these are quantities which appear in formulae which describe the velocity profile; they are used as the dependent variables of the integration.

The majority of methods using the momentum and kinetic-energy equations, for example those of Truckenbrodt[1] and Walz[5], are of the explicit type; the method of Patankar and Spalding[11] is a parametric one. This method has the advantages of greater flexibility and of reduced reliance on empirical inputs; unfortunately it is this type which is prone to the matrix-singularity difficulty*, referred to, in the region of the disappearance of velocity maxima. On the other hand, the previously existing explicit methods are incapable of application in this region.

*This difficulty has been overcome (as described by Spalding[12]), but by abandonment of the kinetic-energy equation. It appears that this equation is particularly unsuited to appear in a parametric method when velocity maxima are present.

The authors and their colleagues are currently developing general methods of calculating the flow and transport processes which take place in turbulent boundary layers (Refs. 10-18); both parametric and explicit methods are in use. The purpose of the present paper is to show that a general explicit calculation procedure exists which provides satisfactory predictions of boundary layer development in the special region described, that in which the momentum and displacement thicknesses change sign.

1.3. OUTLINE OF THE PRESENT PAPER

The new calculation procedure is summarised briefly in Section 2, which presents the basic differential equations and the empirically-based auxiliary relations necessary for their solution. A few notes are appended in explanation of the less conventional features of the method.

In Section 3 are presented the results of some predictions of integral boundary layer properties for situations, of the type in question, for which experimental data have been reported, or for which new experiments have been carried out by the authors. It is shown firstly that the integrations can be carried out successfully, and secondly that the agreement between the predictions and the measurements is as good as is customary in more conventional boundary layer circumstances.

Because explicit methods do not employ assumptions about the algebraic form of the velocity profile (they import their empirical information in more direct ways), such methods do not provide any prediction of velocity profiles which could be compared with experiment. However, once the integral properties of the boundary layer have been predicted by the explicit method, it is possible, by employing further empirical information about the regularities which appear in velocity profiles, to associate a velocity distribution with each station along the wall. A method of doing this is explained in Section 4; it is applied to the particular cases in question. The agreement between prediction and experiment is shown to be tolerably good.

Notation

A, n constants in equation (13)

$c_f/2$ local drag coefficient $= \tau_S/(\rho u_G^2)$

E constant associated with wall roughness

F_2 pressure gradient parameter $= R_2 d(\log_e u_G)/dR_x$

H_{12} velocity profile shape factor $= R_1/R_2$

H_{32} velocity profile shape factor $= R_3/R_2$

l logarithmic function in drag law (see equation (10))

l' logarithmic function $= \log_e [E u_G y_G \sqrt{(c_f/2)}/\nu]$

R_x Reynolds number based on u_G and $x = \int_0^x (u_G/\nu)\, dx$

R_1 Reynolds number based on u_G and $\delta_1 = u_G \delta_1/\nu$

R_2 Reynolds number based on u_G and $\delta_2 = u_G\delta_2/\nu$

R_3 Reynolds number based on u_G and $\delta_3 = u_G\delta_3/\nu$

$\bar{s}$ shear-work integral $= \int_0^{y_G} [\tau/(\rho u_G^3)]\,(\partial u/\partial y)\,dy$

u, u_G mean velocity in main-stream direction and main-stream velocity respectively

x, y distance measured along wall in main-stream direction and normal to wall respectively

y_e slot height

y_G boundary layer thickness

z non-dimensional velocity $= u/u_G$

z_E parameter in velocity profile model $= \sqrt{(c_f/2)}l'/\kappa$

δ_1 displacement thickness $= \int_0^{y_G} (1-u/u_G)\,dy$

δ_2 momentum-deficit thickness $= \int_0^{y_G} (u/u_G)\,(1-u/u_G)\,dy$

δ_3 kinetic-energy-deficit thickness $= \int_0^{y_G} (u/u_G)\,(1-u^2/u_G^2)\,dy$

κ von Kármán constant

ζ shape factor $= \frac{2}{3}H_{32} - 1 + \sqrt{\left(\frac{4}{9}H_{32}^2 - \frac{2}{3}H_{32}\right)}$

ξ dimensionless distance from wall $= y/y_G$

ρ fluid density

τ total (laminar plus turbulent) shear stress

τ_S value of τ at wall ($y = 0$)

ν molecular kinematic viscosity of fluid

Suffixes

G pertaining to main stream ($y \geqslant y_G$)

S pertaining to wall ($y = 0$)

2. Method of Prediction

2.1. THE INTEGRAL EQUATIONS

Beyond the immediate vicinity of the slot, say ten or more slot heights downstream, the experimental velocity profiles have been shown by Spalding[10] and by Escudier and Nicoll[13] to be adequately described by two parameters. The choice of parameters is to some extent arbitrary; in the present work the Reynolds numbers R_2 and R_3 are used. These are defined by

$$R_2 \equiv \frac{\delta_2 u_G}{\nu} \tag{1}$$

and $$R_3 \equiv \frac{\delta_3 u_G}{\nu}, \tag{2}$$

where δ_2 and δ_3 are the momentum and kinetic-energy thicknesses respectively, u_G is the main-stream velocity and ν is the kinematic viscosity of the fluid.

With the usual boundary layer approximations, the equations describing the development of R_2 and R_3, i.e. the integral momentum and mean-kinetic-energy equations, can be written[16] as

$$\frac{dR_2}{dR_x} + (1 + H_{12}) F_2 = c_f/2 \tag{3}$$

and $$\frac{dR_3}{dR_x} + 2H_{32}F_2 = 2\bar{s}. \tag{4}$$

Here R_x is the Reynolds number based upon u_G and on x, the distance measured along the wall in the main-stream direction; it is defined as

$$R_x \equiv \int_0^x (u_G/\nu)\, dx; \tag{5}$$

F_2 is a pressure gradient parameter defined by

$$F_2 \equiv R_2\, d\,(\log_e u_G)/dR_x. \tag{6}$$

The shape factors H_{12} and H_{32} are defined respectively as the ratios δ_1/δ_2 and δ_3/δ_2, where δ_1 is the displacement thickness; $c_f/2$ is the local drag coefficient and $\bar{s}$ the shear-work integral*. The latter quantity is defined by

$$\bar{s} \equiv \int_0^{y_G} [\tau/(\rho u_G^3)]\, (\partial u/\partial y)\, dy, \tag{7}$$

where τ is the total (laminar plus turbulent) shear stress and y_G the boundary layer thickness.

2.2. THE AUXILIARY EQUATIONS

To solve equations (3) and (4), relationships are required between the three quantities H_{12}, $c_f/2$ and $\bar{s}$ and the dependent variables R_2 and R_3. The three relationships used in this paper are:

$$(i) \qquad H_{32} \equiv \frac{R_3}{R_2} = \begin{cases} 1{\cdot}431 - \dfrac{0{\cdot}0971}{H_{12}} + \dfrac{0{\cdot}775}{H_{12}^2}, & 2{\cdot}8 > H_{12} \geqslant 1{\cdot}25 \\ 2{\cdot}674 - 0{\cdot}66 H_{12}, & 1{\cdot}25 \geqslant H_{12} \geqslant 0{\cdot}85 \\ 0{\cdot}82 + \dfrac{1{\cdot}10}{H_{12}}; & 0{\cdot}85 \geqslant H_{12} > 0{\cdot}06 \end{cases} \tag{8}$$

*Frequently, this term is called the "dissipation integral".

(*ii*) $$c_f/2 = \frac{0{\cdot}2430\zeta^3 + 0{\cdot}03759\zeta - 0{\cdot}00106 + 0{\cdot}0914\zeta^2/(1+65/\zeta)}{l^2} \quad , \tag{9}$$

where $$l \equiv \log_e \left[\frac{3{\cdot}389 R_2 \zeta}{(1-\zeta)(1+2\zeta)} \right] ; \tag{10}$$

(*iii*) $$\bar{s} = \frac{1}{3}(1+2\zeta)\, c_f/2 + \left\{ \begin{array}{ll} 0{\cdot}00565\,(1-\zeta)^{2{\cdot}715}, & \zeta \leqslant 1 \\ 0{\cdot}01\,(\zeta-1)^3, & \zeta \geqslant 1 \end{array} \right\} , \tag{11}$$

where $$\zeta \equiv \frac{2}{3} H_{32} - 1 + \sqrt{\left[\frac{2}{3} H_{32} \left(\frac{2}{3} H_{32} - 1 \right) \right]} \quad . \tag{12}$$

These relationships possess certain novel features, of which it may be of interest to indicate the origins.

(*i*) The empirical shape-factor relation, equation (8), is that recommended by Nicoll and Escudier[14]. It should be noted that, in the range $1{\cdot}25 > H_{12} > 0{\cdot}85$, this relation does not properly describe real velocity profiles; examination of the inequality

$$0 < \int_0^\infty (1-u/u_G)^2\, dy = \delta_1 - \delta_2$$

reveals that, for real profiles, $H_{12}\,(\equiv \delta_1/\delta_2)$ cannot take the value unity. However, the error engendered by the use of this relation is negligible, since both $(1+H_{12})F_2$ and $H_{32}F_2$ are small in the region within which it is applied.

(*ii*) The drag law, equation (9), was recommended by Escudier, Nicoll and Spalding[15]; like equation (8) it is applicable to boundary layers both with and without velocity maxima.

(*iii*) The $\bar{s}$ function given in equation (11) is that found by Escudier and Nicoll[16] to fit a large collection of experimental data. Its form was chosen as follows: the expression given in equation (12) was obtained by assuming the velocity profile to be linear between $y=0$, $u=u_G\zeta$ and $y=y_G$, $u=u_G$. The additional assumption that the Prandtl mixing length varies linearly near the wall, and is in a constant ratio with y_G over the outer region of the boundary layer, permitted an expression for the shear-work integral to be deduced:

$$\bar{s} = \zeta c_f/2 + \text{constant} \times |\, 1-\zeta \,|^3.$$

This equation was modified to ensure that $R_2/(1-\zeta)$ remained finite when $R_2=0$; this is necessary if the drag coefficient is to remain finite when $R_2=0$, as must be the case if reasonable predictions are to result.

A suitably modified form of this equation is

$$\bar{s}=\tfrac{1}{3}\ (1+2\zeta)\, c_f/2+A\ |\ 1-\zeta\ |^n, \tag{13}$$

provided $n>1$, and $n\longrightarrow 3$ for $\zeta\longrightarrow\infty$. Values for the constants A and n were obtained by fitting experimental data.

2.3. NUMERICAL CALCULATION PROCEDURE

With the aid of the auxiliary equations, the differential equations, (3) and (4), can be integrated numerically on a digital computer by a standard (Runge-Kutta) forward-integration technique. Initial values of R_2 and R_3 and the variation of u_a with x must, of course, be known. The integration will proceed smoothly except in the immediate vicinity of $\zeta=1$, where special care must be taken to ensure that integration errors do not cause the logarithmic term (l) in the drag law to become singular. Spalding[10] has shown that this quantity varies slowly with R_x; consequently, we may treat it as constant in the small region $|\ R_2\ |<5$ (corresponding with a change in R_x of about 4×10^3).

The solutions so obtained yield R_2, R_3, $c_f/2$, H_{12} etc. as functions of R_x.

3. Comparison of Predicted and Measured Flow Properties

In this section, comparisons are presented between predicted hydrodynamic properties, based on the method outlined in Section 2, and the measurements of Wieghardt[19] and of the present authors. Wieghardt's measurements were obtained in a 1·4 m × 0·4 m test section, the slot geometry being as shown in Fig. 2(*a*). In these measurements, the free-stream velocity was 12·2 m/s and the slot velocity (based on measured mass flow rate through the slot) 17·7 m/s. The maximum velocity at the slot was of the order of 22 m/s.

The measurements recorded by the present authors were obtained in the 18 in × 12 in test section of a wind tunnel designed to investigate wall jets. A detailed description of this apparatus and of the experimental procedures is given by Whitelaw[20]. Two sets of data, obtained in this apparatus, are reported in this paper; the geometric configurations of the two slots used for these experiments are shown in Figs. 2(*b*) and 2(*c*). The main-stream velocities were approximately 88 ft/sec and 68 ft/sec respectively, and the mean slot velocities (obtained by integrating the velocity profiles at the slot) 104 ft/sec and 82 ft/sec respectively. The maximum velocities at the slot were approximately 120 ft/sec and 100 ft/sec respectively.

Values of the integral quantities R_1 and R_2 and of the drag coefficient ($c_f/2$), measured by Wieghardt and by the present authors are shown plotted in Figs. 3(*a*), 3(*b*) and 3(*c*). Also shown in these figures are curves calculated by the procedure outlined in Section 2. Values of R_1 and R_2 are shown, rather than of the more usual combination of R_2 and H_{12} ($\equiv R_1/R_2$), because the shape factor loses its usual significance in the region where R_2 becomes small.

Experimental values of R_1 and R_2 were chosen for the initial conditions required to start the integrations. In the case of Wieghardt, the values were those at the first reported downstream position, i.e. at a distance of 38 slot heights downstream of the slot. For the present measurements, initial conditions were taken at distances

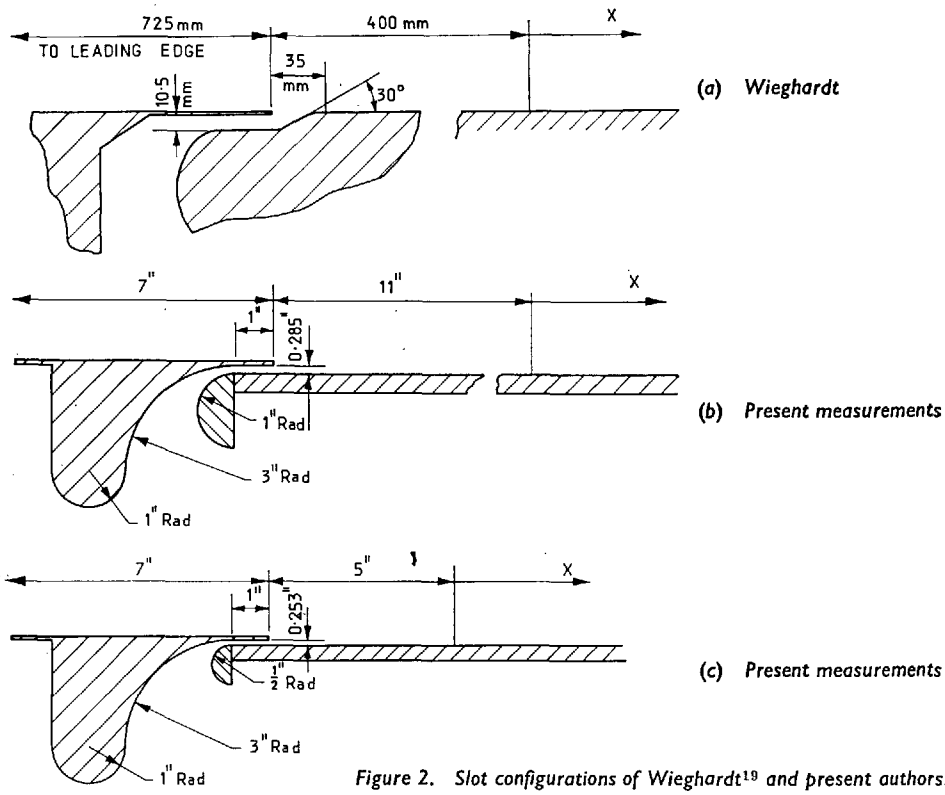


Figure 2. Slot configurations of Wieghardt[19] and present authors.

of 35 and 20 slot heights downstream of the slot, as may be seen from Figs. 2(*b*) and 2(*c*). Velocity profiles were obtained for locations upstream of these starting values but these possessed velocity minima, due to the lip of the slot having a finite thickness, and were not well represented by two parameters.

Comparison of the experimental points and predicted curves of R_1 and R_2 indicate that the predicted values tend to be high. The curves of $c_f/2$ were obtained using these predicted values of R_1 and R_2: in spite of the discrepancies which exist between measured and predicted shape factors, the calculated shear stress is not subject to large errors. In general, the calculated values of $c_f/2$ tend to be higher than measured values, the maximum discrepancy being of the order of 20 per cent. However, there is a general tendency for this discrepancy to decrease as R_x increases; the discrepancy at the larger values of R_x is of the order of 5 per cent. In the case of the measurements of the present authors, the velocity profiles at low values of R_x were not of the universal form. Consequently, the discrepancies at low values of R_x may, in part, result from errors in the "experimental" values, which were derived by Clauser's method.

4. Velocity Profile Generation

4.1. PROFILE ASSUMPTION; IDENTIFICATION OF PROFILE PARAMETERS

The variables normally used to describe boundary layer flows with negative momentum thickness ("wall jets") are the maximum velocity u_m and the half-width

$y_{1/2}$, the distance from the wall where $u=\frac{1}{2}(u_m+u_G)$. Values of these quantities can be obtained from R_2 and R_3 if assumptions are made about the velocity profile.

Escudier and Nicoll[13] have demonstrated that experimental profiles are well represented by the formula adopted by Spalding[10]:

$$z=z_E\,[1+\log_e(\xi)/l']+(1-z_E)\,[1-\cos(\pi\xi)]/2\,. \tag{14}$$

In this equation, z is the non-dimensional velocity u/u_G and ξ the non-dimensional distance y/y_G; z_E and l' are profile parameters which are related to the boundary layer thickness, y_G, and the drag coefficient, $c_f/2$, by the definitions:

$$z_E \equiv \sqrt{(c_f/2)}\,l'/\kappa \tag{15}$$

and

$$l' \equiv \log_e[Eu_G y_G \sqrt{(c_f/2)}/\nu]. \tag{16}$$

The constant E is associated with wall roughness, it has a value of about 7·7 for smooth surfaces; κ is the von Kármán constant, with value taken here as 0·41.

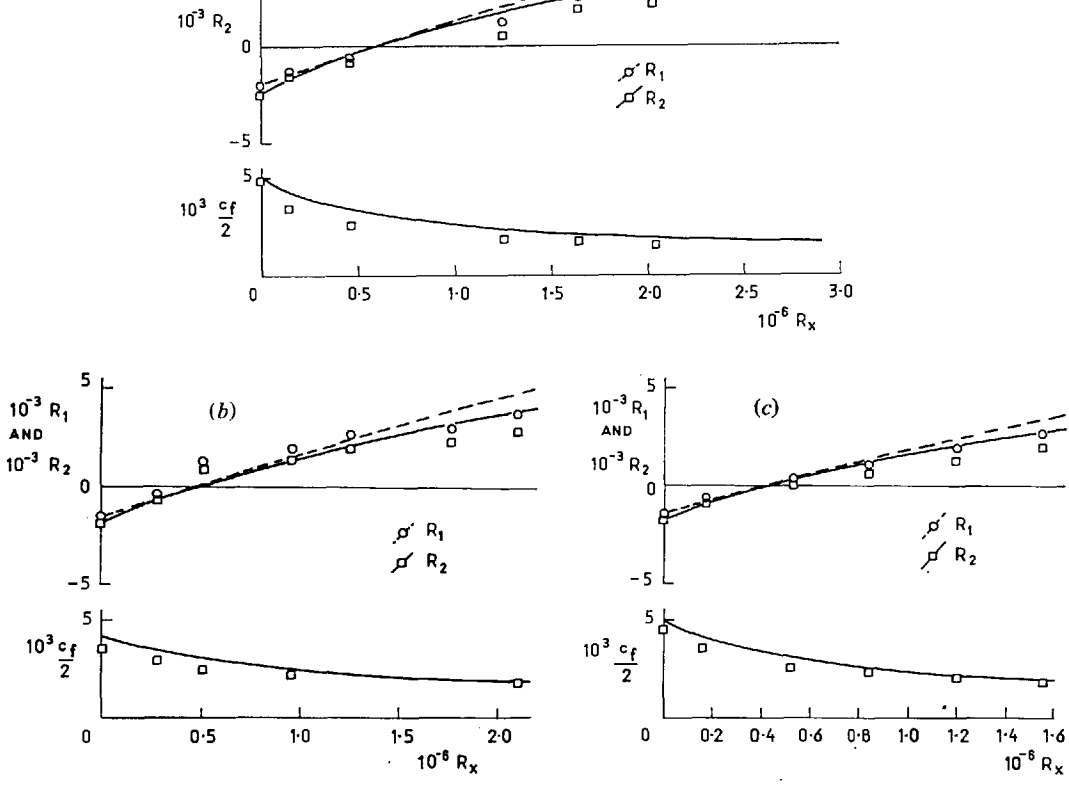


Figure 3. Comparison of measured and predicted variations of R_1, R_2 and $c_f/2$. Data of (a) Wieghardt[19] (b) Present authors (c) Present authors.

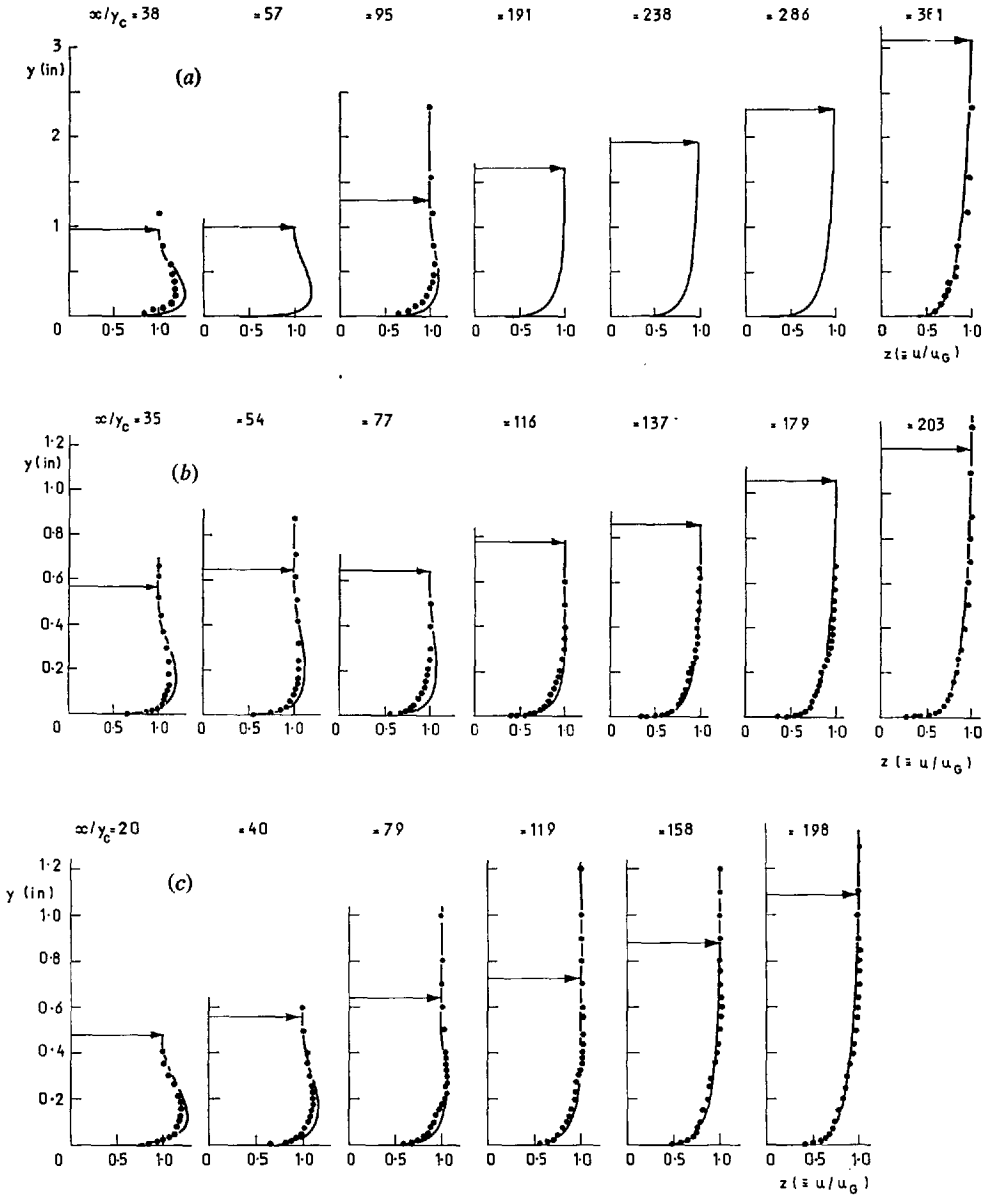


Figure 4. Comparison of measured and predicted velocity profile development. Data of (a) Wieghardt[19] (b) Present authors (c) Present authors.

Thus if z_E and l' are known, values of R_2 and R_3 may readily be obtained with the aid of equation (14). The converse is also true, except in the region where z_E is close to unity; there, it is either impossible to obtain values of z_E and l' from R_2 and R_3, or the values obtained are not unique. However, the constant 3·389 in the expression for l', equation (10), was determined by Escudier, Nicoll and Spalding[15]

to give agreement between values of l and of l' deduced from experimental data. Consequently, it is assumed that the two logarithmic functions are equal; thus

$$\log_e [Eu_G y_G \sqrt{(c_f/2)}/\nu] = \log_e \left[\frac{3{\cdot}389 R_2 \zeta}{(1-\zeta)(1+2\zeta)} \right] .$$

Thus, in the region of z_E close to unity, l' is obtained as just described, $c_f/2$ is obtained from the drag law, equation (9), and z_E and y_G are subsequently obtained from equations (15) and (16).

4.2. COMPARISON BETWEEN MEASURED AND GENERATED PROFILES

The measured velocity profiles are compared with those predicted by the procedure already outlined in Figs. 4(*a*), 4(*b*) and 4(*c*). Figure 4(*a*) presents the data of Wieghardt, and Figs. 4(*b*) and 4(*c*) those of the present authors. As may be seen, the predicted profiles closely resemble the measured ones; the maximum discrepancy is equivalent to an error of about 5 ft/sec in velocity.

5. Conclusions

Application of the general calculation procedure outlined in Section 2 leads to satisfactory predictions of the displacement- and momentum-thickness Reynolds numbers and of the drag coefficient in the region where the former quantities change sign.

The precautions taken to avoid singularities in the immediate vicinity of $R_2=0$ appear to be adequate.

It is possible to use the predicted values of $c_f/2$ and R_2 to generate realistic velocity profiles, in the region under discussion, if a suitable two-parameter family of profiles is assumed.

Acknowledgment

The financial support of the Trustees of the Beit Fellowships is gratefully acknowledged by M. P. Escudier and that of the Ministry of Aviation (Contract numbers PD/37/027 and PD/37/043) by W. B. Nicoll and J. H. Whitelaw.

References

1. TRUCKENBRODT, E. Ein Quadraturverfahren zur Berechnung der laminaren und turbulenten Reibungschicht bei ebener und rotationssymmetrischer Strömung. *Ingenieur Archiv*, Vol. 20, p. 211, 1952.

2. SPENCE, D. A. The development of turbulent boundary layers. *Journal of the Aeronautical Sciences*, Vol. 23, p. 3, 1956.

3. HEAD, M. R. Entrainment in the turbulent boundary layer. ARC R & M 3152, 1960.

4. THOMPSON, B. G. J. A critical review of existing methods of calculating the turbulent boundary layer. ARC Report 26 109, FM 3492, 1964.

5. WALZ, A. Über Fortschritte in Näherungstheorie und Praxis der Berechnung kompressibler laminarer und turbulenter Grenzschichten mit Wärmeübergang. *Zeitschrift für Flugwissenschaften (ZFW)*, Vol. 13, p. 89, 1965.

6. GLAUERT, M. B. The wall jet. *Journal of Fluid Mechanics*, Vol. 1, p. 625, 1956.

7. MYERS, G. E., SCHAUER, J. J. and EUSTIS, R. H. The plane turbulent wall jet flow development and friction factor. Transactions of the American Society of Mechanical Engineers, *Journal of Basic Engineering*, Vol. 85, p. 47, 1963.

8. GARTSHORE, I. S. The streamwise development of two-dimensional wall jets and other two-dimensional turbulent shear flows. PhD Thesis, Department of Mechanical Engineering, McGill University, 1965.

9. HARRIS, G. L. The turbulent wall jet in a moving stream. AGARDograph 97, (1), p. 125, 1965.

10. SPALDING, D. B. A unified theory of friction, heat transfer and mass transfer in the turbulent boundary layer and wall jet. ARC Report 25 925, 1964.

11. PATANKAR, S. V. and SPALDING, D. B. A calculation procedure for heat transfer by forced convection through two-dimensional uniform-property turbulent boundary layers on smooth impermeable walls. Proceedings of the Third International Heat Transfer Conference, Chicago, 1966.

12. SPALDING, D. B. Progress in the development of a unified theory of friction, heat transfer and mass transfer in boundary layers and jets. Imperial College, Department of Mechanical Engineering Tech. Note TWF/TN/10, 1966.

13. ESCUDIER, M. P. and NICOLL, W. B. The entrainment function in turbulent boundary-layer and wall-jet calculations. *Journal of Fluid Mechanics*, Vol. 25, p. 337, 1966.

14. NICOLL, W. B. and ESCUDIER, M. P. Empirical relationships between the shape factors H_{32} and H_{12} for uniform-density turbulent boundary layers and wall jets. *AIAA Journal*, Vol. 4, p. 940, 1966.

15. ESCUDIER, M. P., NICOLL, W. B. and SPALDING, D. B. An explicit drag law for uniform-density turbulent boundary layers on smooth impermeable walls. Imperial College, Department of Mechanical Engineering Tech. Note TWF/TN/12, 1966.

16. SPALDING, D. B. The kinetic-energy deficit equation of the turbulent boundary layer. AGARDograph 97, (1), p. 191, 1965.

17. ESCUDIER, M. P. and SPALDING, D. B. A note on the turbulent uniform-property hydrodynamic boundary layer on a smooth impermeable wall; comparisons of theory with experiment. ARC Current Paper 875, 1965.

18. ESCUDIER, M. P. and NICOLL, W. B. The shear-work integral in calculations of turbulent boundary layers with and without velocity maxima. Imperial College, Department of Mechanical Engineering Tech. Note TWF/TN/18, 1966.

19. WIEGHARDT, K. Hot air discharge for de-icing. AAF Translation No. F-Ts-919—RE, 1946.

20. WHITELAW, J. H. An experimental investigation of the two-dimensional wall jet. ARC Report 28 179, HMT 106, 1966.

Escudier, M.P., Ph.D.

Empirical Relationships between the Shape Factors H_{32} and H_{12} for Uniform-Density Turbulent Boundary Layers and Wall Jets

W. B. NICOLL and M. P. ESCUDIER
Imperial College, London, England

Reprinted from **AIAA Journal**

Volume 4, Number 5, Pages 940–942, May 1966
Copyright, 1966, by the American Institute of Aeronautics and Astronautics,
and reprinted by permission of the copyright owner

Empirical Relationships between the Shape Factors H_{32} and H_{12} for Uniform-Density Turbulent Boundary Layers and Wall Jets

W. B. NICOLL* AND M. P. ESCUDIER†
Imperial College, London, England

THE methods proposed by Rotta,[1] Truckenbrodt,[2] Walz,[3] and Spalding[4] for the prediction of two-dimensional turbulent-boundary-layer flows involve the simultaneous solution of the momentum and kinetic-energy integral equations. Basic to these methods are relationships between the momentum and kinetic-energy thicknesses δ_2 and δ_3, and the displacement thickness δ_1, the wall shear stress and the dissipation integral. In the present note a recommendation is made for the relation between the first three quantities for boundary-layer and wall-jet flows.

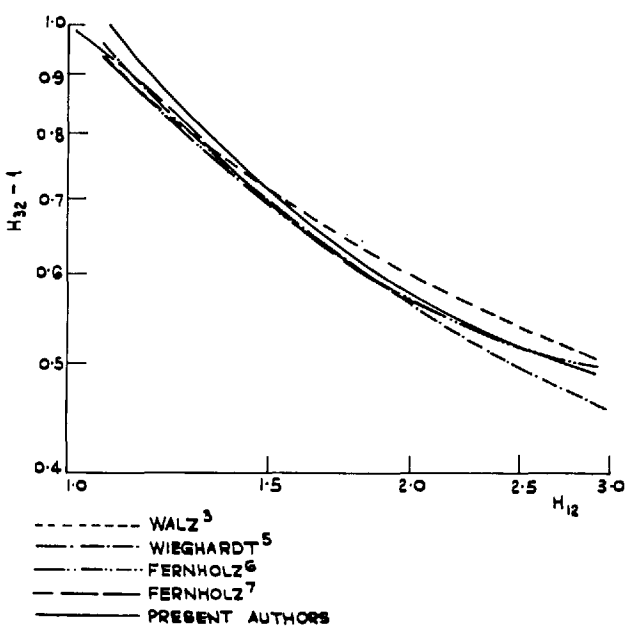


Fig. 1 Recommendations for an $H_{32} \sim H_{12}$ relation for boundary layers.

Received August 17, 1965; revision received January 18, 1966. The support of the Ministry of Aviation (Contract PD/37/27) is gratefully acknowledged by W. B. Nicoll. The authors thank D. B. Spalding for his advice in this work which forms part of a program of research coordinated by Spalding into turbulent flows near walls. Thanks are also due to P. Bradshaw, F. H. Clauser, S. Eskinazi, V. Kruka, G. B. Schubauer, W. Spangenberg, and J. H. Whitelaw for making available unpublished details of their experimental work.

* Lecturer, Department of Mechanical Engineering.
† Beit Scientific Research Fellow.

Reprinted from AIAA JOURNAL

Copyright, 1966, by the American Institute of Aeronautics and Astronautics, and reprinted by permission of the copyright owner

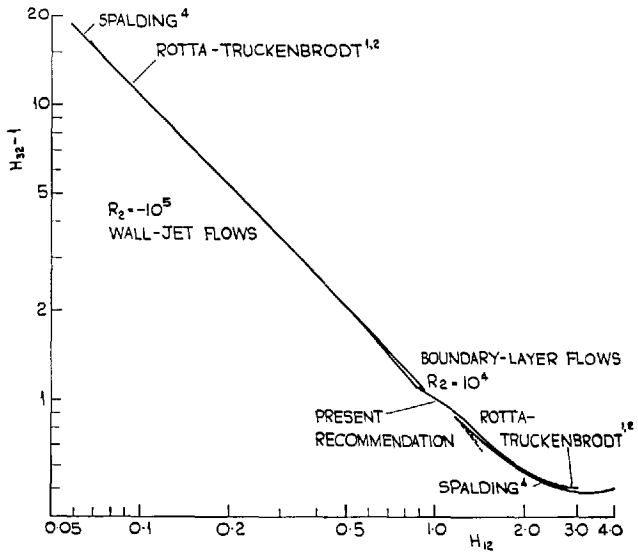


Fig. 2 $H_{32} \sim H_{12}$ relations deduced from theoretical velocity profiles.

It is convenient to express the relation in terms of the velocity-profile shape factors H_{12} and H_{32}, these being defined by

$$H_{12} \equiv \delta_1/\delta_2 \qquad H_{32} \equiv \delta_3/\delta_2$$

where

$$\delta_1 \equiv \int_0^\infty 1 - \frac{u}{u_G}\, dy \qquad \delta_2 \equiv \int_0^\infty \frac{u}{u_G}\, 1 - \frac{u}{u_G}\, dy$$

$$\delta_3 \equiv \int_0^\infty \frac{u}{u_G}\, 1 - \frac{u^2}{u_G{}^2}\, dy$$

and where u is the velocity within the boundary layer in the mainstream direction, u_G is the value of u in the mainstream, and y is the distance from the boundary. Previous recommendations for an $H_{32} \sim H_{12}$ relationship for boundary layers have come from a number of authors, and those of Walz,[3] Wieghardt,[5] and Fernholz[6,7] are shown in Fig. 1.

The present authors are not aware of any previous explicit recommendation for an $H_{32} \sim H_{12}$ relation for wall jets. The assumption of a velocity profile, however, implies such a relation; Truckenbrodt,[2] for example, assumed the two-component profile proposed by Rotta.[1] The Rotta-Truckenbrodt relation is shown in Fig. 2, together with its extension

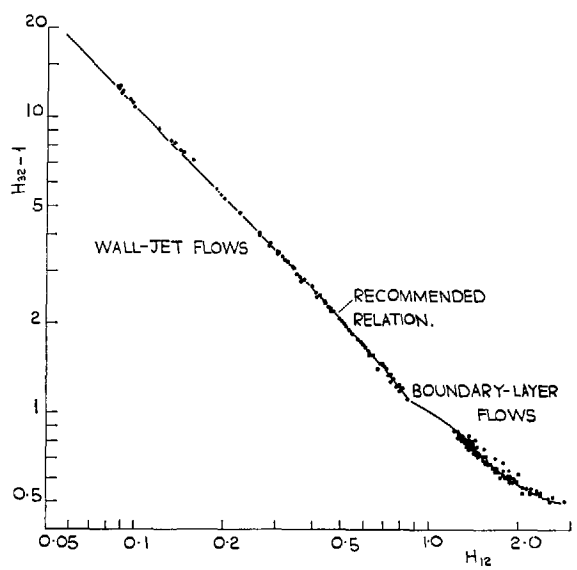


Fig. 3 $H_{32} \sim H_{12}$ data for wall jets and boundary layers.

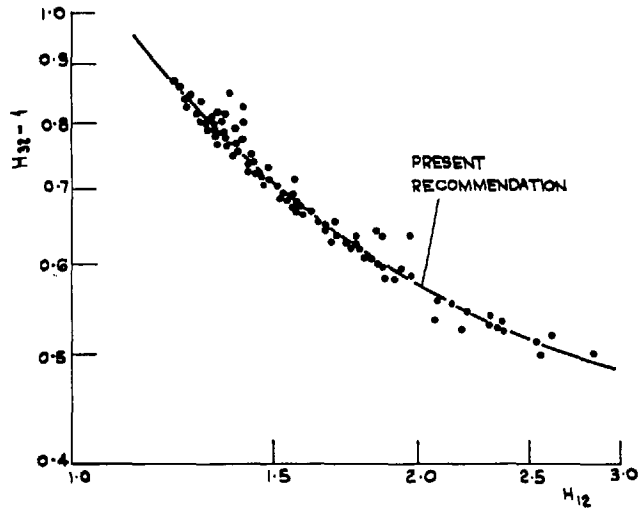


Fig. 4 $H_{32} \sim H_{12}$ data for boundary layers.

to wall-jet flows. Also shown is the relation evaluated from the velocity-profile family adopted by Spalding.[8] The discontinuities in the curves near H_{12} equal to unity are due to the singular behaviour of the shape factors when δ_2 approaches zero. The precise behaviour in this region is sensitive to the profile assumption; since both the profiles referred to are approximate, no significance should be attached to those portions of the curves in Fig. 2 which are shown dashed.

The experimental data of a large number of authors[9–21] have been examined. In each case the values of δ_1, δ and δ_3 were computed from the measured velocity profiles using the same integration procedure (Simpson's rule generalized for integration with unevenly spaced pivotal points). The shape factors so determined are shown in Fig. 3. The data for wall jets are well fitted by

$$H_{32} = 0.82 - \frac{1.10}{H_{12}} \qquad \begin{cases} -6 \times 10^5 \leqslant R_2 \leqslant -4 \times 10^3 \\ 0.06 \leqslant H_{12} \leqslant 0.85 \end{cases}$$

where R_2 is the Reynolds number based upon δ_2 and u_G.

The boundary-layer data, shown in larger scale in Fig. 4, exhibit more scatter than do the wall-jet data. No consistent Reynolds-number or pressure-gradient effect was discernible however. The following relation fits the data with a root-mean-square deviation of only 1.03%

$$H_{32} = 1.431 - \frac{0.0971}{H_{12}} + \frac{0.7749}{H_{12}{}^2} \qquad \begin{cases} 10^3 \leqslant R_2 \leqslant 7.6 \times 10^4 \\ 1.25 \leqslant H_{12} \leqslant 2.8 \end{cases}$$

Figures 1 and 2 indicate that all previous recommendations, including those derived from velocity profiles, yield too small values of H_{32} at small H_{12}. For large H_{12}, the recommendation of Walz[3] gives values of H_{32} which are too large, whereas that of Wieghardt[5] gives values that are too small; the other recommendations are adequate in this region.

The absence of data for H_{12} in the vicinity of unity does not permit the question of the behaviour of the $H_{32} \sim H_{12}$ relation in that region to be answered. For computational purposes, it is recommended that until more information is available, a linear interpolation be used to bridge the gap

$$H_{32} = 2.674 - 0.660\, H_{12} \qquad 0.85 \leqslant H_{12} \leqslant 1.25$$

References

[1] Rotta, J., "On the theory of the turbulent boundary layer," NACA TM 1344 (1953).

[2] Truckenbrodt, E., "Ein Quadraturverfahren zur Berechnung der laminaren und turbulenten Reibungsschicht bei ebener und rotationssymmetrischer Strömung," Ing.-Arch. **20**, 211–228 (1952).

[3] Walz, A., "Beitrag zur Näherungstheorie kompressibler turbulenter Grenzschichten," Deutsche Versuchsanstaldt für Luft- und Raumfahrdt Bericht **136** (1960).

[4] Spalding, D. B., "The kinetic-energy-deficit equation of the turbulent boundary layer," AGARDograph 97, Pt. 1 (1965).

[5] Wieghardt, K., "Turbulente Reibungsschichten," Göttinger Monograph **B5** (1945).

[6] Fernholz, H., "A new empirical relationship between the formparameters H_{32} and H_{12} in boundary layer theory," J. Roy. Aeronaut. Soc. **66**, 588–589 (1962).

[7] Fernholz, H., "Halbempirische Gesetze zur Berechnung turbulenter Grenzschichten nach der Methode der Integralbedingungen," Ing.-Arch. **33**, 384–395 (1964).

[8] Spalding, D. B., "A unified theory of friction, heat transfer and mass transfer in the turbulent boundary layer and wall jet," Brit. Aeronaut. Res. Coun. **25**, 988 (1964).

[9] Bradshaw, P. and Ferriss, D. H., "The response of a retarded equilibrium turbulent boundary layer to the sudden removal of pressure gradient," National Physical Lab. Aerodynamics Rept. 1145, Brit. Aeronaut. Res. Coun. **26**, 758 (1965).

[10] Clauser, F. H., "Turbulent boundary layers in adverse pressure gradients," J. Aerospace Sci. **21**, 91–108 (1954).

[11] Escudier, M. P., unpublished work, Imperial College, London (1965).

[12] Fage, A. and Falkner, V. M., "An experimental determination of the intensity of friction on the surface of an aerofoil," British Aeronautic Research Council R&M 1315 (1930).

[13] Herring, H. J. and Norbury, J. F., "Some experiments on equilibrium turbulent boundary layers in favourable pressure gradients," Princeton Univ., Dept. Aerospace and Mechanical Sciences FLD Rept. 15 (1963).

[14] Klebanoff, P. S., "Characteristics of turbulence in a boundary layer with zero pressure gradient," NACA Rept. **1247** (1955).

[15] Kruka, V. and Eskinazi, S., "The wall jet in a moving stream," J. Fluid Mech. **20**, 555–579 (1964).

[16] Moses, H. L., "The behaviour of turbulent boundary layers in adverse pressure gradients," Massachusetts Institute of Technology, Gas Turbine Lab. Rept. 73 (1964).

[17] Newman, B. G., "Some contributions to the study of the turbulent boundary layer near separation," Australian Dept. Supply Rept. ACA-53 (1951).

[18] Nicoll, W. B., "Wall jet velocity profiles and entrainment," Imperial College, London, Mechanical Engineering Dept. Rept. IC/HRJ/23 (1965).

[19] Schubauer, G. B. and Klebanoff, P. S., "Investigation of separation of the turbulent boundary layer," NACA Rept. 1030 (1951).

[20] Schubauer, G. B. and Spangenberg, W., "Forced mixing in boundary layers," J. Fluid Mech. **8**, 10–32 (1960).

[21] Whitelaw, J. H., unpublished work, Imperial College, London (1965).

Escudier, M.P., Ph.D.

C.P. No. 875

C.P. No. 875



MINISTRY OF AVIATION

AERONAUTICAL RESEARCH COUNCIL

CURRENT PAPERS

A Note on the Turbulent Uniform-Property Hydrodynamic Boundary Layer on a Smooth Impermeable Wall; Comparisons of Theory With Experiment

By

M. P. Escudier and D. B. Spalding

Imperial College

LONDON: HER MAJESTY'S STATIONERY OFFICE

1966

Price 5s. 6d. net

A Note on the Turbulent Uniform-Property Hydrodynamic Boundary Layer on a Smooth Impermeable Wall; Comparisons of Theory with Experiment

- By -
M. P. Escudier and D. B. Spalding,
Imperial College

C.P. No.875*

August, 1965

SUMMARY

The recent experimental data of Bradshaw and Ferriss[1] are compared with generalisations deduced from earlier data, in respect of the mixing-length distribution and the dissipation integral; the agreement is satisfactory.

Also presented is a preliminary theory of boundary-layer development, employing an empirical formula for the relation between the dissipation integral, the drag coefficient and the shape factor; the integral momentum and kinetic-energy equations are solved numerically. The predictions of this theory are compared, in respect of shape factor, with the experiments of Bradshaw and Ferriss and those of many other experimenters. The agreement is satisfactory except for large adverse pressure gradient, where divergences of both positive and negative sign are observed; the reasons for these divergences are discussed.

1. Introduction

Bradshaw and Ferriss[1] have recently published the results of a set of particularly careful and detailed measurements on turbulent boundary layers in adverse pressure gradients; specifically, they studied both: an equilibrium boundary layer; and one in which the adverse pressure gradient fell from a positive value upstream to zero downstream. As Bradshaw and Ferriss rightly remark, their data can be used to test the generality of prediction procedures for turbulent boundary layers; the test will be particularly significant for prediction procedures which have been adjusted to fit data for boundary layers in which the adverse pressure gradient increases in the streamwise direction.

The present authors are developing prediction procedures for turbulent boundary layers, and have accordingly made use of the opportunity provided by Ref. 1 ; the results of their study are contained in the present note; also provided are comparisons of prediction and experiment for a large number of other boundary layers. The latter comparisons are provided to give perspective to the study of the data of Ref. 1 .

The impression might be gained from the paper of Bradshaw and Ferriss that the boundary layers which they have studied differ greatly, from those investigated by earlier authors, in respect of the relations between the profiles of shear stress and velocity profile. In the present note we therefore make some comparisons which show that the similarities are at least as pronounced as the differences; it cannot indeed be said with certainty that the latter are not merely the result of experimental scatter.

2./

*Replaces A.R.C.27 302

2. The Relation Between Shear Stress and Velocity

In order to demonstrate the common features of the Bradshaw-Ferriss and other turbulent boundary layers, we make use, as a definition, of the Prandtl[2] mixing-length formula:

$$\ell \equiv \left\{ \frac{\tau}{\rho \left|\frac{\partial u}{\partial y}\right| \left(\frac{\partial u}{\partial y}\right)} \right\}^{\frac{1}{2}}, \qquad \ldots (1)$$

where ℓ is the mixing length,

τ is the shear stress,

ρ is the fluid density,

u is the (time-mean) velocity in the mainstream direction, and

y is the distance normal to the wall.

With the aid of this formula, $\ell(y)$ can obviously be evaluated from data for $\tau(y)$ and $u(y)$.

We choose to represent the $\ell(y)$ distributions resulting from our evaluations in dimensionless form; both ℓ and y have been divided by the y-value of the outer edge of the boundary layer, y_G. Thus:

$$\lambda \equiv \ell / y_G \ , \qquad \ldots (2)$$

$$\xi \equiv y / y_G \ . \qquad \ldots (3)$$

The values of y_G were determined by inspection of the reported velocity profiles, with an estimated accuracy of $\pm 5\%$.

The resulting mixing-length distributions across the boundary layers are shown in Fig.1*, which has been extracted from a wider survey by Escudier[3]. The curves represent the experimental data; the two straight lines, which are repeated in each graph to provide a base of reference, represent the formulae which have been used by the authors elsewhere as the foundation of a prediction procedure[4].

$$\left.\begin{aligned} 0 \leqslant \xi \leqslant \lambda_G/\kappa \ : \ \lambda &= \kappa \xi \ , \\ \lambda_G/\kappa < \xi \leqslant 1 \ : \ \lambda &= \lambda_G \ , \end{aligned}\right\} \qquad \ldots (4)$$

where the values 0·075 and 0·4 have been chosen for λ_G and κ respectively.

The data of Bradshaw and Ferriss appear in graphs (a) and (b) of Fig.1; evidently the $\lambda(\xi)$ profiles of these authors do not differ greatly among themselves; and they are not radically different from those of the other authors. Further data could have been taken from Ref. 3 to support the same trends.

When assessing the degree of similarity between the curves, it is helpful to remember:

(i) That the shear stress is proportional to the square of mixing length; so the $\lambda(\xi)$ representation tends to minimise the differences in the shear-stress-versus-velocity relation;

(ii)/

---

* A list of all figures, with brief descriptions, is given on page 14.

(ii) That where ξ lies between 0·8 and 1·0, although the mixing length tends to rise rapidly and the differences between the profiles may be great, the velocity gradients are small; consequently the shear stresses are small and errors in λ are of slight importance;

(iii) The values of λ rest on determinations of the slope of the velocity profile; the inevitable experimental error thus introduces a large scatter in the $\lambda(\xi)$ curves. In this respect therefore the method of plotting magnifies the differences between boundary layers.

Fig. 1 is the first piece of evidence which we put forward for the similarity between the Bradshaw-Ferriss boundary layers and those studied by earlier authors.

3. The Dissipation Integral

The method of boundary-layer prediction pioneered by Rotta[5] and Truckenbrodt[6], based on the integral momentum and kinetic-energy equations, requires knowledge of the dissipation integral $\bar{s}$, defined by:

$$\bar{s} \equiv \frac{1}{\rho_G u_G^3} \int_0^{y_G} \tau \frac{\partial u}{\partial y} \, dy \quad . \qquad \ldots (5)$$

Here ρ_G and u_G are respectively the density and velocity of the main stream. The quantity $\bar{s}$ is sometimes represented symbolically by: $(d_1 + t_1)/(\rho U^3)$.

As has been shown elsewhere, the particular recommendations for the $\bar{s}$ function made in Refs. 5 and 6 are valid only in very restricted circumstances; better ones can be based on the mixing-length profile of equation (4) and on suitable velocity-profile assumptions[4]. Here however we draw attention to an empirical formula derived by the present authors from a least-squares analysis of shear-stress data, measured with hot-wire equipment in a variety of boundary-layer situations by: Bradshaw and Ferriss[1], Klebanoff[7], Moses[8], Newman[9], Sandborn and Slogar[10], and Schubauer and Klebanoff[11].

The formula is:

$$\bar{s} = 0{\cdot}547 \left(\frac{c_f}{2} \right) + 10^{-3}(2{\cdot}107H - 2{\cdot}286) \quad , \qquad \ldots (6)$$

where c_f is the local drag coefficient, and H is the shape factor (displacement thickness divided by momentum thickness).

Fig. 2 displays the data from which equation (6) was derived. The plain dots represent the data of references 7 to 11 ; the encircled dots represent the data of Bradshaw and Ferriss[1]. Fig.2 gives little reason for believing that the latter data deviate radically from the former. The deviations that exist may be systematic; but they are of the order of a few tens per cent.

Fig.2 is the second item of evidence for the similarity between the data of reference 1 and those of other workers.

4./

4. The Prediction of the Development of Turbulent Boundary Layers

The present authors have investigated, among other methods* of predicting boundary-layer development on smooth impermeable walls when the density is uniform, the implications of the following set of assumptions:-

(i) The dissipation integral obeys equation (6);

(ii) The local drag coefficient is related to the Reynolds number and the shape factor by the well-known Ludwieg-Tillmann relation (12).

(iii) The shape factor H is related to the quantity H_3, representing the kinetic-energy thickness divided by the momentum thickness, by the formulae recommended by Nicoll and Escudier[13], namely:

$$2{\cdot}8 \geq H \geq 1{\cdot}25 \quad : \quad H_3 = 1{\cdot}431 - 0{\cdot}097/H + 0{\cdot}775/H^2 . \qquad \ldots (7)$$

The data from which this formula was deduced are shown in Fig.3.

Predictions have been made, by this means, for many of the experiments which can be found in the literature. The differential equations in question were integrated numerically, for the prescribed main-stream velocity distribution, and the predicted values of momentum thickness, shape factor, etc., were then compared with the reported values. The initial conditions of the integration were the experimental values of momentum thickness and shape factor; but otherwise no individual adjustments were made to improve the agreement between prediction and experiment.

Some of the results of the comparison are displayed in Fig.4, the shape factor H being the boundary-layer property selected for consideration. The abscissa is the length Reynolds number, R_x, defined by:

$$R_x \equiv \int_0^x (\rho_G u_G / \mu_G)\, dx \ , \qquad \ldots (8)$$

where x is the distance along the surface in the mainstream direction and μ_G is the fluid viscosity. The individual diagrams are distinguished by the names of the experimenters who reported the data; dots represent experimental values while curves represent predictions.

Inspection of the diagrams, with particular reference to the degree of agreement between prediction and experiment, seems to justify the following conclusions:-

(i) Apart from a few failures, the extent of agreement is generally satisfactory, at least when judged against the poor results reported in Thompson's recent survey[14] of the predictive ability of earlier theories.

(ii) The predictions for the two Bradshaw-Ferriss boundary layers are not notably better or worse than those for other experiments. (Incidentally, a complete failure to predict the H-variation for the first u_G-x variation reported in Ref. 1 , revealed that the reported u_G values were in error; the diagram marked "Bradshaw and Ferris 1" is based on corrected values, subsequently confirmed by those authors.)

The/

*For example, as was mentioned earlier, a procedure has been developed which is based on the mixing length formula (4)[4].

The second Bradshaw-Ferriss experiment, for the "recovering" boundary layer (H diminishing in the main-stream direction) is not the only one of its kind, as may be seen from Fig.4. For example, the experiments of Klebanoff and Diehl[15] are of this character; in their case the disturbance was a roughness element, distributed or local, upstream of a flat surface. Also two of the experiments of Moses[8] embody the recovery from the effects of an adverse pressure gradient; our theory predicts one of them satisfactorily; but the computation for the other was stopped when H attained the separation value of 3.

(iii) Although there are some fairly successful predictions of separation (e.g. Moses 2, Schubauer and Spangenberg[23] C, E and F), the failures are more numerous; most of these are such that H rose more rapidly than predicted.

(iv) On some cases, the disagreement between prediction and experiment may perhaps be more probably ascribed to the latter than the former. For example, the downstream H-values of experiments 1 and 2 of Klebanoff and Diehl seem implausibly high.

5. Discussion of Fig.4

The comparisons of theory with experiment in Fig.4 do not, of course, settle the question of whether it is possible to predict boundary-layer development with a theory which rests, as does the present one, on the assumption that the shear-stress profile is uniquely determined by the velocity profile; for no attempt has so far been made systematically to seek the $\bar{s}$ and c_f functions of H and Reynolds number which give the best predictions.

That the $\bar{s}$ function must be chosen with care can be recognised by writing the equation for dH/dx which follows from the momentum and kinetic-energy equations, namely:

$$\delta_2 \frac{dH}{dx} = \frac{dH}{dH_3} \left\{ 2\bar{s} - H_3 \left(\frac{c_f}{2} \right) + H_3 \, (H - 1) F_2 \right\}, \qquad \ldots (9)$$

where δ_2 stands for the momentum thickness, dH/dH_3 is a negative quantity varying somewhat with H, and:

$$F_2 \equiv \frac{\delta_2}{u_G} \frac{du_G}{dx} \, . \qquad \ldots (10)$$

Near separation, c_f is of course small and F_2 is negative, dH/dx is therefore proportional to the difference between the dissipation integral and the quantity $\frac{1}{2} H_3 (H - 1)(-F_2)$. Obviously, a 10% error in the $\bar{s}$ value may easily change dH/dx from a positive to a negative value when the two terms have about the same size. It is therefore not surprising, in view of the scatter displayed on Fig.2, and of the unsophisticated nature of equation (6), that predictions are sometimes in error when $-F_2$ is large.

When weighing this consideration, two points deserve particular attention. The first is that the aerodynamicist's interest in separation lies chiefly in preventing its occurrence; and engineering good practice demands that a safety factor should be incorporated in a design. For this purpose, the criterion is already quite clear; the quantity $-F_2$ should never be allowed to increase above (say) 0·002. The predictions of F_2 by the present authors are fortunately quite accurate.

The/

The second point is that there are many possible influences on the $\bar{s}$ function, the systematic exploration of which may lead to improved methods of prediction. Among these influences are: free-stream turbulence, the rate of enlargement of the boundary-layer thickness, the rate of change of the velocity profile, the convexity of the surface, and the local pressure gradient itself. If these influences exist at a significant level, research can disclose them; and, whether they require expression by algebraic equations or by differential ones, modern computing facilities are more than adequate for their incorporation in the prediction procedure.

6. Conclusions

It is the opinion of the present authors that the experimental results of Bradshaw and Ferriss[1] reveal a heartening similarity to exist between their boundary layers and those reported elsewhere in the literature. The near universality of the mixing-length distribution may form a valuable jumping-off point for theoretical studies.

The procedure outlined in Section 4 is fairly successful in predicting the development of the boundary-layer shape factor; but it is clearly not likely to be the optimum procedure, even among procedures of its own kind. The exploration of the factors influencing the dissipation integral is one of the most urgent topics of turbulent-boundary-layer research.

7. Acknowledgements

The authors' thanks are due to Mr. P. Bradshaw, Prof. F. H. Clauser, and Mr. W. Spangenberg for making available unpublished details of their experimental work. Thanks are also due to Mr. J. A. P. Stoddart for supplying tabulated information about the Ludwieg-Tillmann experiments.

List of Symbols/

List of Symbols

		Equation of first mention
$c_f/2$	Local drag coefficient	(6)
F_2	Pressure-gradient parameter	(9)
H, H_3	Boundary-layer shape factors	(6), (7)
ℓ	Prandtl mixing length	(1)
R_x	Length Reynolds number	(8)
$\bar{s}$	Dissipation integral	(5)
u	Velocity of fluid in mainstream direction	(1)
u_G	Value of u in mainstream	(5)
x	Distance along wall in mainstream direction	(8)
y	Distance from wall in direction towards the fluid	(1)
y_G	Value of y at the outer "edge" of the boundary layer	(2)
δ_2	Boundary-layer momentum thickness	(9)
$\varkappa$	Constant appearing in mixing-length distribution near the wall	(4)
λ	Non-dimensional mixing length	(2)
λ_G	Value of λ in outer region of boundary layer	(4)
μ_G	Dynamic viscosity of fluid in mainstream	(8)
ξ	Non-dimensional distance from wall	(3)
ρ	Fluid density	(1)
ρ_G	Value of ρ in mainstream	(5)
τ	Shear stress in fluid	(1)

Subscript

G	Appertaining to conditions in the mainstream

References/

References

No.	Author(s)	Title, etc.
1	P. Bradshaw and D. H. Ferriss	The response of a retarded equilibrium turbulent boundary layer to the sudden removal of pressure gradient. A.R.C.26 758, March, 1965.
2	L. Prandtl	Bericht über Untersuchungen zur ausgebildeten Turbulenz. ZAMM 5, pp.136-139, 1925.
3	M. P. Escudier	The distribution of the mixing length in turbulent flows near walls. Mech. Eng. Dept. Imperial College, TWF/TN/1, 1965.
4	M. P. Escudier, W. B. Nicoll, S. V. Patankar and D. B. Spalding	Unpublished work at Imperial College.
5	J. Rotta	Über die Theorie der turbulenten Grenzschichten Strom. Forsch. Nr.1 (1950). Transl. as "On the theory of the turbulent boundary layer". NACA TM 1344, 1953.
6	E. Truckenbrodt	Ein Quadraturverfahren zur Berechnung der laminaren und turbulenten Reiburg-Schicht bei ebener und rotations symmetrischer Strömung. Ing.-Arch. 20, pp.211-228, 1952.
7	P. S. Klebanoff	Characteristics of turbulence in a boundary layer with zero pressure gradient. NACA Rep.1247, 1955.
8	H. L. Moses	The behaviour of turbulent boundary layers in adverse pressure gradients. MIT GTL Rep. No.73, 1964.
9	B. G. Newman	Some contributions to the study of the turbulent boundary layer near separation. ARCC Rep. ACA-53, 1951.
10	V. A. Sandborn and R. J. Slogar	Study of the momentum distribution of turbulent boundary layers in adverse pressure gradients. NACA TN 3264, 1955.
11	G. B. Schubauer and P. S. Klebanoff	Investigation of separation of the turbulent boundary layer. NACA Rep.1030, 1951.

12/

No.	Author(s)	Title, etc.
12	H. Ludwieg and W. Tillman	Untersuchungen über die Wandschubspannung in Turbulenten Reibungsschichten. Ing.-Arch. 17, pp.288-299, (1949). Transl. as "Investigations of the wall shearing stress in turbulent boundary layers". A.R.C.14 800, April, 1952.
13	W. B. Nicoll and M. P. Escudier	Empirical relationships between the shape factors H_{32} and H_{12} for uniform-density turbulent boundary layers and wall jets. Mech. Eng. Dept. Imperial College, TWF/TN/3, 1965.
14	B. G. J. Thompson	A critical review of existing methods of calculating the turbulent boundary layer. A.R.C. R. & M.3447, August, 1964.
15	P. S. Klebanoff and Z. W. Diehl	Some features of artificially thickened fully developed turbulent boundary layers with zero pressure gradient. NACA Rep.1110, 1952.
16	G. G. Brebner and J. A. Bagley	Pressure and boundary-layer measurements on a two-dimensional wing at low speed. A.R.C. R. & M.2886, February, 1952.
17	F. H. Clauser	Turbulent boundary layers in adverse pressure gradients. J. Aero. Sci. 21, pp.91-108, 1954.
18	A. E. von Doenhoff and N. Tetervin	Determination of general relations for the behaviour of turbulent boundary layers. NACA Rep.772, 1943.
19	A. Fage	Profile and skin-friction aerofoil drags. A.R.C. R. & M.1852, April, 1938.
20	D. E. Gault	Boundary-layer and stalling characteristics of the NACA 63-009 airfoil section. NACA TN 1894, 1949.
21	H. J. Herring and J. F. Norbury	Some experiments on equilibrium turbulent boundary layers in favourable pressure gradients. Princeton University, Dept. Aerospace and Mech. Sci. FLD No.15, 1963.

22/

No.	Author(s)	Title, etc.
22	G. B. Schubauer and P. S. Klebanoff	Investigation of separation of the turbulent boundary layer. NACA Rep.1030, 1951.
23	G. B. Schubauer and W. Spangenberg	Forced mixing in boundary layers. J. Fluid Mech., 8, (1), pp.10-32, 1960.
24	F. Schultz-Grunow	Neues Reibungswiderstandsgezetz für glatte Platten. Luftfahrtforschung, 17, pp.239-246, (1940). Transl. as "New frictional resistance law for smooth plates". NACA TM 986, 1941.

Description/

Description of Figures

Fig. 1. Experimental mixing-length profiles for various turbulent boundary layers. $\lambda \equiv \ell/y_G$, $\xi \equiv y/y_G$; $\ell \equiv$ Prandtl mixing length; $y_G \equiv$ boundary-layer thickness.

(a) Bradshaw and Ferris[1] 1: Equilibrium boundary layer.

(b) Bradshaw and Ferriss[2] 2: Boundary layer recovering from adverse pressure gradient.

(c) Klebanoff[7] : Flat-plate boundary layer.

(d) Moses[8]: Axisymmetric boundary layer along a horizontal cylinder, adverse pressure gradient.

(e) Newman[9] 1: Boundary layer on rear-stalling aerofoil.

(f) Newman[9] 2: Boundary layer on rear-stalling aerofoil.

Fig.2. Experimental data for the dissipation integral $\bar{s}$ related to the local drag coefficient $\frac{c_f}{2}$ and to the shape factor H.

Fig.3. Experimental data for the relation between the shape factors H_3 and H.

Fig.4. Comparison of measured shape factors with the predictions (curves) made by the method described in the text.

Bradshaw and Ferriss[1] 1: Equilibrium boundary layer.

Bradshaw and Ferriss[1] 2: Boundary layer recovering from adverse pressure gradient.

Brebner and Bagley[16] 1: Symmetrical wing RAE 101, $\alpha = 0°$.

Brebner and Bagley[16] 2: Symmetrical wing RAE 101, $\alpha = 4{\cdot}09°$.

Brebner and Bagley[16] 3: Symmetrical wing RAE 101, $\alpha = 8{\cdot}18°$.

Clauser[17] 1: Equilibrium boundary layer, pressure distribution 1.

Clauser[17] 2: Equilibrium boundary layer, pressure distribution 2.

von Doenhoff and Tetervin[18] 1: Aerofoil NACA 65 (216) - 222 (approx.), $R = 0{\cdot}92 \times 10^6$, $\alpha = 8{\cdot}1°$.

von Doenhoff and Tetervin[18] 2: Aerofoil NACA 65 (216) - 222 (approx.), $R = 2{\cdot}67 \times 10^6$, $\alpha = 8{\cdot}1°$.

von Doenhoff and Tetervin[18] 3: Aerofoil NACA 65 (216) - 222 (approx.), $R = 2{\cdot}64 \times 10^6$, $\alpha = 10{\cdot}1°$.

von Doenhoff and Tetervin[18] 4: Aerofoil NACA nose-opening shape 13, $R = 4{\cdot}18 \times 10^6$, $\alpha = 9{\cdot}1°$.

Fage[19] 1: Joukowski aerofoil, $R = 1{\cdot}665 \times 10^6$.

Fage[19] 2: Joukowski aerofoil, $R = 1{\cdot}248 \times 10^6$.

Gault[20] 1: Aerofoil NACA 63-009, $\alpha = 0°$.

Gault[20] 2: Aerofoil NACA 63-009, $\alpha = 4°$.

Gault[20] 3: Aerofoil NACA 63-009, $\alpha = 6°$.

Gault[20] 4: Aerofoil NACA 63-009, $\alpha = 8{\cdot}5°$.

Herring and Norbury[21]: Equilibrium boundary layer, $\beta \approx -0{\cdot}35$.

Klebanoff and Diehl[15] 1: Flat-plate boundary layer, natural transition.

Klebanoff and Diehl[15] 2: Flat-plate boundary layer recovering from 0·04 in. rod disturbance.

Klebanoff and Diehl[15] 3: Flat-plate boundary layer recovering from 0·25 in. rod disturbance.

Klebanoff and Diehl[15] 4: Flat-plate boundary layer recovering from mesh-screen disturbance.

Klebanoff and Diehl[15] 5: Flat-plate boundary layer recovering from sandpaper-strip disturbance, $u_G = 35$ ft/s.

Klebanoff and Diehl[15] 6: Flat-plate boundary layer recovering from sandpaper-strip disturbance, $u_G = 55$ ft/s.

Klebanoff and Diehl[15] 7: Flat-plate boundary layer recovering from sandpaper-strip disturbance, $u_G = 108$ ft/s.

Ludwieg and Tillmann[12] A: Moderate adverse pressure gradient.

Ludwieg and Tillmann[12] B: High adverse pressure gradient.

Ludwieg and Tillmann[12] C: Favourable pressure gradient.

Ludwieg and Tillman[1] (unpublished) : Adverse pressure gradient.

Ludwieg and Tillman[2] (unpublished) : Adverse pressure gradient.

Ludwieg and Tillman[3] (unpublished) : Adverse pressure gradient.

Ludwieg and Tillmann[4] (unpublished) : Adverse pressure gradient.

Moses[8] 1: Axisymmetric boundary layer along horizontal cylinder, adverse pressure gradient.

Moses[8] 2: Axisymmetric boundary layer along horizontal cylinder, adverse pressure gradient.

Moses[8] 3: Axisymmetric boundary layer along horizontal cylinder, adverse pressure gradient.

Moses[8] 4: Axisymmetric boundary layer along horizontal cylinder, adverse pressure gradient.

Moses[8] 5: Axisymmetric boundary layer along horizontal cylinder, adverse pressure gradient followed by near-zero favourable pressure gradient.

Moses/

Moses[8] 6: Axisymmetric boundary layer along horizontal cylinder, adverse pressure gradient followed by near-zero pressure gradient.

Newman[9]: Symmetrical rear-stalling aerofoil.

Sandborn and Slogar[10] : Adverse pressure gradient.

Schubauer and Klebanoff[11]: Convex wall, adverse pressure gradient.

Schubauer and Spangenberg[23] A: Moderate adverse pressure gradient.

Schubauer and Spangenverg[23] B: Adverse pressure gradient.

Schubauer and Spangenberg[23] C: Moderate adverse pressure gradient.

Schubauer and Spangenberg[23] D: Adverse pressure gradient.

Schubauer and Spangenberg[23] E: Adverse pressure gradient.

Schubauer and Spangenberg[23] F: Adverse pressure gradient.

Schultz-Grunow[24]: Flat-plate boundary layer.

SJ

D 74195/1/125875 K4 10/66 XL

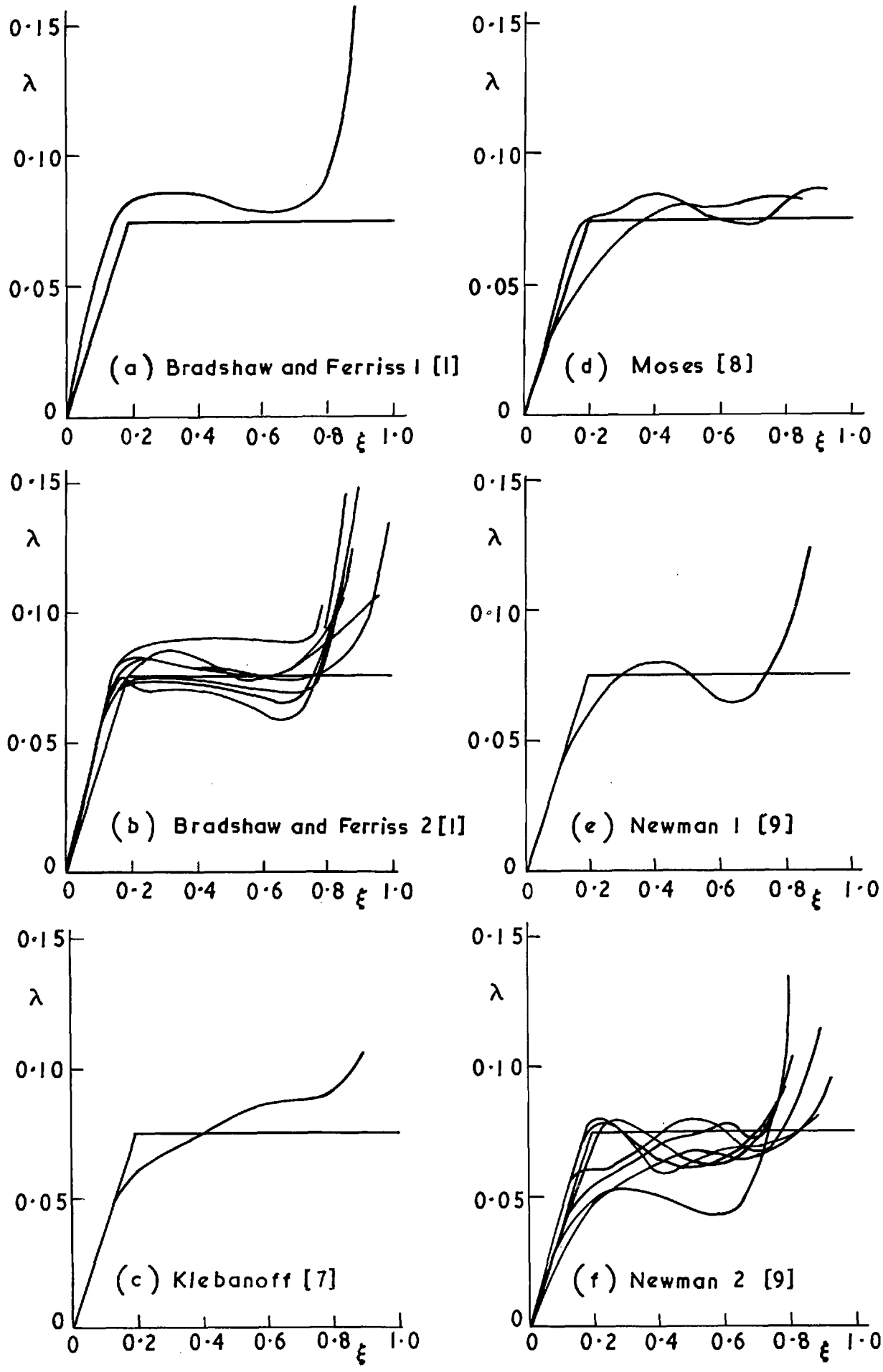


FIG. 1 Experimental mixing-length profiles for various turbulent boundary layers. $\lambda \equiv l/y_G$, $\xi \equiv y/y_G$; $l \equiv$ Prandtl mixing length ; $y_G =$ boundary-layer thickness

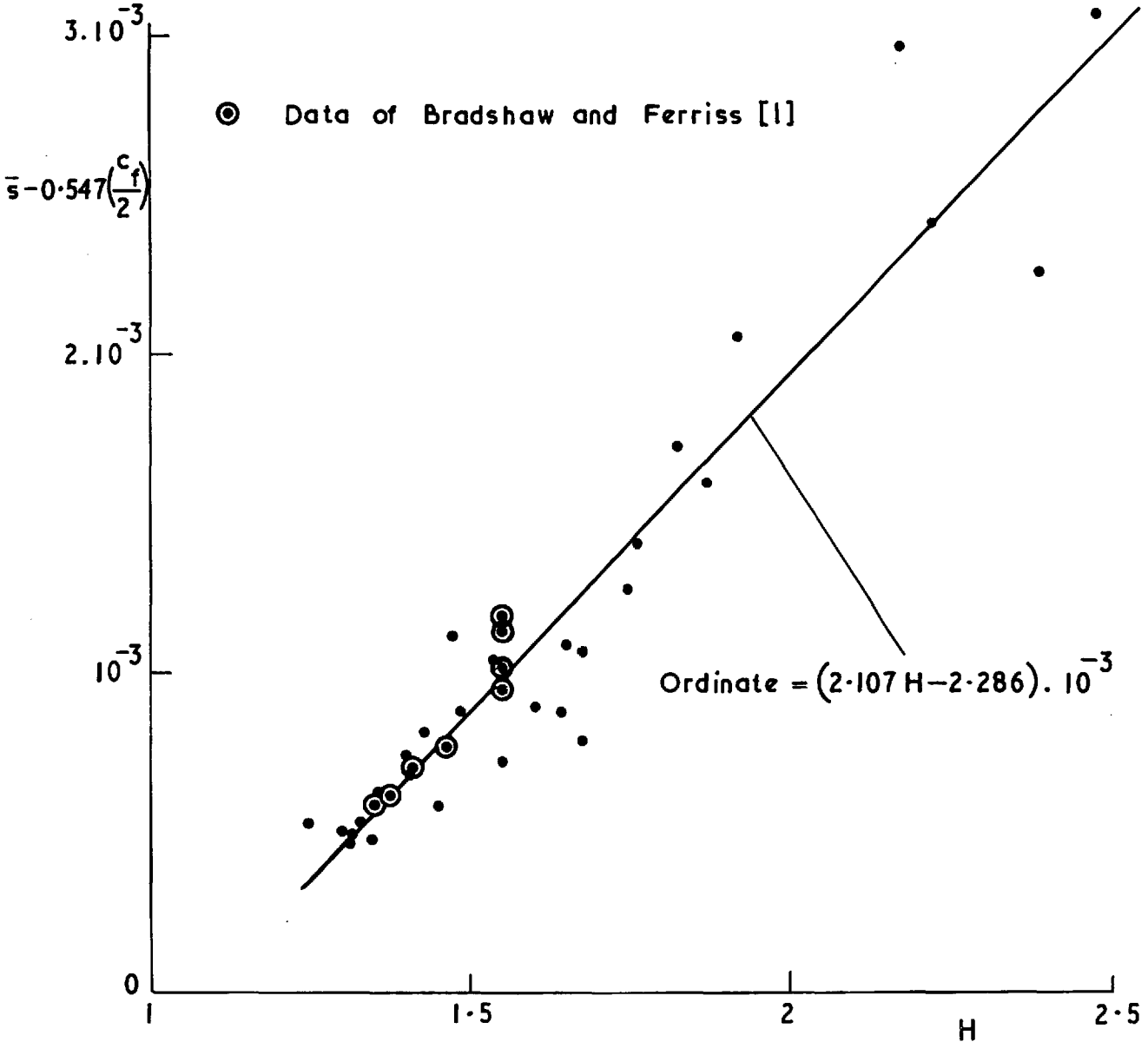


FIG. 2 Experimental data for the dissipation integral $\bar{s}$, related to the local drag coefficient $c_f/2$ and to the shape factor H

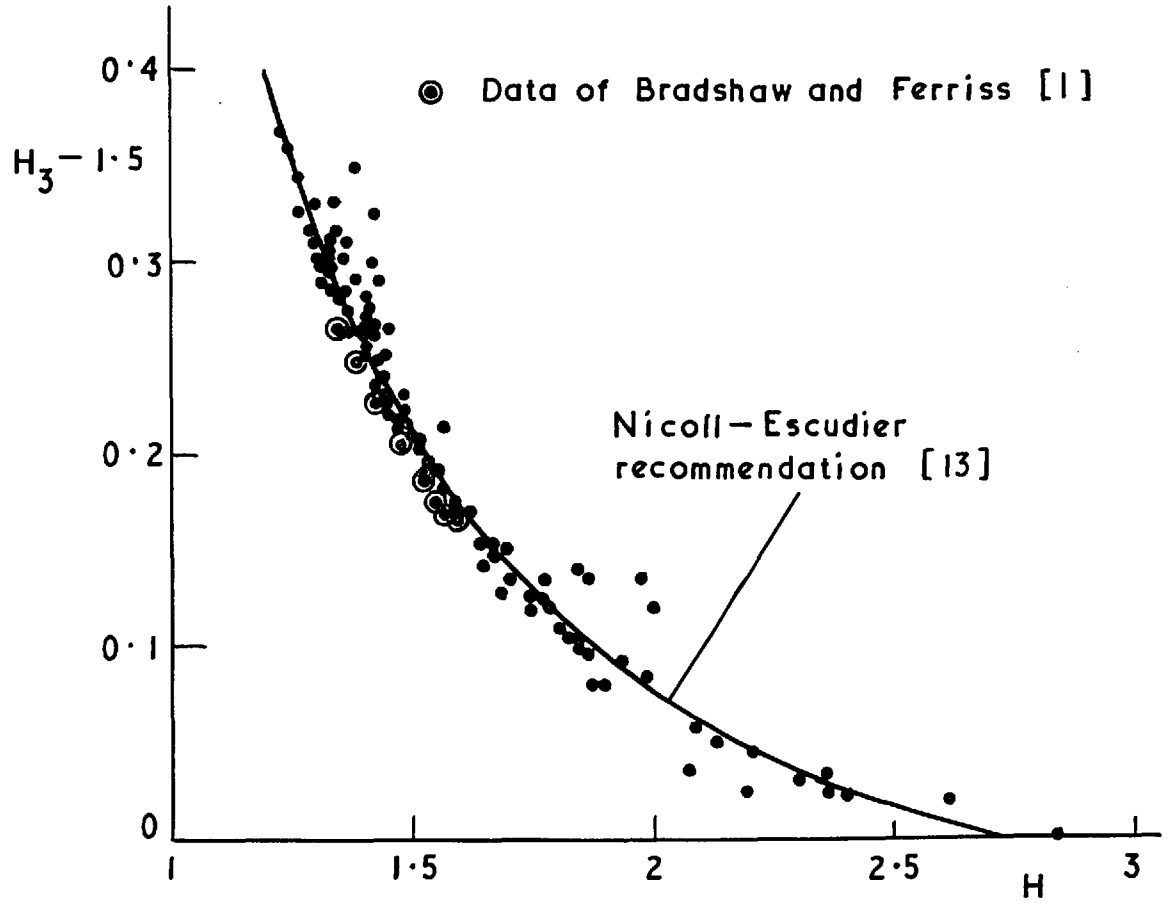


FIG. 3 Experimental data for the relation between the shape factors H_3 and H

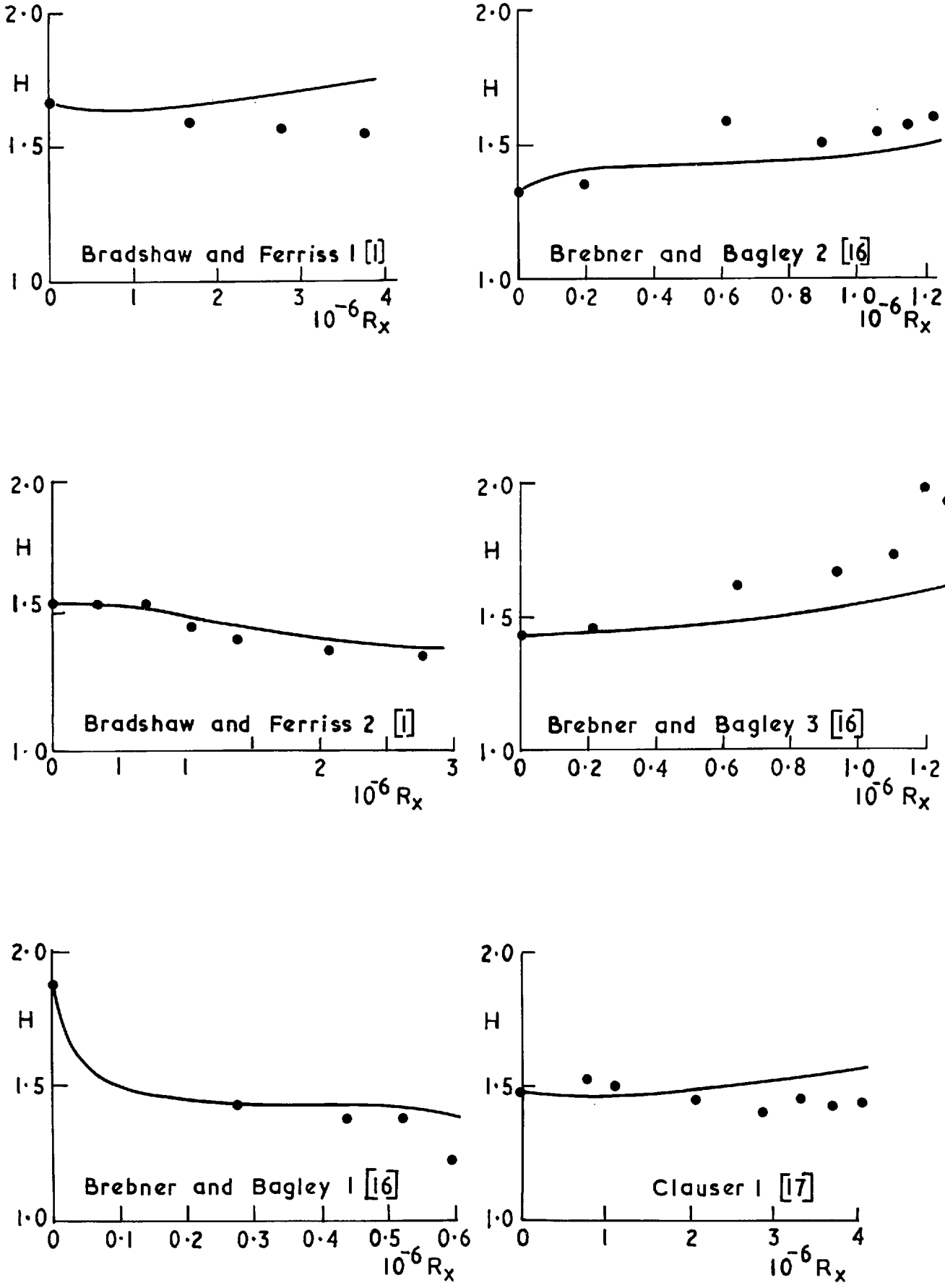


FIG. 4: Comparison of measured shape factors with the predictions (curves) made by the method described in the text

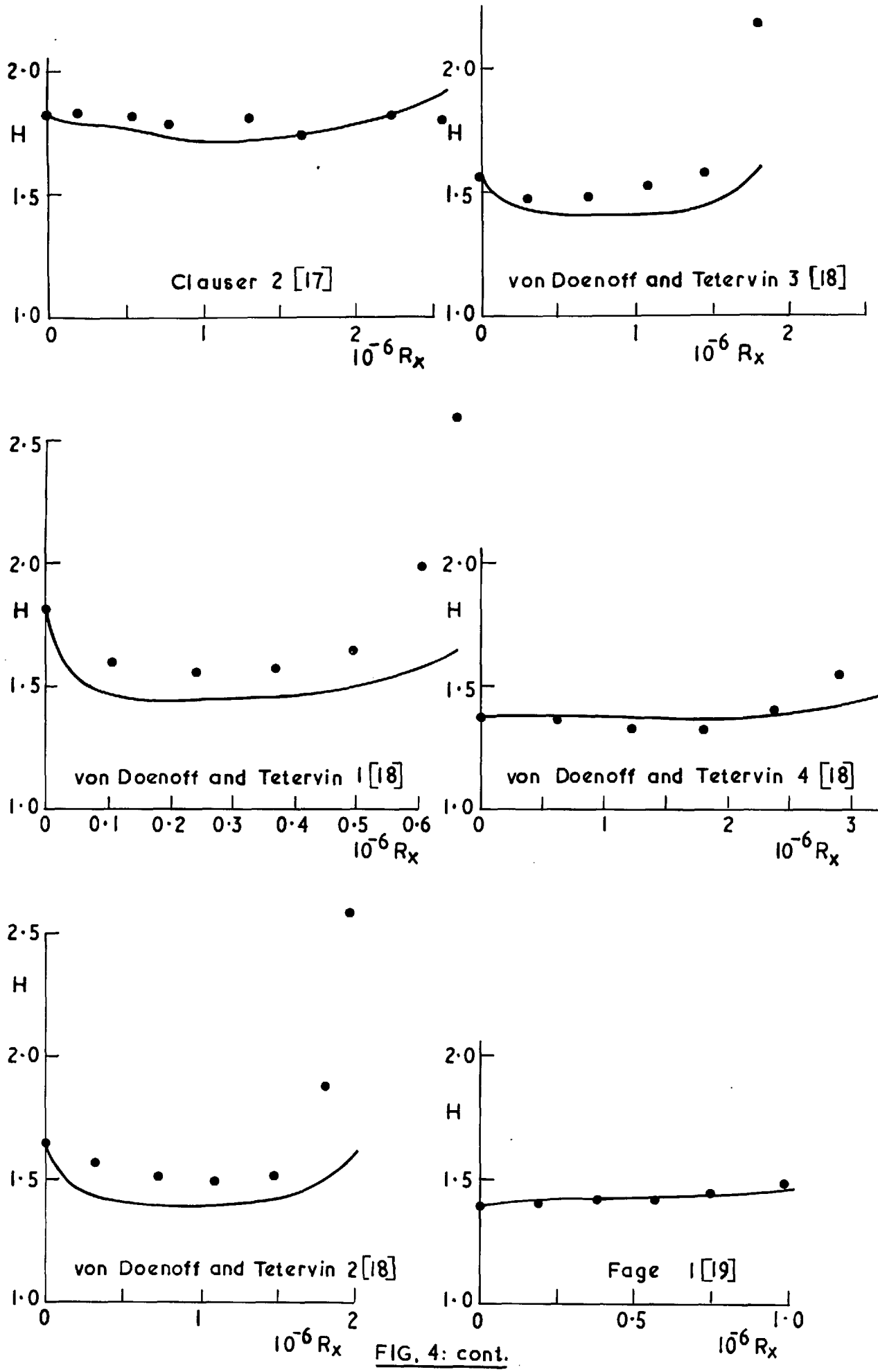
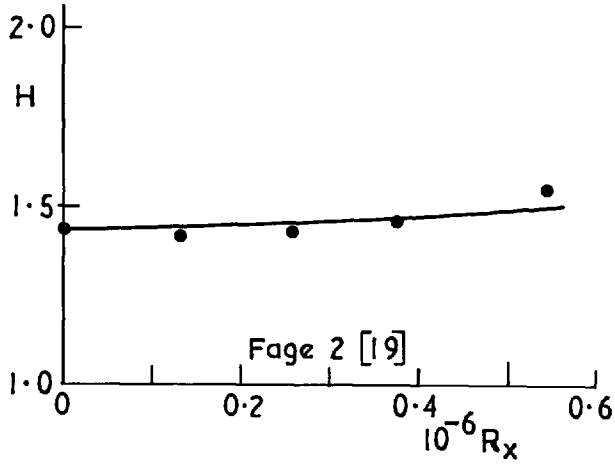
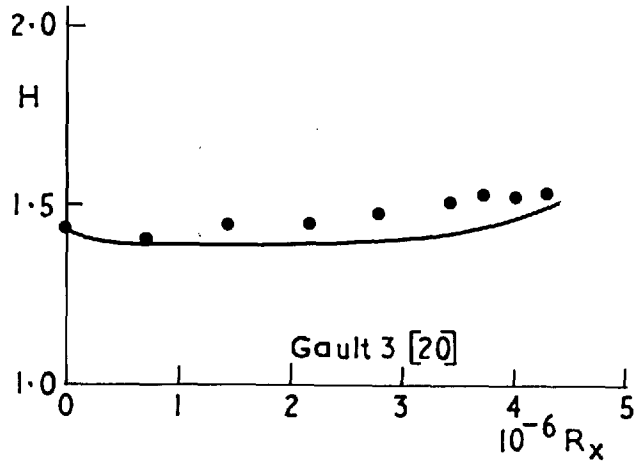
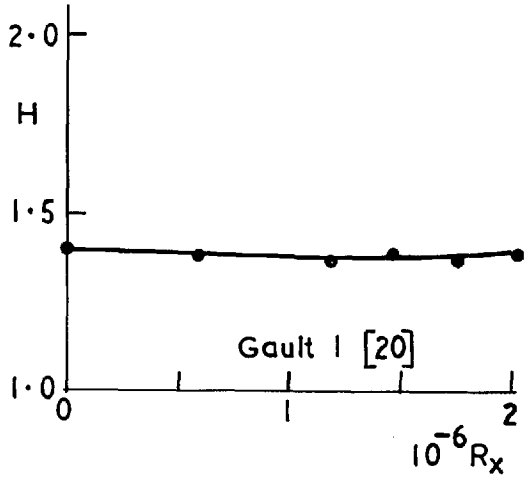
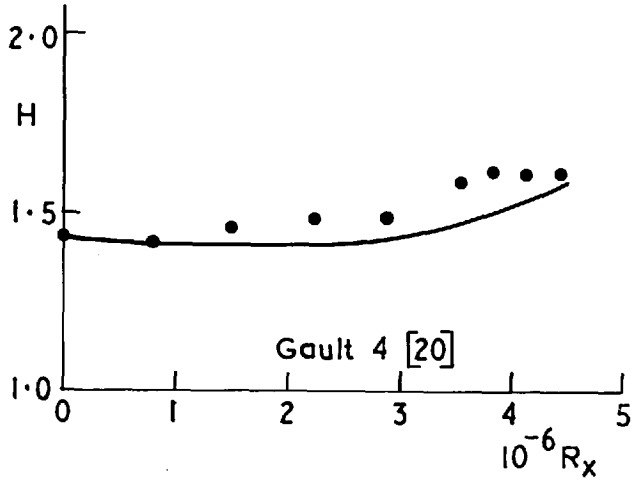

2·0
H
1·5
1·0
Clauser 2 [17]
0
1
2
10⁻⁶ Rx
2·0
H
1·5
1·0
von Doenoff and Tetervin 3 [18]
0
1
2
10⁻⁶ Rx
2·5
2·0
H
1·5
1·0
von Doenoff and Tetervin 1 [18]
0
0·1
0·2
0·3
0·4
0·5
0·6
10⁻⁶ Rx
2·0
H
1·5
1·0
von Doenoff and Tetervin 4 [18]
0
1
2
3
10⁻⁶ Rx
2·5
H
2·0
1·5
1·0
von Doenoff and Tetervin 2 [18]
0
1
2
10⁻⁶ Rx
2·0
H
1·5
1·0
Fage 1 [19]
0
0·5
1·0
10⁻⁶ Rx

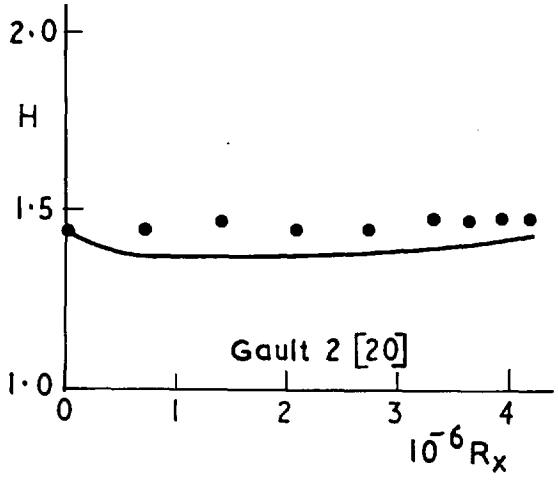
FIG. 4: cont.


2·0
H
1·5
1·0
Fage 2 [19]
0
0·2
0·4
0·6
$10^{-6}R_x$


2·0
H
1·5
1·0
Gault 3 [20]
0
1
2
3
4
5
$10^{-6}R_x$


2·0
H
1·5
1·0
Gault 1 [20]
0
1
2
$10^{-6}R_x$


2·0
H
1·5
1·0
Gault 4 [20]
0
1
2
3
4
5
$10^{-6}R_x$


2·0
H
1·5
1·0
Gault 2 [20]
0
1
2
3
4
$10^{-6}R_x$

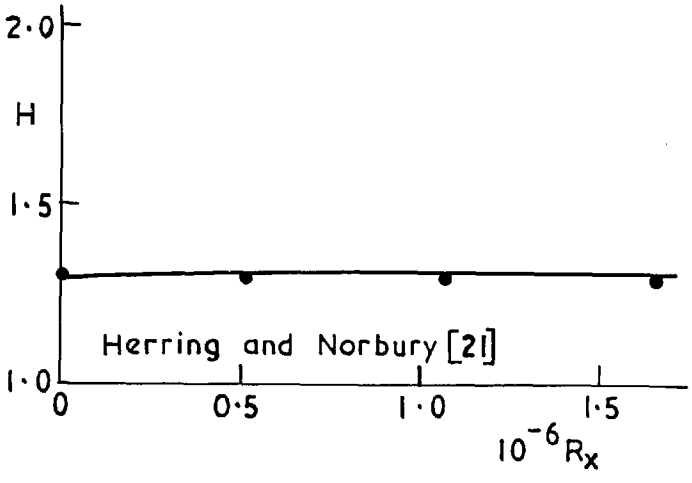
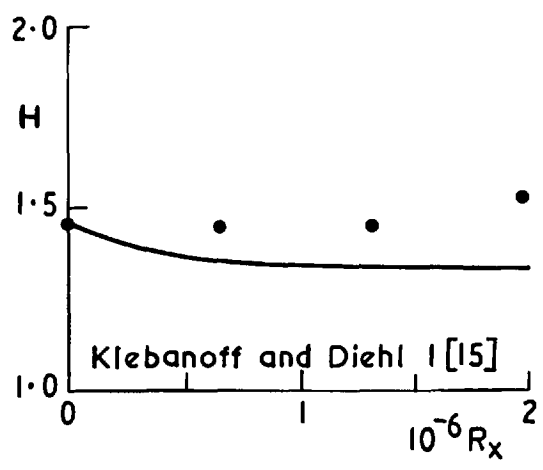
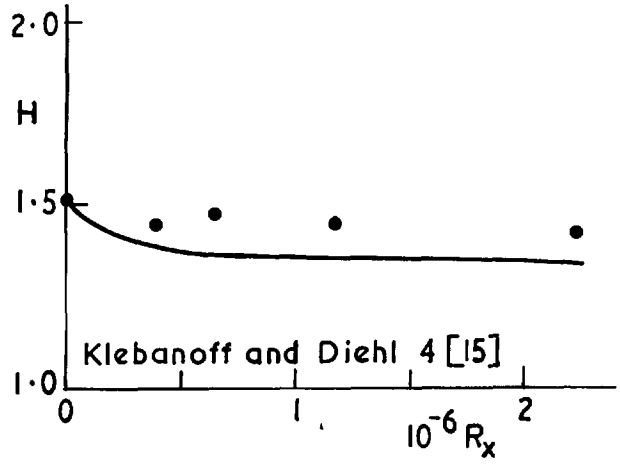
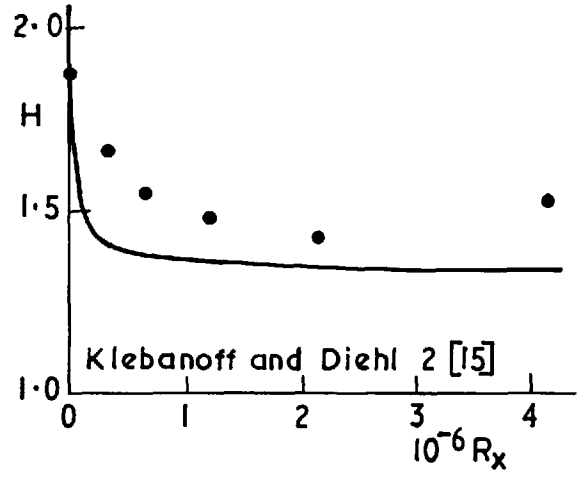
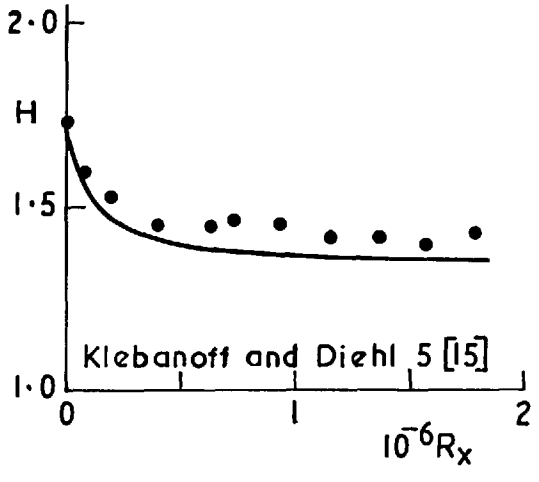

2·0
H
1·5
1·0
Herring and Norbury [21]
0
0·5
1·0
1·5
$10^{-6}R_x$

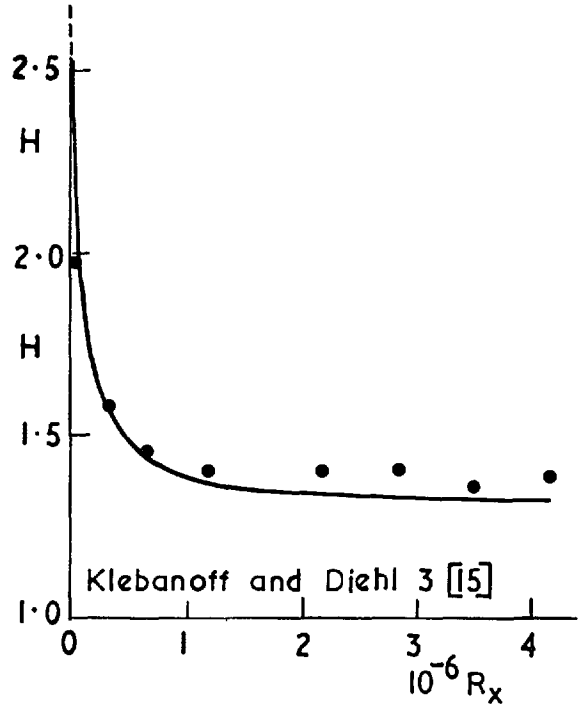
FIG. 4 cont.


2·0
H
1·5
1·0
Klebanoff and Diehl 1 [15]
0
1
2
$10^{-6} R_x$


2·0
H
1·5
1·0
Klebanoff and Diehl 4 [15]
0
1
2
$10^{-6} R_x$


2·0
H
1·5
1·0
Klebanoff and Diehl 2 [15]
0
1
2
3
4
$10^{-6} R_x$


2·0
H
1·5
1·0
Klebanoff and Diehl 5 [15]
0
1
2
$10^{-6} R_x$


2·5
H
2·0
H
1·5
1·0
Klebanoff and Diehl 3 [15]
0
1
2
3
4
$10^{-6} R_x$

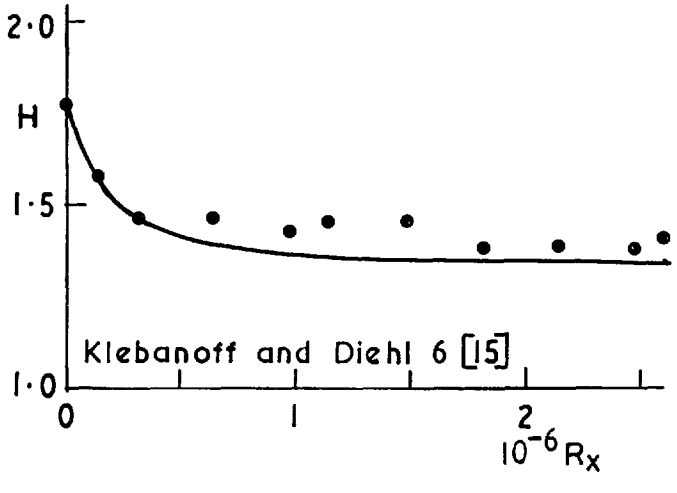

2·0
H
1·5
1·0
Klebanoff and Diehl 6 [15]
0
1
2
$10^{-6} R_x$

FIG. 4 cont.

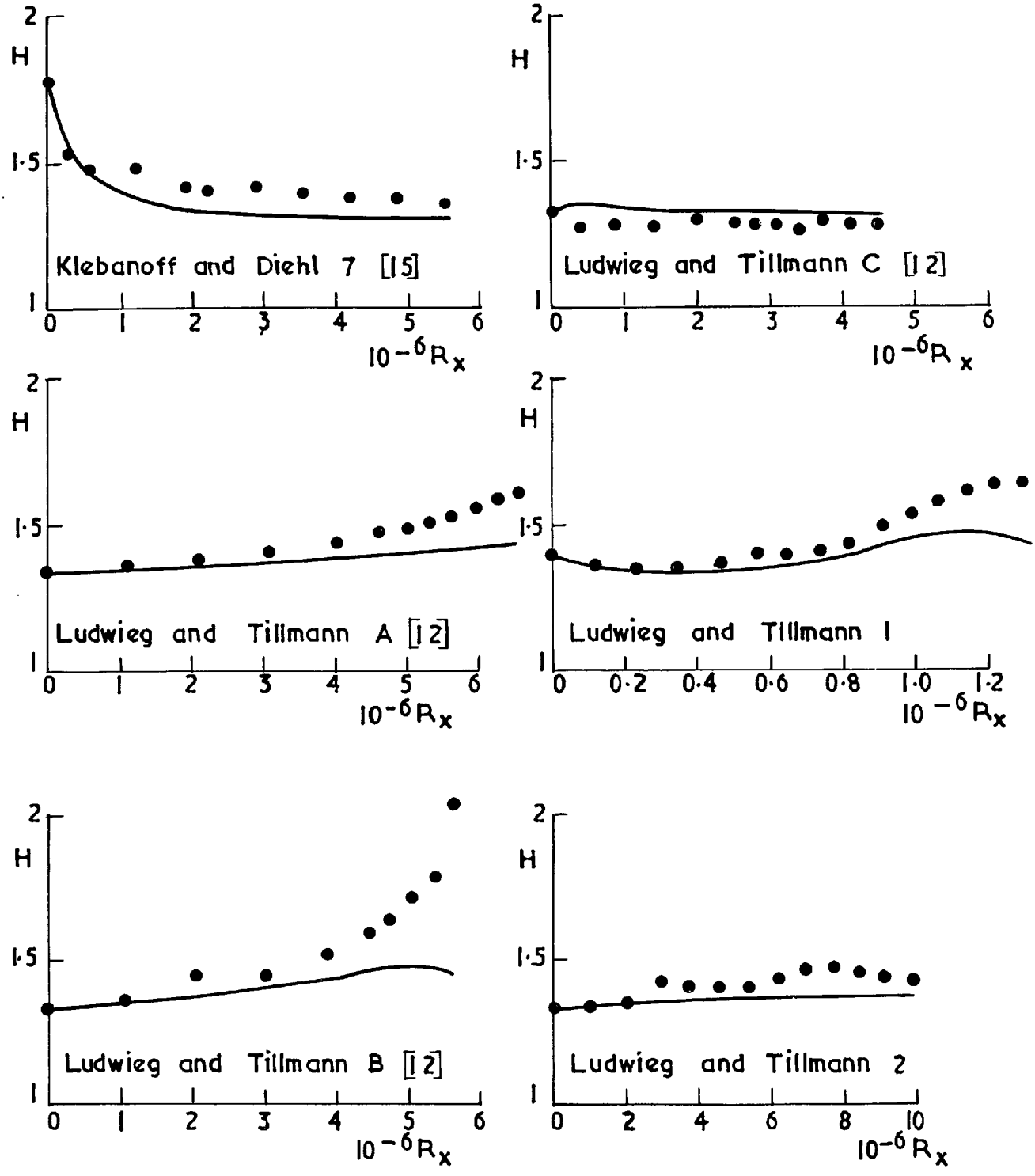

H
2
1·5
1
Klebanoff and Diehl 7 [15]
Ludwieg and Tillmann C [12]
Ludwieg and Tillmann A [12]
Ludwieg and Tillmann I
Ludwieg and Tillmann B [12]
Ludwieg and Tillmann 2
0 1 2 3 4 5 6
0 0·2 0·4 0·6 0·8 1·0 1·2
0 2 4 6 8 10
$10^{-6}R_x$

FIG. 4. cont.

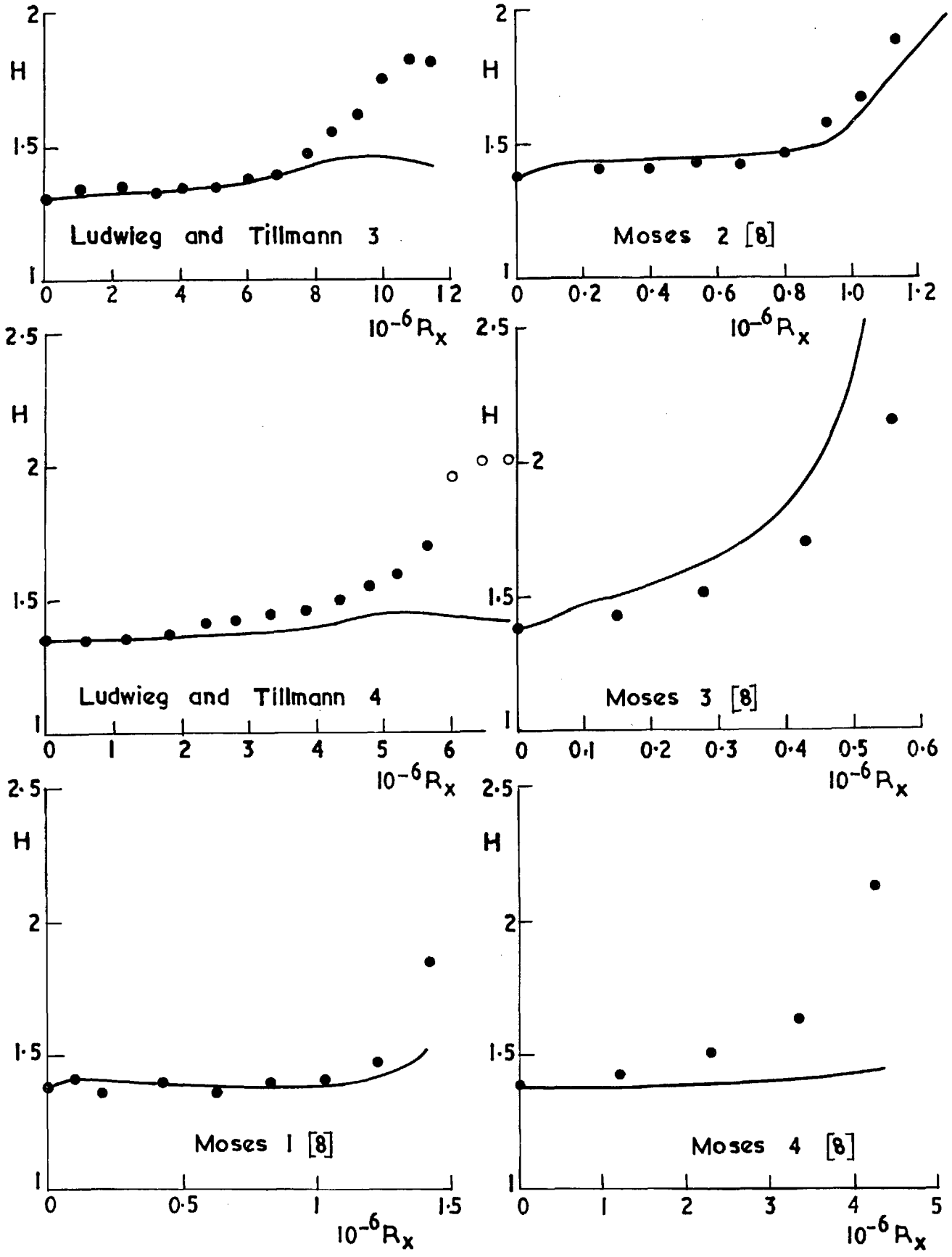

Ludwieg and Tillmann 3
Moses 2 [8]
Ludwieg and Tillmann 4
Moses 3 [8]
Moses 1 [8]
Moses 4 [8]
H
$10^{-6} R_x$

FIG.4 cont.

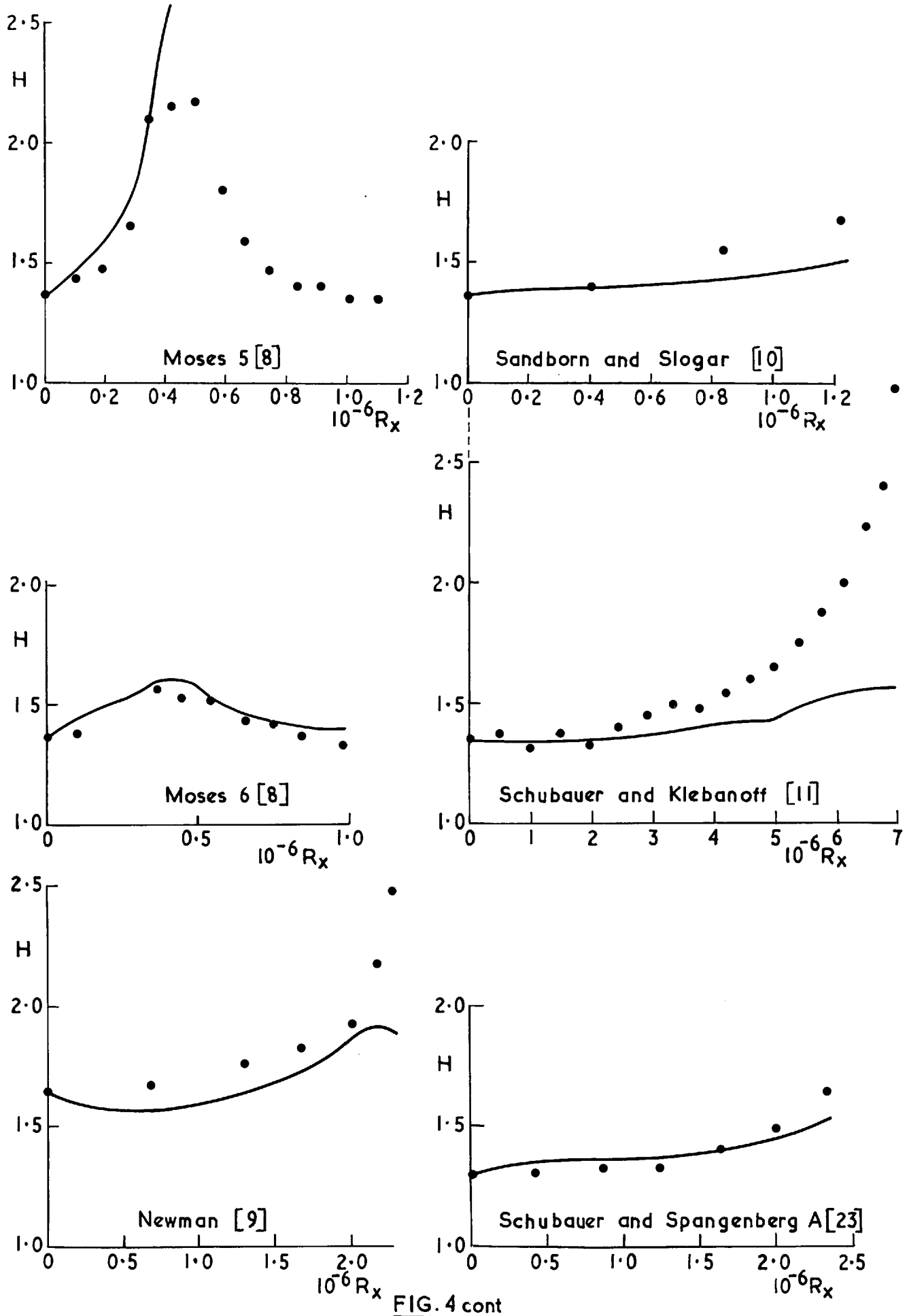

Moses 5 [8]
Sandborn and Slogar [10]
Moses 6 [8]
Schubauer and Klebanoff [11]
Newman [9]
Schubauer and Spangenberg A[23]
H
$10^{-6}R_x$

FIG. 4 cont

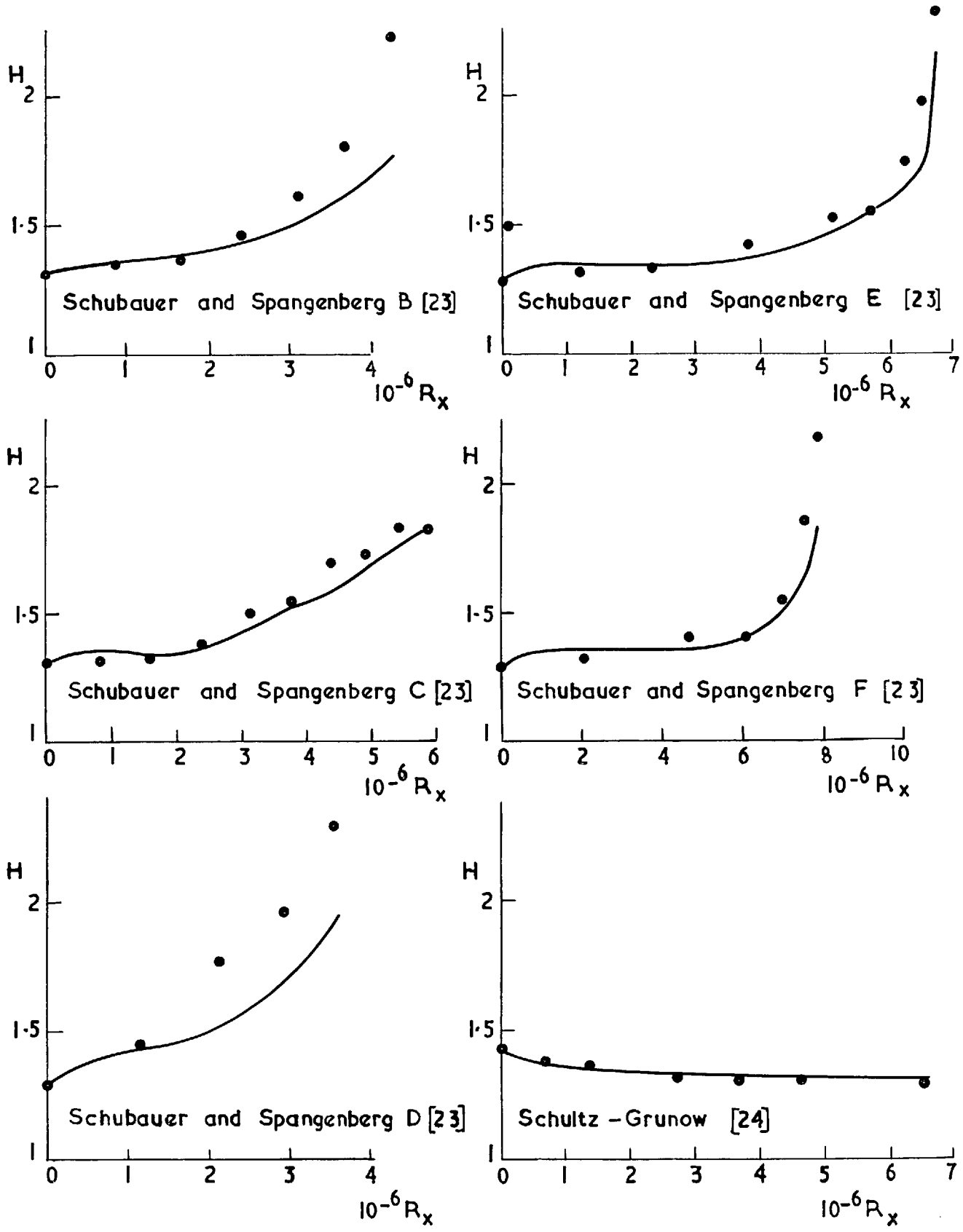

H
2
1·5
1
Schubauer and Spangenberg B [23]
0 1 2 3 4
10⁻⁶ Rx
Schubauer and Spangenberg E [23]
0 1 2 3 4 5 6 7
Schubauer and Spangenberg C [23]
0 1 2 3 4 5 6
Schubauer and Spangenberg F [23]
0 2 4 6 8 10
Schubauer and Spangenberg D [23]
Schultz - Grunow [24]

FIG. 4. conc.

A.R.C. C.P. No.875
August, 1965
Escudier, M. P. and Spalding, D. B.

A NOTE ON THE TURBULENT UNIFORM-PROPERTY HYDRODYNAMIC BOUNDARY LAYER ON A SMOOTH IMPERMEABLE WALL; COMPARISONS OF THEORY WITH EXPERIMENT

The recent experimental data of Bradshaw and Ferriss[1] are compared with generalisations deduced from earlier data, in respect of the mixing-length distribution and the dissipation integral; the agreement is satisfactory.

Also presented is a preliminary theory of boundary-layer development employing an empirical formula for the relation between the dissipation integral, the drag coefficient and the shape factor; the integral momentum and kinetic-energy equations are solved numerically. The predictions of this theory are compared, in respect of shape factor, with the experiments of Bradshaw and Ferriss and those of many other experimenters. The agreement is satisfactory except for large adverse pressure gradient, where divergences of both positive and negative sign are observed; the reasons for these divergences are discussed.

A.R.C. C.P. No.875
August, 1965
Escudier, M. P. and Spalding, D. B.

A NOTE ON THE TURBULENT UNIFORM-PROPERTY HYDRODYNAMIC BOUNDARY LAYER ON A SMOOTH IMPERMEABLE WALL; COMPARISONS OF THEORY WITH EXPERIMENT

The recent experimental data of Bradshaw and Ferriss[1] are compared with generalisations deduced from earlier data, in respect of the mixing-length distribution and the dissipation integral; the agreement is satisfactory.

Also presented is a preliminary theory of boundary-layer development employing an empirical formula for the relation between the dissipation integral, the drag coefficient and the shape factor; the integral momentum and kinetic-energy equations are solved numerically. The predictions of this theory are compared, in respect of shape factor, with the experiments of Bradshaw and Ferriss and those of many other experimenters. The agreement is satisfactory except for large adverse pressure gradient, where divergences of both positive and negative sign are observed; the reasons for these divergences are discussed.

A.R.C. C.P. No.875
August, 1965
Escudier, M. P. and Spalding, D. B.

A NOTE ON THE TURBULENT UNIFORM-PROPERTY HYDRODYNAMIC BOUNDARY LAYER ON A SMOOTH IMPERMEABLE WALL; COMPARISONS OF THEORY WITH EXPERIMENT

The recent experimental data of Bradshaw and Ferriss[1] are compared with generalisations deduced from earlier data, in respect of the mixing-length distribution and the dissipation integral; the agreement is satisfactory.

Also presented is a preliminary theory of boundary-layer development employing an empirical formula for the relation between the dissipation integral, the drag coefficient and the shape factor; the integral momentum and kinetic-energy equations are solved numerically. The predictions of this theory are compared, in respect of shape factor, with the experiments of Bradshaw and Ferriss and those of many other experimenters. The agreement is satisfactory except for large adverse pressure gradient, where divergences of both positive and negative sign are observed; the reasons for these divergences are discussed.

A.R.C. C.P. No.875
August, 1965
Escudier, M. P. and Spalding, D. B.

A NOTE ON THE TURBULENT UNIFORM-PROPERTY HYDRODYNAMIC BOUNDARY LAYER ON A SMOOTH IMPERMEABLE WALL; COMPARISONS OF THEORY WITH EXPERIMENT

The recent experimental data of Bradshaw and Ferriss[1] are compared with generalisations deduced from earlier data, in respect of the mixing-length distribution and the dissipation integral; the agreement is satisfactory.

Also presented is a preliminary theory of boundary-layer development employing an empirical formula for the relation between the dissipation integral, the drag coefficient and the shape factor; the integral momentum and kinetic-energy equations are solved numerically. The predictions of this theory are compared, in respect of shape factor, with the experiments of Bradshaw and Ferriss and those of many other experimenters. The agreement is satisfactory except for large adverse pressure gradient, where divergences of both positive and negative sign are observed; the reasons for these diverg nces are discussed.

DETACHABLE ABSTRACT CARDS